



UNIVERSITY OF
BIRMINGHAM

**ASSESSING THE CONDITION OF
BURIED PIPE USING GROUND
PENETRATING RADAR**

by

SAIFUL WAZLAN WAHAB

A Thesis submitted to
The University of Birmingham
For the degree of
MASTER OF PHILOSOPHY (MPhil)

School of Civil Engineering
College of Engineering and Physical Science
The University of Birmingham
August 2013

UNIVERSITY OF
BIRMINGHAM

University of Birmingham Research Archive

e-theses repository

This unpublished thesis/dissertation is copyright of the author and/or third parties. The intellectual property rights of the author or third parties in respect of this work are as defined by The Copyright Designs and Patents Act 1988 or as modified by any successor legislation.

Any use made of information contained in this thesis/dissertation must be in accordance with that legislation and must be properly acknowledged. Further distribution or reproduction in any format is prohibited without the permission of the copyright holder.

ABSTRACT

The invention of Ground Penetrating Radar (GPR) technology has facilitated the possibility of detecting buried utilities and has been used primarily in civil engineering for detecting structural defects, such as voids and cavities in road pavements, slabs and bridge decks, but has not been used to assess the condition of buried pipes. Pipe deterioration can be defined as pipes where, for example, cracking, differential deflection, missing bricks, collapses, holes, fractures and corrosion exists. Assessing the deterioration of underground pipes is important for service efficiency and asset management. This thesis describes a research project that focused on the use of GPR for assessing the condition of buried pipes. The research involved the construction of a suitable GPR test facility in the laboratory to conduct controlled testing in a dry sand. Plastic pipes were chosen for the experiments. A series of laboratory experiments were conducted to determine the validity and effectiveness of standard commercially available GPR technology in assessing the condition of buried utilities with common types of damage. Several types of damage to the plastic pipe were investigated with respect to different GPR antenna frequencies. The GPR surveys were carried out in order to obtain signal signatures from damaged and undamaged pipes buried at 0.5m depth. These surveys were organised on a grid pattern across the surface of the sand in the test facility. The results presented in this thesis show that GPR can identify certain types of damage associated with a buried pipe under these controlled laboratory conditions.

ACKNOWLEDGMENTS

First of all, I wish to express my truthful appreciation to my thesis supervisor, Dr David Chapman and Professor Christopher Rogers, Civil Engineering, University of Birmingham for their guidance, advise, understanding and encouragement. It has been an honour for me to be supervised by people with such wide knowledge and top notch ideas. Without their continued support and interest, this thesis would not have been the same as presented here.

I also wish to thank my colleague Dr Andrew, Dr Aziman and everyone in the Mapping the Underworld group, University of Birmingham, for sharing idea and discussion during the period of completing the studies.

I owe my loving and sincere thanks to my father Wahab Abd Rahman, my mother Leha Mohd Noor, my wife Azyanty Mohd Arifin, my children Aqil Safwan, Nur Auni Nahwah and Alma Saffiyyah. My special gratitude and loving thanks are also due to my siblings. Their prayers and duas, support, encouragement, understanding and sacrifices have helped and motivated me a lot throughout the entire time I worked on my thesis.

Last but not least, thanks to all the staff in Department of Survey and Mapping Malaysia especially in Utility Mapping Section and Public Service Department of Malaysia (JPA) for the financial support and MPhil sponsorship.

PUBLICATIONS

Conferences

1. **Wazlan, S.**, Chapman,D.N., Rogers,C.D.F., Foo, K.Y.and Nawawi S.W., “Assessing the condition of buried pipe using GPR”11th International Symposium and Exhibition on Geoinformation 2012 (ISG2012), 25-26 Sept 2012, Kuala Lumpur, Malaysia.
2. Royal, A. C. D., Rogers, C. D. F., Atkins, P. R., Chapman, D. N., Curioni, G. , Foo, K. Y. , T. Hao, Metje, N. , Moghareh Abed, T. , Shirgiri, N. , **Wazlan, S.** , “Pipeline Engineering in the Ground: The Impact of Ground Conditions on Pipeline Condition and Maintenance Operations”,Proc. ICPTT 2011, American Society of Civil Engineers, 1598-1609, Oct 2011.

TABLE OF CONTENTS

Abstract	i
Acknowledgment	ii
Publications	iii
List of figures	x
List of tables	xxii
List of abbreviations	xxiii
List of notations	xxiv
CHAPTER 1- INTRODUCTION	1
1.1 Background	1
1.2 Aim and objectives.....	4
1.3 Layout of the thesis	5
1.4 Summary	5
CHAPTER 2- LITERATURE REVIEW	7
2.1 Introduction	7
2.2 History of GPR.....	8
2.3 Overview of GPR techniques.....	9

2.4 Basic GPR concept.....	11
2.5 GPR method.....	13
2.6 GPR limitations.....	21
2.7 Properties of materials.....	23
2.7.1 Dielectric permittivity (ϵ).....	26
2.7.2 Electrical conductivity (σ).....	28
2.7.3 Magnetic permeability (μ).....	29
2.8 Ground Penetrating Radar signal signature.....	30
2.9 Condition assessment of utilities.....	35
2.10 Summary.....	41
CHAPTER 3- RESEARCH METHODOLOGY.....	44
3.1 Introduction.....	44
3.2 Materials.....	46
3.2.1 GPR test facility preparation.....	46
3.2.2 Fill material for the tank.....	50
3.2.3 Pipes.....	54
3.3 Details of the GPR equipment used.....	57

3.4 Data acquisition and analysis	62
3.4.1 Data acquisition	62
3.4.2 Data processing	64
3.5 Research methodology diagram	69
3.5.1 Test 1	71
3.5.2 Test 2	72
3.5.3 Test 3	73
3.5.4 Test 4	74
3.5.5 Test 5	75
3.5.6 Test 6	76
3.5.7 Test 7	77
3.6 Summary	78
CHAPTER 4- RESULTS AND DISCUSSION	79
4.1 Introduction	79
4.2 Test 1	80
4.2.1 Identifying the best configuration	81
4.2.2 Identifying the signal signature of damaged and undamaged pipes.....	87

4.2.3 Identifying the effects of the GPR signal related to the damaged regions relative to the undamaged regions under ‘ideal’ ground conditions	100
4.3 Test 2	113
4.3.1 Identifying the signal signature of the damaged and undamaged pipe	115
4.3.2 Identifying the effects of the GPR signal related to the damaged regions relative to the undamaged regions under ‘ideal’ ground conditions	120
4.4 Test 3	124
4.4.1 Identifying the signal signature of the damaged and undamaged pipe	125
4.4.2 Identifying the effects of the GPR signal related to the damaged regions relative to the undamaged regions under ‘ideal’ ground conditions	130
4.5 Test 4	135
4.5.1 Identifying the signal signature of the damaged and undamaged pipe	136
4.5.2 Identifying the effects of the GPR signal related to the damaged regions relative to the undamaged regions under ‘ideal’ ground conditions	141
4.6 Test 5	145
4.6.1 Identifying the signal signature of the damaged and undamaged pipe	147
4.6.2 Identifying the effects of the GPR signal related to the damaged regions relative to the undamaged regions under ‘ideal’ ground conditions	151
4.7 Test 6	155

4.7.1 Identifying the signal signature of the damaged and undamaged pipe	156
4.7.2 Identifying the effects of the GPR signal related to the damaged regions relative to the undamaged regions under ‘ideal’ ground conditions	161
4.8 Test 7	165
4.8.1 Identifying the signal signature of the damaged and undamaged pipe	166
4.8.2 Identifying the effects of the GPR signal related to the damaged regions relative to the undamaged regions under ‘ideal’ ground conditions	175
4.9 Result Comparison and Discussion.....	182
CHAPTER 5- CONCLUSION AND RECOMMENDATIONS	188
5.1 Introduction	188
5.2 Conclusions	189
5.3 Recommendations for Further Work.....	192
REFERENCES	194

APPENDICES

Appendix 1 - Matlab Script for identifying the related matrices	205
Appendix 2 - Calculating Mean Square Error (MSE)	206

LIST OF FIGURES

Figure 2.1	One of commercial GPR systems in market	11
Figure 2.2	Functional diagram of GPR equipment (Kuo et al.,2005)	12
Figure 2.3	Radar scan generation (Dusan & Aleksandar, 2007)	15
Figure 2.4	Ground penetrating radar uses radio waves to probe the subsurface of lossy dielectric materials. Two modes of measurement are common: (a) detection of reflected or scattered energy is used, and (b) variation after transmission through the material is used to probe a structure (Annan, 2002)	16
Figure 2.5	General relationship of the EM field phase velocity and attenuation with frequency illustrating the ‘ GPR plateau’ (Annan, 2002)	17
Figure 2.6	Type and material detection of utilities (Paniagua et al., 2004)	32
Figure 2.7	Optical cable in a PVC pipe with a diameter of 110mm (Paniagua et al., 2004)	33
Figure 2.8	Scan along PVC pipe (Dusan & Aleksandar, 2007)	34
Figure 2.9	Broken metal pipe with 160mm diameter	36
Figure 2.10	10mm hole in metal pipe with 180mm diameter	36
Figure 2.11	Metal bent pipe with 60mm diameter	37
Figure 2.12	Multiple crack pipes (www.rdg.com.my)	37

Figure 2.13	Longitudinal crack (www.rdg.com.my)	38
Figure 2.14	Metal corroded pipes	38
Figure 3.1	Minimum width of test facility	48
Figure 3.2	A schematic model of the test facility indicating the pipe position	49
Figure 3.3	Test facility during construction	49
Figure 3.4	Particle size distribution line for the Leighton Buzzard Sand	51
Figure 3.5	The compaction test results for the sand	52
Figure 3.6	Moisture content measurements were taken at five different positions within the test facility	53
Figure 3.7	Arrangement of the two plastic pipes in the test box prior to burial	55
Figure 3.8	Detector Duo GPR unit with shielded dual frequency antennas	57
Figure 3.9	Radar section perpendicular to the pipes	59
Figure 3.10	Radar section axially along the pipes	60
Figure 3.11	Survey grid lines used for each experiment	61
Figure 3.12	Three different configurations of an example GPR image	63
Figure 3.13	Signal contrast between (a) a damaged pipe and (b) an undamaged pipe	65
Figure 3.14	15 radar images relating to 15 crossing points on the survey grid along the damaged pipe (position 8 is where the break in the pipe occurs in this example (Test 1))	66

Figure 3.15	18 radar images relating to 18 crossing points on the survey grid along the damaged pipe (position 14 is where the break in the pipe occurs in this example (Test 1)).	67
Figure 3.16	Example Mean Square Error (MSE) analysis for a pipe where there is damage in the region of survey grid number 8 (Test 1, frequency 250MHz, as described in Table 3.2)(The red dotted circle indicates that the greatest MSE occurs at grid number 8.)	68
Figure 3.17	Flow diagram outlining the research methodology	70
Figure 3.18	Test 1 during filling of the test facility	71
Figure 3.19	Broken pipe with a 2cm gap under a plastic cover	72
Figure 3.20	Broken pipe with a 5cm gap under a plastic cover	72
Figure 3.21	Hole in the pipe with a diameter of 5cm	73
Figure 3.22	Hole in pipe with a diameter of 5cm gap in polystyrene cover	74
Figure 3.23	Hole in pipe with a diameter of 5cm gap in fabric cover	75
Figure 3.24	Broken pipe with a 5cm gap under a fabric cover	76
Figure 3.25	Hole in the pipe with a diameter of 5cm with a sponge covering the inside of the pipe	77
Figure 4.1	Broken pipe split into two sections with a 5cm gap without a plastic cover	81
Figure 4.2(a)	Configuration of radar setting	82 - 84
Figure 4.2(b)	Radar images in three configurations	85-86

Figure 4.3	Test 1- 15 radar images (perpendicular to the pipes) using the 250MHz antenna with 10 integrations.(The red dotted circles indicate areas where visual differences are evident in the scans associated with damaged pipe section.)	88
Figure 4.4	Test 1- 15 radar images (perpendicular to the pipes) using the 700MHz antenna with 10 integrations.(The red dotted circles indicate areas where visual differences are evident in the scans associated with damaged pipe section.)	89
Figure 4.5	Test 1- 15 radar images (perpendicular to the pipes) using the 250MHz antenna with 5 integrations.(The red dotted circles indicate areas where visual differences are evident in the scans associated with damaged pipe section.)	90
Figure 4.6	Test 1- 15 radar images (perpendicular to the pipes) using the 700MHz antenna with 5 integrations.(The red dotted circles indicate areas where visual differences are evident in the scans associated with damaged pipe section.)	91
Figure 4.7	Test 1- 15 radar images (perpendicular to the pipes) using the 250MHz antenna with 2 integrations.(The red dotted circles indicate areas where visual differences are evident in the scans associated with damaged pipe section.)	92
Figure 4.8	Test 1- 15 radar images (perpendicular to the pipes) using the 700MHz antenna with 2 integrations.(The red dotted circles indicate areas where visual differences are evident in the scans associated with damaged pipe section.)	93
Figure 4.9	Test 1- 18 radar images (axially along the pipes) using the 250MHz	94

	antenna with 10 integrations	
Figure 4.10	Test 1- 18 radar images (axially along the pipes) using the 700MHz antenna with 10 integrations	95
Figure 4.11	Test 1- 18 radar images (axially along the pipes) using the 250MHz antenna with 5 integrations	96
Figure 4.12	Test 1- 18 radar images (axially along the pipes) using the 700MHz antenna with 5 integrations	97
Figure 4.13	Test 1- 18 radar images (axially along the pipes) using the 250MHz antenna with 2 integrations.	98
Figure 4.14	Test 1- 18 radar images (axially along the pipes) using the 700MHz antenna with 2 integrations.	99
Figure 4.15	Example GPR radar image in the Matlab program used for determining the area for the subsequent MSE analysis (black rectangle)	101
Figure 4.16	Test 1- MSE for the 250MHz radar at 10 integrations perpendicular to the pipes	103
Figure 4.17	Test 1- MSE for the 250MHz radar at 5 integrations perpendicular to the pipes	103
Figure 4.18	Test 1- MSE for the 250MHz radar at 2 integrations perpendicular to the pipes	104
Figure 4.19	Test 1- MSE for the 700MHz radar at 10 integrations perpendicular to the pipes	104

Figure 4.20	Test 1- MSE for the 700MHz radar at 5 integrations perpendicular to the pipes	105
Figure 4.21	Test 1- MSE for the 700MHz radar at 2 integrations perpendicular to the pipes	105
Figure 4.22	Test 1- MSE for the 250MHz radar at 10 integrations axially along the pipes	106
Figure 4.23	Test 1- MSE for the 250MHz radar at 5 integrations axially along the pipes	107
Figure 4.24	Test 1- MSE for the 250MHz radar at 2 integrations axially along the pipes	108
Figure 4.25	Test 1- MSE for the 700MHz radar at 10 integrations axially along the pipes	109
Figure 4.26	Test 1- MSE for the 700MHz radar at 5 integrations axially along the pipes	110
Figure 4.27	Test 1- MSE for the 700MHz radar at 2 integrations axially along the pipes	111
Figure 4.28	Test 2- Broken pipe with a 5cm gap with a plastic cover	114
Figure 4.29	Test 2- Broken pipe with a 2cm gap with a plastic cover	114
Figure 4.30	15 radar images (perpendicular to the pipes) using the 250MHz antenna with 10 integrations (Test 2).	116
Figure 4.31	15 radar images (perpendicular to the pipes) using the 700MHz	117

	antenna with 10 integrations (Test 2).	
Figure 4.32	18 radar images (axially along the pipes) using the 250MHz antenna with 10 integrations (Test 2).	118
Figure 4.33	18 radar images (axially along the pipes) using the 700MHz antenna with 10 integrations (Test 2).	119
Figure 4.34	MSE for the 250MHz radar at 10 integrations perpendicular to the pipes (Test 2)	120
Figure 4.35	MSE for the 700MHz radar at 10 integrations perpendicular to the pipes (Test 2)	121
Figure 4.36	MSE for the 250MHz radar at 10 integrations axially along the pipes (Test 2)	122
Figure 4.37	MSE for the 700MHz radar at 10 integrations axially along the pipes (Test 2)	123
Figure 4.38	Test 3 –5cm hole in the pipe prior to being covered with sand	124
Figure 4.39	15 radar images perpendicular to the pipes using the 250MHz antenna with 10 integrations (Test 3). (The red dotted circles indicate where visually there is potential evidence of damage due to differences in the scans.)	126
Figure 4.40	15 radar images perpendicular to the pipes using the 700MHz antenna with 10 integrations (Test 3). (The red dotted circles indicate where visually there is potential evidence of damage due to differences in the scans.)	127
Figure 4.41	18 radar images axially along the pipes using the 250MHz antenna	128

	with 10 integrations (Test 3).	
Figure 4.42	18 radar images axially along the pipes using the 700MHz antenna with 10 integrations (Test 3).	129
Figure 4.43	MSE for the 250MHz radar at 10 integrations perpendicular to the pipes (Test 3)	131
Figure 4.44	MSE for the 700MHz radar at 10 integrations perpendicular to the pipes (Test 3)	131
Figure 4.45	MSE for the 250MHz radar at 10 integrations axially along the pipes (Test 3)	132
Figure 4.46	MSE for the 700MHz radar at 10 integrations axially along the pipes (Test 3)	133
Figure 4.47	Test 4 – 5 cm hole in the pipe covered by polystyrene prior to being covered with sand	135
Figure 4.48	15 radar images perpendicular to the pipes using the 250MHz antenna with 10 integrations (Test 4).	137
Figure 4.49	15 radar images perpendicular to the pipes using the 700MHz antenna with 10 integrations (Test 4).	138
Figure 4.50	18 radar images axially along the pipes using the 250MHz antenna with 10 integrations (Test 4).	139
Figure 4.51	18 radar images axially along the pipes using the 700MHz antenna with 10 integrations (Test 4).	140
Figure 4.52	MSE for the 250MHz radar at 10 integrations perpendicular to the	142

	pipes (Test 4)	
Figure 4.53	MSE for the 700MHz radar at 10 integrations perpendicular to the pipes (Test 4)	142
Figure 4.54	MSE for the 250MHz radar at 10 integrations axially along the pipes (Test 4)	143
Figure 4.55	MSE for the 700MHz radar at 10 integrations axially along the pipes (Test 4)	144
Figure 4.56	Test 5 – 5cm diameter hole in the pipe covered by fabric prior to being covered by sand.	146
Figure 4.57	15 radar images perpendicular to the pipes using the 250MHz antenna with 10 integrations (Test 5).	147
Figure 4.58	15 radar images perpendicular to the pipes using the 700MHz antenna with 10 integrations (Test 5).	148
Figure 4.59	18 radar images axially along the pipes using the 250MHz antenna with 10 integrations (Test 5)	149
Figure 4.60	18 radar images axially along the pipes using the 700MHz antenna with 10 integrations (Test 5)	150
Figure 4.61	MSE for the 250MHz radar at 10 integrations perpendicular to the pipes (Test 5)	151
Figure 4.62	MSE for the 700MHz radar at 10 integrations perpendicular to the pipes (Test 5)	152
Figure 4.63	MSE for the 250MHz radar at 10 integrations axially along the pipes	153

	(Test 5)	
Figure 4.64	MSE for the 700MHz radar at 10 integrations axially along the pipes (Test 5)	154
Figure 4.65	Test 6- Broken pipe with a 5cm gap (sand prevented from passing through the gap by a fabric cover)	156
Figure 4.66	15 radar images perpendicular to the pipes using the 250MHz antenna with 10 integrations (Test 6).	157
Figure 4.67	15 radar images perpendicular to the pipes using the 700MHz antenna with 10 integrations (Test 6).	158
Figure 4.68	18 radar images axially along the pipes using the 250MHz antenna with 10 integrations (Test 6)	159
Figure 4.69	18 radar images axially along the pipes using the 700MHz antenna with 10 integrations (Test 6)	160
Figure 4.70	MSE for the 250MHz radar at 10 integrations perpendicular to the pipes (Test 6)	161
Figure 4.71	MSE for the 700MHz radar at 10 integrations perpendicular to the pipes (Test 6)	162
Figure 4.72	MSE for the 250MHz radar at 10 integrations axially along the pipes (Test 6)	163
Figure 4.73	MSE for the 700MHz radar at 10 integrations axially along the pipes (Test 6)	164
Figure 4.74	Test 7 - A 5cm diameter hole in the pipe	165

Figure 4.75	Test 7 - A sponge was used to block the hole in the pipe that could be subsequently removed	166
Figure 4.76	Test 7 - 15 radar images perpendicular to the pipes using the 250MHz antenna (before the sponge was removed).	167
Figure 4.77	Test 7 - 15 radar images perpendicular to the pipes using the 700MHz antenna (before the sponge was removed).	168
Figure 4.78	Test 7 - 15 radar images perpendicular to the pipes using the 250MHz antenna (after the sponge was removed).	169
Figure 4.79	Test 7- 15 radar images perpendicular to the pipes using the 700MHz antenna (after the sponge was removed).	170
Figure 4.80	Test 7 - 18 radar images axially along the pipes using the 250MHz antenna (before the sponge was removed)	171
Figure 4.81	Test 7 - 18 radar images axially along the pipes using the 700MHz antenna (before the sponge was removed)	172
Figure 4.82	Test 7 - 18 radar images axially along the pipes using the 250MHz antenna (after the sponge was removed)	173
Figure 4.83	Test 7 - 18 radar images axially along the pipes using the 700MHz antenna (after the sponge was removed).	174
Figure 4.84	Test 7 - MSE for the 250MHz radar at 10 integrations perpendicular to the pipe (before the sponge was removed)	175
Figure 4.85	Test 7 - MSE for the 700MHz radar at 10 integrations perpendicular to the pipes (before the sponge was removed).	176

Figure 4.86	Test 7 - MSE for the 250MHz radar at 10 integrations perpendicular to the pipes (after the sponge was removed).	176
Figure 4.87	Test 7 - MSE for the 700MHz radar at 10 integrations perpendicular to the pipes (after the sponge was removed).	177
Figure 4.88	Test 7 - MSE for the 250MHz radar at 10 integrations axially along the pipes (before the sponge removed)	178
Figure 4.89	Test 7 - MSE for the 700MHz radar at 10 integrations axially along the pipes (before the sponge was removed).	179
Figure 4.90	Test 7 - MSE for the 250MHz radar at 10 integrations axially along the pipes (after the sponge was removed)	180
Figure 4.91	Test 7 - MSE for the 700MHz radar at 10 integrations axially along the pipes (after the sponge was removed)	181
Figure 4.92	All tests of MSE for the 250MHz radar scans perpendicular to the pipes, the green circle highlights position of undamaged pipe, while the red circle highlights position of damaged pipe, both are known <i>a priori</i>	184
Figure 4.93	All tests of MSE for the 700MHz radar scans perpendicular to the pipes	185
Figure 4.94	All tests of MSE for the 250MHz radar scans axially along the pipes	185
Figure 4.95	All tests of MSE for the 700MHz radar scans axially along the pipes	186

LIST OF TABLES

Table 2.1	Dielectric values for common materials (Daniels, 2004)	20
Table 2.2	Typical range of dielectric characteristics of various materials measured at 100 MHz (Daniels, 2004)	24
Table 3.1	Electromagnetic properties and soil moisture content	53
Table 3.2	Description of the experimental arrangements used in each test	56

LIST OF ABBREVIATIONS

ASCE	American Society of Civil Engineers
CI	Cast iron
CCTV	Closed Circuit Television system
EM	Electromagnetic
GPR	Ground Penetrating Radar
HDPE	High-density polyethylene
IDS	IngegneriadeiSistemi
MSE	Mean Square Error
PVC	Polyvinyl chloride
RF	Radio Frequency
SSET	Sewer Scanning Evaluation Technology
SIP	Structural insulated panel
TDR	Time Domain Reflectometry
USEPA	US Environmental Protection Agency

LIST OF NOTATIONS

t_R	The time necessary for the propagation of the EM waves from the transmit antenna to the boundary surface and its reflection back to the receiver antenna
ε	Dielectric permittivity
θ	Angle (degree)
R_x	Receiver
T_x	Transmitter
α	Attenuation
t	Two way travel time (nsec)
v	Average propagation velocity of the signal (m/nsec)
ε_r	Dielectric constant of materials/ relative permittivity (unitless)
c	Velocity of light (m/nsec)
D	Depth of penetration (m)
σ	Electrical conductivity (Sm ⁻¹)
μ	Magnetic permeability (H/m)

Chapter 1

INTRODUCTION

1.1 Background

The quality of life in a city is usually associated with the quality of infrastructure and utility services. Provision of essential services in an efficient and reliable way is the minimum expectation of a modern city. Since the 19th Century, the UK has been developing its modern utility systems, which involve five main utility services: electricity, gas, sewer, telecommunications and water (Beck et al., 2007). These systems are important to all aspects of urban living and form capital-intensive infrastructure systems. Without

them, life in crowded cities would be impossible. Unfortunately, many of the utilities laid beneath the street have not been properly managed and utility providers hold inaccurate records of their location (and condition). This brings additional challenges as utilities are buried in the ground, and are thus not visible. Difficulties in carrying out maintenance and rehabilitation, planning and designing new routes for utilities or repairing existing utilities are common problems in utility works. Pickering et al. (1993) demonstrates how important it is for all utility information to be recorded properly, not only to contribute to service efficiency, but also for maintaining those assets. Rana (2011) also mentions that poor records, improper notification, and excavation errors of underground utilities contribute to increased costs, delays, and public inconvenience. In order to improve the quality of utility records, Beck et al. (2007) suggest a framework for data utility integration in the UK.

Asset management might include how to determine the structure of deteriorated pipes. Structural deterioration, which is characterised by structural defects, reduces the physical integrity of pipes and can eventually lead to pipe failure (Tran, 2007). This can occur in many different ways from either the inner surface or the outer surface of the pipe. For instance, leakage from buried water pipes is a major issue facing all water distribution companies (Yin & Pineda, 1996). Leakage in pipes might be due to aging, excessive demand, misuse and lack of maintenance of the pipe. In the UK, much of the existing drinking water distribution system has been constructed using cast iron pipes, which are subject to corrosion (often resulting in holes in the pipes) (Long et al., 2003). Studies by Makar (1999) have shown that many sewer system failures are caused by pipe deformation, cracking and missing bricks. Failure to identify deterioration of the pipe will increase the risk of asset failure and thus increase the capital required for maintaining,

repairing or replacing the asset. Structural deterioration is a continuing process that reduces the load bearing capacity of the pipe and can be observed through structural defects such as cracks and fractures (Tran, 2007). In this study, pipe deterioration is described as deformation, cracking, fractures, holes and corrosion which lead to structural failure of the pipe. The detection of pipe deterioration is a crucial step in assessing the condition of a pipe and is the subject in this research. It is appreciated that many different approaches have been investigated before such as automatic crack detection in buried concrete pipes (Sinha & Fieguth, 2006), Closed Circuit Television (CCTV) system, Sewer Scanning Evaluation Technology (SSET), Sonar Systems, and Laser Scanning Systems for assessing sewer pipes (Koo & Ariaratnam, 2006).

The invention of Ground Penetrating Radar (GPR) technology has facilitated the possibility of detecting buried utilities and has been used primarily for detecting structural defects, such as voids and cavities in pavements, slabs and bridge decks (Koo & Ariaratnam, 2006). In the current study it is considered as a possible additional non-destructive technique to investigate the condition of pipes or the remaining serviceability of pipes. The range of applications for GPR methods is wide and the sophistication of signal recovery techniques, hardware designs and operating practices is increasing as the technology matures (Daniels, 2004). In order to improve data interpretation in complex situations, basic studies are still required for the recognition of individual target signatures (such as objects, layers and fractures); these studies can be addressed primarily through laboratory or field based physical modelling. However, there is a potential to extend the use of GPR to explore whether it can assess the condition of existing buried utilities as well as to differentiate the signal signatures between new and damaged or corroded pipes.

1.2 Aim and objectives

The aim of this research is to investigate whether an off-the-shelf Ground Penetrating Radar (GPR) unit can be used to assess the condition of existing buried utilities under controlled laboratory conditions.

Even though the GPR is a well-established technique for locating buried utilities and identifying underground disturbances and voids (Farley et al., 2008), as far as the author is aware, it has not been used to assess the condition of pipes. The objectives for this research were:

- i. To conduct a thorough critical review of the literature related to GPR and pipe deterioration.
- ii. To construct a suitable test facility in the laboratory to conduct controlled testing using an off-the-shelf GPR unit.
- iii. To study the different signal signatures obtained from GPR for damaged and undamaged pipes using different frequencies.
- iv. To study the limitations of GPR with respect to identifying different levels of deterioration in pipes.
- v. To study the effects of GPR signal related to damaged regions relative to undamaged regions under 'ideal' ground conditions.

1.3 Layout of the thesis

Following this introductory chapter, Chapter 2 includes a critical review of the relevant literature and provides the necessary background required to understand and appreciate the need for this research. The chapter provides details of the characteristics and performance of GPR systems. The chapter also investigates properties of materials which affect the radar signals. Chapter 3 presents the methodology of the main experimental programme. It details the materials and the novel methods used for this research. Chapter 4 indicates the data acquisition with various parameter configurations and discusses the results obtained from the experimental programme. Chapter 5 presents the conclusions of this research and finally the recommendations for future work are made.

1.4 Summary

Since many utility networks are poorly recorded and mapped, the opportunities to locate accurately the existing buried utilities are crucial. Unable to locate the position accurately will cause damages to the adjacent services, delay to traffic and damage to the environment during maintenance of the asset. Many different approaches have been investigated before such as CCTV, SSET, laser scanning and GPR but these approaches still have limitations. The author decided to study the capability of GPR for detecting the

location of deteriorated pipes. In doing so, a literature review is needed in order to understand the topic and determine what related research has been made before.

Chapter 2

LITERATURE REVIEW

2.1 Introduction

As mention in Chapter 1, understanding GPR and reviewing previous research is a critical part in this Chapter. This chapter includes a review of GPR techniques, GPR concepts, GPR limitations, properties of materials, GPR signal signature and soil science, which form a critical part of the understanding of GPR characteristics and performance. This should provide an indication as to the applicability of GPR to investigating the condition of buried pipes and hence the gaps on current knowledge.

2.2 History of GPR

This section will cover the history of GPR which consists of previous and latest research that has been made. GPR's origins lie in research carried out during the early 20th century by German scientists trying to patent techniques to investigate the nature of various buried features (Daniels, 1996; Reynolds, 1997). Pulse electromagnetic waves were first used in the mid-1920s introduced by Hulsbeck (1926) to determine the structure of buried features. Following these initial developments, pulsed techniques were developed extensively over the next 50 years as a means of probing to considerable depths in ice, fresh water, salt deposits, desert sand and rock formations (Daniels et al., 1988). However, it was not until the 1980s that applications started to grow because of the availabilities of the technology and a better understanding of geology (Annan, 2002). Since the mid-1990s there has been an explosion of interest in GPR, with an ever-increasing number of research articles published on the technique each year (Neal, 2004). It is of interest to note that most of these papers were directed towards environment concerns and a variety of applications such as in locating buried agricultural drainage (Allred et al., 2004), in leaking pipelines under road pavements (Kuo et al., 2005), in rebar detection (He et al., 2009), detecting tunnels and mines (Peters et al., 1994), in the mining industry (Yelf, 1990), in archaeology (Goodman et al., 2011), in police work (Davenport, 2001), were covered including geological structures and even buried corpses.

In summary, GPR represents one of the most promising new non-destructive inspection techniques in providing detail such as in pipe position, existence of soil voids and areas with water leakage. In conclusion, much research has been made previously in terms of a

variety of GPR applications, but there still appears to be a lack of knowledge on the use of GPR to assess the condition of buried utilities. Thus, an overview of GPR techniques is important in order to understand how the GPR techniques work.

2.3 Overview of GPR techniques

This section will cover the GPR techniques in various applications. Nowadays, there are many commercial GPR systems in the market with one of those shown in Figure 2.1. GPR can be defined as a technique which is able to detect buried objects and to characterise the subsurface structure and properties in a wide variety of applications.

Numerous studies describe how GPR techniques are able to detect electromagnetic anomalies under a variety of conditions, such as the location and orientation of plastic and metal pipes or barrels, reinforcing steel bars, metal nets, voids and fractures in concrete, walls and pavements (Zeng & McMechan, 1997; Power & Olheoft, 1994; Tong, 1993; Annan et al., 1990; Pettinelli et al., 2008).

Griffin & Pippett (2002) stated that the GPR method provides a high resolution image of subsurface features in the form of a cross-section view that is essentially a map of the variation in ground electrical properties. They found that these can be correlated with physical changes such as the soil/bedrock interface, the boundary between different soil types, the water table, underground structures such as pipes, cables and tunnels as well as voids and cavities. In addition, features in the GPR section will correlate with the geological profile if, for instance, stratigraphic boundaries representing different rock

types correspond to significant variations in the electrical properties, but not necessarily to other physical properties such as density, grain size or chemical composition (Griffin & Pippett, 2002).

Meanwhile Daniels et al. (1988) noted that GPR relies for its operational effectiveness on successfully meeting the following requirements:

- Efficient coupling of the electromagnetic radiation into the ground;
- Adequate penetration of the radiation through the ground to the target depth;
- Obtaining from the buried object, or other dielectric discontinuities, a sufficiently large scattered signal for detection at or above the ground surface;
- An adequate band width in the detected signal to the desired resolution and noise level.

Generally, the idea of GPR techniques is not very different from free space radar (conventional techniques), as any radar system depends on the design and operational factors. However, GPR is clearly different in propagation loss, clutter characteristics and target characteristics (Daniels et al., 1988).

A study by Daniels (2004) mentioned that a GPR can provide a continuous record of the sub-surface showing the presence, depth, and lateral extent of certain soil horizons and features which it is useful in soil classification, characterisation and mapping. A GPR provides high-resolution information that can aid interpretation and the extrapolation of information obtained with traditional surveying techniques (Davis & Annan, 1989).

In summary, how the GPR technique is applied in a particular application, such as the location and orientation to buried utilities and any physical changes in the soil, can affect the radar image. It is therefore evident that understanding the GPR concept is important in order to minimize these limitations.



Figure 2.1: One of commercial GPR systems in market

2.4 Basic GPR concept

This section will cover the understanding of the GPR concept, which is fundamental of the equipment performance. GPR is a device used for non-invasive scanning which is able to record an accurate depth reading and the signature of targets (radagram) for further property interpretation, and can detect shallow or deep targets depending on the applied frequency of the antenna. However, the accuracy of the depth information is limited since

it depends on the speed of travel of the wave in an unknown soil or rock. GPR produces high frequency pulsed electromagnetic waves (generally 10 MHz to 1.5 GHz) that travel through the ground until these waves meet the target and then they bounce back to the surface (Kuo et al., 2005). The function of GPR wave transmission and reflection is shown in Figure 2.2.

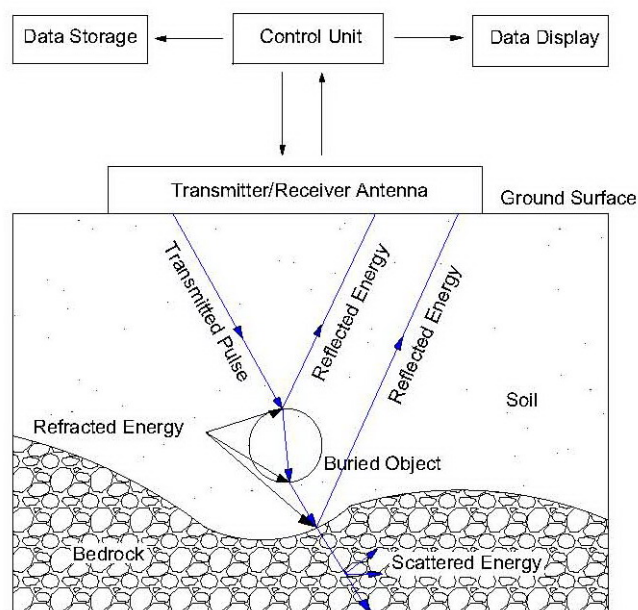


Figure 2.2: Functional diagram of GPR equipment (Kuo et al., 2005)

GPR is composed of a receiver and transmitter antenna, a control unit, battery supply and a survey cart. The control unit is the main part of the GPR because it controls the whole system. It manages the IP protocol link with the laptop and provides the trigger signal and power supply to the antenna. The survey cart is equipped with an incremental encoder. The incremental encoder is used for precise positioning (cm level) of the centre of the antenna

above the ground surface. The antenna receives the electrical pulse produced by the control unit, amplifies it and transmits it into the ground or other medium at a particular frequency. The antenna frequency is a major factor in depth penetration. The higher the frequency of the antenna, the shallower into the ground it will penetrate. Although, a higher frequency should be better at detecting smaller targets (this is a function of the wavelength of the transmitted wave). At the same time, the GPR can be equipped and synchronised with the Global Positioning System (GPS) to determine the planar sub-centimetre accurate location.

In summary, the GPR uses an electromagnetic energy signal to penetrate through the structure. It records two way travel time and amplitude of the signal. The amplitude is the strength of the signal coming back. It is therefore apparent that the strength of the GPR signal depends on soil structure and thus understanding the GPR method is important in order to understand signal propagation and the information ultimately obtained from the system.

2.5 GPR method

This section will cover in more detail aspects of the GPR signal. Generally, when the GPR survey cart moves on the site surface the transmitting antenna sends polarized, high frequency electromagnetic (EM) waves into the ground. Due to different existing heterogeneities in the ground, e.g. soil layers, underground utilities, stones, gravel, cavities and other anomalies, a proportion of the EM waves are reflected from the dielectric

boundary between different materials and the rest is refracted and continues to deeper layers. The process is repeated until the EM waves become too weak. Reflection of the EM waves from the dielectric boundary is the consequence of differences in the electric and magnetic properties of the materials of the infrastructural objects and soil layers (Daniels, 2004).

The time necessary for the propagation of the EM waves from the transmit antenna to the boundary surface and its reflection back to the receiver antenna is defined as a two way travel time, t_R (ns) (Daniels, 2004). The GPR measures t_R , and from this calculates the relative depth of the underground object. As each location has its own specific soil structure, the ϵ (dielectric permittivity) has to be recalculated for each site. Usually, the GPR recalibration method is used on site. This method is based on a GPR scan of an underground object with known depth. The methodology of the radar scan generation is shown in Figure 2.3.

The antenna's linear trajectory is shown on the X axis, and the Y axis shows the two way travel time t_R , i.e. the relative depth z from the ground surface to the underground object. The distance between the transmitter and receiver antenna is very small. Because of this, the distance from the transmit antenna to the boundary surface is approximately equal to the distance from the boundary surface to the receiver antenna. The distance from the antenna to the underground object continuously changes. Distances r_0, r_1, \dots, r_N are projected orthogonally on the movement axis, see points $x_{-N} \dots x_0 \dots x_N$ (see Figure 2.3 (b)). By sequentially connecting the ends of these segments, a geometrical hyperbola is formed (Daniels, 2004).

All points on the scan include the reflected wave amplitude data. Points on top of the segments have the peak amplitude value. The peak on the shortest segment r_0 the antenna centre is above the pipe axis is the highest (positive or negative). This value is the criteria for scan searching and determination of the location and the depth of the underground utility.

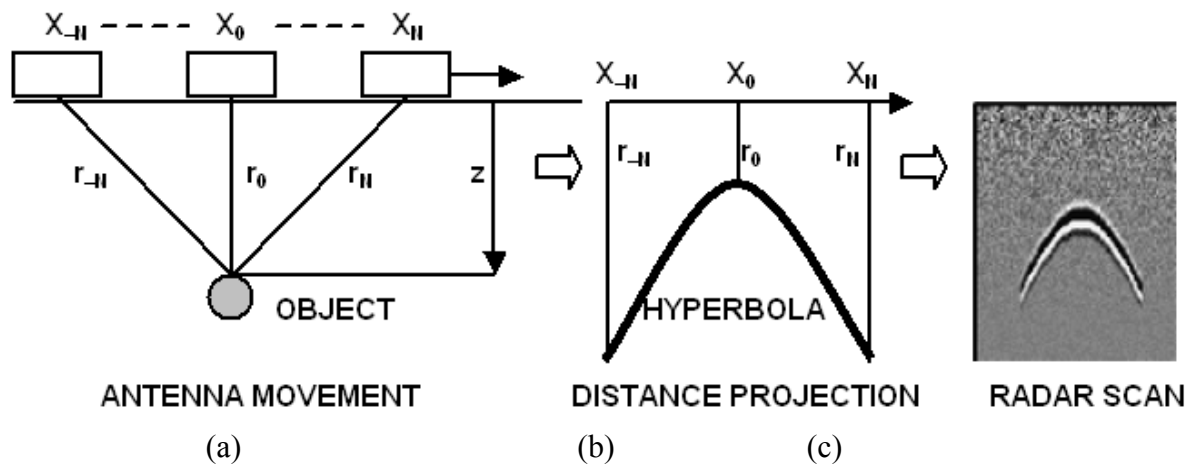


Figure 2.3: Radar scan generation (Dusan & Aleksandar, 2007)

The transmit antenna radiates a conical EM wave beam with a bandwidth $\theta=35^{\circ}-45^{\circ}$. Based on these facts, it is not necessary for the centre of the antenna to be above the underground object to detect it. Figure 2.3 shows an ideal one-pipe radar scan in a homogenous soil layer. The antenna moves orthogonally to the pipeline axis. Under real conditions, the scan will have different noises and hyperbolic reflections, caused by electrical installations, trees or other infrastructure objects. Post-processing can eliminate this (Daniels, 2004).

Annan (2002) describes how GPR uses electromagnetic fields to probe lossy dielectric materials in order to detect structures and changes in material properties within the

materials. Reflection and transmission measurements, as shown in Figure 2.4, are therefore employed.

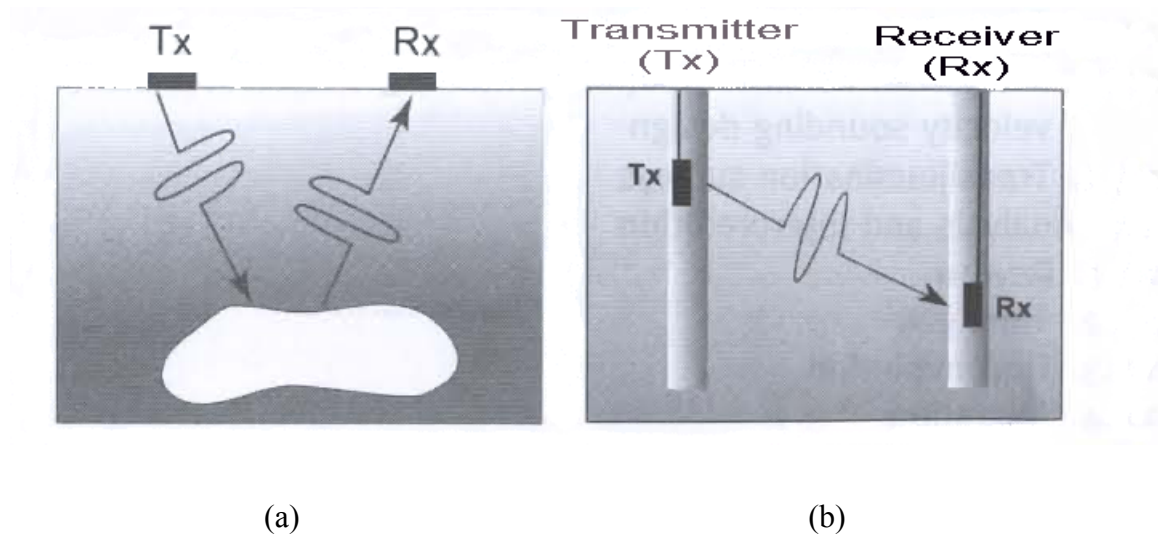


Figure 2.4: Ground penetrating radar uses radio waves to probe the subsurface of lossy dielectric materials. Two modes of measurement are common: (a) detection of reflected or scattered energy is used, and (b) variation after transmission through the material is used to probe a structure (Annan, 2002).

This author added that with GPR, the electromagnetic fields transmit essentially non-dispersive waves. The signal discharged travels through the materials and is scattered and/or reflected by changes in impedance giving rise to events similar to the discharged signal. This means signal recognition is simple because the return signal looks like the discharged signal. Figure 2.5 shows the general relationship of the electromagnetic (EM) field phase velocity and attenuation in lossy dielectric material versus frequency and illustrates the ‘GPR plateau’.

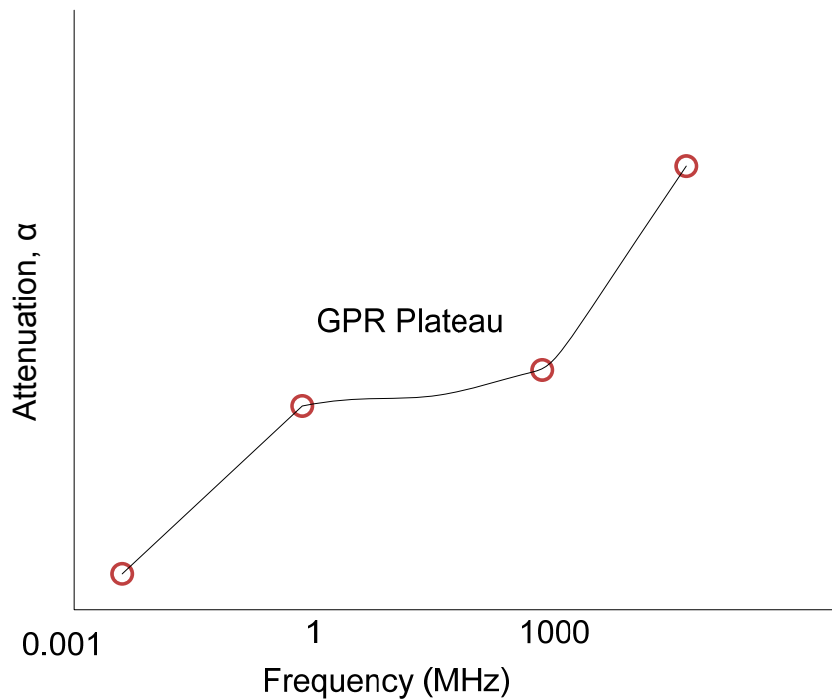


Figure 2.5: General relationship of the EM field phase velocity and attenuation with frequency illustrating the ‘GPR plateau’(Annan, 2002).

GPR field behaviour occurs over a finite frequency range generally referred to as the GPR plateau, where velocity and attenuation are frequency independent. The GPR plateau usually occurs in the 1 MHz to 1000 MHz frequency range. At lower frequencies the fields become diffusive in character and pulses are dispersed. At higher frequencies several factors increase the signal absorption meaning that penetration is extremely limited (Annan, 2002).

According to Griffin & Pippett (2002), the short pulse of Radio Frequency (RF) energy is radiated into the ground from a transmitting antenna placed either on the ground surface or in close proximity. Energy reflected back to the surface from subsurface targets is detected by the receiving antenna, also located in close proximity to the surface. The antennas’

physical size or dimension limits the frequency (or wavelength) of the transmitted pulse. A high frequency waveform (short wavelength) will provide a more detailed or higher resolution image than a low frequency waveform, but the higher frequencies are attenuated or absorbed at a greater rate so the penetration depth is not as great as for lower frequencies. For any specific application, the appropriate choice of antenna frequency involves a compromise between resolution (or size of objects/features to be detected) and the depth of interest.

In addition, Griffin & Pippett (2002) noted that the transmission is characterised as a single burst of energy after which the receiver then ‘listens’ and ‘records’ any reflected energy such that the recoding time (from the point of transmission) representing the depth to the source of the reflection. This means, a reflection from a deeper target will appear later in time in the GPR trace since the energy has travelled further than for the shallower targets (Griffin & Pippett, 2002). In calculating depth of penetration, two way travel time and propagation velocity of the radar signal must be known. The two way travel time can be determined from the graphic representation of the reflected radar signal (Kuo et al., 2005). The propagation velocity of the radar signal can be calculated by Equation 2.1 as follow:

$$v=c/(\sqrt{\epsilon_r}) = 0.3/(\sqrt{\epsilon_r}) \quad \text{(Equation 2.1)}$$

where v is the average propagation velocity of the signal (m/nsec), ϵ_r is the dielectric constant of the materials (unitless), and c is the velocity of light (≈ 0.3 m/nsec). Meanwhile the depth of penetration can be determined using Equation 2.2 as follow:

$$D=(tv)/2 \quad \text{(Equation 2.2)}$$

Where D is the depth of the penetration (metres) and t is two way travel time (nsec)

Daniels et al. (1988) state that the radar technique is usually employed to detect backscattered radiation from a target. Forward scattering can also yield target information, although for subsurface work at least one antenna would need to be buried, and some kind of imaging transform would need to be applied to the measured data.

Therefore, GPR works by sending pulses of energy into the ground and recording the strength and the time for the return of any reflected signal. These series of pulses over a single area are called a scan. Reflection occurs whenever the energy pulses are transmitted through various materials on their way to the buried target feature thus changing the velocity. The velocity changes depend basically on two primary electrical properties of the subsurface: electrical conductivity (σ) and dielectric permittivity (ϵ). Reflections are produced by changes in the dielectric contrast due to changes in the subsurface materials (Eyuboglu et al., 2003). The greater the contrast between two materials at the subsurface interface, the stronger the reflected signal, resulting in a higher amplitude reflected wave (Kuo et al., 2005). For instance, a pulse which moves from dry sand (dielectric permittivity (ϵ) of 5) to wet sand (dielectric permittivity (ϵ) of 30) will produce a very strong, visible reflection, rather than from dry sand (ϵ of 5) to limestone (ϵ of 7), which produces a very weak reflection. Table 2.1 shows the dielectric values for common materials. This means, any materials with a high dielectric constant are very conductive. Void spaces in the ground or buried pipes or conduits will also generate strong reflections due to a significant change in radar wave velocity.

In summary, a GPR pulse penetration depends on the soil properties and differs for each site. Thus, an understanding of the limitations of GPR is crucial in order to minimise the factors affecting the GPR performance and these are discussed in the next section.

Table 2.1: Dielectric values for common materials (Daniels, 2004)

Material	Dielectric constant	Velocity (mm/ns)
Air	1	300
Water (fresh)	81	33
Water (sea)	81	33
Polar snow	1.4-3	194-252
Sand (dry)	3-6	120-170
Sand (wet)	25-30	55-60
Clay (wet)	8-15	86-110
Clay soil (dry)	3	173
Concrete	6-8	55-112
Asphalt	3-5	134-173
PVC	3	173

2.6 GPR limitations

The capability of GPR could be improved by looking at several factors. Generally, the factors affecting the GPR performance, and should be considered, are the design of the GPR unit (hardware), target types, material of the target and the surrounding (environment) (Jol, 2009). Some parts of a GPR system are controllable by the designer while others are set by the nature of the task. Daniels, et al., (1988) state that, the principal constraint on the design process of any GPR is the set of electromagnetic properties of the ground itself, which dictates the design options available elsewhere. Generally, the antenna design for high frequency antenna is smaller than low frequency antenna.

A high frequency waveform (short wavelength) will provide a more detailed or higher resolution image than a low frequency waveform, but the higher frequencies are attenuated or absorbed at a greater rate so the penetration depth is not as great as lower frequencies (Daniels, 2004). Meanwhile the shape of the target such as a sphere, a cuboid or a long thin cylindrical object will affect the choice of antenna type and configuration as well as the kind of signal processing techniques to be employed (Daniels et al., 1988). Detection of pipe materials (metal or non-metal pipe) is possible by measuring differences between the reflected waves (reflection strength) (Paniagua et al., 2004).

Fortuny-guasch (2002) mentioned that there are some difficulties associated with the limitations of GPR such as, multiple internal reflections, clutter generated by the air-ground interface, and poor impedance matching at the antenna and a heterogonous velocity distribution in the subsurface. Meanwhile, Daniels (2004) mentioned that the GPR performance can be improved by considering a few factors such as path loss, target

reflectivity, clutter and system dynamic range. He added that the spatial resolution of the radar can be determined by considering the depth and plan resolution separately.

A study by Rogers et al. (2008) considered the signal attenuation when the signal is going through a variety of ground conditions especially in clay soils.

Inagaki & Okiyasu (2008) noted that the depth penetration of GPR signals depends on the type of soil. These authors knew that a GPR pulse penetrates deeper into rocks compared to soils, especially soils with finer particles. In addition, dry sandy soil can potentially attenuate energy when it contains hydrous salt, as they are electrically conductive and will readily dissipate radar energy. It is well known that an increase in conductivity reduces the penetration depth of GPR signals in soils (Sternberg & Levitskaya, 2001)

As soils have a large effect on the strength and velocity of GPR signals, which can vary significantly with frequency as a result of the phenomenon known as electromagnetic dispersion, a full understanding of its electromagnetic properties must be considered central to an understanding of the difficulties inherent in geophysical detecting buried utilities (Rogers et al., 2008).

Studies by Thomas et al. (2006) indicated that the accuracy of geophysical utility location can vary significantly due to soil attenuation of electromagnetic waves, with the contrast between soil and utilities determining the strength of reflection.

Daniels (2004) in his study found that the performance of GPR is dependent upon the electrical conductivity of soils. This author stated that soils having high electrical conductivity rapidly attenuate the radar energy, restrict penetration depths, and severely limit the effectiveness of GPR. In addition, Doolittle & Collins (1998) in their research

noted that depending on antenna frequency and the chemistry of the soil materials, penetration could range from 5 to 30 metres in sandy soil, 1 to 5 metres in loamy (7 to 35% clay) soils, to less than 0.5 metres in clayey (>35% clay) soils. This author clarified that the range of depth penetration depends on the signal passing through the materials and hence the selection of a suitable antenna frequency is very important.

In summary, the key issue affecting GPR performance is the properties of the materials through which the GPR signal must pass, including any objects expected in the ground. If one can understand better these properties prior to using the GPR system and potentially tune the GPR to these properties, then a better performance of the system is likely. These material properties are discussed in more detail in the next section.

2.7 Properties of materials

Generally, the GPR technique is based on the propagation and reflection of electromagnetic energy in the subsurface. In this section, it is necessary to understand those characteristics of the materials which affect both the velocity of propagation and attenuation. The basic dielectric characteristics of various materials are shown in Table 2.2. The velocity of propagation is related to the relative permittivity of a material, which depends primarily upon its water content. At low microwave frequencies (most in GPR), water has a relative permittivity (ϵ_r) of ≈ 80 , while in dry condition of the solid constituents of most soils and man-made materials the relative permittivity is in the range 2 to 9. Meanwhile, materials containing appreciable amounts of moisture will behave as

conducting dielectric, especially if the water contains ions. Mostly, water has some degree of ionic conduction (Daniels, 2004).

Table 2.2: Typical range of dielectric characteristics of various materials measured at 100 MHz (Daniels, 2004).

Materials	Conductivity, Sm^{-1}	Relative permittivity(ϵ_r)
Air	0	1
Clay dry	$10^{-1}:10^{-0}$	2-6
Clay wet	$10^{-1}:10^{-0}$	5-40
Concrete dry	$10^{-3}:10^{-2}$	4-10
Concrete wet	$10^{-2}:10^{-1}$	10-20
Freshwater	$10^{-6}:10^{-2}$	81
Freshwater ice	$10^{-4}:10^{-3}$	4
Sand dry	$10^{-7}:10^{-3}$	2-6
Sand wet	$10^{-3}:10^{-2}$	10-30

The (frequency dependent) properties that play a role in the behaviour of the electromagnetic energy in a medium are the dielectric permittivity (ϵ), the electrical conductivity (σ) and the magnetic permeability (μ) (Hippel, 1954).

Each subsurface material is described by a complex permittivity, conductivity and magnetic permeability spectrum and, although the effect of the permeability is often negligible, it must be included when iron-oxide rich materials are present (Daniels, 2004).

Meanwhile Neal (2004) mentioned that the material properties that control the behavior of electromagnetic energy in a medium are dielectric permittivity (ϵ), electrical conductivity (σ) and magnetic permeability (μ). When an alternating electric field is applied to a material, those electric charges that are bound, and, therefore, unable to move freely, still respond to the applied field by undergoing a small amount of displacement. When the resulting internal electric field balances the external electric field, the charges stop moving (Olheoft, 1998). This charge separation in distance is called polarisation and can be of various types (Power, 1997): circular orbits of electrons become elliptical (electronic polarisation), charged molecules undergo slight distortion (molecular polarisation), neutrally charged dipole molecules rotate into alignment with the applied field (orientation polarisation), and ions accumulate at interfaces (interfacial polarisation). Polarisation processes store electric field energy, the amount stored during each cycle of the alternating electric field determines the real dielectric permittivity at that frequency (Power, 1997). In addition, a small amount of energy is lost as heat due to resistance to the transportation of charge resulting from the polarisation processes. The amount of energy dissipated determines the imaginary component of the dielectric permittivity at that frequency

(Power, 1997). The real and imaginary dielectric permittivities are often quoted relative to the dielectric permittivity of free space (i.e. a region where there is no matter and no electromagnetic or gravitational fields). Dielectric permittivity is measured in units of electrical capacitance (farads) per metre, and represents a measure of the material's ability to store electrical charge (Neal, 2004). The permittivity spectrum is described by a superposition of individual electric field and electric flux density relaxation times combined with a static permittivity (Daniels, 2004).

2.7.1 Dielectric permittivity (ϵ)

Dielectric permittivity describes the ability of a material to store and release EM energy in the form of electric charge and classically relates to the storage ability of capacitors. Alternatively, it can be described as the ability to restrict the flow of free charges or the degree of polarisation (in F/m) exhibited by the material under the influence of an applied electric field. It is usually quoted in terms of a non-dimensional, relative permittivity term (ϵ_r) where

$$\epsilon_r = \text{permittivity of the material } (\epsilon) / \text{permittivity of free space or vacuum } (\epsilon_0)$$

(Equation 2.3)

The permittivity of free space (or permittivity constant) is given as 8.8542×10^{-12} F/m and differs negligibly from the permittivity of air (Jol, 2009). Dielectric constant can be considered as relative permittivity.

Dielectric permittivity is in part dependent upon the frequency of the applied, alternating electric field (Power, 1997; Olheoft, 1998). At low frequencies, charges move the full distance required to balance the applied field, but only spend a fraction of the time moving and the rest waiting for the field to reverse (Olheoft, 1998). This results in maximum energy storage and minimum energy loss. At high frequency, polarity reversals occur much more quickly and charge movement may not be complete before the field reverses. This results in charge storage proportional to the distance moved and a proportionally small energy loss through dissipation (Olheoft, 1998). At a certain intermediate frequency, a charge will move the full distance required to balance the external in the same time as one cycle of that field. This will produce maximum energy loss and energy storage that is an average of the high and low frequency limits (Power, 1997; Olheoft, 1998). Clearly, each polarisation process will vary in its ability to respond to the applied electric field and the net effect will be very much dependent upon the medium involved. In porous media, grain edges or pores walls may also limit electrical charge motions (Olheoft, 1998). Freshwater has a high ϵ in comparison to air and typical rock-forming minerals (Olheoft, 1981). Freshwater content exerts a primary control over dielectric properties of common geologic materials (Topp et al., 1980; Davis & Annan, 1989).

With respect to water, maximum energy losses occur around 10-20 GHz (GHz= 10^9 Hz), and are caused by relaxation (dissipation) processes associated with the dipolar nature of the water molecule (Power, 1997). This effectively limits the upper frequency range for the GPR systems. At low frequencies, a significant relaxation frequency often associated with rocks and sediments, and of unknown origin, is around 10 MHz (Power, 1997).

2.7.2 Electrical conductivity (σ)

The complex conductivity is described by a static conductivity component and a conductivity relaxation time. These parameters can be obtained either by the dielectric testing of sub-surface materials or from theoretical/ empirical models developed by Cole and Debye as mentioned in Daniel (2004).

Conductivity is a measure of the ability to transport charge on application of a static electric field. These charge motions are in addition to those associated with the polarisation phenomena and occur throughout each half cycle of an alternating electric field, irrespective of its frequency. With respect to GPR, the most important conduction-based energy losses occur due to ionic charge transport in water and electrochemical processes associated with cation exchange on clay minerals (Olheoft, 1998). For low-loss materials, such as clean sand and gravel, the influence of σ over the GPR frequency range is minimal and it is assumed ≈ 0 (Davis & Annan, 1989; Reynolds, 1997).

Due to the nature of ϵ and σ , as the frequency of an applied field changes the energy dissipated through charge transport and the energy stored in charge displacements also changes. Hence, conduction losses can also be frequency dependent. For typical earth materials, below a transition frequency 10-300 MHz, energy losses due to σ greatly exceed energy stored by polarisation processes and the propagation will be dispersive. This limits low frequency applications of GPR. Above the transition frequency, energy losses due to conduction are approximately independent of frequency. High frequency propagation is

instead limited by scattering losses, which become particularly important when the wavelengths approach the size of the particles (Power, 1997). Scattering is also influenced by electromagnetic contrast between object and host, object shape, object orientation relative to electromagnetic field polarisation vectors, and antennae geometry (Olheoft, 1998). Most GPR systems are designed to perform within a frequency range of 50 MHz- 1 GHz.

2.7.3 Magnetic permeability (μ)

Magnetic permeability is essentially the magnetic equivalent of dielectric permittivity and is a measure of the magnetic field energy stored and lost through induced magnetisation (Power, 1997). Magnetic permeability can, like dielectric permittivity, be divided into its real and imaginary parts and is often expressed relative to the magnetic permeability of free space. Magnetic permeability is measured in inductance (henrys, H) per metre. All substances respond to an applied magnetic field and various types of magnetic behavior exist (Walden et al., 1999). In naturally occurring materials, the strongest magnetic response is usually seen in ferromagnetic oxides or sulphides, particularly iron and iron-titanium oxides. Laboratory experiments of GPR frequencies have identified important magnetic relaxation losses associated with both natural and artificial iron-rich sands. However, the majority of natural magnetic minerals have never undergone measurement (Olheoft, 1998).

Studies by Van Dam & Schlager (2000) mentioned that there was an impact of iron oxides on GPR waves and layers rich in iron oxide were identified as possible GPR reflectors. They used time domain reflectometry (TDR) and sedimentological analyses to show in a qualitative way that iron oxides significantly lower the electromagnetic wave velocity of sediments.

Meanwhile Daniels (2004) stated that each sub-surface material is described by a complex permittivity, conductivity and magnetic permeability spectrum and, although the effect of the permeability is often negligible, it must be included when iron-oxide rich materials are present.

In summary, this section has shown that the soil properties such as dielectric permittivity, conductivity and magnetic permeability are very important in order to measure the strength of the signal coming back to the GPR unit. These soil properties will affect the signal signature of the radar as discussed in the next section.

2.8 Ground Penetrating Radar signal signature

GPR has been used extensively to determine the depth to soil horizons and as a quality control tool for soil mapping and investigation. The application of GPR has been extended to Civil Engineering work such as in rebar and tension cable detection, slab thickness, voids detection and underneath pipelines detection. For pipeline detection, orthogonal scanning has been used to determine the depth and direction of pipelines. In order to

determine pipeline direction, at least two scans are needed (Paniagua et al., 2004). Generally, a regular hyperbola shows up on the scan when orthogonally crossing above the pipeline axis. The wave amplitude of the radar signal is a maximum whenever the antenna is crossing above the pipeline axis orthogonally. However, when the antenna passing parallel above the pipeline axis, the hyperbola (reflection signature) has a totally different shape, which is no longer hyperbolic. In an extreme case, when the antenna trajectory is along the pipeline axis, the hyperbola is distorted into a straight line (Paniagua et al., 2004).

The shape of the hyperbola and the type of peaks (maximum or minimum) depends on the material of the utility (Paniagua et al., 2004). By analyzing the above data, it is possible to define the type and material of the utility. Figure 2.6 shows hyperbolas with various characteristics. By analysing the shape of the hyperbola, it is possible to identify the type of the object: cable or pipe. A study by Paniagua et al., (2004) found that the light segments of the hyperbola indicate positive peaks, while dark parts indicate negative peaks. If the positive peaks are the highest, it indicates a cable or a pipe filled with a liquid. The highest negative peaks indicate empty pipes. Figure 2.6A shows the reflection from an electrical cable, about 35mm in diameter. Figure 2.6B shows the reflection from a filled metal pipe, whose diameter is 100 mm. Figure 2.6C shows the reflection from an empty concrete pipe, diameter 150 mm. Figure 2.6D and Figure 2.6E show the comparative view of an empty metal pipe and an empty PVC pipe with an optic cable. Both pipes have a diameter of 110 mm.

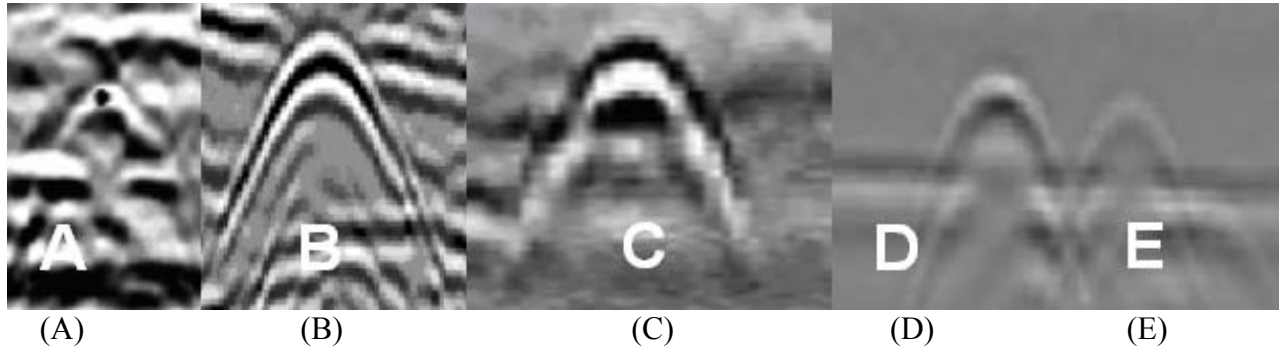


Figure 2.6: Type and material detection of utilities (Paniagua et al., 2004)

It can be seen, that the electric cables (Figure 2.6A) differ from empty PVC pipe the most, and also that it can be difficult to differentiate reflections of concrete and PVC pipes (Figure 2.6). It is also shown, that metal utilities have better reflections than those made of non-metallic (concrete, PVC) (Paniagua et al., 2004). This difference is caused by various reflective capabilities of metals and non-metals. Metals reflect most of the EM waves, while PVC is transparent to EM waves. A study by Paniagua et al. (2004) found that GPR is able to detect metal cables in PVC cladding. Figure 2.7 shows a processed scan of an optic cable in PVC cladding with a diameter of 110mm.

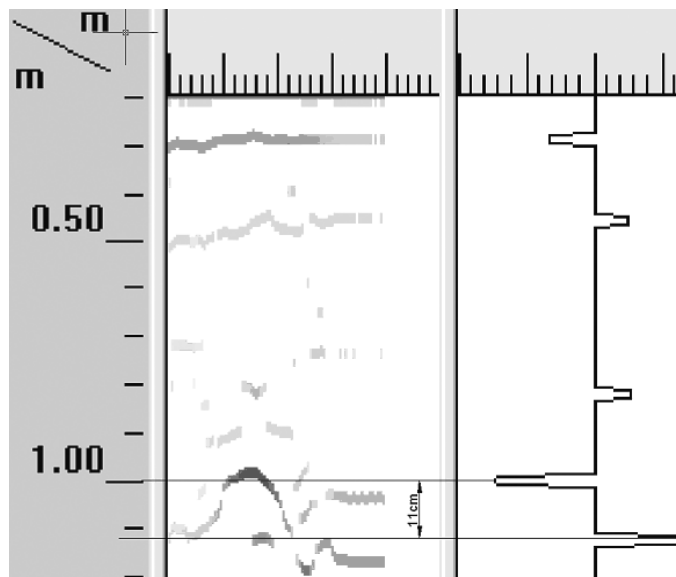


Figure 2.7: Optical cable in a PVC pipe with diameter of 110mm (Paniagua et al., 2004)

As a result of their study, Figure 2.7 shows a radar scan with marked positive and negative peaks. The negative peak shows the depth of the PVC pipe ($h=1.00$ m), while the positive peak shows the depth of the optic cable ($h=1.12$ m). PVC pipes have standard diameters, so it is possible to determine their diameters indirectly.

Another study by Dusan & Aleksandar (2007) indicated that if the antenna moves along the pipeline axis – the longitudinal scan transforms the hyperbola into a straight line. They also stated that the metal objects have weak reflections caused by the minimal radar cross-section of the longitudinal scans. Empty non-metal pipes (concrete, PVC, ceramics) have opposite polarisation, which cause negative peaks and good quality of longitudinal scans. Figure 2.8 shows the longitudinal scan of a PVC pipe with a length of 12 metres (diameter 200 mm) taken in Novi Sad. It also illustrates the parameters which can be estimated: pipe, for examples inclination, length, junctions, and reductions.

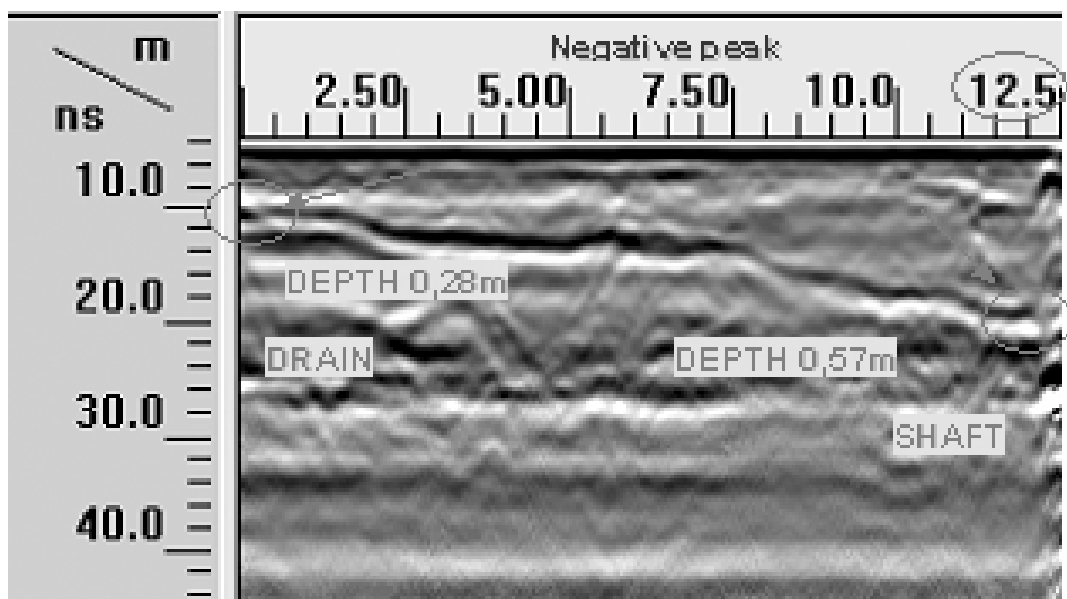


Figure 2.8: Scan along PVC pipe (Dusan & Aleksandar, 2007)

In terms of GPR images, Neto & Medeiros (2006) has mentioned that the quality of images is then strongly dependent on the adequate correction of the attenuation effects. However, studies by Chen (2011) found that the GPR images are often contaminated with noise and it is impossible to ensure the processed GPR data are free from noise.

In summary, this section has shown that different materials, orientation to the buried object and 'noise' effects all contribute to the quality of the signature signal obtained from GPR surveys. These are all issues that complicate the interpretation of GPR scans and need to be considered in any condition assessment analysis.

2.9 Condition assessment of utilities

In the UK, many utilities have been installed a few hundred years ago as an essential role in sustaining urban life. Since then, a majority of existing underground infrastructure systems or buried utility services have become degraded, thus have been replaced. The pipes degradation has been caused by many factors. Basically, the problem of buried pipe deterioration includes pipes cracking, vertical and horizontal deflection, missing bricks, root intrusion, sagging, open joints and deteriorated mortar (Koo & Ariaratnam, 2006). Meanwhile Sinha & Knight (2004) in their study mentioned that the sewer condition is rated based on general defect criteria including crack patterns (transverse, longitudinal, major or minor), joint conditions (minor, major, or multiple), lateral conditions (minor, major, or multiple), and structural defects (sagging, collapsing, or crushed) as shown in Figure 2.9-2.14. Meanwhile, a study by Silva et al. (2002) mentioned that the common causes of pipe deterioration involve temperature, external load, aeration, soil characteristics, groundwater, movement, pressure, minor joint defects, and cracks and fractures.



Figure 2.9: Broken metal pipe with 160mm diameter



Figure 2.10: 10mm hole in metal pipe with 180 mm diameter



Figure 2.11: Metal bent pipe with 60mm diameter



Figure 2.12: Multiple cracked pipe at the joint (www.rdg.com.my)



Figure 2.13: Cements longitudinal crack with 2000mm diameter (www.rdg.com.my)



Figure 2.14: Metal corroded pipes

Normally, pipes are designed as either rigid or flexible pipes. The study by Sinha & Knight (2004) found that buried pipe structural behaviour will depend on the soil surrounding the

pipe and the type of pipe material (rigid or flexible). Pipes are considered to be rigid when they have sufficient inherent strength to resist vertical applied loads. Thus, rigid pipes will not deflect much due to changes in the soil pressure distribution surrounding the pipe. Common rigid pipes are reinforced concrete, asbestos cement, gray cast iron, and vitrified clay (Sinha & Knight, 2004). In contrast to rigid pipes, flexible pipes have little inherent stiffness. Thus, their ability to support vertical loads is mostly derived from lateral pipe support (confinement) provided by the surrounding fill. Common flexible pipes include ductile iron, thin shell steel, fibre, PE and PVC (Sinha & Knight, 2004).

Most major problems for buried rigid pipes are caused by surface defects such as holes and cracks (Sinha & Karray, 2002). In addition, the American Society of Civil Engineers (ASCE) (1994) reported that most structural failures are caused by corrosion, soil movement or roots that puncture or grow inside the pipe. Studies by Romanoff, (1964), Makar & Rajani (2000), Makar et al. (2001) found that the deterioration of cast iron (CI) water mains through pitting corrosion and graphitisation has been the subject of many investigations. Meanwhile, buried flexible pipes suffer from dents, cracks, holes and fractures as well.

Several study cases in the United States by the US Environmental Protection Agency (USEPA) (2002) and ASCE (2004) mentioned that the majority of the current underground utility infrastructure was built after World War II with their sewer systems on average more than 40 years old and overall their wastewater system a failing grade of “D”. This means the deterioration of these systems has become a society issue and an enormous financial burden to utility owners in the United States (Koo & Ariaratnam, 2006). A

similar situation occurs in the UK with many of the existing gas and water mains and sewers reaching the end of their lives: NGTransco will replace all of their iron mains in the UK within 30 m of a property within the next 30 years; and Thames Water is to replace more than 1600 km of iron mains in London over the next five years (Costello et al., 2007)

As new installation can be very costly and disruptive, the best course of action is to maintain the present infrastructure in a more effective way to maximize life span and prevent catastrophic failures (Ariaratnam & Guercio, 2006). Underground utilities in particular have been prone to neglect, mainly due to a lack of visibility (Costello et al., 2007). This has led to catastrophic failures occurring in the network resulting in difficult and costly rehabilitation (Gokhale et al., 1997). The accurate evaluation of current underground infrastructure must be done before any crucial decisions including lifecycle, rehabilitation and replacement interval, and appropriate remedial methods can be made (Koo & Ariaratnam, 2006). Unfortunately, traditional technologies and management approaches have been limited by the use of insufficient data in the evaluation of the structural integrity of an aging infrastructure (Ariaratham & Guercio, 2006).

In general, various non-destructive inspection and data collection systems are currently available for condition assessment including closed-circuit television (CCTV), sewer scanning and evaluation technology (SSET), sonar systems, laser scanning systems and GPR to assess the interior and exterior of the pipe (Koo & Ariaratnam, 2006; Costello et al., 2007). However, each of the methods has its limitations, for example CCTV imaging and SSET are only operational above the waterline and cannot detect any abnormalities found behind of the limit of a visual image. Even though the sonar system and laser based

technology can detect corrosion pits, voids and perpendicularly oriented cracks on the pipe's inner wall, in fact it still has limitations (Koo & Ariaratnam, 2006). Laser based technologies are only operational above the waterline, while sonar, although capable of operating in both media, cannot be operated in water air and water simultaneously (Costello et al., 2007). Meanwhile GPR technology has been used primarily for detecting structural defects, such as voids and cavities in pavements (Grote et al., 2005), slabs (Laurens et al., 2005), rebar (He et al., 2009), bridge decks (Wang et al., 2008), and detecting the water leakage from metallic pipeline (Crocco et al., 2009). However, the limitation of this technology is that it requires highly trained and experienced individuals to interpret the results (Guercio, 2002).

In summary, there are many reasons why buried utilities degrade, and due to the age of many of these assets it is important to be able to assess their condition. There are a number of techniques for determining the condition of these assets. However, most of these require access to the inside of the utility. Although GPR has been used for assessing the condition of a number of civil engineering related infrastructures, the assessment of buried infrastructure is currently limited to voids and leaks.

2.10 Summary

This literature review has outlined the important subjects related to GPR, including a brief history of GPR, a view of GPR techniques, a review of the basic concepts of GPR, a review of the GPR's limitations, a review of the properties of materials including related

elements, a review of the GPR signature signal and a review of the pipe condition assessment.

In conclusion, the key findings of the review can be listed as follows;

- Even though much research has been made into various GPR applications (i.e. archaeology, forensic etc.) there is still a lack of knowledge on a use of GPR to assess the condition of buried utilities, with very little literature related to this subject. Therefore a greater understanding is needed with respect to the ability of GPR to assess the condition of buried pipes.
- The GPR systems still have limitations in terms of hardware such as the type of antenna frequency, in order to match it to the types of materials found in the ground, such as metal, plastic or concrete, and the shapes of these materials, such as cylindrical or box, and the size of these materials, such as large, small, thick and thin utilities.
- The GPR systems can be used in a variety of media, including rock, soil, ice, fresh water, pavements and structures. However, this variety of media has different dielectric constants as previously stated in Table 2.2 and hence this needs careful consideration.
- The depth range of the GPR is limited by the electrical conductivity of the ground. For instance, as the conductivity decreases, the penetration depth increases.
- Higher frequencies do not penetrate as far as lower frequencies, but give better resolution.

- The soil properties such as dielectric permittivity, conductivity and magnetic permeability are the parameters that need to be considered for measuring the strength of the signal coming back.
- Deeper penetration is achieved in dry sandy soils or massive dry materials such as granite and limestone. Meanwhile, the opposite is true in wet soils and soils with high electrical conductivity.

Chapter 3

RESEARCH METHODOLOGY

3.1 Introduction

Based on the key findings from the review of the literature in Chapter 2, it was evident that there were some areas, particularly related to using GPR for monitoring the condition of buried infrastructure, where information is lacking. It was therefore proposed to investigate this subject area in this research. Due to the complex nature of the problem it was decided that large scale controlled laboratory tests were the best way to do a preliminary investigation of whether GPR could assess the condition of buried services. Selecting

suitable materials in this experiment is an important part in order to differentiate the signal contrast between undamaged and damaged pipes by using an off-the-shelf GPR. A full-scale test facility was constructed and dry sand was selected as the material to fill in this tank. Dry sand was chosen because it is the best material for GPR to get the greatest penetration (less dispersion) and has characteristics of low-electrical-loss-materials, low relative dielectric constant and low absorption coefficient. Meanwhile the plastic pipe was chosen in order to create simple pipe damage.

This chapter describes the methodology followed to achieve the objectives of the project, and hence the aim, described in Chapter 1. The construction of a suitable GPR test facility in the laboratory to conduct controlled testing was required for the experiments. In these experiments, only a plastic pipe was chosen as the main pipe material. This plastic pipe has been selected because it is an easy material to conduct some tests (hole in pipe and gap). Besides, it has good signal contrast between the selected sand. A series of laboratory experiments were conducted to determine the validity and effectiveness of the GPR technology in assessing the condition of buried utilities with common types of damage to plastic pipes. Several types of damage in the plastic pipe were tested with respect to different GPR antenna frequencies. Three configurations of equipment setting were conducted during these experiments and are explained in Section 3.4.1. The GPR surveys were carried-out in order to obtain signal signatures from damaged and undamaged pipes and compare these. The surveys were organised using a grid pattern across the test facility. Ultimately, the information of all the radar signals were extracted and were further examined and analysed.

3.2 Materials

3.2.1 GPR test facility preparation

There are various material options in order to make a suitable GPR test facility for the experiments, for example wood, plastic or concrete. The most suitable material for GPR test facility is wood because it has less signal reflection and it is practical to construct. Meanwhile the plastic or concrete materials are less preferable because it could give strong signal reflection whenever the signal is hitting the boundary of the test facility. In addition, some other factors needed to be considered during the design of the GPR test facility, such as the minimum size of the GPR test facility, the type(s) of soil and pipes to be used in the testing, as well as health and safety issues.

In this research, a laboratory test facility consisting of a box of dimensions 2.4m (length) x 2.2m (width) x 1.2m (height) was constructed from structural by insulated panel material (SIP). SIP is a composite building material. It is consist of an insulating layer of rigid polymer foam sandwiched between two layers of structural board. The reasons for using SIP included that it had enough strength to support the volume of soil, it was easier to construct the test facility compared to other materials and importantly, it had less signal reflection compare to other potential materials, for example plastic or metal. The size of the box was determined as the minimum required for the GPR unit based on the beam width antenna calculations, so as to avoid signal reflection from the edges or the base of the box and to ensure that the complete shape of the hyperbolic trace from the targets could be captured.

The size of the IDS GPR antenna footprint is 60cm x 37cm (based upon the specification provided by IDS). In this case, the beamwidth of the antenna spreads laterally at 90° (θ in Figure 3.1) and spreads longitudinally at 60°. In these experiments, the depth of the buried pipe was fixed at 0.5m from the soil surface. This depth was chosen as an ideal depth which could minimise those signals that are unrelated to the target (clutter). Clutter can be caused by a breakthrough between the transmit and receive antennas as well as multiple reflections between the antenna and the ground surface (Daniels, 2004). Generally, clutter is more significant at short range times (shallow target) and decreases at longer times (deep target). In theory, in order to get the complete shape of hyperbola from two parallel targets (Figure 3.1), using equation 3.1 the width of the test facility must be at least 4y, i.e. $X=4y$:

$$y = \tan^{-1}\theta (0.5) \quad (3.1)$$

where y and θ are defined on Figure 3.1.

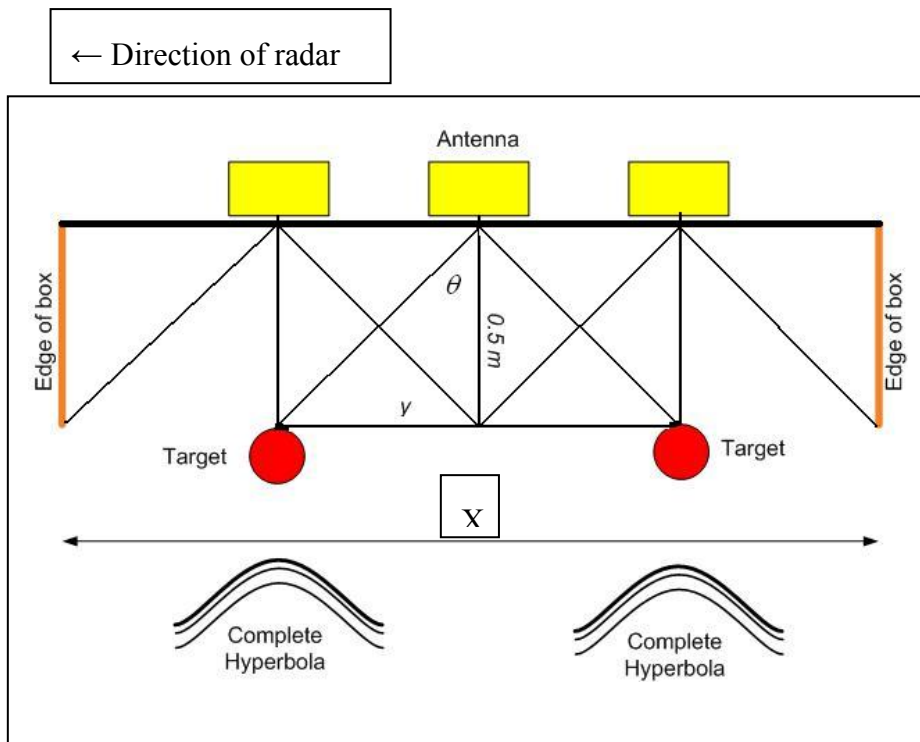


Figure 3.1: Minimum width of test facility

Using simple trigonometry, the dimension X can be estimated as 2m in order to have sufficient clearance from the walls of the box with respect to minimising reflection. The design of the test facility is shown in Figure 3.2 and constructed as shown in Figure 3.3. In order to improve the strength of the test facility and for safety reasons, safety rails were installed around the box.

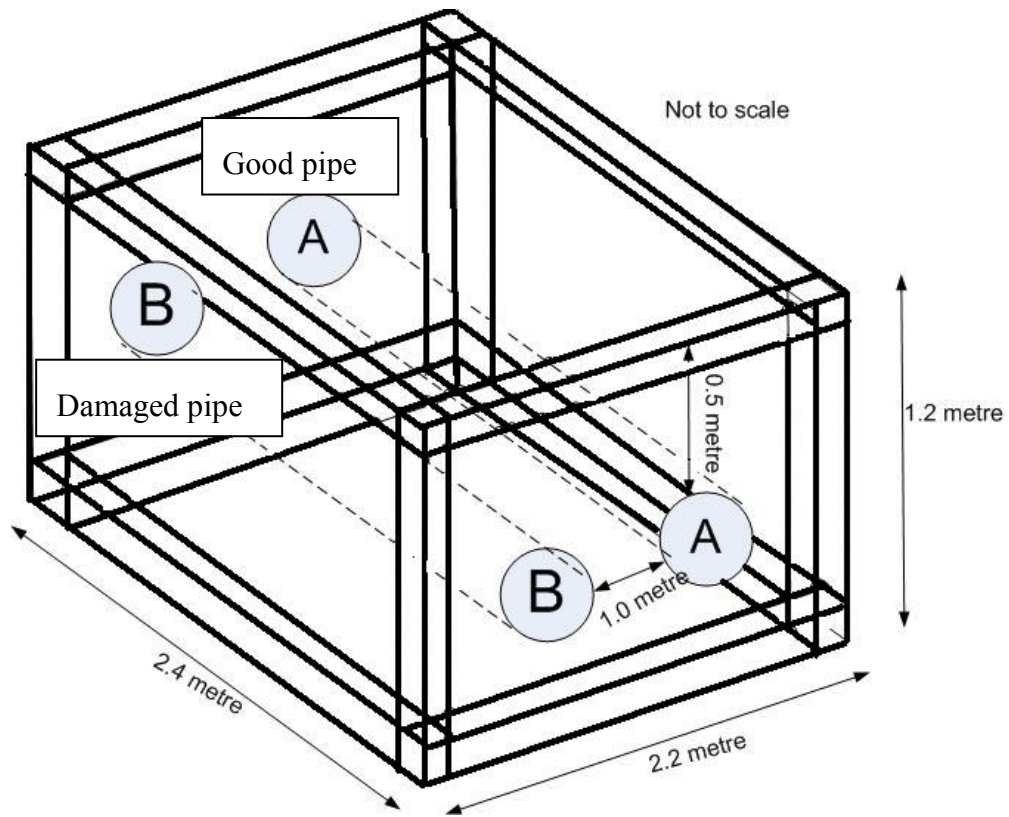


Figure 3.2: A schematic model of the test facility indicating the pipe position



Figure 3.3: Test facility during construction

3.2.2 Fill material for the tank

The GPR technique is based on the propagation and reflection of electromagnetic energy through the ground. In theory, the strength of the electromagnetic waves depends on the medium they are passing through. The GPR signal can travel further in ‘low-electrical-loss’ materials. The speed and effective detection depth of electromagnetic waves are affected by the relative permittivity and absorption coefficient (conductivity) of the media (Reppert et al., 2000). If the electrical conductivity equals zero, the GPR signals would penetrate to a greater depth (Jol, 2009). Therefore, soil characteristics as low-electrical-loss materials, low relative dielectric constant and low absorption coefficient are selected and important for these experiments so as to represent the ‘best’ conditions to observe the pipe condition in these initial tests (if it was not possible to see any differences in the pipes using the GPR under this condition then it would not be worth doing further experiments with more ‘realistic’ soils).

Hence for these experiments, a Leighton Buzzard sand was selected as the soil medium. A sieve analysis was conducted in order to classify the soil particle size distribution. Three measurements were carried out and Figure 3.4 shows the average of the sieve analysis results. The material is classified as a uniform coarse grained sand with particle sizes ranging from 0.6mm to 2.0mm. These sand particles were identified through sieve analyses as low-electrical-loss materials.

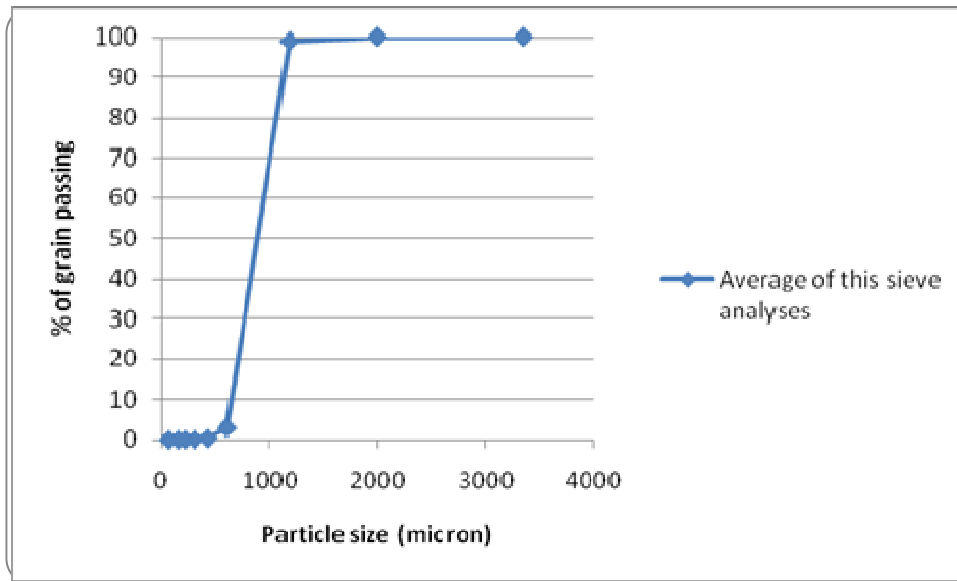


Figure 3.4: Particle size distribution for the Leighton Buzzard Sand

As mentioned, the strength of electromagnetic waves depends on the medium they are passing through and the GPR signal can travel further in ‘low-electrical-loss materials. That means the GPR signal is weaker in wet materials compared with dry materials. Materials containing appreciable amounts of moisture will behave as conducting dielectrics, especially if the water contains ions (Daniels, 2004). The attenuation of GPR signal rises in wet materials. Therefore, a compaction test was carried out to identify the behaviour of the material. Three measurements were taken at each moisture content and Figure 3.5 shows the average results for the compaction test. The optimum moisture content for this sand was determined as 5.9% with an achieved maximum dry density of 1861kg/m³.

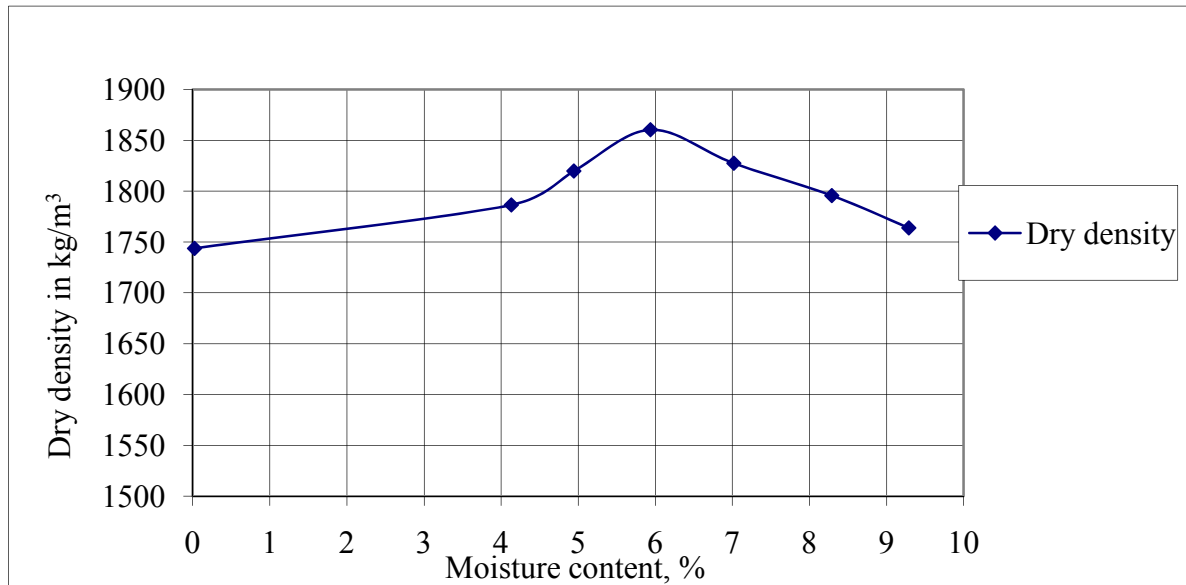


Figure 3.5: The compaction test results for the sand

In these experiments, the optimum moisture content was not chosen for a number of reasons, e.g. reducing signal attenuation as the water content increases, therefore the minimum moisture content was preferred in these tests, and also the difficulty of maintaining the optimum moisture content during the tests (data acquisition). The sand was therefore placed as dry as possible (a small amount of water was needed to keep the dust to a minimum during placement for health and safety reasons). Measurements of soil moisture content were taken at five different positions within the test facility (Figure 3.6) and the average of soil moisture content was 0.02% with a standard deviation (σ) of 0.007.

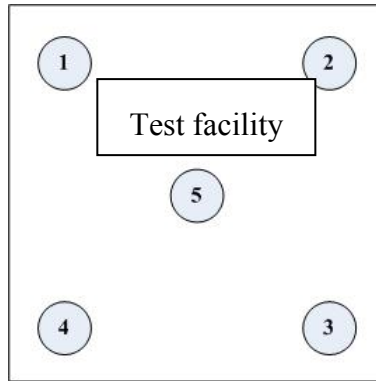


Figure 3.6: Moisture content measurements were taken at five different positions within the test facility

During these experiments, the relative dielectric permittivity and conductivity of the sand was determined using Time Domain Reflectometry (TDR). These properties were identified as identical properties during these experiments as shown in Table 3.1. These data properties are essential to the subsequent data analysis and interpretation.

Table 3.1: Electromagnetic properties and soil moisture content

Relative dielectric permittivity (ϵ_r)	2.72
Conductivity (σ)	0.01Sm^{-1}
Velocity of the signal (V)	180 mm/ns
Average soil moisture content	0.02%

The sand in the test facility was filled by large bags of sand being lifted and emptied using a laboratory crane. However, by doing different tests, the tank had to be emptied after each test and this was done manually with the sand being put into tear-resistant sand bags,

which were subsequently used to fill the test facility. During these experiments, the sand was compacted in layers to provide a uniform material throughout the test facility. The thickness of compaction of each layer was 0.5m. The plate compactor was used for 30 seconds of a vibrating compactor across the surface of each layer. The sand's characteristic is a uniformly sized material and so it was important that the filling and compaction process did not disturb the characteristic of the sand, which it will create another variable during the test. During data acquisition, an uneven surface will affect the radar scan. In order to ensure uniformity across the test bed, a very thin (3mm) plywood sheet was laid on the sand surface. This plywood was useful in order to push and pull the GPR across the surface of the sand during the tests. The gap between the surface and the radar antenna contributes to the 'static correction'. It was practically quite hard to maintain a uniform surface throughout the test facility. However, a simple broom was used to minimise any uneven the top surface of the sand. All the tests were conducted in order to understand the soil characteristics and were very useful for replicating the conditions in each experiment.

3.2.3 Pipes

In these experiments, only a high-density polyethylene (HDPE) pipe was used. This pipe was chosen because it is easier to create simple damage to the pipe and it would give a good signal contrast when buried in dry sand materials and the pipe. The greater the contrast between two materials at a subsurface interface, the stronger the reflected signal, resulting in a higher amplitude reflected wave (Kuo et al., 2005). The tests involved burying a 0.2m diameter plastic pipes in 2.0m long lengths in the test facility (Figure 3.7).

The reason for choosing this pipe size was to increase the level of the return signal and decrease the target scattering loss compared to choosing smaller pipes. Daniels (2004) mentioned that for a small physical dimension of an anomaly it will increase the target scattering loss due to the geometry of the situation and the return signal becomes smaller. Two pipe lengths were buried in the test facility, with one of these pipes being in a ‘good’ state (undamaged) and the other pipe having a defect in it (for example a break or a hole), i.e. damaged. The pipes were buried in pairs at a depth of 0.5m (± 0.02 m). The depth was defined as the distance between the ground surface and the top surface of the pipes. The descriptions of the deteriorated pipes and the experimental parameters investigated are defined in Table 3.2.



Figure 3.7: Arrangement of the two plastic pipes in the test box prior to burial

Table 3.2: Description of the experimental arrangements used in each test

Test number	Description of pipe defect	GPR antenna frequency
1	Broken pipe (i.e. a pipe split into two sections) with a 5cm gap without a plastic cover (i.e. sand was allowed to pass through the gap)	250MHz
		700MHz
2	Broken pipe with a 2cm and a 5cm gap (i.e. the pipe was split into three sections), with the gaps covered with plastic (i.e. sand prevented from passing through the gap by the plastic cover)	250MHz
		700MHz
3	Hole in the pipe with a diameter of 5cm (sand allowed to pass through the hole)	250MHz
		700MHz
4	Hole in the pipe with a diameter of 5cm (sand prevented from passing through the gap by a polystyrene cover)	250MHz
		700MHz
5	Hole in the pipe with a diameter of 5cm (sand prevented from passing through the gap by a fabric cover)	250MHz
		700MHz
6	Broken pipe with a 5cm gap (sand prevented from passing through the gap by a fabric cover)	250MHz
		700MHz
7	Hole in the pipe with a diameter of 5cm (sand prevented from passing through the gap by a polystyrene cover)	250MHz

Test number	Description of pipe defect	GPR antenna frequency
		700MHz

3.3 Details of the GPR equipment used

A Detector Duo GPR unit (manufactured by IDS) with shielded dual frequency antennas of 250 MHz and 700 MHz, which can decrease the effects of background noise, was used for all the experiments (Figure 3.8). This dual frequency GPR in a single unit can reduce the time for each test, as it permitted two frequencies to be investigated simultaneously with just a single scan. It also reduced the possibility of errors.



Figure 3.8: Detector Duo GPR unit with shielded dual frequency antennas

Fourteen tests were conducted as part of this research as previously described in Table 3.2 (seven arrangements at two different frequencies). Details of these tests are provided in Section 3.5. Each test took at least 11 working days to complete including filling the test

facility (3 days), conducting the test (4 days) and emptying the test facility (4 days). These experiments were conducted over a 7 month period. The GPR surveys during each test involved radar sections both perpendicular to the pipe (Figure 3.9) and along the pipe (Figure 3.10). These surveys were conducted by establishing a grid pattern across the test facility. Typically, reference flags were inserted into the ground at uniform intervals along the grid lines. The purpose of this survey grid was to identify, and to evaluate, the effectiveness of the GPR resolution. In practice, the interval spacing of the GPR survey grid should be varied depending on the purpose of the survey required, i.e. larger for location, and smaller for utility assessment. For this research a number of grid spacings were tried and based on the findings, a 0.1m spaced GPR survey grid was found to be appropriate for the current experiments in both the direction of the pipes (Y direction) and perpendicular to the pipes (X direction). This spacing was chosen as an ideal spacing for GPR to enable it to be towed or dragged across the soil surface and avoid overlap or duplicate grid lines due to its size, and also to be appropriate for the type and size of the damaged sections on the buried pipes. Meanwhile the direction of the pipes were chosen in order to capture a uniform GPR image to assist processing and analysing the data at a later time. Figure 3.11 shows the GPR survey grid line arrangement. A survey wheel or odometer was used to record the position of the GPR unit.

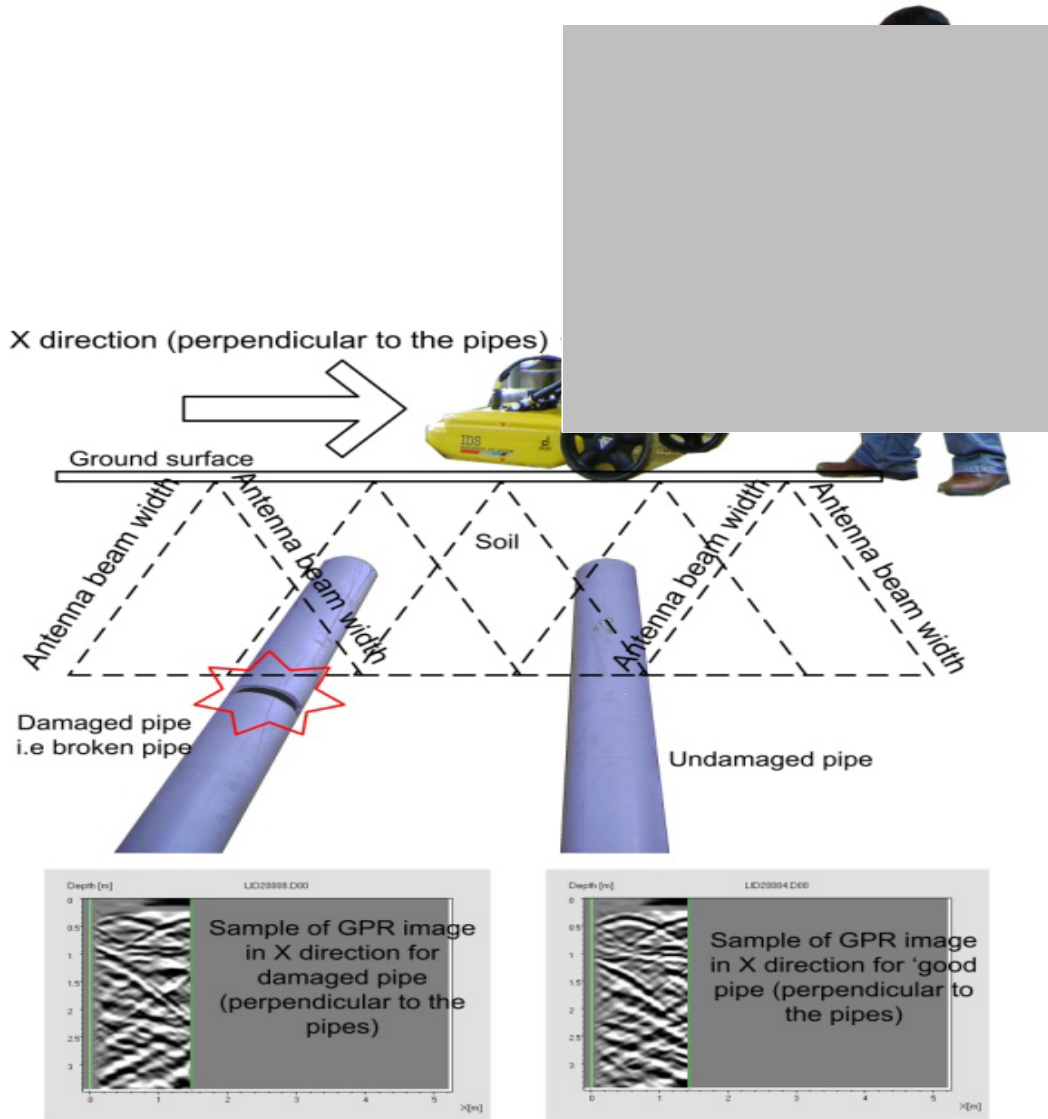


Figure 3.9: Radar section perpendicular to the pipes

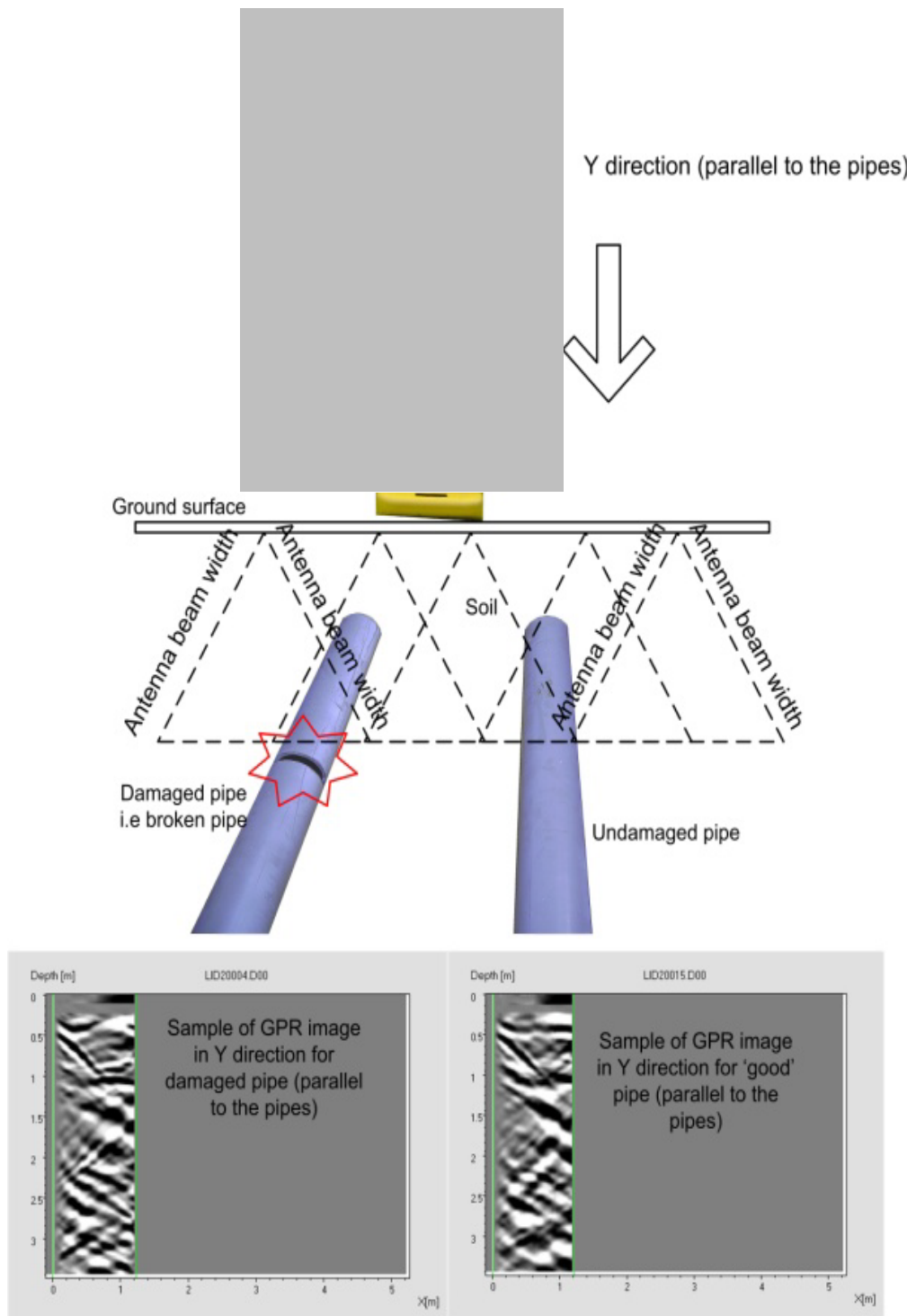


Figure 3.10: Radar section axially along the pipes

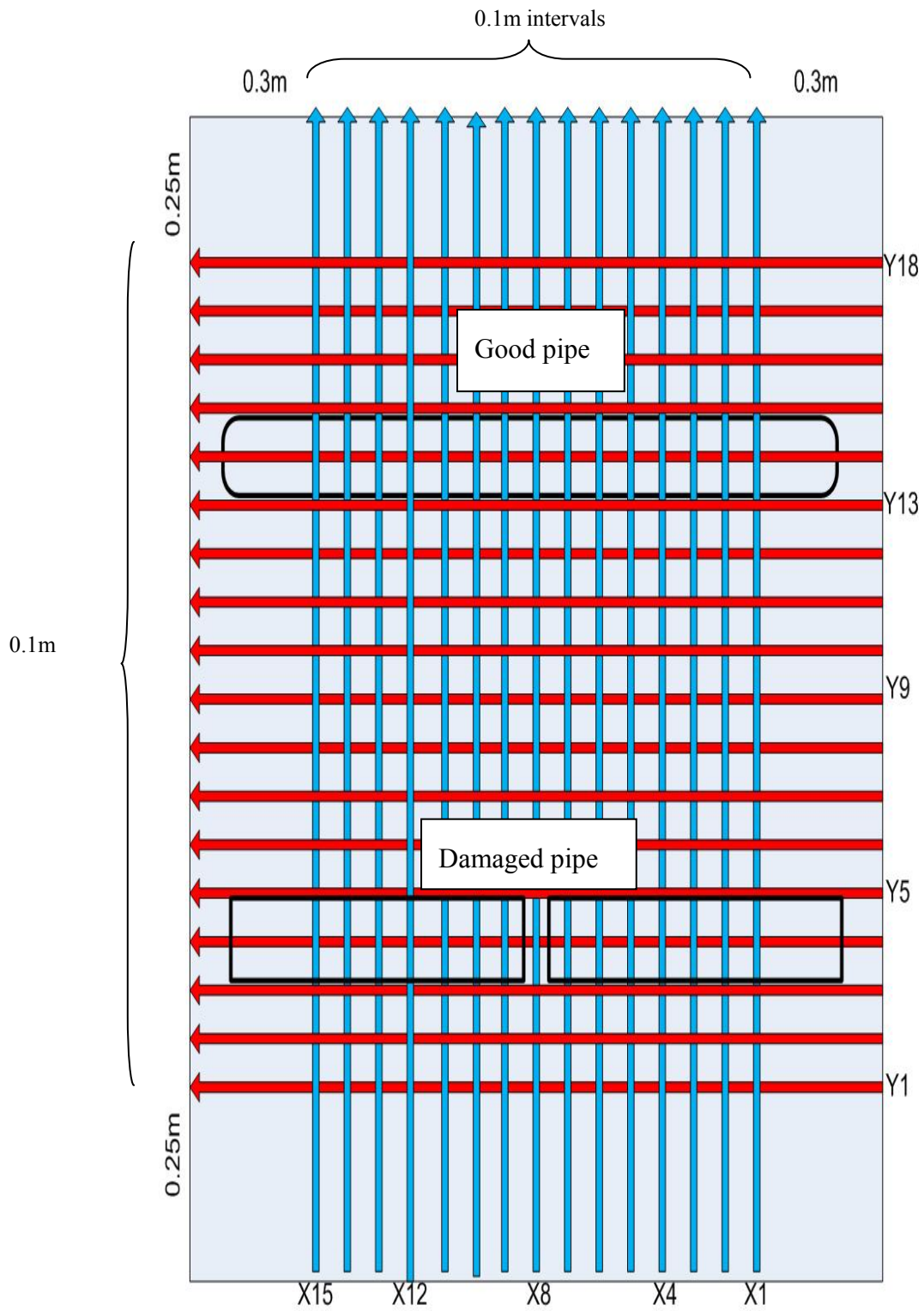


Figure 3.11: Survey grid lines used for each experiment

3.4 Data acquisition and analysis

3.4.1 Data acquisition

During these experiments, the IDS K2-Fastwave software was used to capture the data. This software was developed by I.D.S. IngegneriadeiSistemiS.p.A, Italy and operates on the Windows platform. However, understanding the configuration of the equipment setting (radar settings) is important in order to optimize the data acquisition and also for pre-processing the data. Any changes to the equipment configuration will produce different input to the data acquisition software and may ultimately produce different results. Three configurations were tested and identified as 10 integrations, 5 integrations and 2 integrations during these experiments. A smaller integration number results in a higher resolution of the radar image. This means that the radar images are brighter and sharper compared to a higher integration due to the larger amount of data that can be generated. For example, 10 integrations of 512 samples generate 77 kbyte of data whereas, 2 integrations of 512 samples create 315 kbyte of data. In other words, this configuration is all about how the radar signals are transmitted and captured during the data acquisition. The idea of getting different configurations was to obtain more radar information during the data acquisition based on the matrix array. Each configuration does not involve different ways of data acquisition, but it might change the results that can aid interpretation during the data analysis. Figure 3.12 shows an example GPR data set for the different configurations.

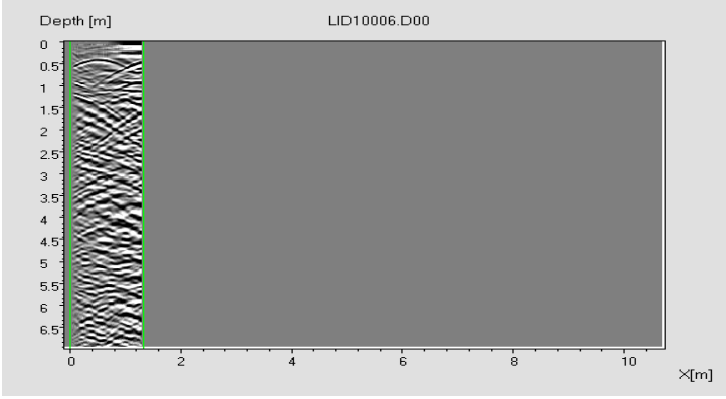
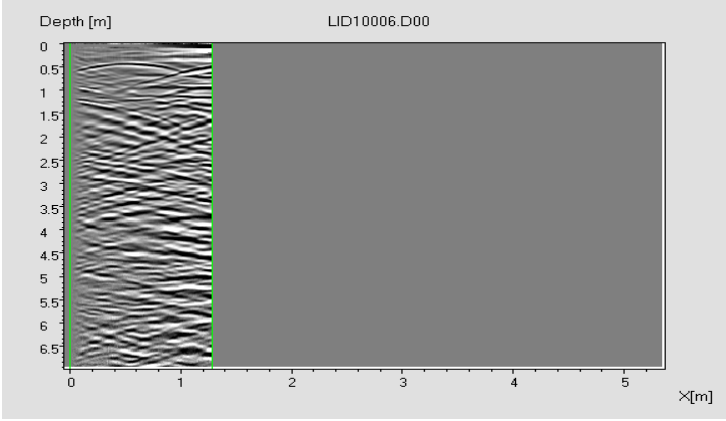
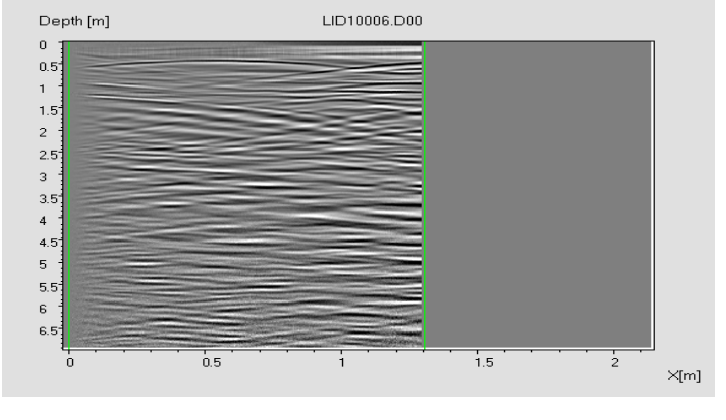
Integrations	GPR sample images
10	
5	
2	

Figure 3.12: Three different configurations of an example GPR image

The integrated dual frequency antenna (250 MHz and 700 MHz) was used to collect the GPR data. As mentioned before, three GPR system configurations were conducted and tested. There were 15 grid lines of 0.1 metre spacing in the X direction (perpendicular to the pipes) and 18 grid lines in the Y direction (axially along the pipes) (Figure 3.10). The GPR survey along each grid line was repeated several times in order to verify the consistency of the GPR data.

3.4.2 Data processing

Generally, it is difficult to interpret subsurface target features from the raw data obtained from GPR systems. This is mainly because of signal attenuation, which reduces the strength of reflected signals, and reflections which can be produced from surface objects. As a result, in order to improve the signal-to-noise ratio, GPR data have to be processed. This should result in a good quality image (after all corrections have been applied) of the raw data so that it can be interpreted and analysed more accurately and precisely.

The main aims of data processing are to eliminate low frequencies from the received signal (called dewow), assign the first break of each trace to a common reference time (known as static corrections), increase the signal-to-noise ratio of a reflected signal (called gain) and increase the visibility of the received signal (known as background removal).

In these studies, all the GPR data captured through the IDS K2-Fastwave software was then processed using the IDS GredBasic software. These data are time domain radar data, which are defined as the time (travel time) and amplitude of the reflected pulses. In

essence, this software is a basic software to process raw GPR data (.dt file), which are acquired during the survey. It has an automatic function to process the raw data allowing visualisation of the radar data. In this experiment, reflected amplitudes and geometry are the primary information used in the GPR data to allow interpretations to be made.

In these experiments, the data analysis was based on the signal contrast between the two types of pipe (damaged and undamaged) by using advanced interpretation (via a Matlab program) to differentiate the signal amplitude between the different pipes using a Mean Square Error (MSE) analysis. The hypothesis is that damage in pipe leads to anomaly in the GPR B-scan when compared to an undamaged pipe. The "error" being quantified is the difference between the damaged and undamaged pipe. The location and of damaged and undamaged pipes are known *a priori*.

The analyses have concentrated on the amplitude changes of a particular area of the GPR data obtained from the undamaged and damaged pipe. An example of the signal contrast between a damaged pipe and an undamaged pipe when the GPR crosses perpendicular to the pipe direction is shown in Figure 3.13.

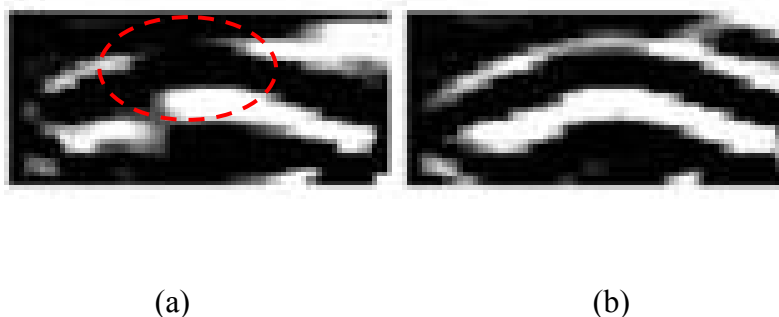


Figure 3.13: Signal contrast between (a) a damaged pipe and (b) an undamaged pipe.

The 0.1m survey grid produces 15 crossing points along the pipe and an example of the data obtained is shown in Figure 3.14.

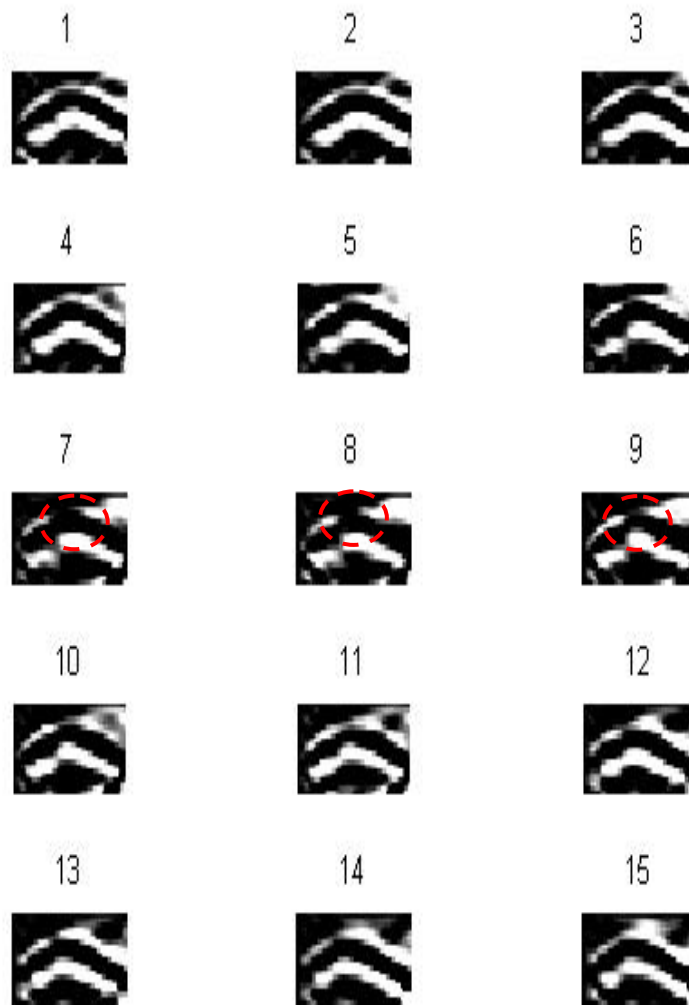


Figure 3.14. 15 radar images relating to 15 crossing points on the survey grid along the damaged pipe (position 8 is where the break in the pipe occurs in this example (Test 1)).

Meanwhile, the 18 radar images for the Y direction are represented in Figure 3.15.

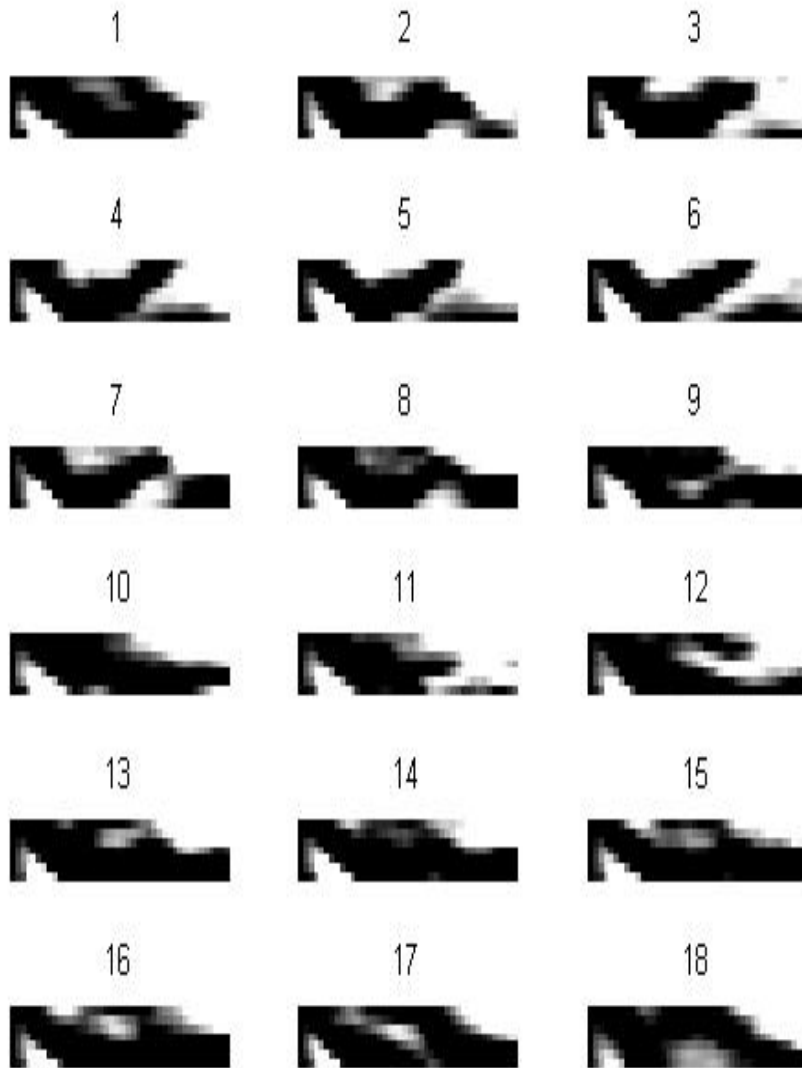


Figure 3.15: 18 radar images relating to 18 crossing points on the survey grid along the damaged pipe (position 14 is where the break in the pipe occurs in this example (Test 1)).

From the analysis of these images using the Mean Square Error (MSE), it is possible to quantify the signal amplitude changes between the undamaged and the damaged pipe section. In this case, grid position 4 is the reference as it contained the undamaged pipe, while grid position 8 has the highest MSE value as compared to the scan at grid 4. This indicates that the scan at position 8 has the largest anomaly. Figure 3.16 shows the results of the analysis, and for the particular example shown in Figure 3.11, it is known *a priori* that point 4 is where the pipe is undamaged and grid point 8 is where the damage occurred on the pipe.

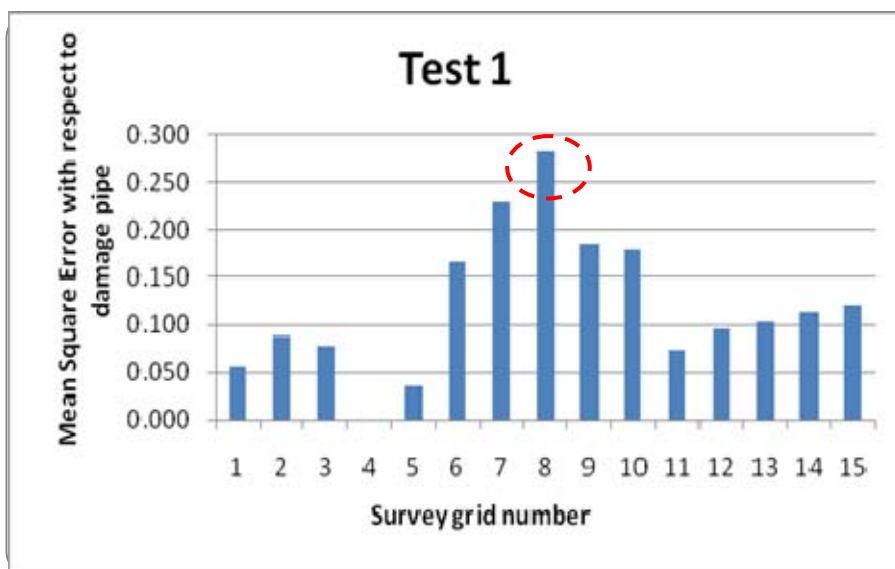


Figure 3.16: Example Mean Square Error (MSE) analysis for a pipe where there is damage in the region of survey grid number 8 (Test 1, frequency 250MHz, as described in Table 3.2) (The red dotted circle indicates that the greatest MSE occurs at grid number 8.)

The test facility wall introduced more clutter into the data. This clutter can be identified by

comparing the results that were obtained for every test. The MSE near to the test facility wall always contributed to the clutter. However, the clutter also always happened because of reflected signals from other sources, e.g. electrical power, cellular phones. As can be seen, survey grid numbers 1,2,3 and 13,14 & 15 are near to the wall. The MSE shows that clutter is coming from test facility wall due to the higher than expected values in these regions.

The high MSE represents the damaged region meanwhile the lowest values represent the undamaged region. The analysis method appeared to show promise and was tested during the experiments conducted as part of this thesis.

3.5 Research methodology diagram

A flow diagram outlining the research methodology is shown in Figure 3.17. General explanations of the materials used, hardware and software development for data analyses have been previously given. Details of each test arrangement are described in the subsequent Section 3.2.3.

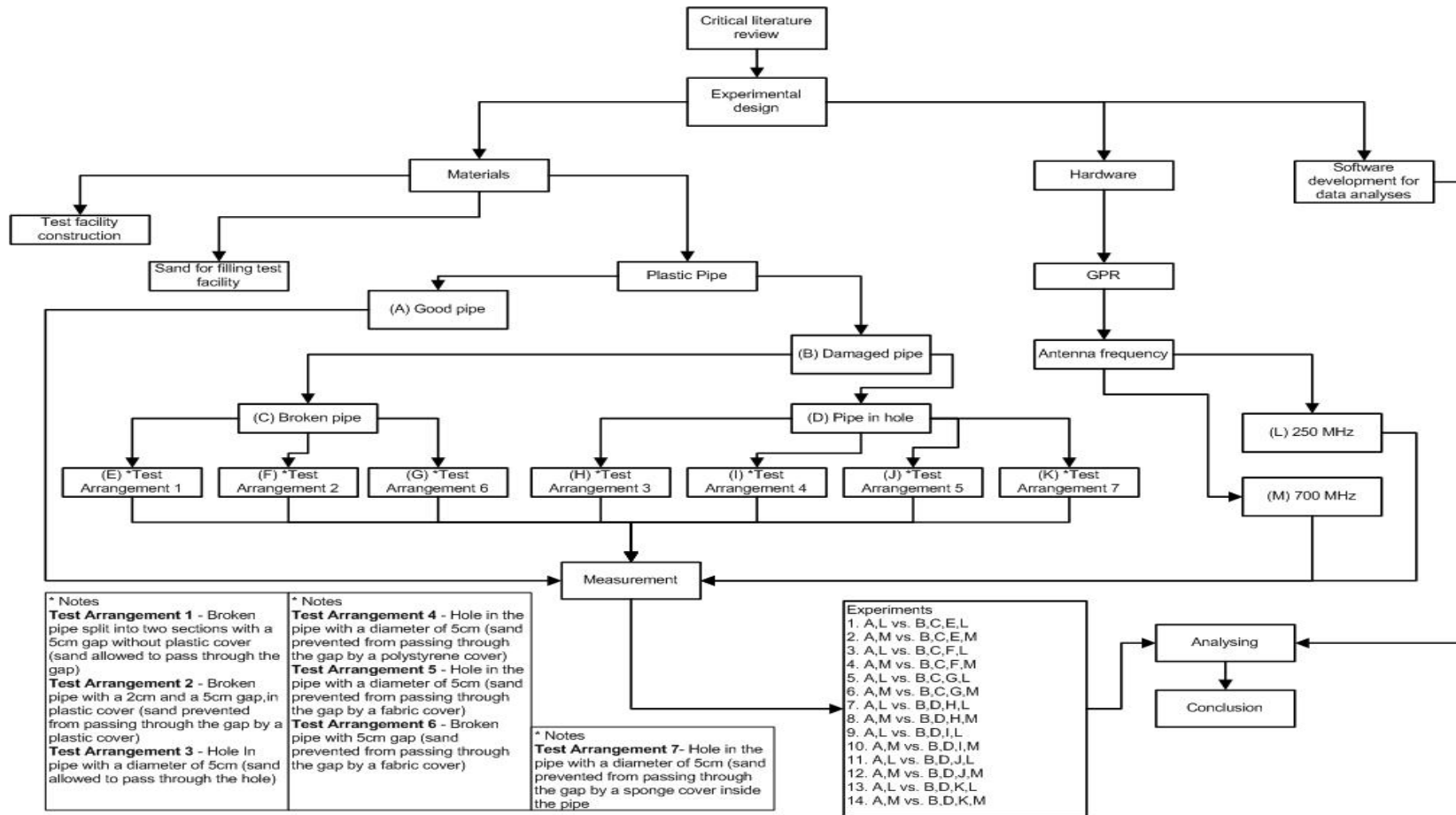


Figure 3.17: Flow diagram outlining the research methodology

3.5.1 Test 1

Test 1 involved burying two parallel 0.2m diameter, 2m long, plastic pipes in the test facility (Figure 3.18). One of these pipes was in a ‘good’ state (undamaged) and the other had a broken pipe with a 5cm gap without any plastic cover. Sand could therefore pass through the gap. The pipes were buried at an approximate depth of 0.5m.



Figure 3.18: Test 1 during filling of the test facility

For all experiments, the integrated dual frequency antenna (250 MHz and 700 MHz) was used to collect the GPR data. Besides, 15 grid lines of 0.1 metre spacing in the X direction (perpendicular to the pipes) and 18 grid line in the Y direction (axially along the pipes) were carried out. However, only on Test 1, three configurations (i.e. the 10 integrations, 5 integrations and 2 integrations) were measured and tested.

3.5.2 Test 2

The tests involved burying 0.2m diameter plastic pipes in 2.0m long lengths in the test facility. One of these pipes was in a 'good' state (undamaged) and the other had broken pipe with a 2cm (Figure 3.19) and a 5cm (Figure 3.20) gap under a plastic cover. Sand was prevented from passing through the gap by a plastic cover. The pipes were buried in pairs at an approximate depth of 0.5m.

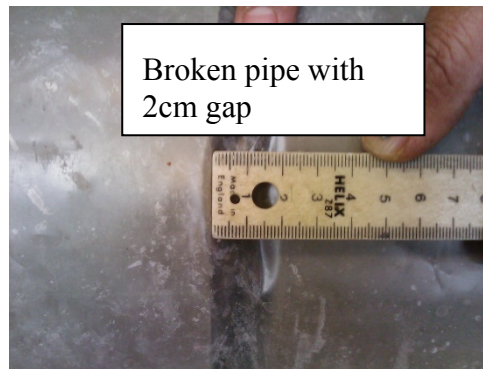


Figure 3.19: Broken pipe with a 2cm gap under a plastic cover

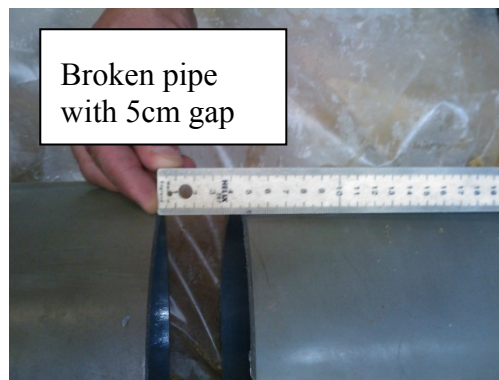


Figure 3.20: Broken pipe with a 5cm gap under a plastic cover

3.5.3 Test 3

The tests involved burying 0.2m diameter plastic pipes in 2.0m long lengths in the test facility. One of these pipes was in a ‘good’ state (undamaged) and the other had a hole in the pipe with a diameter of 5cm (Figure 3.21). Sand was allowed to pass through the hole. The pipes were buried in pairs at an approximate depth of 0.5m.



Figure 3.21: Hole in the pipe with a diameter of 5cm

3.5.4 Test 4

The tests involved burying 0.2m diameter plastic pipes in 2.0m long lengths in the test facility. One of these pipes was in a ‘good’ state (undamaged) and the other had a hole in the pipe with a diameter of 5cm (Figure 3.22). Sand was prevented from passing through the hole by a polystyrene cover. The pipes were buried in pairs at an approximate depth of 0.5m.



Figure 3.22: Hole in pipe with a diameter of 5cm gap in polystyrene cover

3.5.5 Test 5

The tests involved burying 0.2m diameter plastic pipes in 2.0m long lengths in the test facility. One of these pipes was in a ‘good’ state (undamaged) and the other had a hole in the pipe with a diameter of 5cm (Figure 3.23). Sand was prevented from passing through the hole by a fabric cover. The pipes were buried in pairs at an approximate depth of 0.5m.



Figure 3.23: Hole in pipe with a diameter of 5cm gap in fabric cover

3.5.6 Test 6

The tests involved burying 0.2m diameter plastic pipes in 2.0m long lengths in the test facility. One of these pipes was in a 'good' state (undamaged) and the other had broken pipe with a 5cm gap (Figure 3.24). Sand was prevented from passing through the gap by a fabric cover. The pipes were buried in pairs at an approximate depth of 0.5m.



Figure 3.24: Broken pipe with a 5cm gap under a fabric cover

3.5.7 Test 7

The tests involved burying 0.2m diameter plastic pipes in 2.0m long lengths in the test facility. One of these pipes was in a 'good' state (undamaged) and the other had hole in the pipe with a diameter of 5cm. Sand was prevented from passing through the hole by a sponge covering the inside of the pipe (Figure 3.25). The GPR data were taken before and after the sponge was pulled off. The pipes were buried in pairs at an approximate depth of 0.5m.

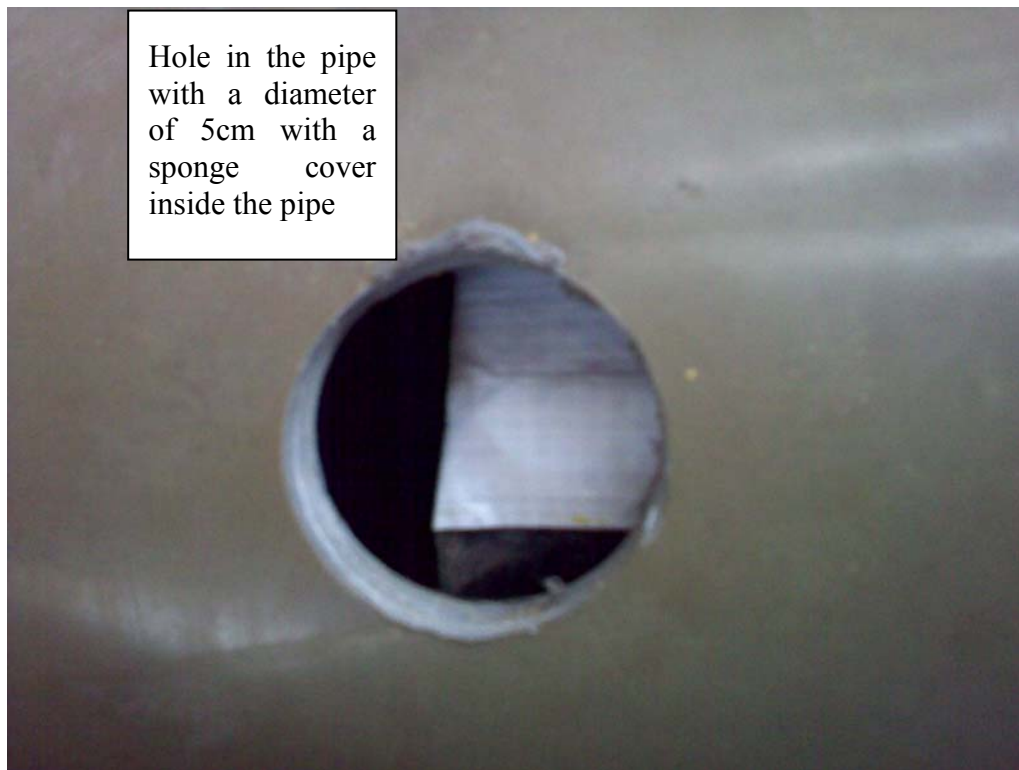


Figure 3.25. Hole in the pipe with a diameter of 5cm with a sponge covering the inside of the pipe

3.6 Summary

This chapter has explained how the experiments were carried out. Many factors have been discussed including the size of test facility, the material of fill, the appropriate size and type of the pipes, the appropriate the grid line spacing and the test parameters for the experiments. The next Chapter will discuss the results of each experiment.

Chapter 4

RESULTS AND DISCUSSION

4.1 Introduction

This chapter presents and discusses the results of the tests carried out. Seven tests were conducted as part of this research (seven tests at two different frequencies as mentioned in Table 3.2). All the signal signatures captured by the GPR were identified and analysed. Commercial (IDS) software was used to capture the data and to process the data. Meanwhile, the data analysis was based on the signal contrast between the two types of pipe (damaged and undamaged). Advanced interpretation (Matlab programming) was used to differentiate the signal amplitude between the different pipes using a Mean Square Error

(MSE) analysis. The analysis focused on the amplitude changes of a particular area of the GPR data obtained from the undamaged and damaged pipe. In order to verify consistency of the data, three sets of GPR data were taken for each test and averaged after the MSE analysis had been done (after confirming that they were similar).

4.2 Test 1

The experimental set up, procedure, and data processing were explained in the Research Methodology Chapter in Sections 3.4 & 3.5. The purpose of Test 1 was to identify the best GPR configurations, to understand whether the GPR is capable of detecting the broken pipe and to identify and quantify the damaged region of broken pipe. In this case, a broken pipe was created with a 5cm gap and the sand was allowed to pass through the gap as shown in Figure 4.1.

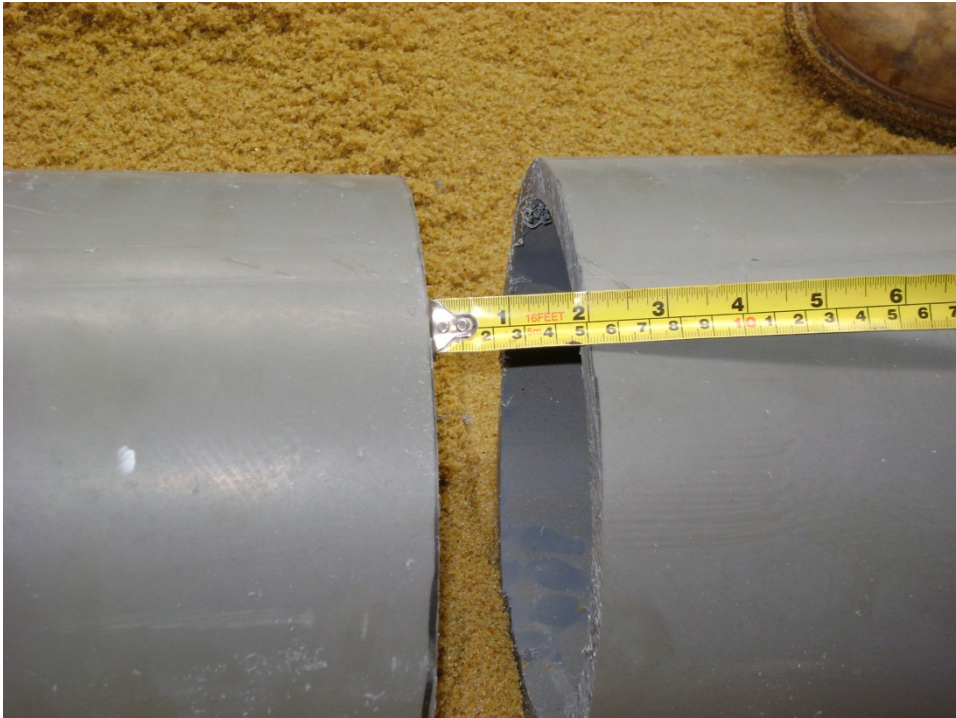
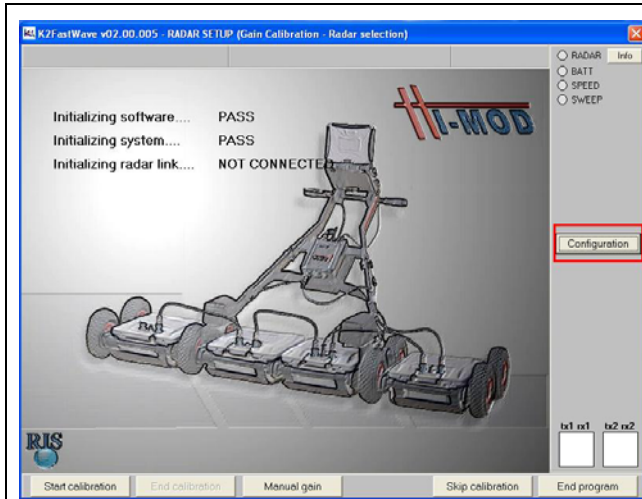


Figure 4.1. Broken pipe split into two sections with a 5cm gap without plastic cover

4.2.1 Identifying the best configuration

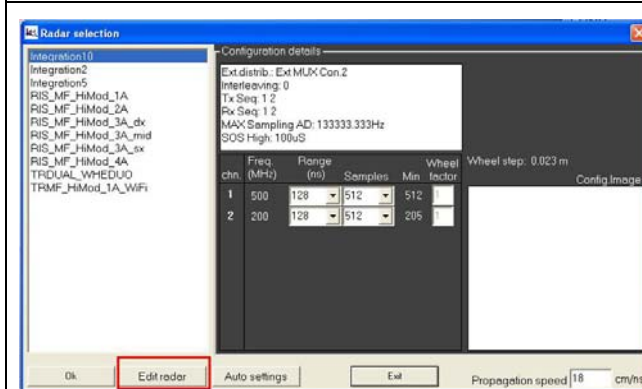
For initial testing, three configurations were tested in order to identify the best configuration for the GPR during data acquisition. The software used for the data acquisition is called IDS K2-FastWave. This configuration was then used for all the experiments. The author believed that any changes of GPR configuration would affect the results thus knowing the configuration and keeping it consistent might help the author during critical data processing. Basically this configuration can be changed from the step below as shown in Figure 4.2(a).



Step 1

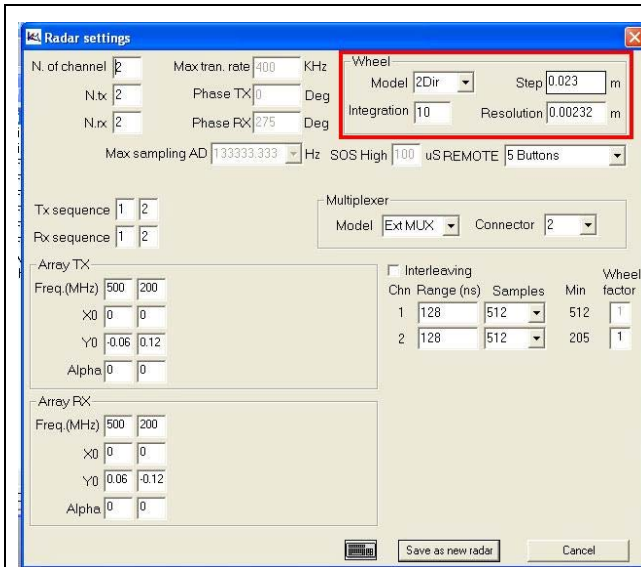
-Run IDS K2-Fastwave program

-Click to Configuration menu



Step 2

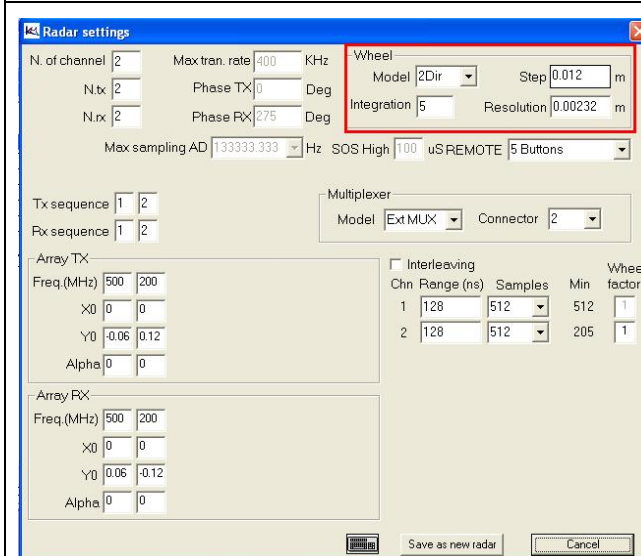
-Click to Edit radar menu



Step 3

-10 integrations is a default configuration for which the Step is 0.023m

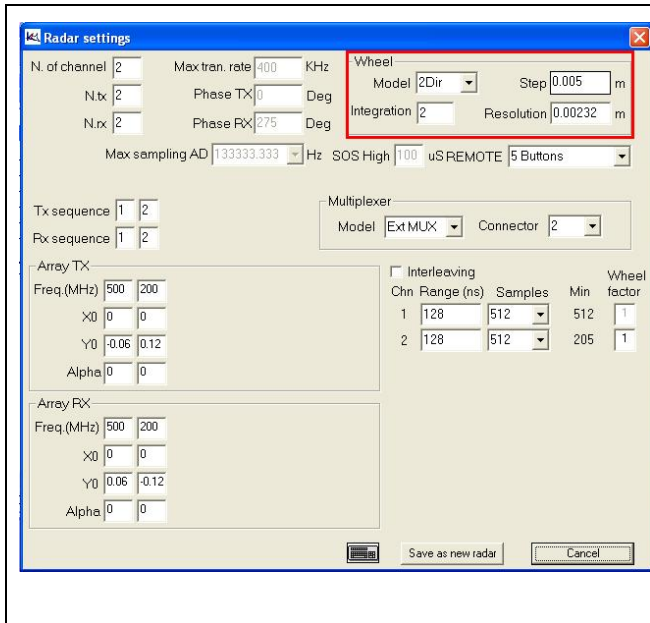
-Then, click to Save as new radar i.e. 10 integrations



Step 4

-Change the integration to a value of 5 and the step will change to 0.012m

-Then, click to Save as new radar i.e. 5 integrations



Step 5

-Change the integration to a value of 2 and the step will change to 0.005m

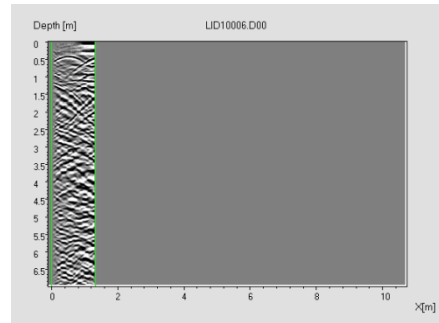
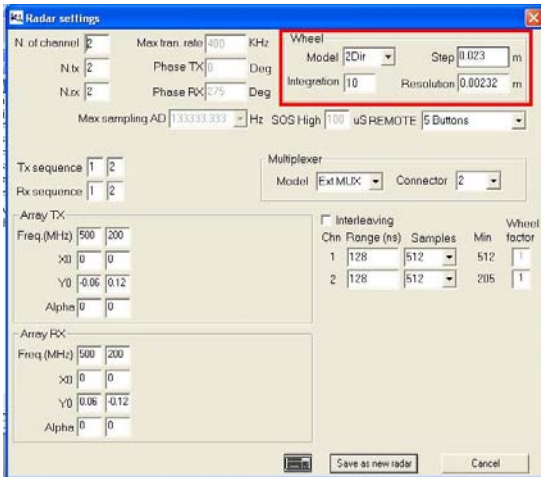
-Then, click to Save as new radar i.e. 2 integrations

Figure 4.2(a): Configuration of radar setting

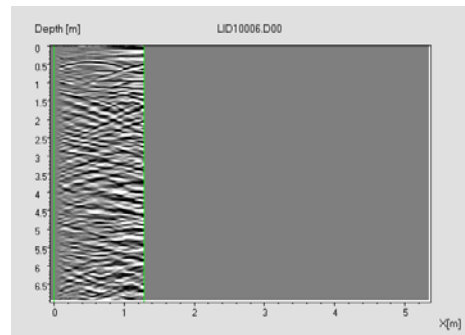
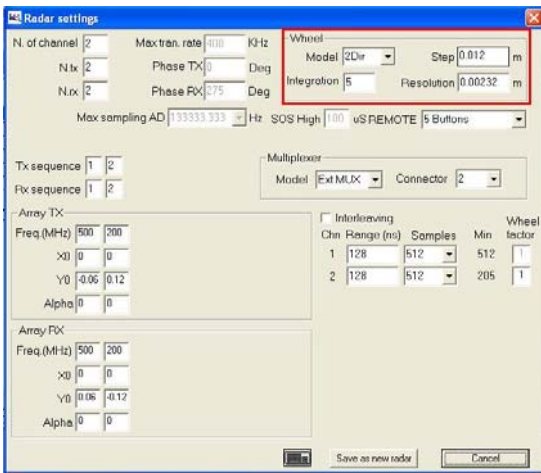
The effect of changing the radar setting is shown in Figure 4.2(b).

Configuration of 10 integrations, 5 integrations and 2 integrations

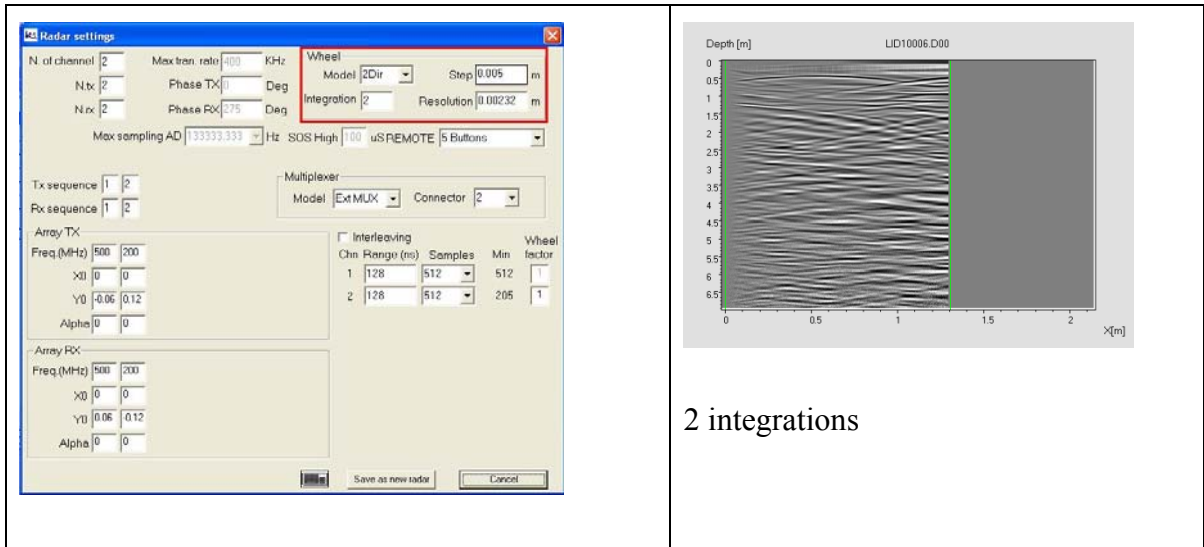
Radar images of different integrations at 700MHz antenna



10 integrations



5 integrations



2 integrations

Figure 4.2(b) Radar images in three configurations

The results in Figure 4.2(b) demonstrated the radar images in the three configurations. These show that a change in the integration is reflected in the value of the Step. For example, for an integrations of 2, the radar transmits the signal every 0.023m. This means the radar will transmit the pulse while the wheels move 0.023m from the starting point then continue to transmit the pulse at a step of every 0.023m. Meanwhile, at an integration of 5 the radar transmitted the signal at every 0.012m. The radar image of an integration of 5 is extended horizontally (i.e. the peaks of the hyperbolae are slightly flattened) compared to '10 integrations'. However, for '2 integrations', the radar image is considered to generate the worst flattening and the hyperbolae in the radar image tend to become one straight line and it is quite hard to identify the hyperbolae.

4.2.2 Identifying the signal signature of damaged and undamaged pipes

Basically, it is difficult to interpret target features because the GPR is affected by the soil conditions, in particular by the soil electrical properties (i.e. permittivity and conductivity). Permittivity is the ability of the soil to transmit electrical signals (in soils this is mainly due to changes in water content). Soil layers with different water content (i.e. different permittivity) can cause multiple reflections and a variation in signal velocity. GPR penetration depth can be reduced to a few centimetres in highly conductive soils. In these experiments, the factors that could reduce the strength of signal had been to be considered. In addition, other signals such as those associated with television, microwaves, and cellular radios will affect the radar scan. However, eliminating all signal attenuation is impossible. In these experiments, two types of antenna have been tested (i.e. 250MHz and 700MHz) with different configurations (i.e. 10 integrations, 5 integrations and 2 integrations). The radar scan results of these experiments perpendicular to the pipes are shown in Figures 4.3-4.8

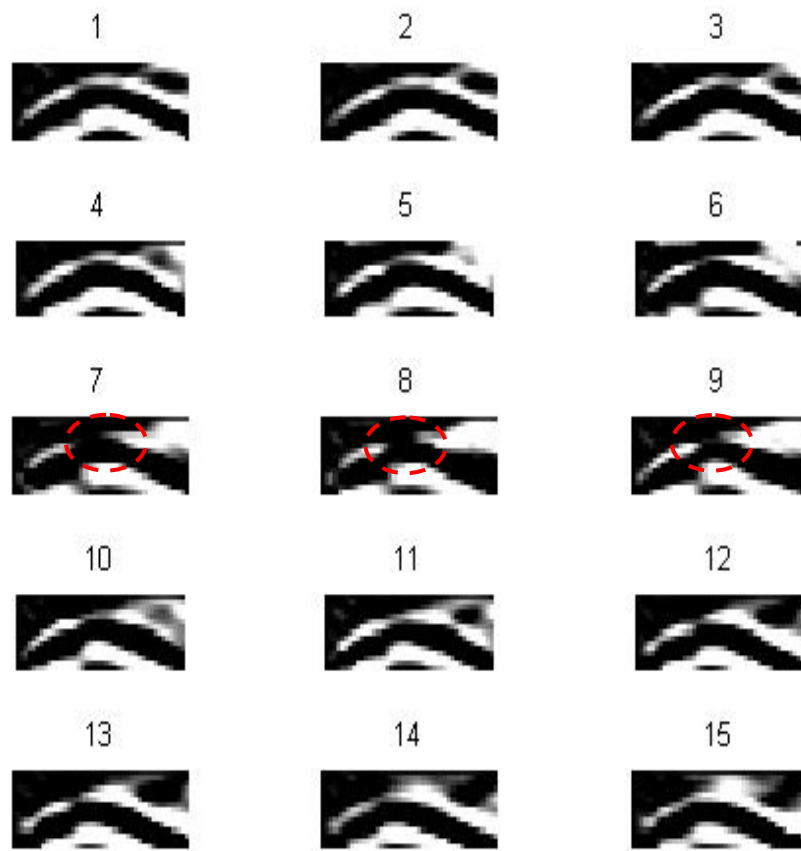


Figure 4.3. Test 1 - 15 radar images (perpendicular to the pipes) using the 250MHz antenna with 10 integrations.(The red dotted circles indicate areas where visual differences are evident in the scans associated with damaged pipe section.)

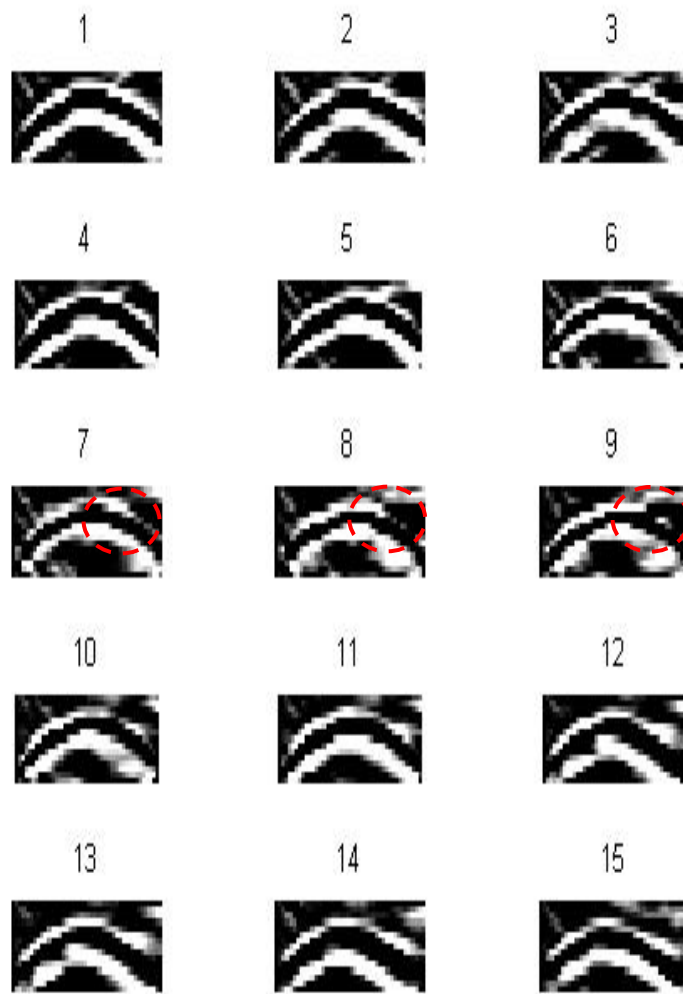


Figure 4.4. Test 1 - 15 radar images (perpendicular to the pipes) using the 700MHz antenna with 10 integrations. (The red dotted circles indicate areas where visual differences are evident in the scans associated with damaged pipe section.)

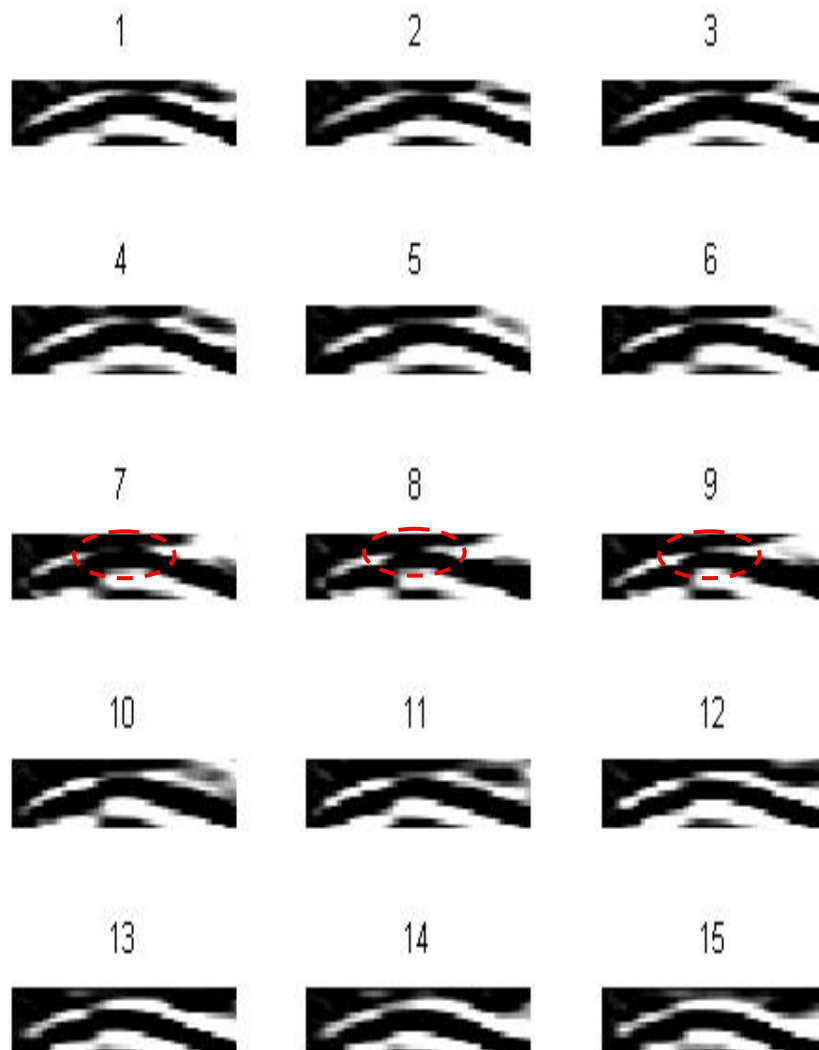


Figure 4.5. Test 1 - 15 radar images (perpendicular to the pipes) using the 250MHz antenna with 5 integrations. (The red dotted circles indicate areas where visual differences are evident in the scans associated with damaged pipe section.)

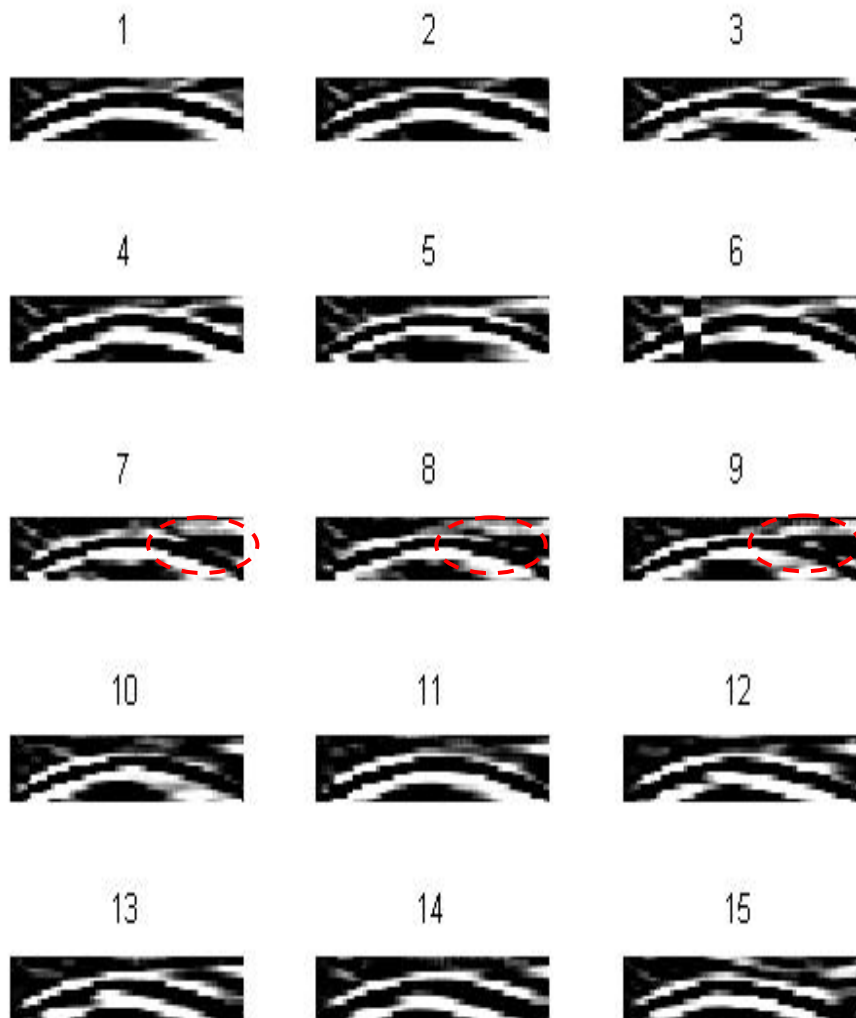


Figure 4.6. Test 1 - 15 radar images (perpendicular to the pipes) using the 700MHz antenna with 5 integrations. (The red dotted circles indicate areas where visual differences are evident in the scans associated with damaged pipe section.)

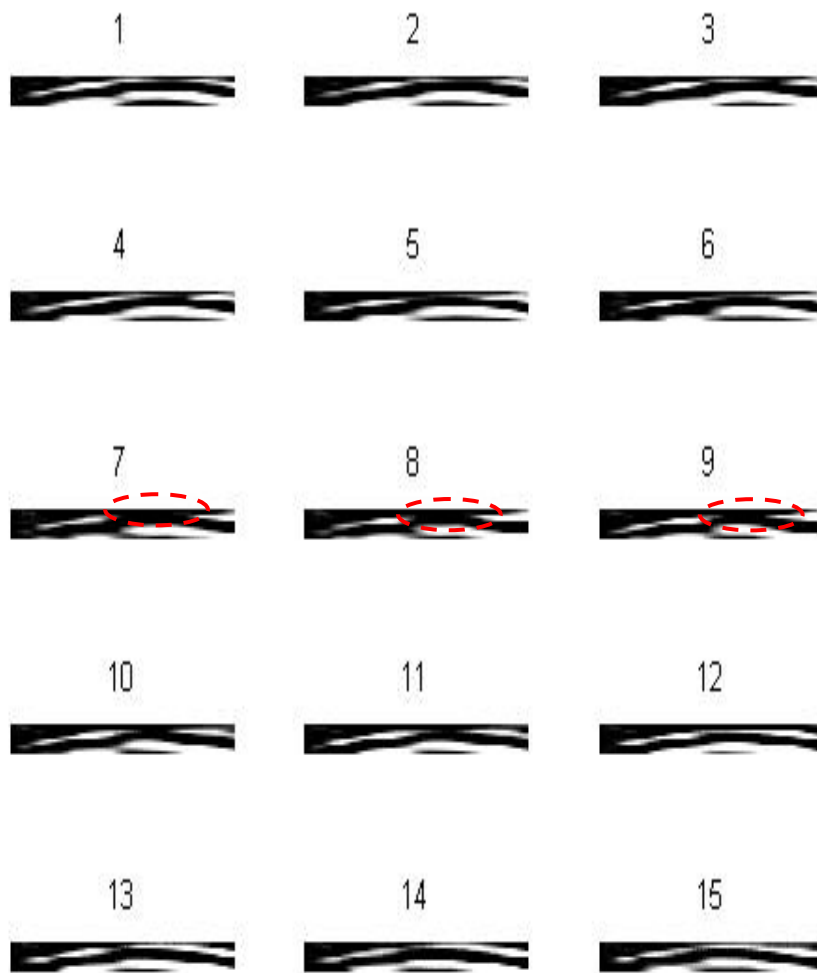


Figure 4.7. Test - 15 radar images perpendicular to the pipes using the 250MHz antenna with 2 integrations. (The red dotted circles indicate areas where visual differences are evident in the scans associated with damaged pipe section.)

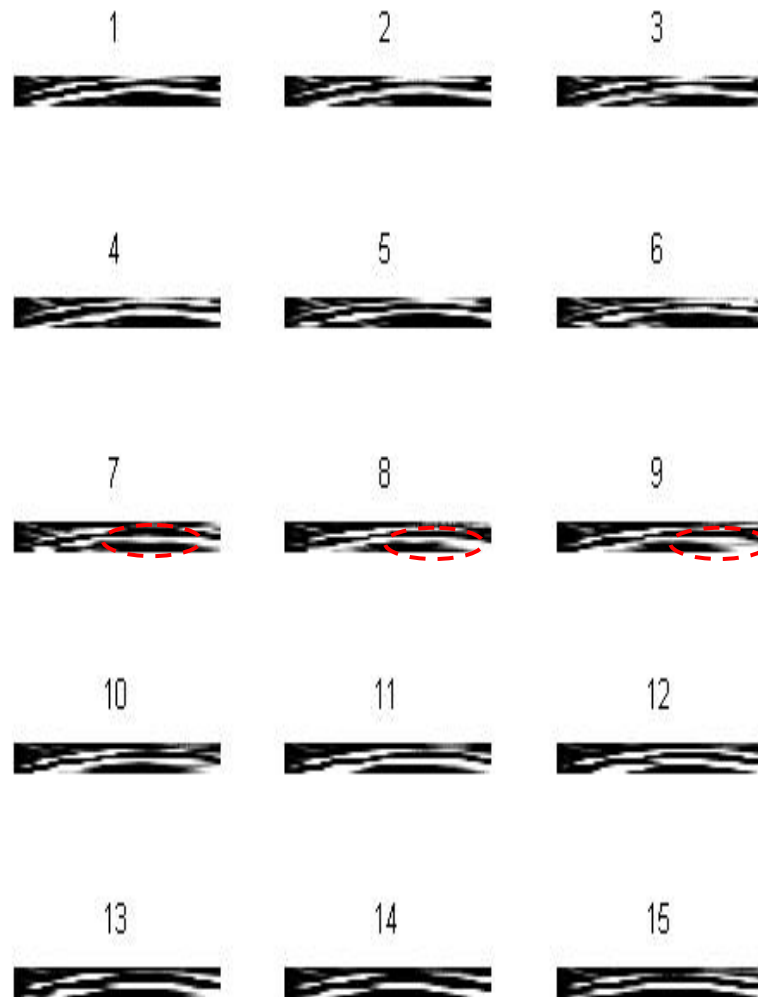


Figure 4.8. Test 1 - 15 radar images perpendicular to the pipes using the 700MHz antenna with 2 integrations. (The red dotted circles indicate areas where visual differences are evident in the scans associated with damaged pipe section.)

As mentioned before, position 8 was where the break in the pipe occurred and position 4 was where the undamaged pipe was located. Referring to Figures 4.3 and 4.8, the signal signature from both antenna frequencies with different configurations can be compared. It can be seen that the hyperbola image was distorted from position 6 to position 10 in these scans (the greatest visual differences are indicated on the Figures by red dotted circles). This means that something had occurred in these locations, i.e. where the damaged pipe was positioned. In terms of radar image resolution, it was quite hard to interpret the radar images from the ‘5 integrations’ and ‘2 integrations’ configurations due to the flattening of the hyperbolae (Figures 4.5-4.8). For comparison, the radar scan results axially along the pipes are shown in Figures 4.9- 4.14.

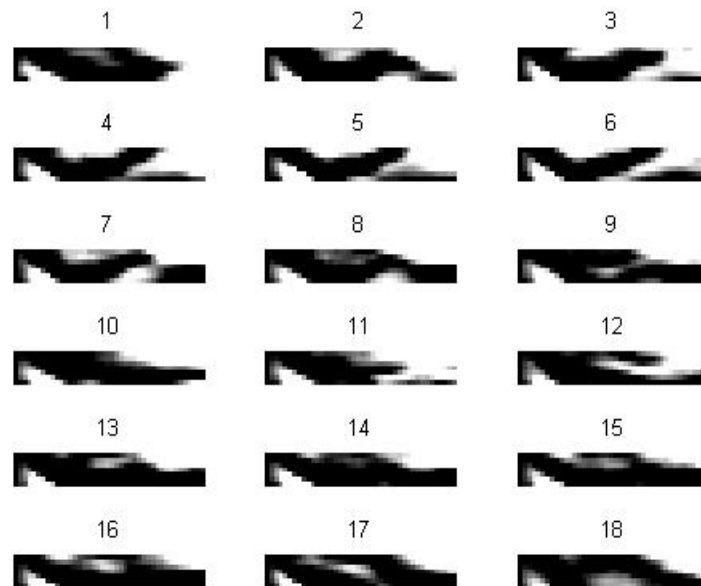


Figure 4.9. Test 1 - 18 radar images axially along the pipes using the 250MHz antenna with 10 integrations.

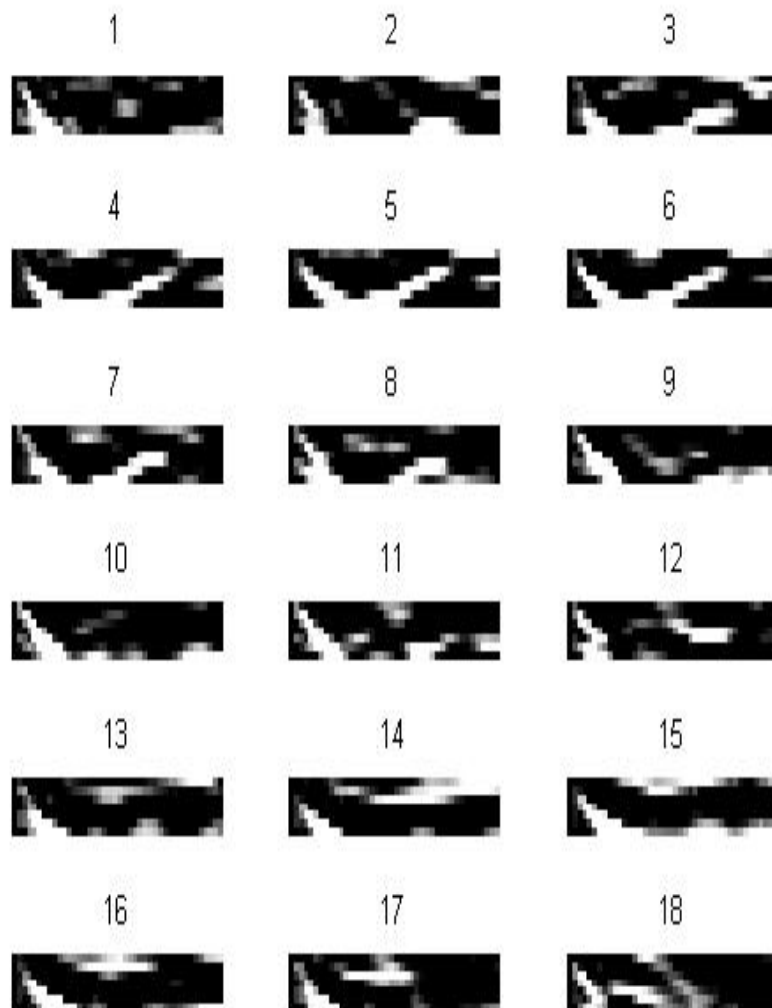


Figure 4.10. Test 1 - 18 radar images axially along the pipes using the 700MHz antenna with 10 integrations.

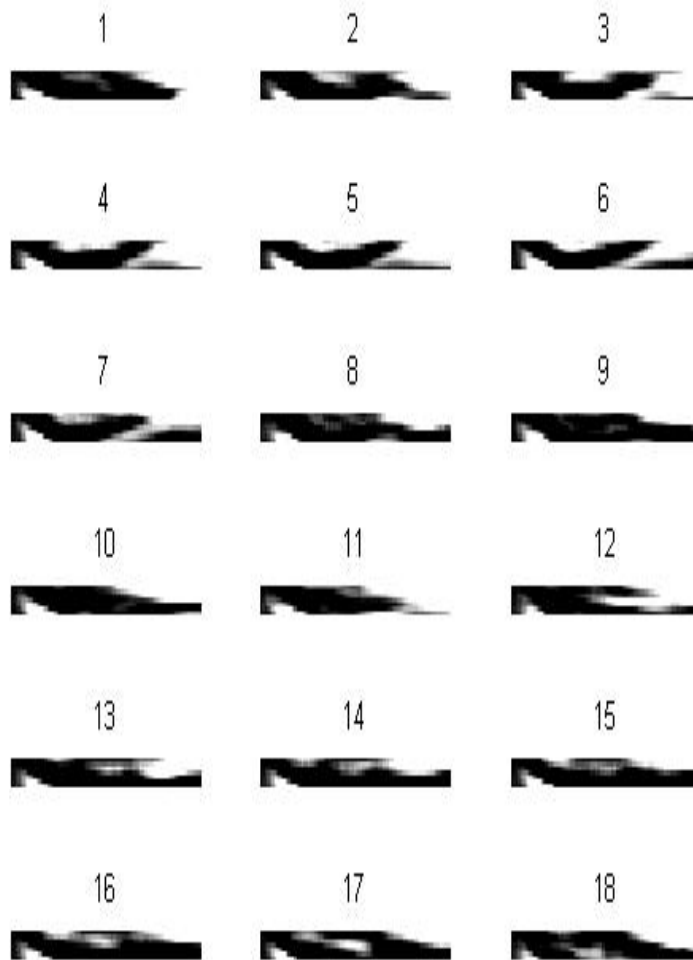


Figure 4.11. Test 1 - 18 radar images axially along the pipes using the 250MHz antenna with 5 integrations.

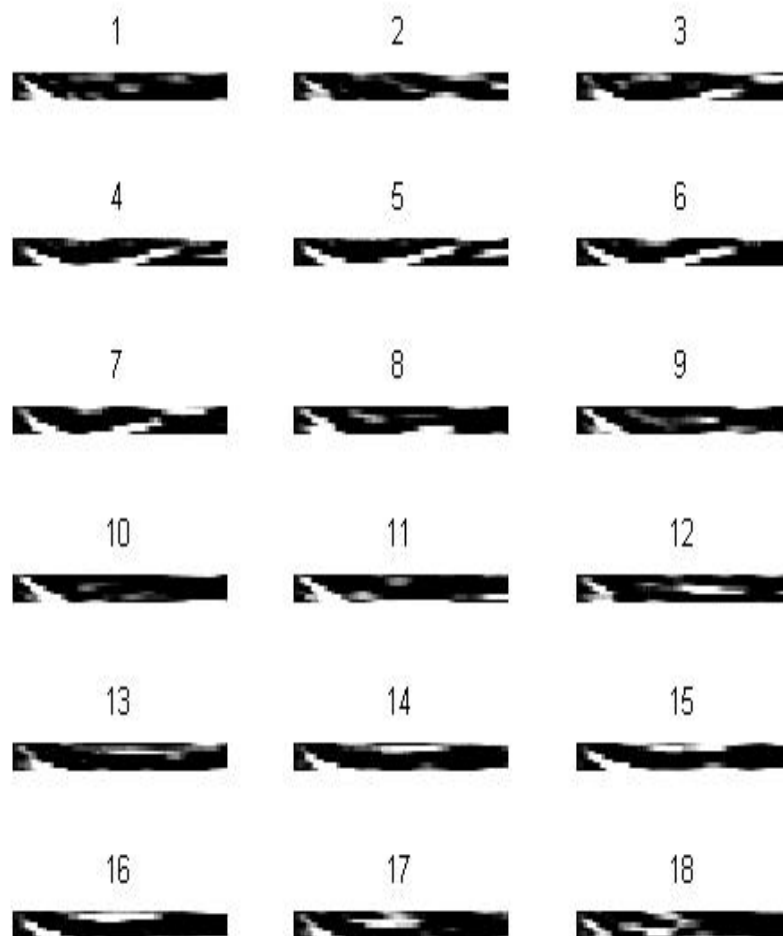


Figure 4.12. Test 1 -18 radar images axially along the pipes using the 700MHz antenna with 5 integrations.

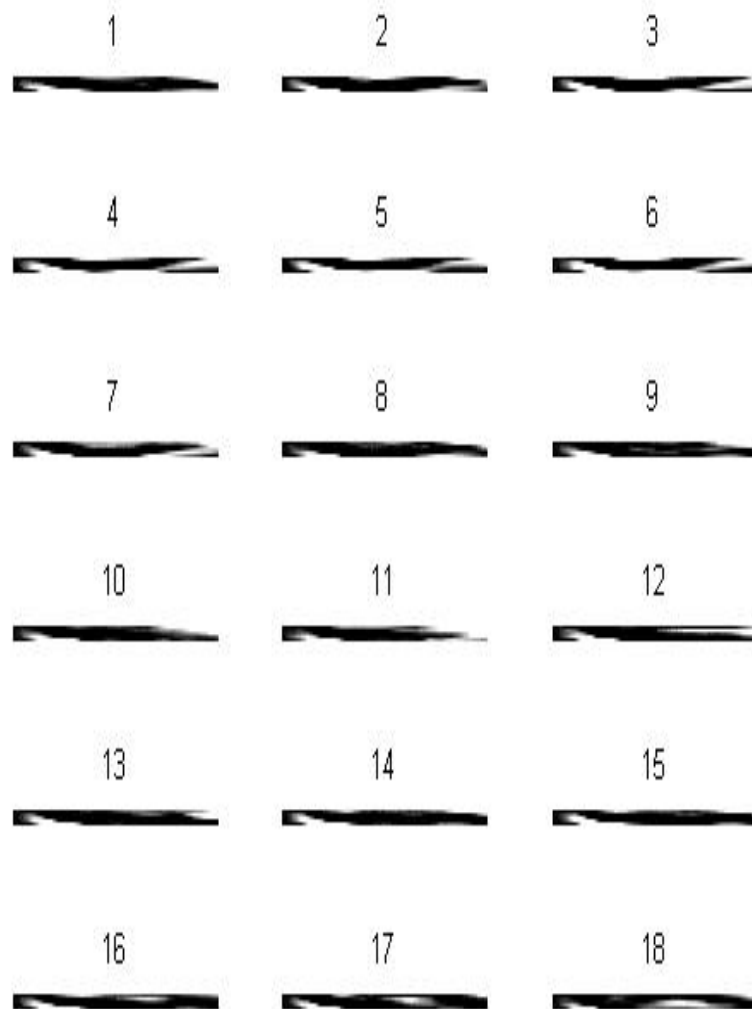


Figure 4.13. Test 1 - 18 radar images axially along the pipes using the 250MHz antenna with 2 integrations.

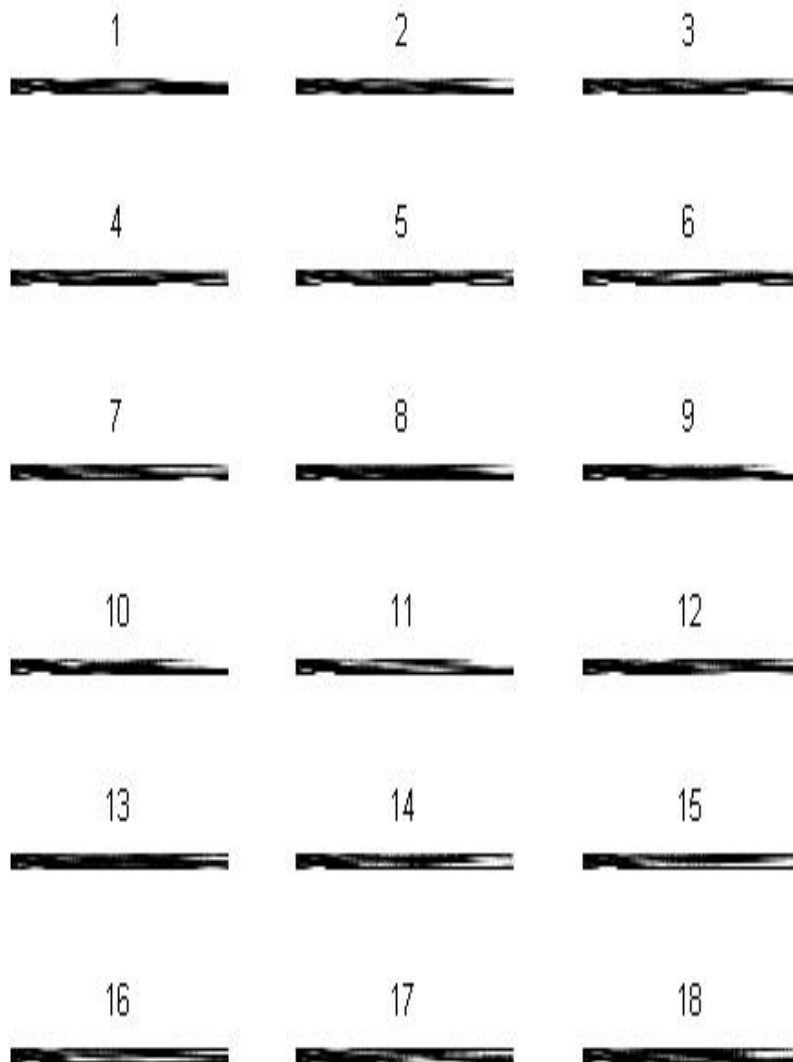


Figure 4.14. Test 1 - 18 radar images axially along the pipes using the 700MHz antenna with 2 integrations.

As mentioned in Figure 3.11 and referring to Figures 4.9-4.14, position 4 was where the break in the pipe occurred and position 14 was where the undamaged pipe was located. Visual inspection of the radar images for the Y direction (axially along the pipe) is quite hard to understand. From all the radar images for both frequencies and different integrations it was difficult to interpret by visual inspection where the damage pipe section occurred. However, the signal amplitude changes in the damaged region were used to quantify the differences by using a Matlab program.

4.2.3 Identifying the effects of the GPR signal related to the damaged regions relative to the undamaged regions under ‘ideal’ ground conditions

Due to the difficulties of visually identifying the damaged regions, a Matlab program was developed in order to quantify the MSE and help identify the damaged region. This program was divided into two parts. The first part was about capturing the images (select the related matrix array involved for further data processing) as shown in Figure 4.15. In order to choose the damaged region for subsequent analysis, the signal signature of the damaged and undamaged pipe need to be identified by the full scan radar images. The full scan radar images were then minimised by cropping the selected signal signature. The signal signature (perpendicular to the pipe) can be identified by choose the complete hyperbola image. However, the signal signature axially along the pipes can be identified

by choose a single straight line image. At this stage, cropping the selected signal signature can be done by visual inspection. Cropping the selected signal signature means selecting the related matrix array, which consists of values on the Y-axis and X-axis. These values were key values in the Matlab program as stated in Appendix 1 (i.e. (50:64, 1:42)). The Y-axis represents the depth and the X-axis represents the horizontal distance (from the starting point of the GPR cart). In this program, 512 samples were captured. This sample is a default menu in the IDS K2-FastWave data acquisition software. Hence, in order to identify the related matrix array, the sample in which the hyperbola is situated (i.e. Y-axis=50:64, X-axis=1:42) needs to be identified.

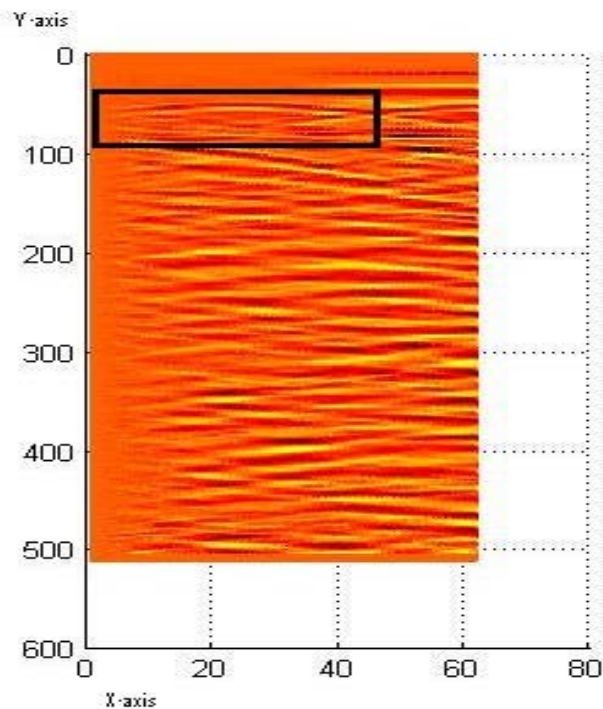


Figure 4.15. Example GPR radar image in the Matlab program used for determining the area for the subsequent MSE analysis (black rectangle)

The second part involved calculating the amplitude of the radar signal for the mean square error (MSE) in order to identify the defect region of the damaged pipe. In this experiment, only 200 positive amplitudes are selected and calculated thus the mean of 200 samples is captured. When all the mean amplitudes are calculated, then calculating the MSE becomes easier. All mean amplitudes (representing each line) were compared to the others with the mean amplitude in the undamaged line as the benchmark. In the case of the X-direction , line number 4 was selected as the benchmark line (undamaged line) for the radar scan perpendicular to the pipe and line number 14 was selected as the benchmark line (undamaged line) for the radar scan along the pipe. Finally, the difference of the mean square error is calculated and recorded. The Matlab script for capturing the images and identifying the related matrix array is given in Appendix 1. Meanwhile, the script for calculating the mean square error is given in Appendix 2.

The MSE results for Test 1 perpendicular to the pipe are shown in Figures 4.16-Figure 4.21. The red dotted circle in these plots indicates the peak MSE value and the most likely position of the damaged region of the pipe.

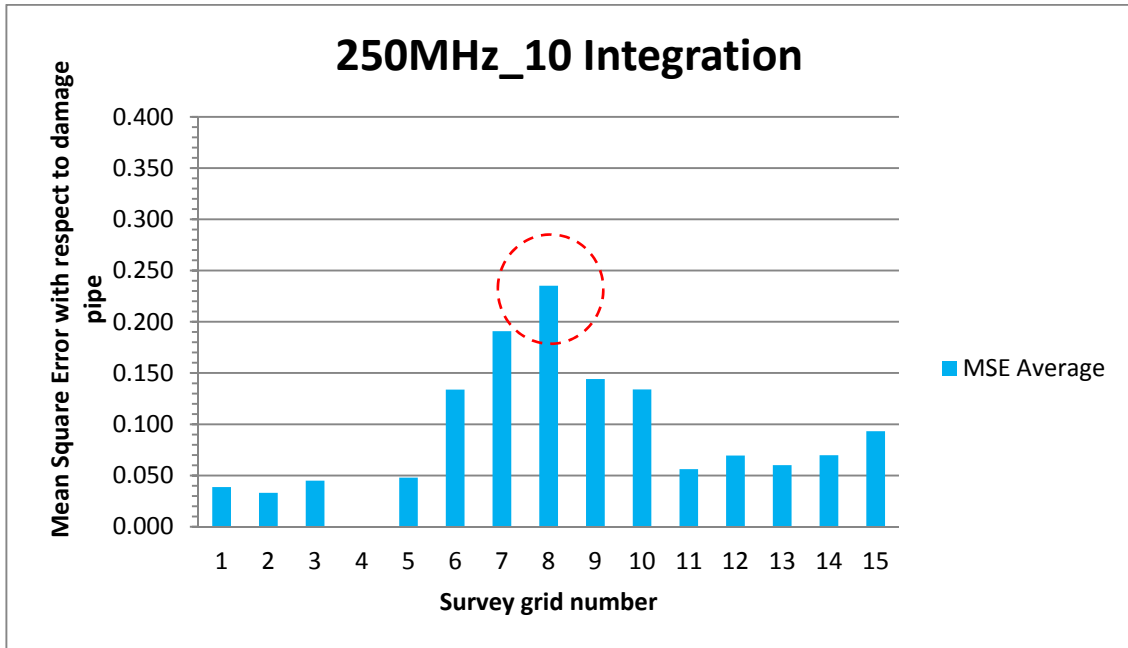


Figure 4.16: Test 1 - MSE for the 250MHz radar at 10 integrations perpendicular to the pipes

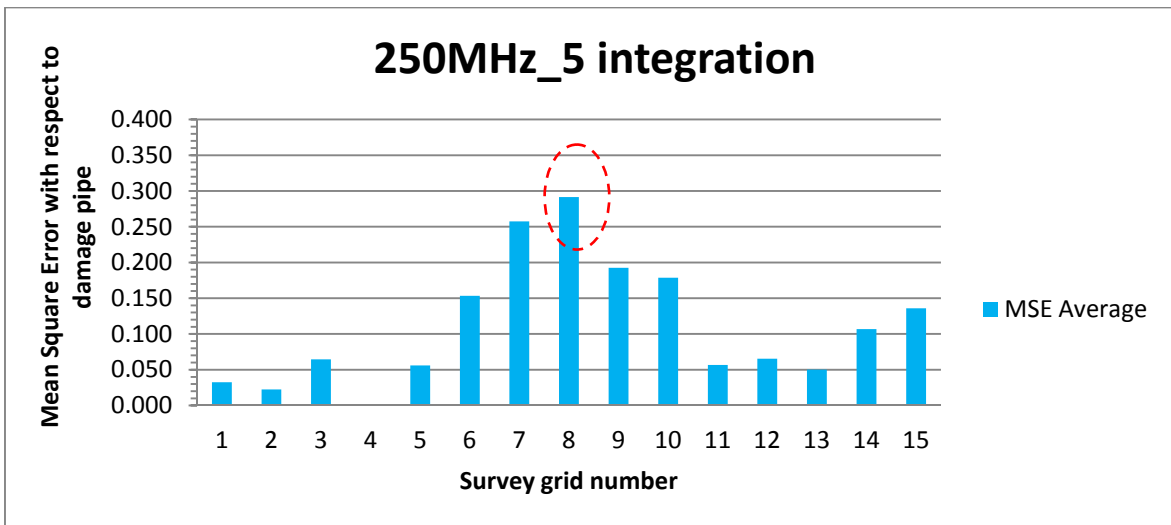


Figure 4.17: Test 1 - MSE for the 250MHz radar for 5 integrations perpendicular to the pipes

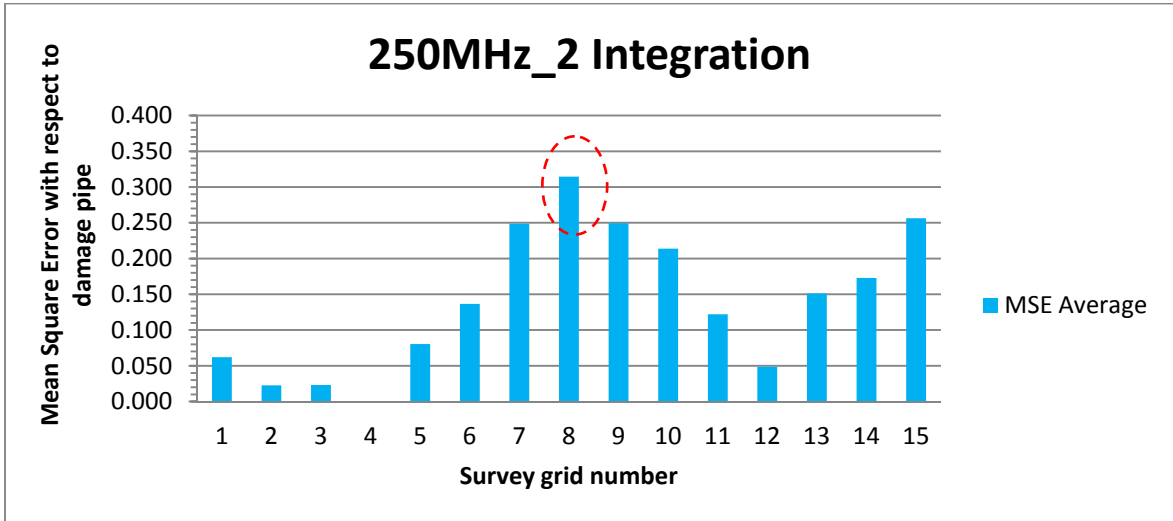


Figure 4.18: Test 1 - MSE for the 250MHz radar at 2 integrations perpendicular to the pipes

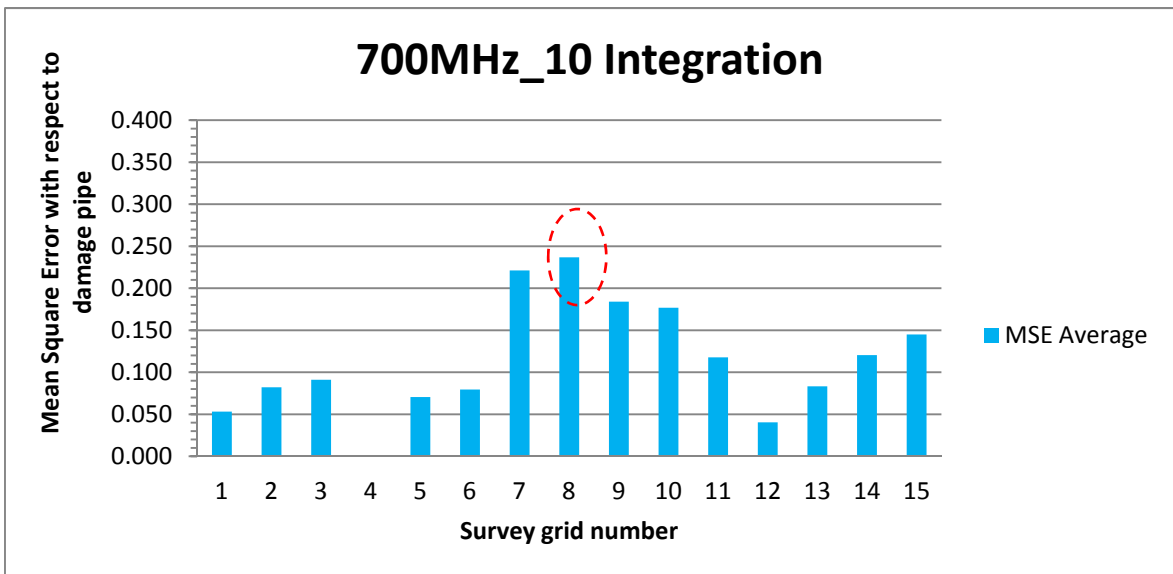


Figure 4.19: Test 1 - MSE for the 700MHz radar at 10 integrations perpendicular to the pipes

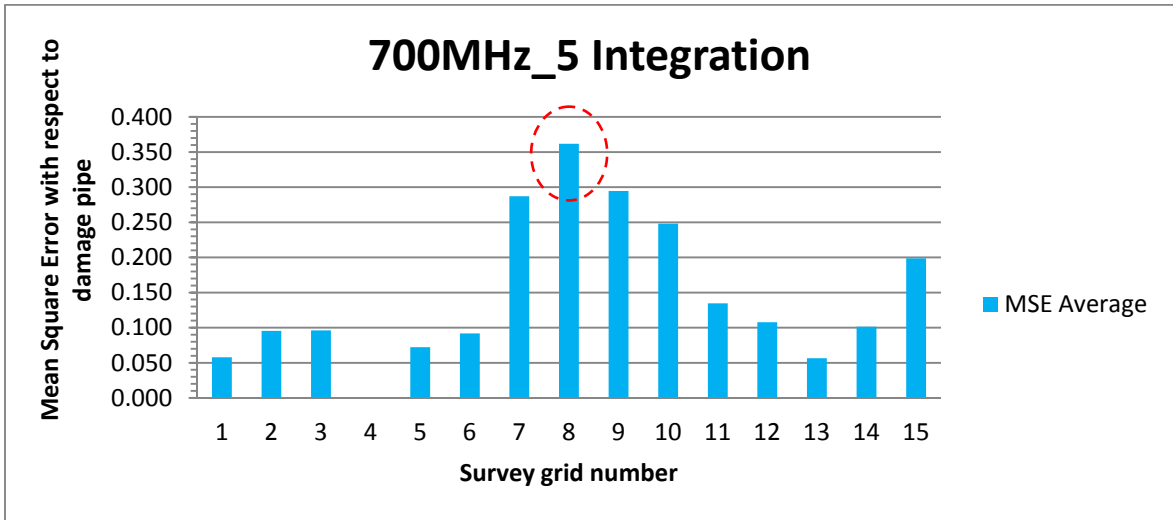


Figure 4.20: Test 1 - MSE for the 700MHz radar at 5 integrations perpendicular to the pipes

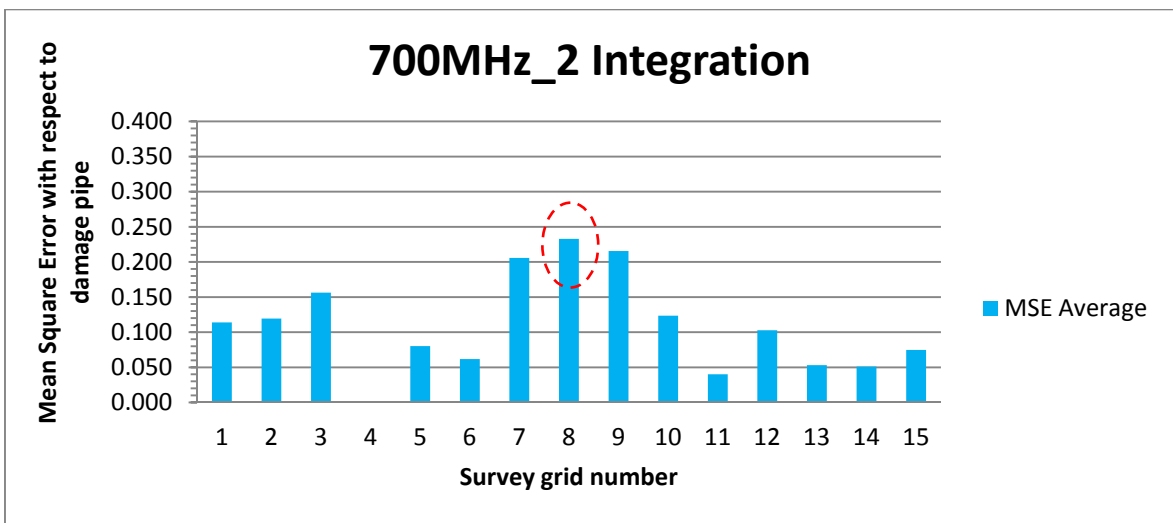


Figure 4.21: Test 1 - MSE for the 700MHz radar at 2 integrations perpendicular to the pipes

From this result, it can be concluded that all the configurations were able to identify the damaged region. However, the best configuration for these experiments appears to be an integration of 10. This decision is based on better images and the value of the mean square error (MSE) at ‘10 integrations’ compare to the others, i.e. a smaller value of the MSE is better.

Meanwhile, the results for the MSE (axially along the pipes) at 250MHz are shown in Figures 4.22-24, while the results at 700MHz are shown in Figures 4.25-27. Once again, the red dotted circle on the plots indicates the highest MSE value and hence the likely location of the damaged section.

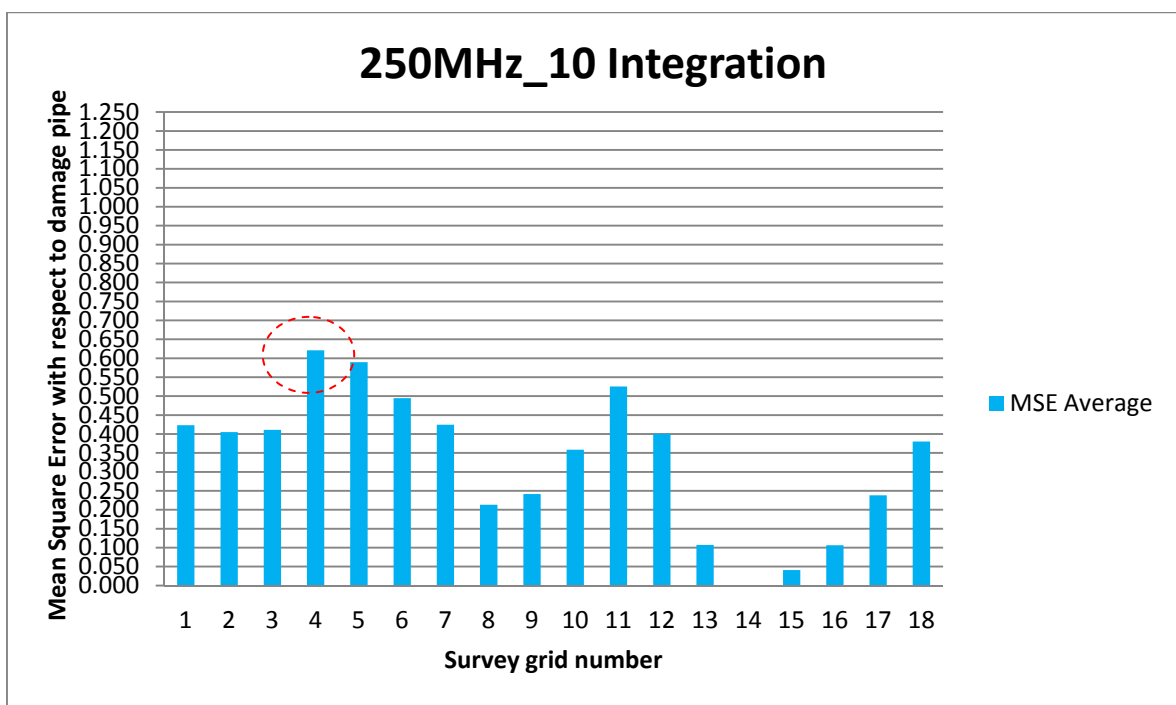


Figure 4.22: Test 1 - MSE for the 250MHz radar at 10 integrations axially along the pipes

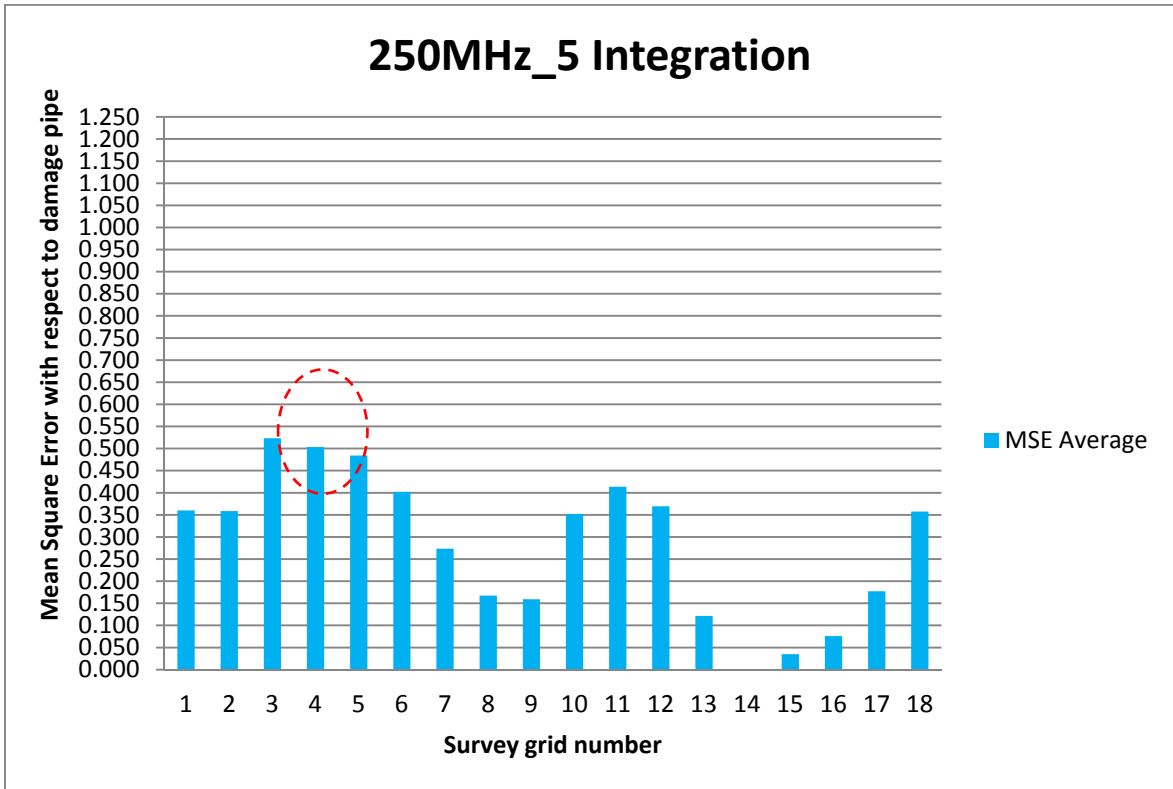


Figure 4.23: Test 1 - MSE for the 250MHz radar at 5 integrations axially along the pipes

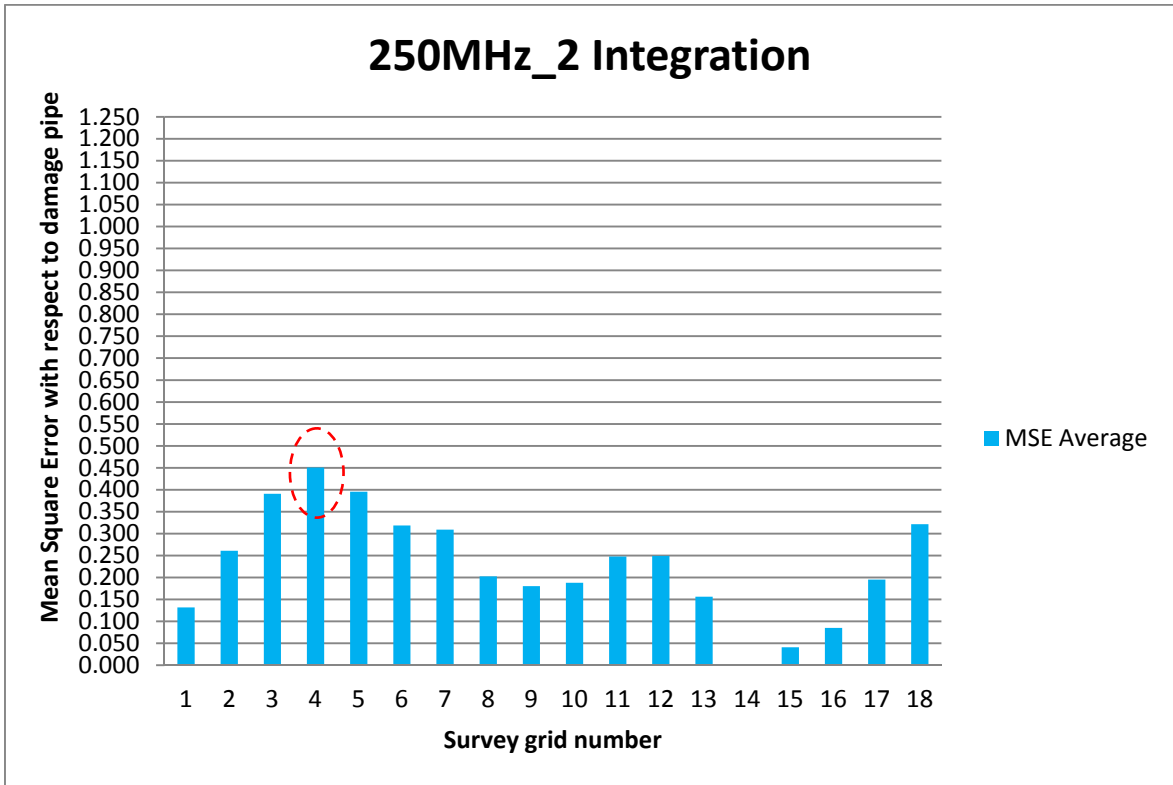


Figure 4.24: Test 1 - MSE for the 250MHz radar at 2 integrations axially along the pipes

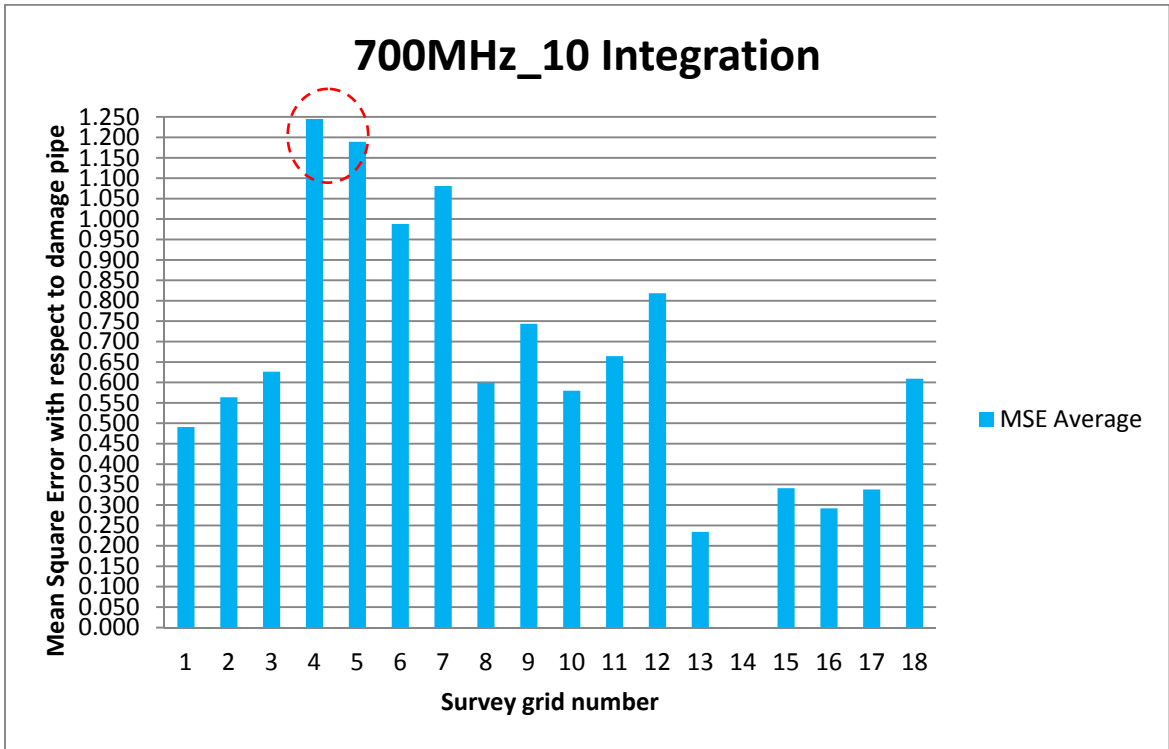


Figure 4.25: Test 1 - MSE for the 700MHz radar at 10 integrations axially along the pipes

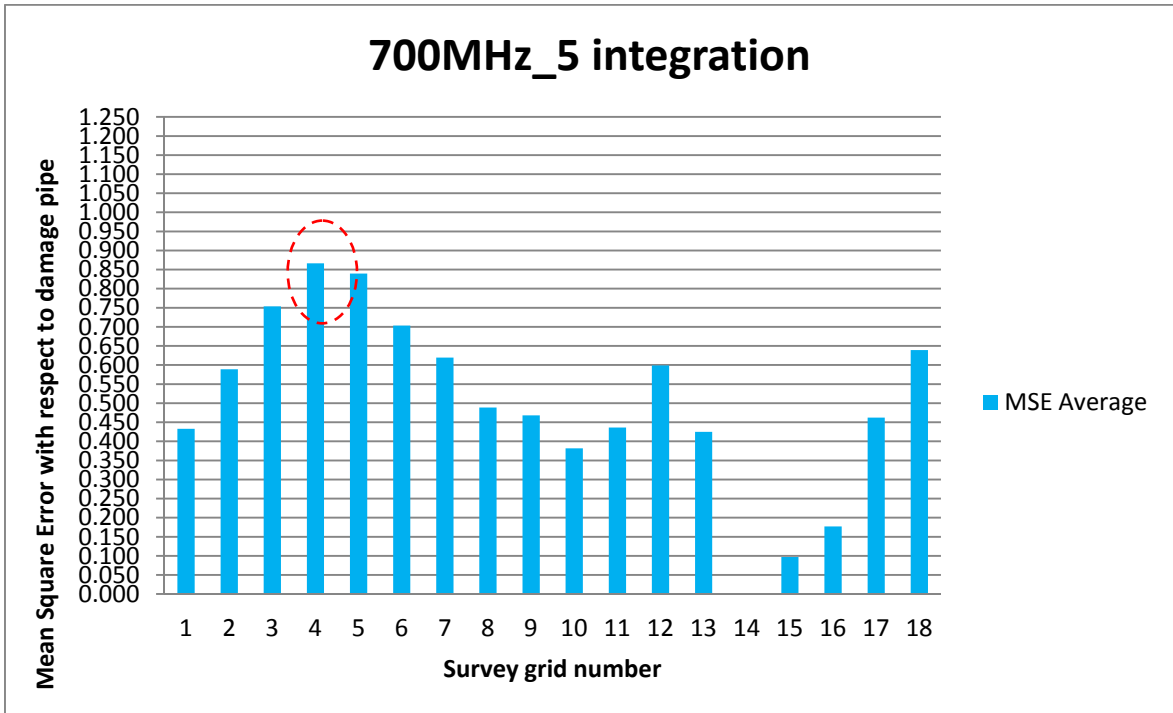


Figure 4.26: Test 1 - MSE for the 700MHz radar at 5 integrations axially along the pipes

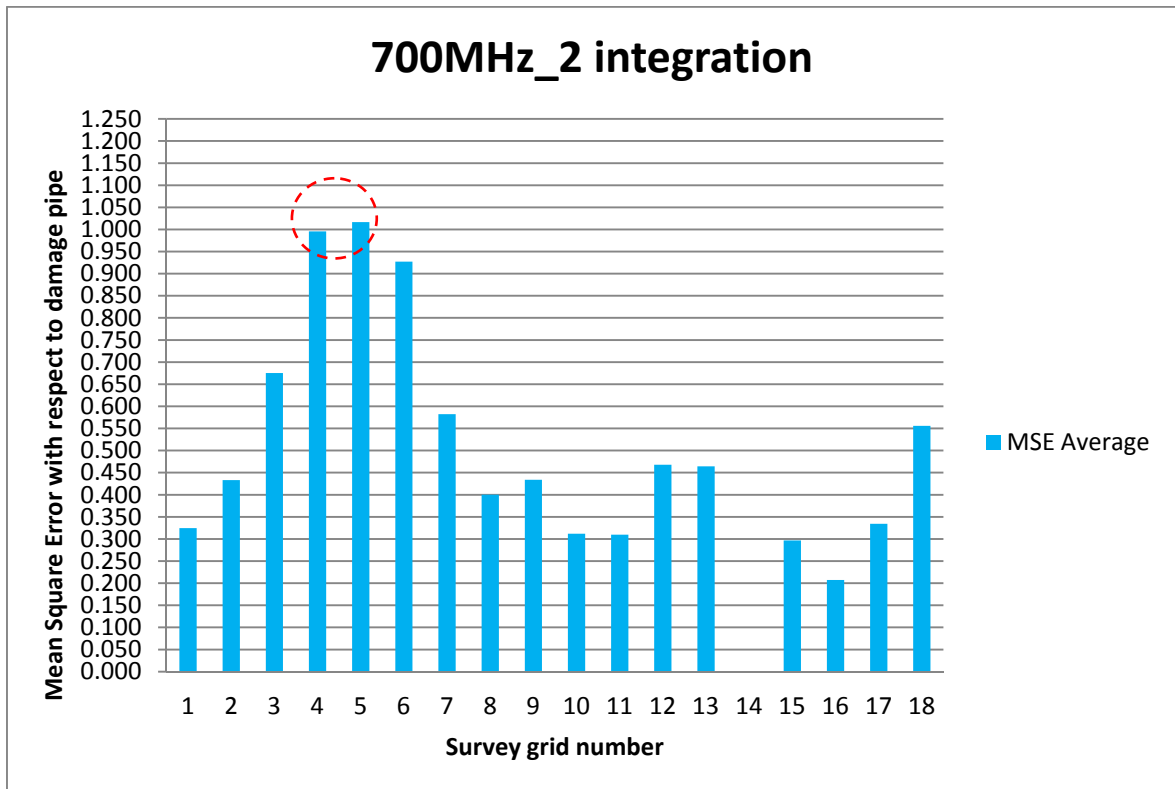


Figure 4.27: Test 1 - MSE for the 700MHz radar at 2 integrations axially along the pipes

Even though it was hard to visually identify the damaged region from the radar images along the pipe, it is possible to quantify the amplitude changes for the damaged region along the pipe.

In summary, the following key findings can be identified from the results for Test 1:

- i. From the analysis using the Mean Square Error (MSE), it is possible to quantify the signal amplitude changes between the undamaged and the damaged pipe section for both frequencies. As the MSE analysis results are positively

correlated to the difference from an undamaged pipe, a large value would indicate an anomaly that in turn points to an observed variation from an undamaged pipe. The peak value in the MSE result indicates the possible position of the damage. For both surveys, perpendicular and along the pipe, the MSE results produced the highest value at the position that corresponded to the location of the damaged pipe section, which were position 8 for the perpendicular scans and position 4 for the scans along the pipe.

- ii. The analysis of the results perpendicular to the pipe showed that grid point 4 was where the pipe was undamaged (and most free from clutter due to wall effects) and grid point 8 was where the damage occurred in the pipe.
- iii. The analysis of the results along the pipe showed that grid point 14 was where the pipe was undamaged and grid point 4 was where the damage occurred in the pipe.
- iv. All integrations were able to quantify the signal amplitude changes.
- v. For both radar frequencies (250 MHz and 700 MHz) it was possible to identify the defective regions in the pipe.
- vi. The 700 MHz radar scan was sharper and brighter due to the higher signal resolution. The same was observed in all subsequent tests, suggesting that the usual assumption of resolution improving with higher frequency remained valid.

- vii. The pipe damage was more easily observed when the survey was conducted perpendicular to the pipe (X direction).
- viii. Even though the antennas were shielded, ‘clutter’ in the data still occurred due to interference from the surroundings. The same observation was recorded in all subsequent tests as the same GPR and setup were used. Clutter is most visible in the radar scans near the walls, and this is likely to be caused by reflections from both the wall/air interface and external objects such as the supporting structure. Different signal calibrations produced different signal amplitude changes. This is a common observation with GPR equipment. Therefore, the same calibration setting was used in the scans for all positions within each test to ensure that any true anomalies in the traces were detected.

4.3 Test 2

The purpose of Test 2 was to understand whether the GPR was capable of detecting a broken pipe with a 2cm and a 5cm gap (i.e. the pipe was split into three sections), and to identify and quantify the damaged region of this broken pipe. The gaps were covered with plastic (i.e. sand was prevented from passing through the gap by the plastic cover) as shown in Figures 4.28 and 4.29. In these experiments 15 crossing points perpendicular to the pipe and 18 points along the pipe were used in the radar scan. The pipe was split into three sections where the broken pipe with 5 cm gap and 2 cm gap were created. These gaps

were located at X12 (2 cm gap) and at X8 (5 cm gap). The GPR survey grid line for this experiment was shown in Figure 3.11.



Figure 4.28. Test 2 - Broken pipe with a 5cm gap with a plastic cover



Figure 4.29. Test 2 - Broken pipe with a 2cm gap with a plastic cover

4.3.1 Identifying the signal signature of the damaged and undamaged pipe

The radar scan perpendicular to the pipe and along the pipe was conducted in order to identify the signal signature of the damaged and undamaged pipe. In these experiments, two types of antenna were tested (i.e. 250MHz and 700MHz). As was shown previously a configuration with 10 integrations showed the best resolution and hence this has been used here. The radar scan results of these experiments perpendicular to the pipes are shown in Figures 4.30 and 4.31. Meanwhile, the radar scans axially along the pipe are shown in Figures 4.32 and 4.33.

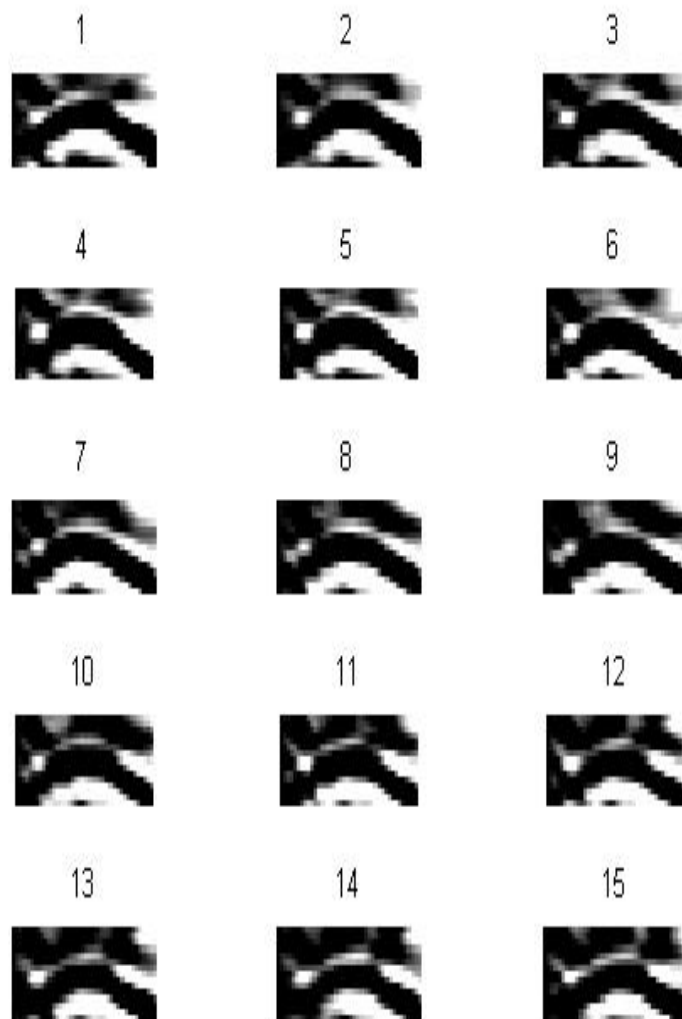


Figure 4.30. 15 radar images perpendicular to the pipes using the 250MHz antenna with 10 integrations (Test 2)

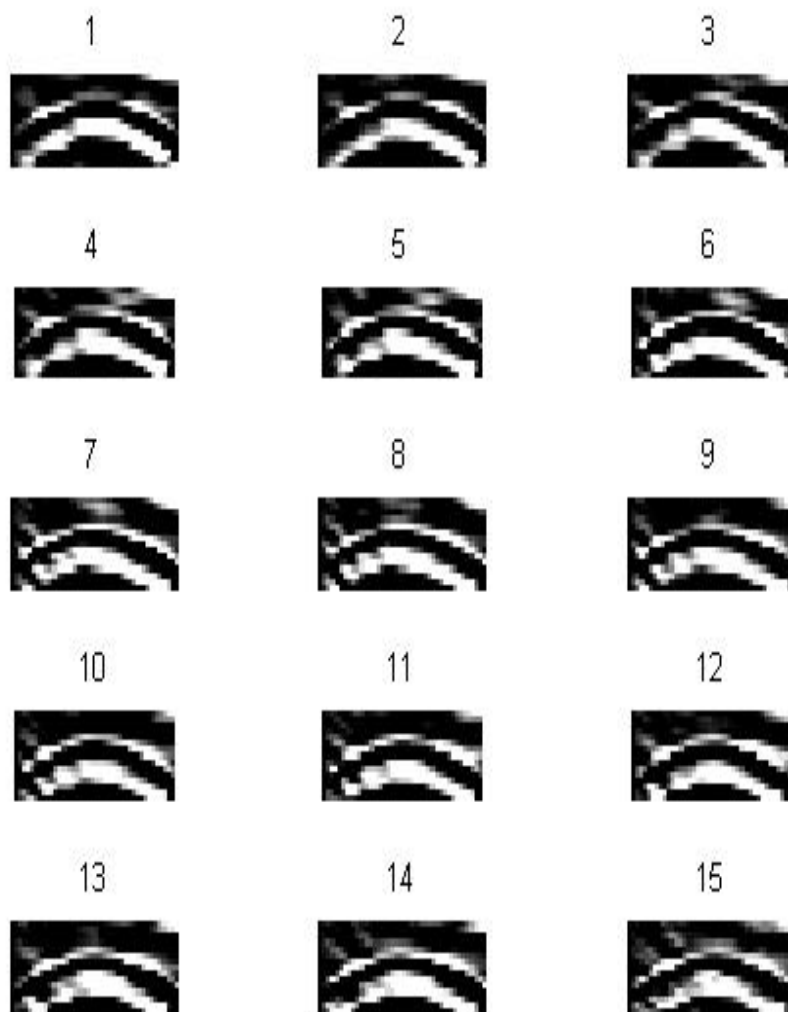


Figure 4.31. 15 radar images perpendicular to the pipes using the 700MHz antenna with 10 integrations (Test 2)

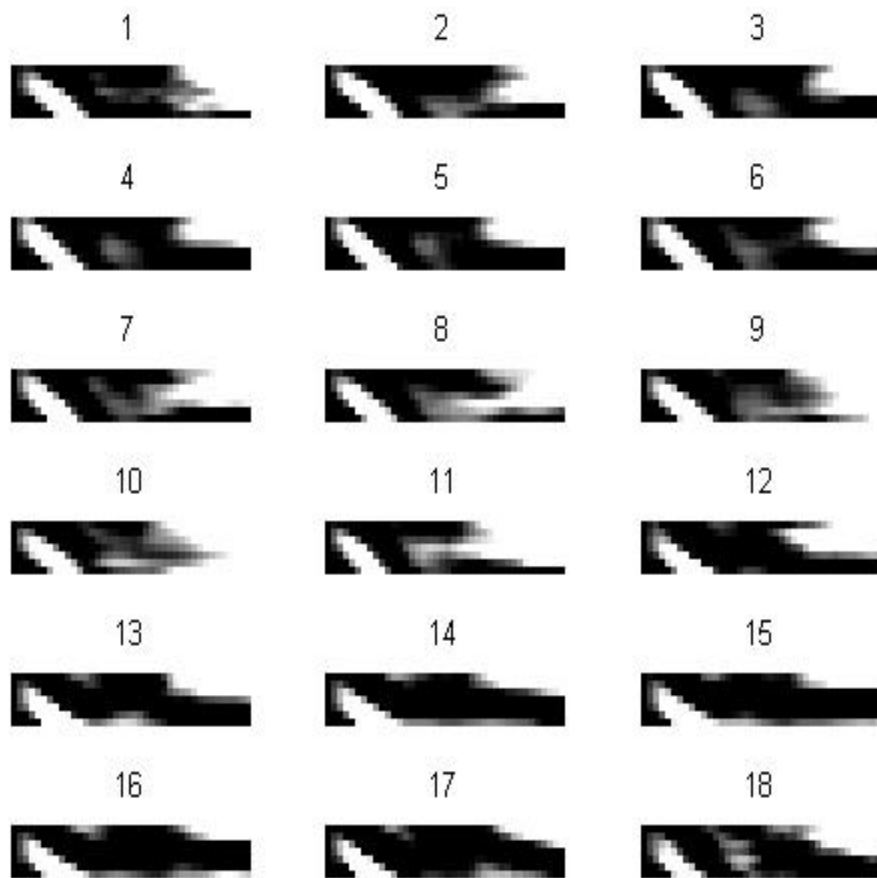


Figure 4.32. 18 radar images axially along the pipes using the 250MHz antenna with 10 integrations (Test 2)

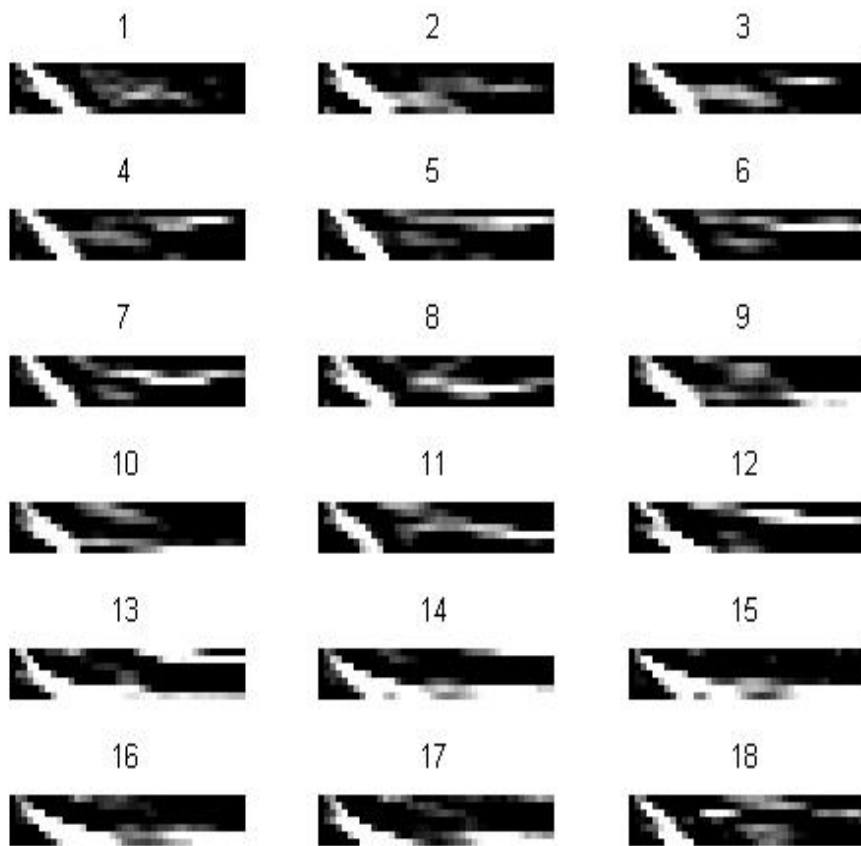


Figure 4.33. 18 radar images axially along the pipes using the 700MHz antenna with 10 integrations (Test 2)

All the radar images for both frequencies were visually inspected, but none could be used to identify the damaged areas. The amplitude changes were therefore investigated in the damaged regions to quantify any differences by using a Matlab program.

4.3.2 Identifying the effects of the GPR signal related to the damaged regions relative to the undamaged regions under ‘ideal’ ground conditions

Even though it is hard to interpret the images, the MSE for both directions was calculated. The results for the MSE perpendicular to the pipes at 250MHz and 700MHz are shown in Figures 4.34 and 4.35, meanwhile the results for the MSE along the pipe are shown in Figures 4.36 and 4.37.

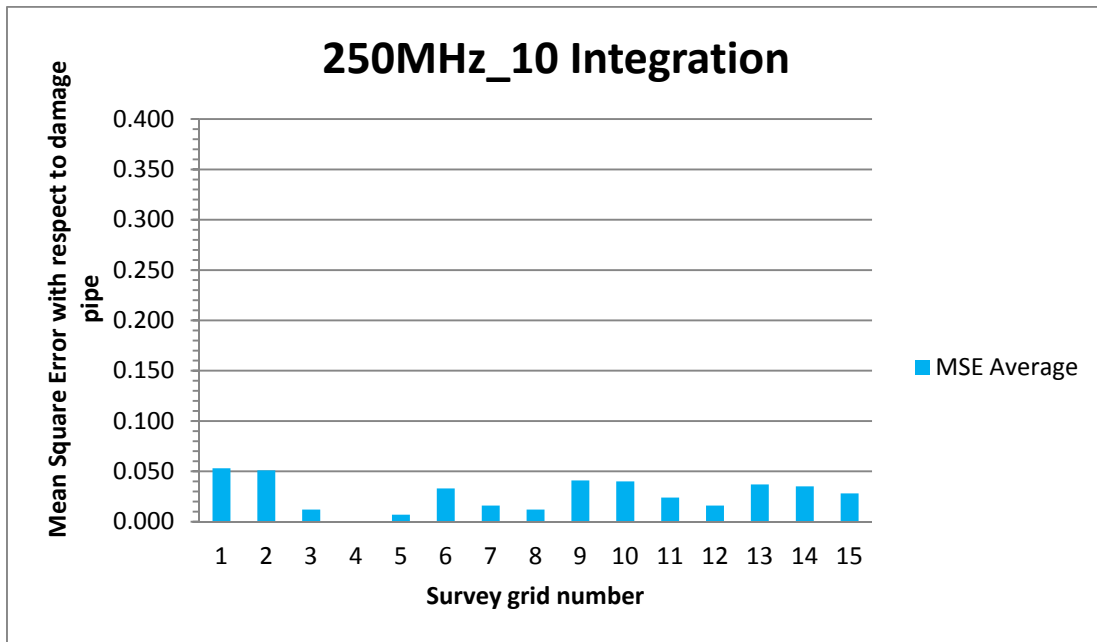
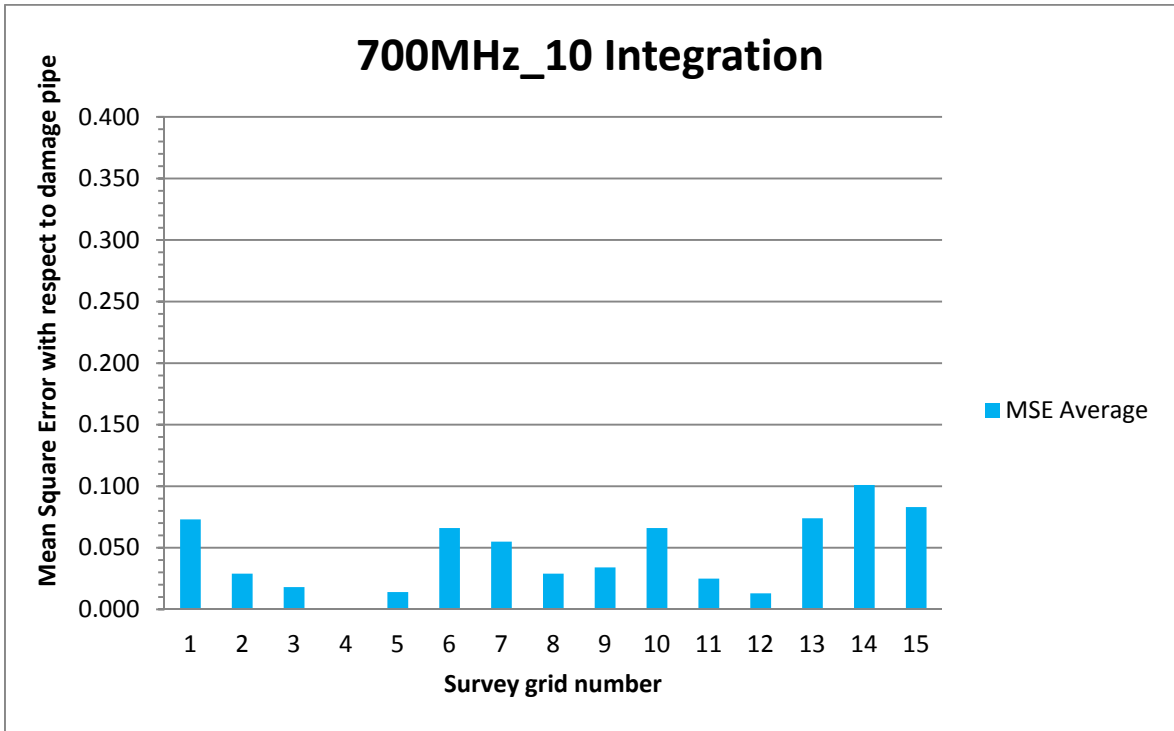
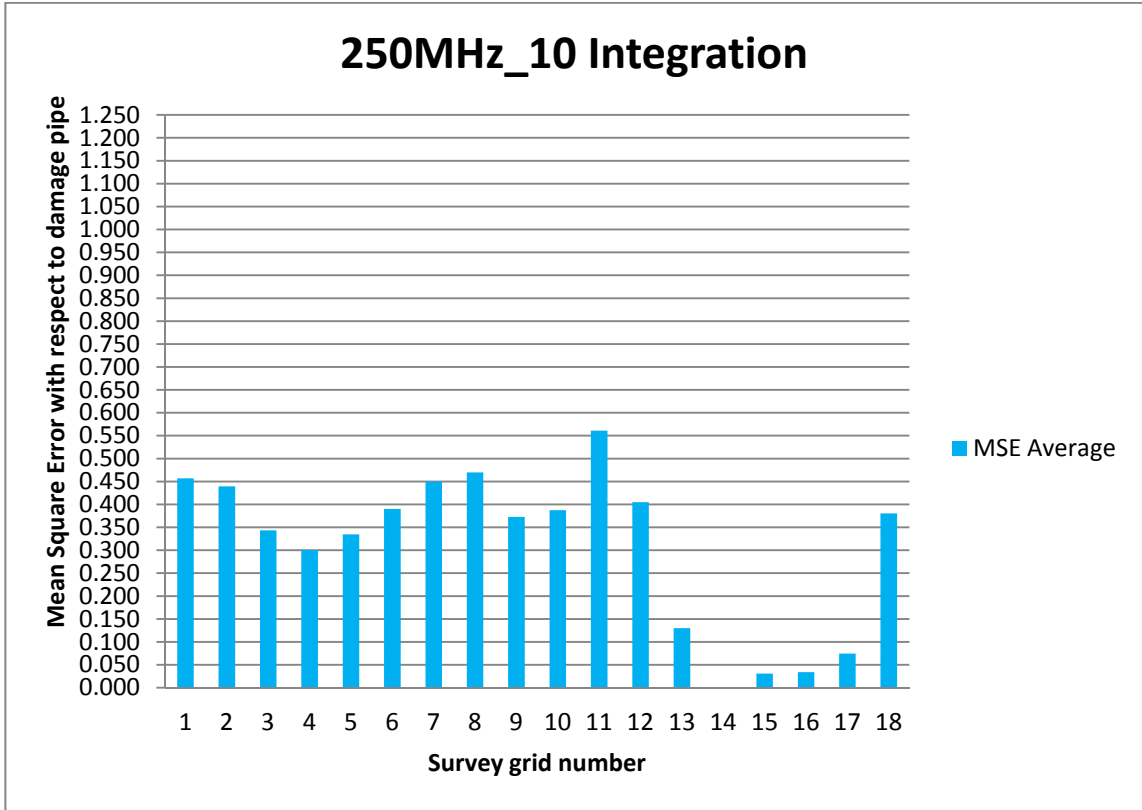


Figure 4.34: MSE for the 250MHz radar at 10 integrations perpendicular to the pipes (Test 2)



**Figure 4.35: MSE for the 700MHz radar at 10 integrations perpendicular the pipes
(Test 2)**



**Figure 4.36: MSE for the 250MHz radar at 10 integrations axially along the pipes
(Test 2)**

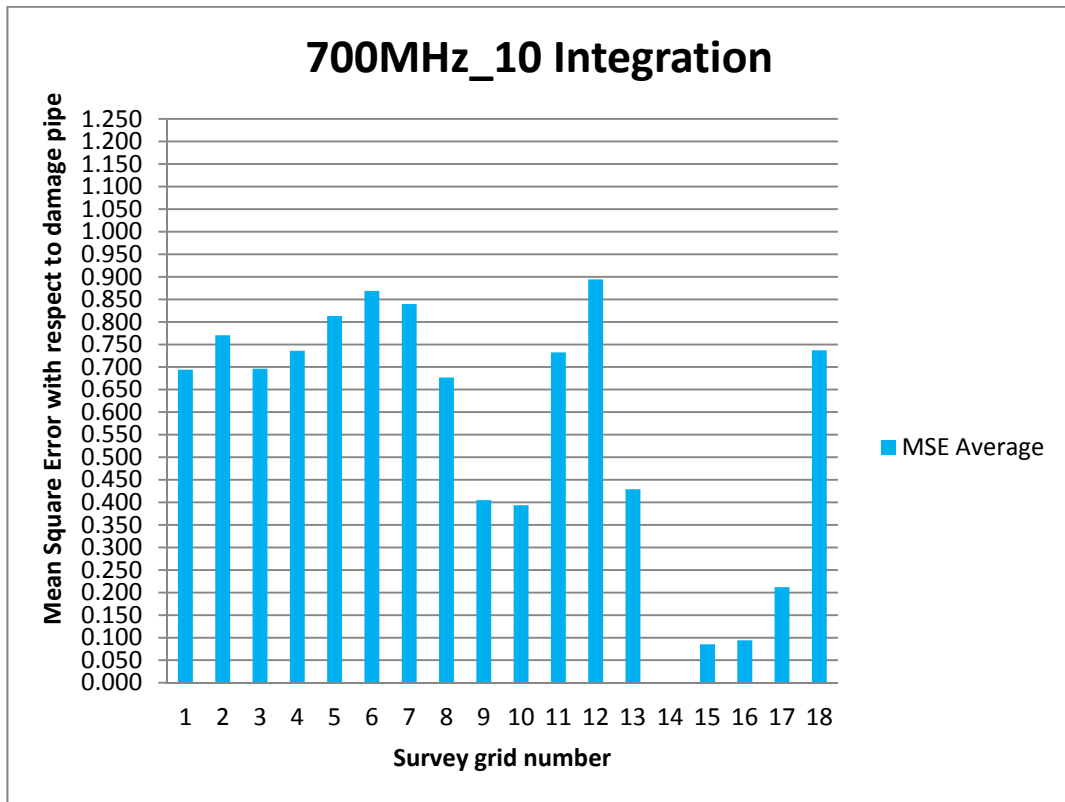


Figure 4.37: MSE for the 700MHz radar at 10 integrations axially along the pipes (Test 2)

The following key findings can be identified from the results for Test 2:

- i. Analysis using the Mean Square Error (MSE) method did not accurately point to the damaged section in this case. This suggests that the method may not be suitable for the detection of this type of damage. As the damaged section was sealed off with a plastic cover and no sand was allowed into the pipe, the damaged section would appear to be very similar to an undamaged pipe to the

GPR as the dielectric constant of the plastic cover is very similar to the dielectric constant of the pipe material.

- ii. Both radar frequencies (250 MHz and 700 MHz) were unable to detect the defective regions on the pipe in this case.

4.4 Test 3

The purpose of Test 3 was to understand whether the GPR was capable of detecting a hole in the pipe with a diameter of 5cm (sand allowed to pass through the hole) and to identify and quantify the damaged region of this pipe. The hole was not covered with any materials, as shown in Figure 4.38. In these experiments, 15 crossing points perpendicular to the pipe and 18 points along the pipe were provided by the radar scan.



Figure 4.38: Test 3 –5cm hole in the pipe prior to being covered with sand

4.4.1 Identifying the signal signature of the damaged and undamaged pipe

A radar scan perpendicular to the pipe and axially along the pipe was conducted in order to identify the signal signature of the damaged and undamaged pipe. Once again in these experiments, two types of antenna were tested (i.e. 250MHz and 700MHz). Only an integration of 10 was tested. The radar scan results of these experiments perpendicular to the pipes are shown in Figures 4.39 and 4.40. Meanwhile the radar scan axially along the pipe is shown in Figures 4.41 and 4.42.

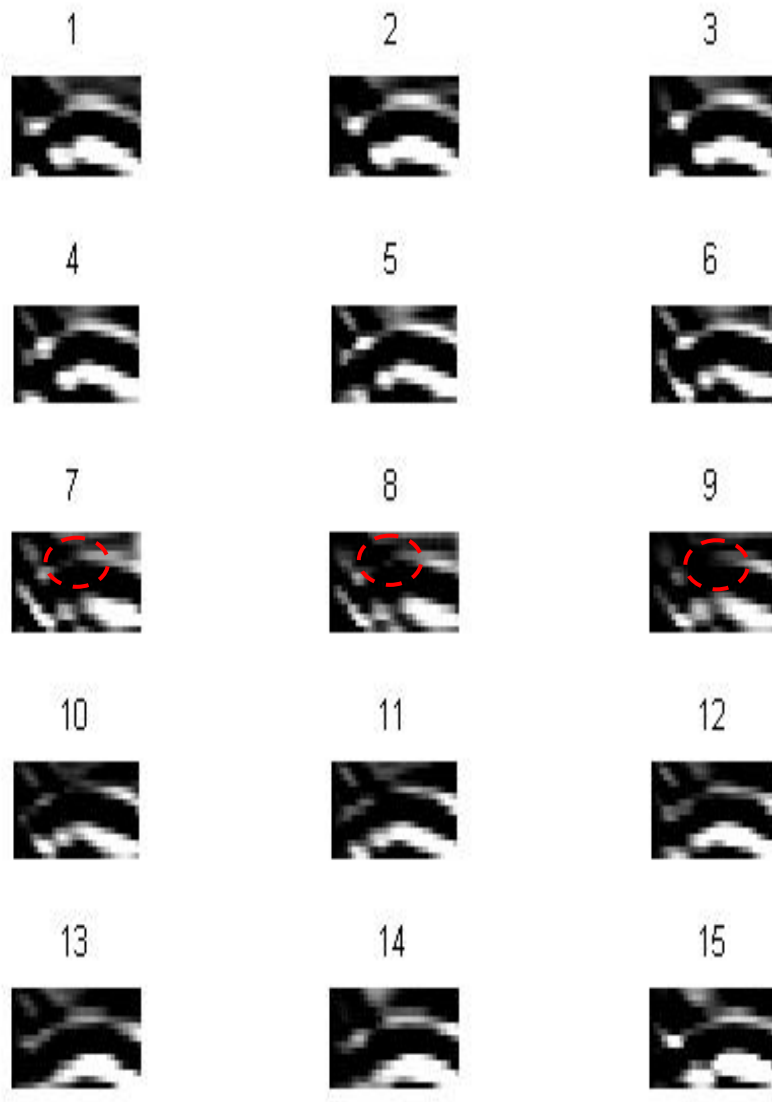


Figure 4.39: 15 radar images perpendicular to the pipes using the 250MHz antenna with 10 integrations (Test 3). (The red dotted circles indicate where visually there is potential evidence of damage due to differences in the scans.)

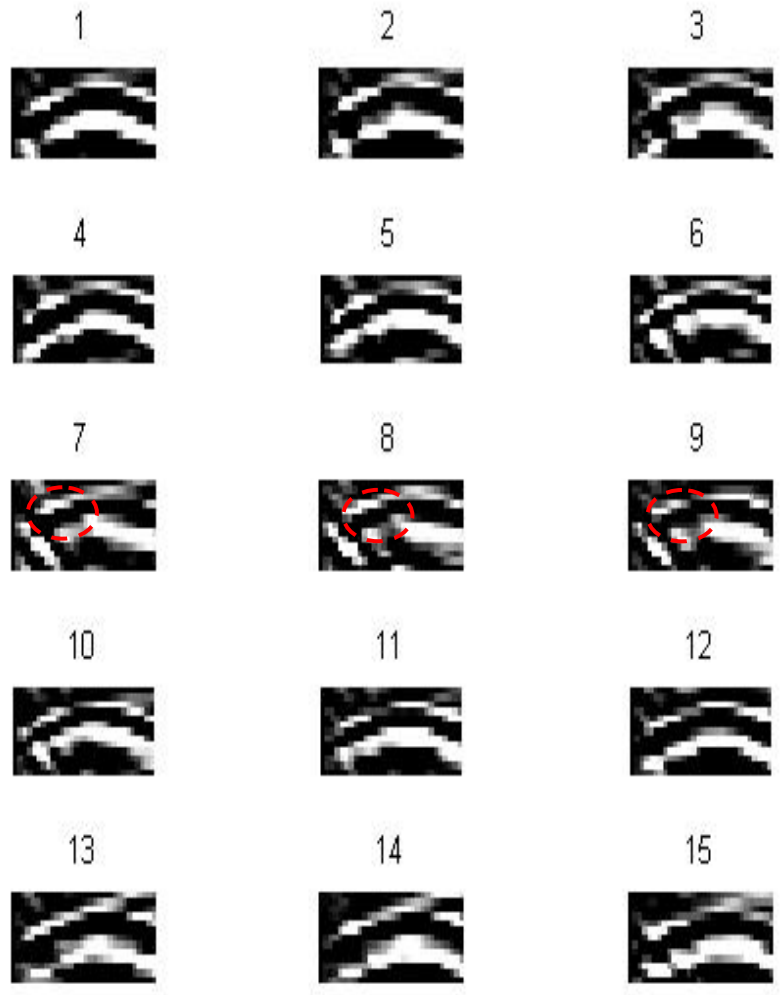


Figure 4.40: 15 radar images perpendicular to the pipes using the 700MHz antenna with 10 integrations (Test 3). (The red dotted circles indicate where visually there is potential evidence of damage due to differences in the scans.)

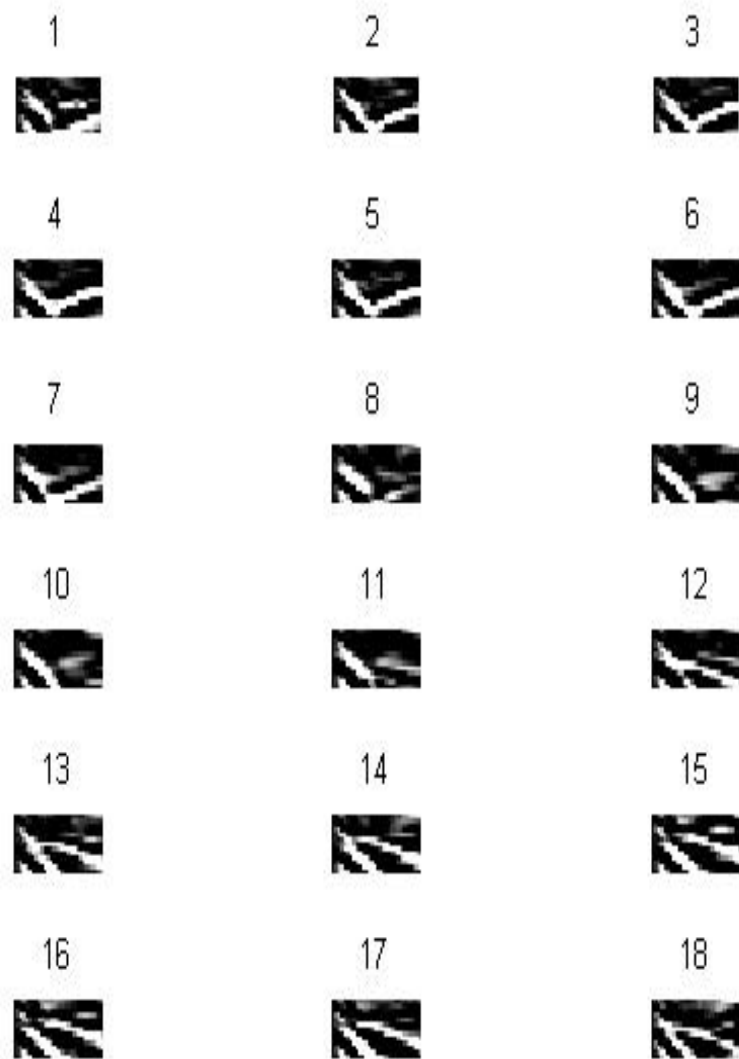


Figure 4.41: 18 radar images axially along the pipes using the 250MHz antenna with 10 integrations (Test 3).

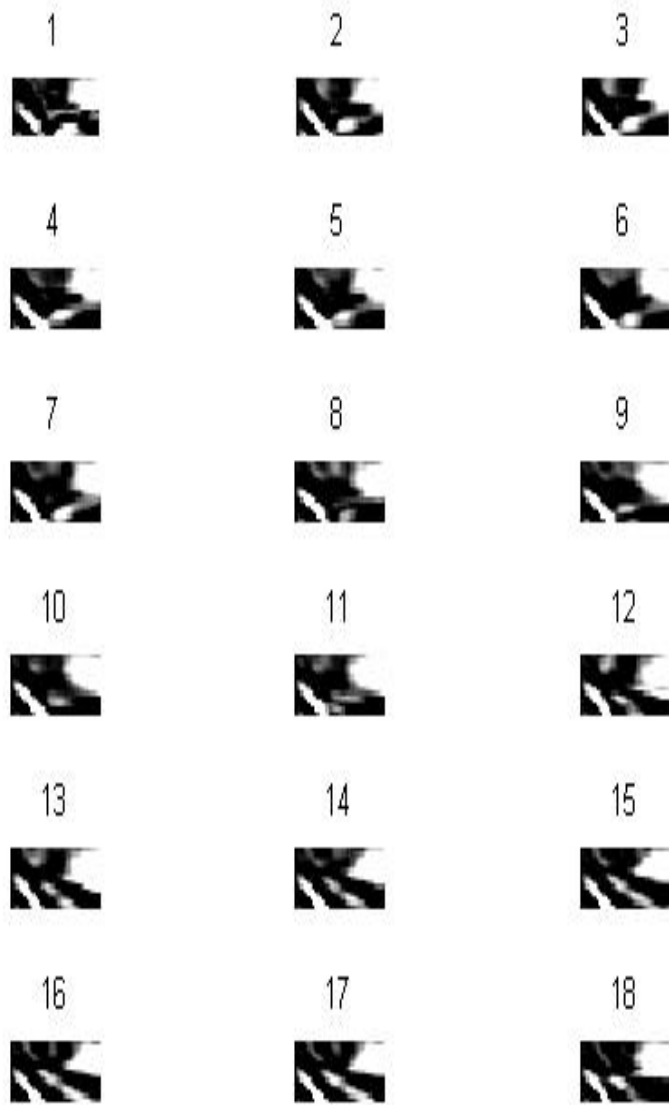


Figure 4.42: 18 radar images axially along the pipes using the 700MHz antenna with 10 integrations (Test 3).

In the experiments where the radar is used perpendicular to the pipe, position 8 is where the hole in the pipe occurs and position 4 is where the undamaged pipe is located (Figure 3.11). Referring to Figures 4.39 and 4.40, we can see that starting from position 7 to position 9, the hyperbola images were slightly distorted. This means that something has occurred in this location and relates to the damaged region in the pipe (this could be related directly to the damage, i.e. the hole, but more likely it is due to the sand entering the pipe, thus creating a different radar response). Meanwhile for Figures 4.41-4.42, it is hard to visually see any change in the signal signature when the GPR is run axially along the pipe.

4.4.2 Identifying the effects of the GPR signal related to the damaged regions relative to the undamaged regions under ‘ideal’ ground conditions

As previously described, in order to identify and quantify the damaged regions the MSE was calculated. The results for the MSE perpendicular to the pipes at 250MHz and 700MHz are shown in Figures 4.43 and 4.44, meanwhile the results for MSE axially along the pipe are shown in Figures 4.45 and 4.46. The red dotted circles in these Figures indicate the maximum MSE values and hence the most likely position for the damaged section of pipe.

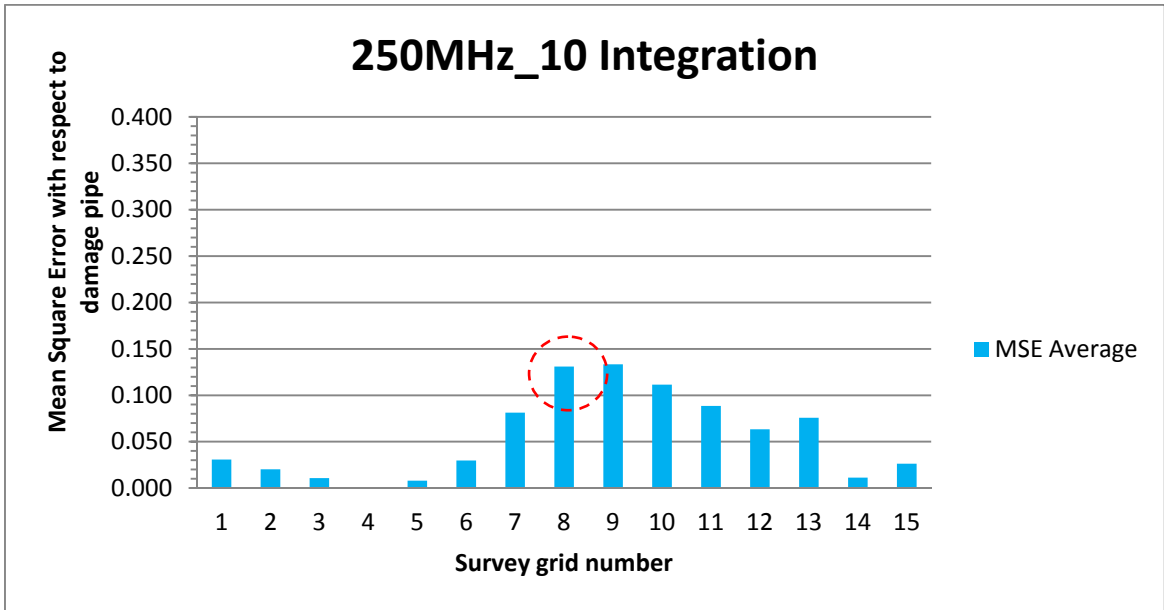


Figure 4.43: MSE for the 250MHz radar at 10 integrations perpendicular to the pipes (Test 3)

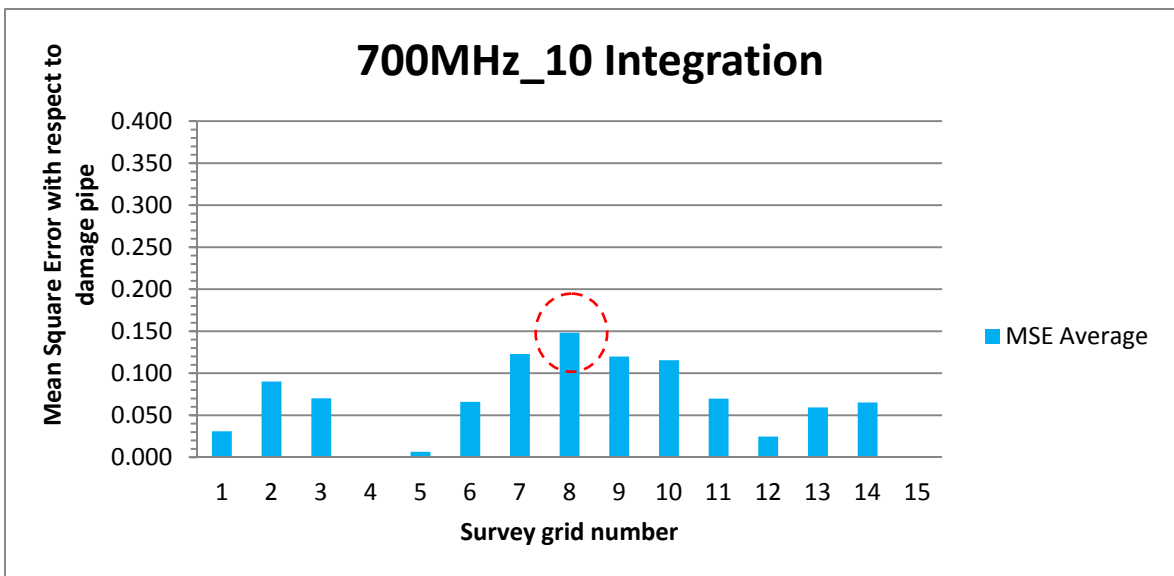
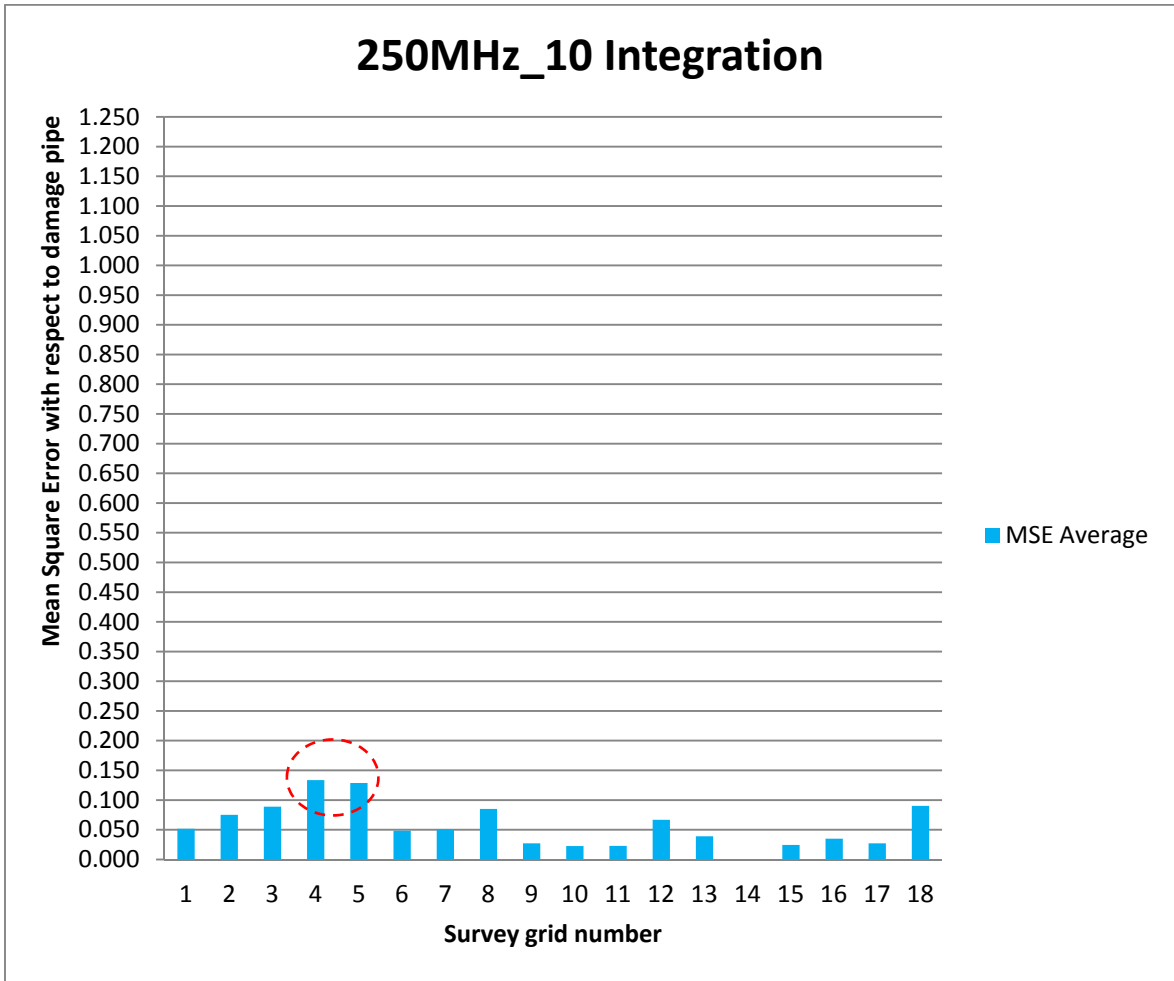
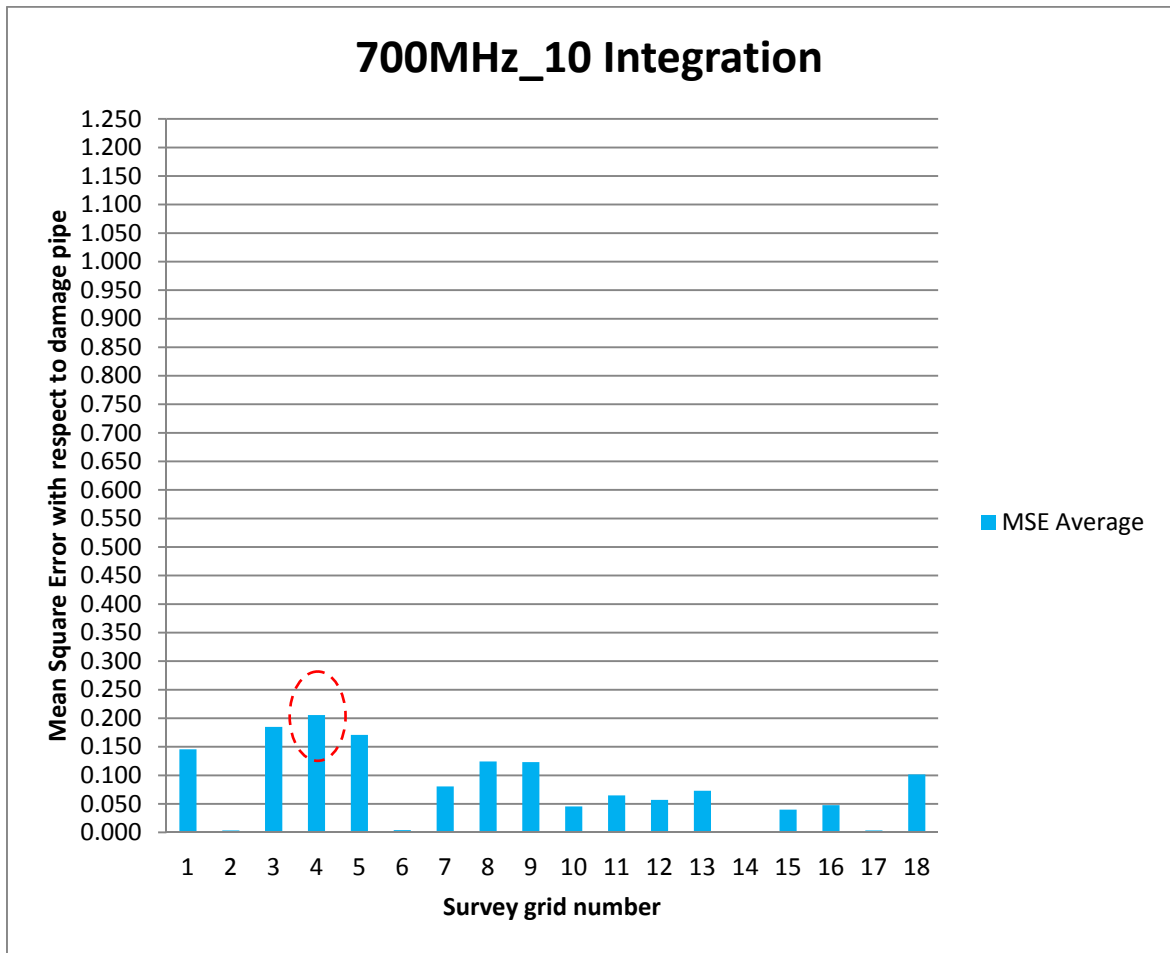


Figure 4.44: MSE for the 700MHz radar at 10 integrations perpendicular to the pipes (Test 3)



**Figure 4.45: MSE for the 250MHz radar at 10 integrations axially along the pipes
(Test 3)**



**Figure 4.46: MSE for the 700MHz radar at 10 integrations axially along the pipes
(Test 3)**

These MSE results for the scans perpendicular to the pipe, confirm the location of the damaged region of pipe seen visually. However, as in the previous test, it was hard to identify the damaged region through visual inspection of the radar images along the pipe, but the results show it was possible to quantify the amplitude changes for the damaged region along the pipe.

A summary of the key findings that can be drawn from these results are:

- i. The result from this test showed that an uncovered hole of 5 cm on the pipe can be detected when sand was allowed to enter the pipe. This is comparable to the result from Test 1 with a completely broken and uncovered section of 5 cm. In both Tests 1 and 3, the Mean Square Error (MSE) methodology located the position of the damage.
- ii. For the survey performed perpendicular to the pipe, grid point 4 is where the pipe is undamaged (well away from the tank wall) and grid point 8 is where the damage occurred in the pipe. The MSE analysis produced a peak relative value at position 8.
- iii. For the survey performed along the pipe, grid point 14 is where the pipe was undamaged and grid point 4 is where the damage occurred in the pipe. The MSE analysis produced a peak relative value at position 4.
- iv. Both frequencies (250 MHz and 700 MHz) are capable of observing the defective regions of the pipe.
- v. The pipe damage was more easily observed, both by visual inspection of the radar scans and by identification of the peak MSE value, when the survey was conducted perpendicular to the pipe (X direction).

4.5 Test 4

The purpose of Test 4 was to understand whether the GPR was capable of detecting a hole in the pipe with a diameter of 5cm (sand prevented from passing through the gap by a polystyrene cover) and to identify and quantify the damaged region of this pipe. The hole was covered with polystyrene as shown in Figure 4.47. As in previous experiments, 15 crossing points perpendicular to the pipe and 18 points along the pipe were conducted for the radar scans.



Figure 4.47: Test 4 – 5 cm hole in the pipe covered by polystyrene prior to being covered with sand

4.5.1 Identifying the signal signature of the damaged and undamaged pipe

The radar scans perpendicular to the pipe and along the pipe was conducted in order to identify the signal signature of the damaged and undamaged pipe. As previously, two types of antenna were tested (i.e. 250MHz and 700MHz). Only the 10 integrations were tested. The radar scan results for the experiments perpendicular to the pipes are shown in Figures 4.48 and 4.49. The red dotted circles once again indicate visual differences in the scans. Meanwhile the radar scans along the pipe as shown in Figures 4.50 and 4.51.

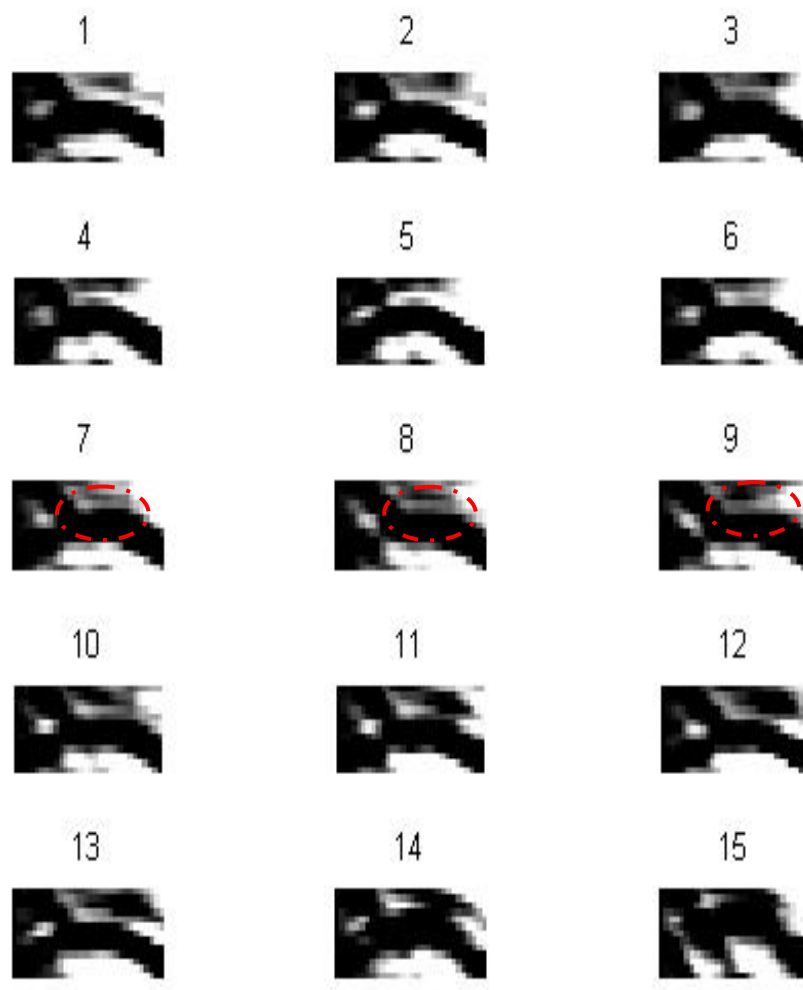


Figure 4.48: 15 radar images perpendicular to the pipes using the 250MHz antenna with 10 integrations (Test 4).

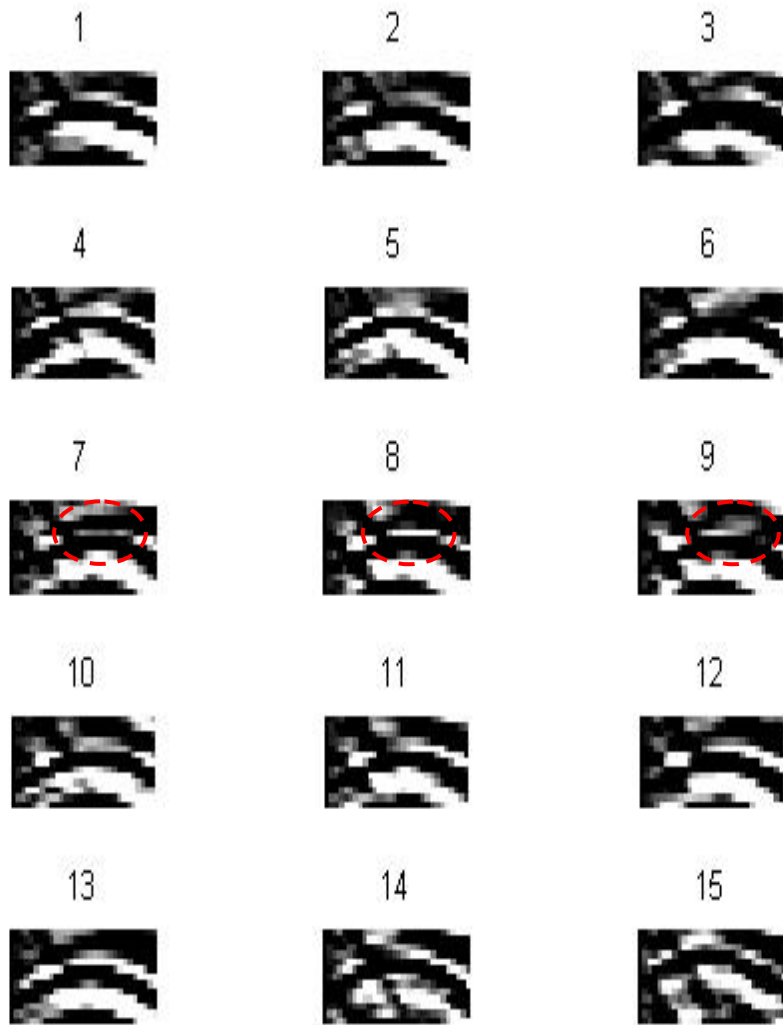


Figure 4.49: 15 radar images perpendicular to the pipes using the 700MHz antenna with 10 integrations (Test 4).

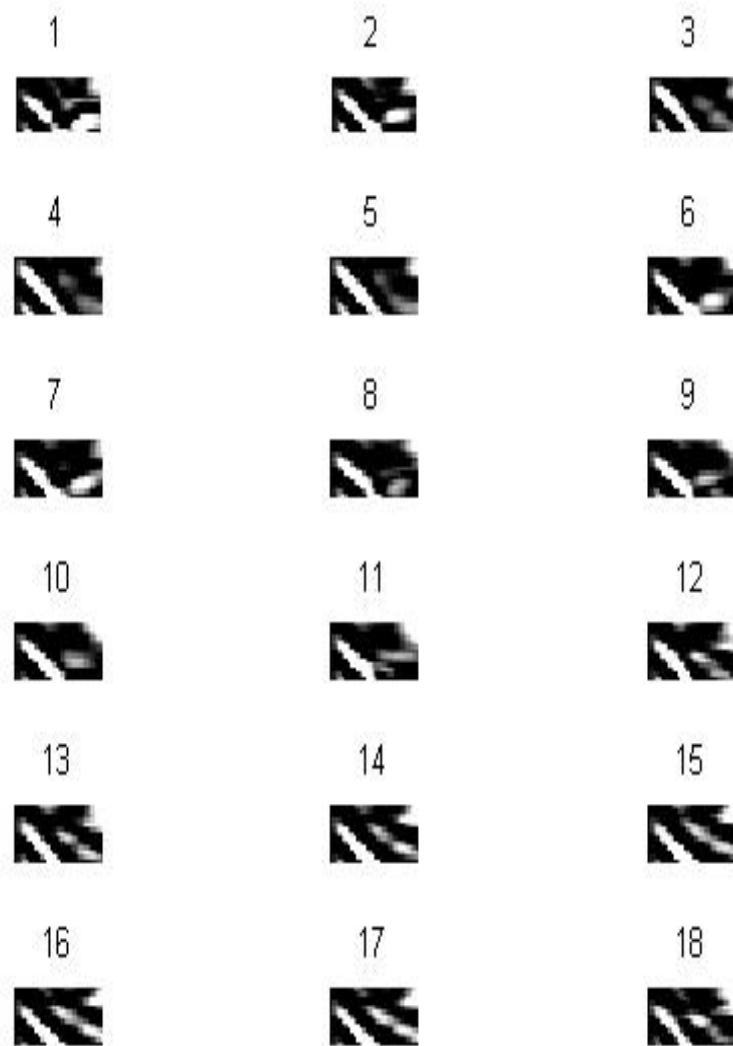


Figure 4.50: 18 radar images axially along the pipes using the 250MHz antenna with 10 integrations (Test 4).

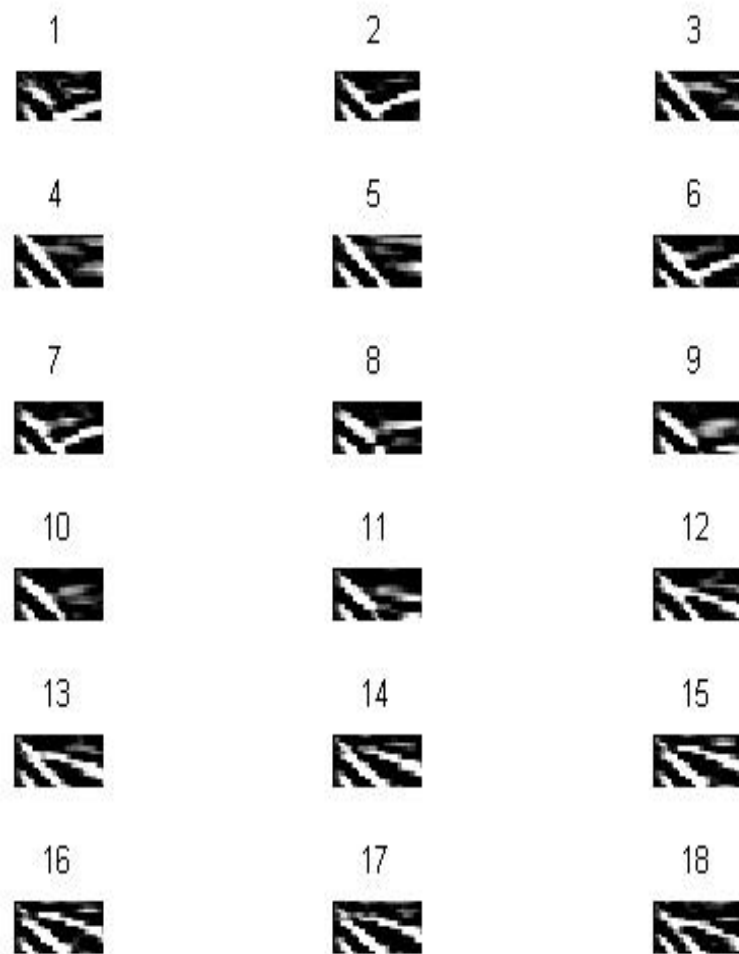


Figure 4.51: 18 radar images axially along the pipes using the 700MHz antenna with 10 integrations (Test 4).

As in the previous experiments for the radar scans perpendicular to the pipe, position 8 is where the hole in the pipe occurs and position 4 is where the undamaged pipe is located

(Figure 3.11). Referring to Figures 4.48 and 4.49, it can be seen that starting from position 7 to position 9, there are some minor differences in the hyperbolae images. This means, something has occurred at these locations potentially related to the damaged region of the pipe. Meanwhile for Figures 4.50 and 4.51, where the radar scans are axially along the pipe, it is hard to visually observe any differences in the signal signatures.

4.5.2 Identifying the effects of the GPR signal related to the damaged regions relative to the undamaged regions under ‘ideal’ ground conditions

As with the previous experiments, in order to help identify the damaged regions, the MSE was calculated. The results for the MSE perpendicular to the pipes at 250MHz and 700MHz are shown in Figures 4.52 and 4.53, meanwhile the results for MSE axially along the pipe are shown in Figures 4.54 and 4.55.

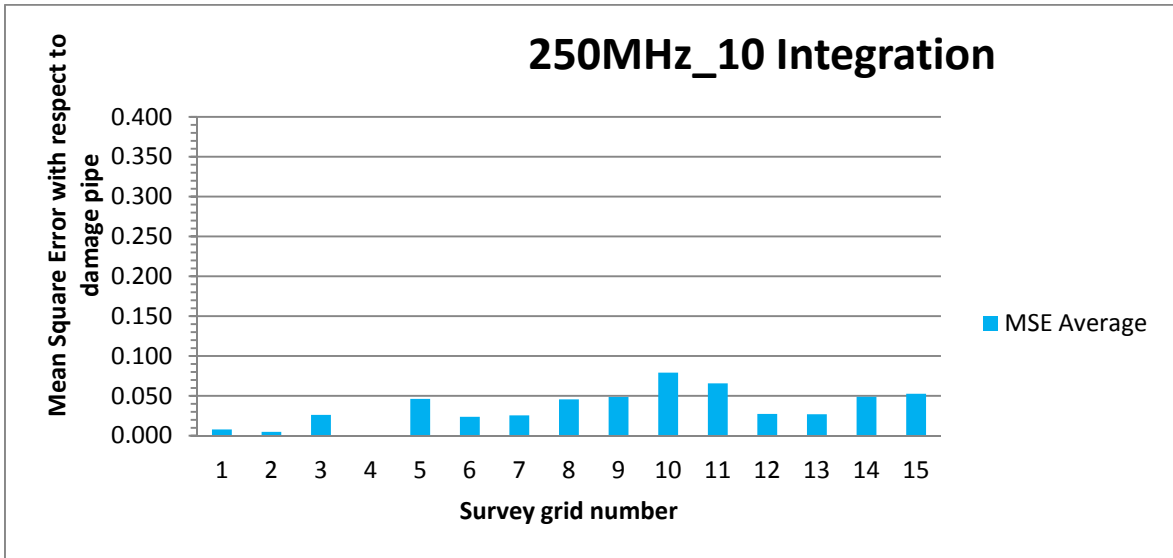


Figure 4.52: MSE for the 250MHz radar at 10 integrations perpendicular to the pipes (Test 4).

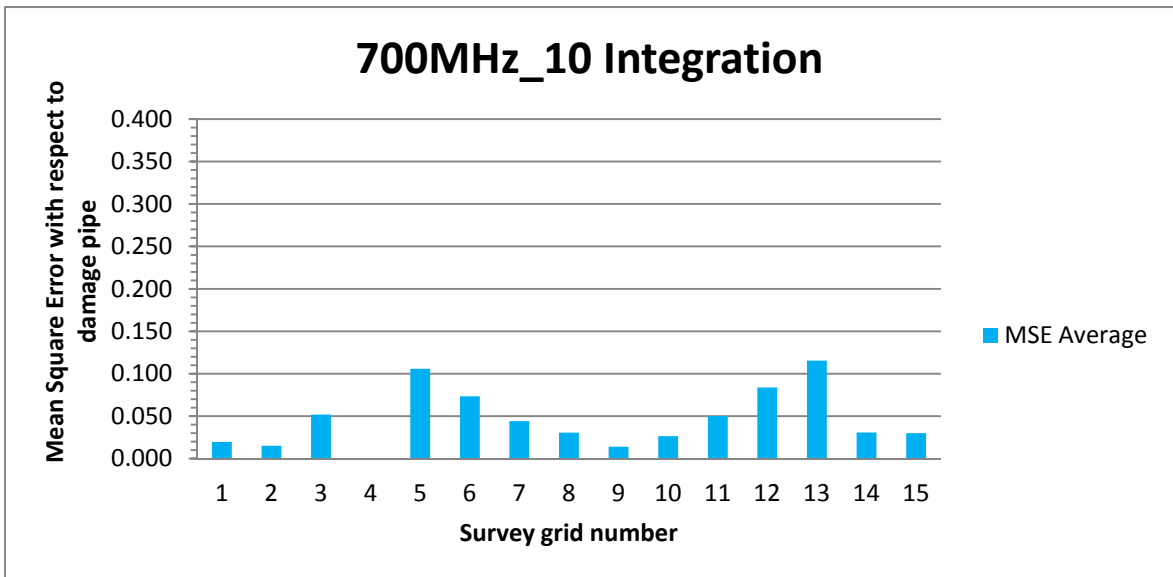


Figure 4.53: MSE for the 700MHz radar at 10 integrations perpendicular to the pipes (Test 4).

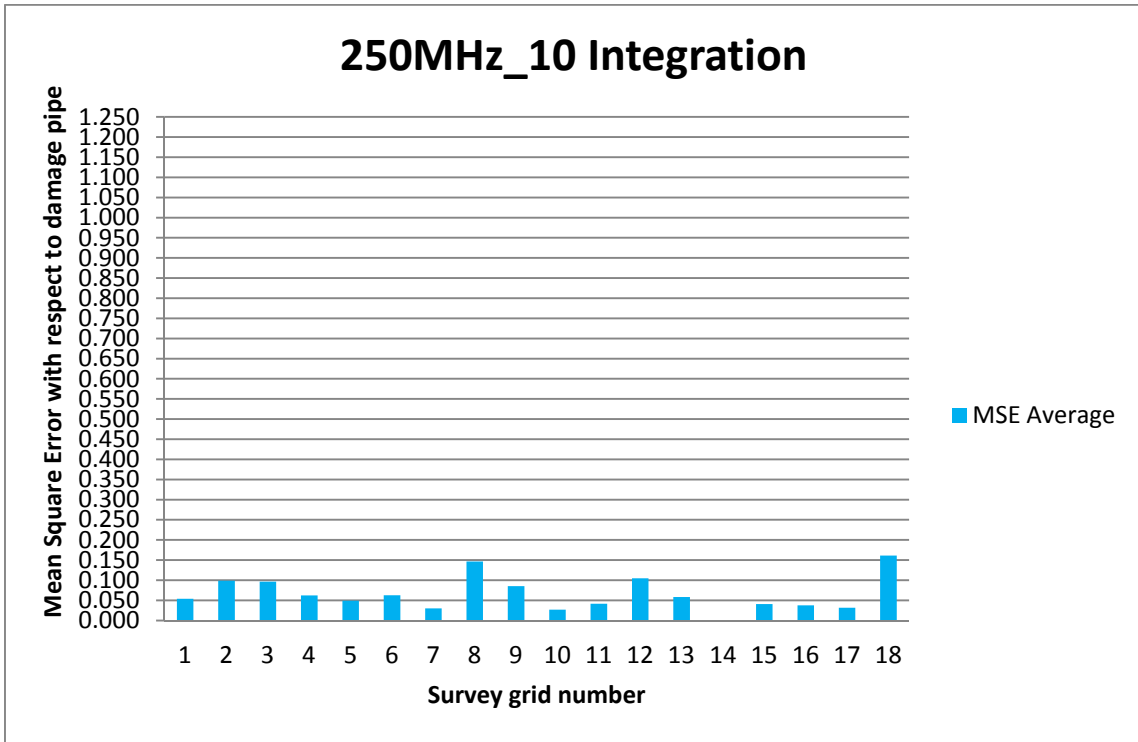


Figure 4.54: MSE for the 250MHz radar at 10 integrations axially along the pipes (Test 4).

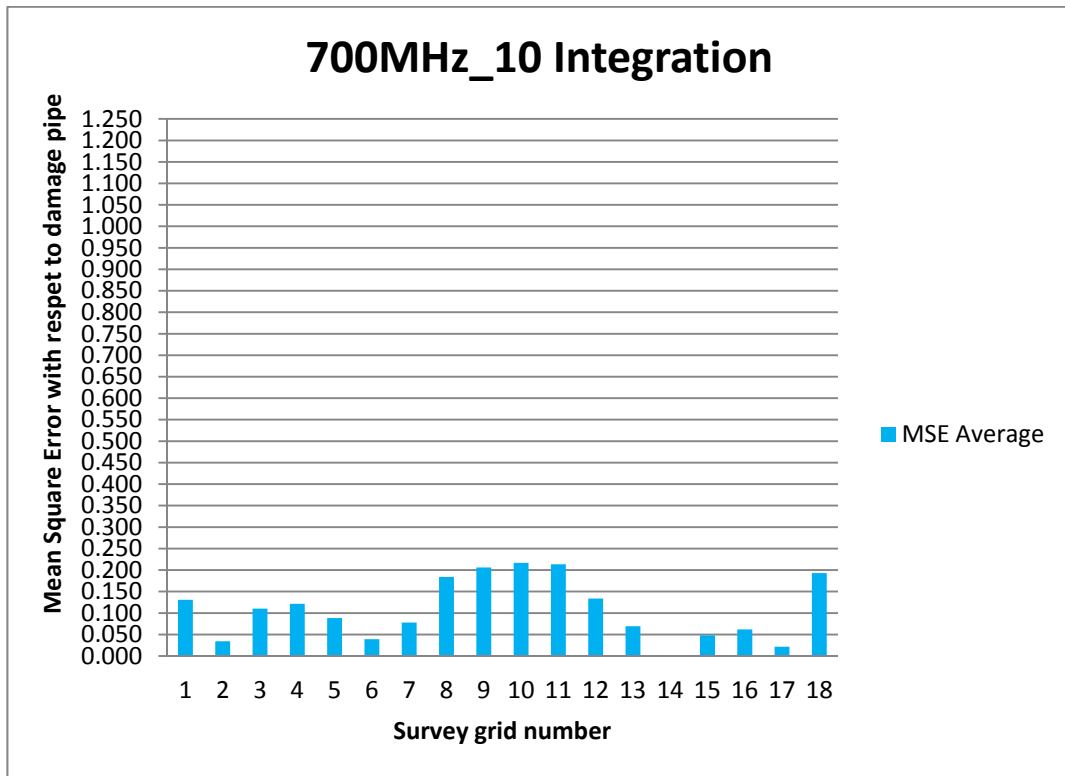


Figure 4.55: MSE for the 700MHz radar at 10 integrations axially along the pipes (Test 4).

Even though it is possible to use the radar images to show that something was occurring at a particular area for scans perpendicular to the pipe (position 8), using the MSE analysis, the damage region cannot be identified. This is also true for the MSE analysis of the radar scans axially along the pipe. As with the results for Test 2, it was hard to identify the damaged region without allowing the sand to pass into the pipe and hence it appears to be the radar response caused by the sand within the pipe rather than the damage itself that is being observed.

A summary of the key findings that can be drawn from these results are:

- i. Although there was a discernible anomaly on the radar traces, it was not immediately obvious by visual inspection, and it may arguably require some a-priori knowledge of the region of damage.
- ii. With the MSE analysis, it is also not possible to accurately locate the position of the damage in this test. The peak MSE value did not correctly indicate the position of the damage for any combination of frequencies and survey directions in this test. This result is similar to Test 2, such that both had damage sections that were covered, preventing sand from entering the pipe. In addition, the materials covering the damage had similar dielectric permittivities as the pipe. The result thus far also suggest that most of the reflected signal is as a result of the pipe-air-pipe interface. It follows that the pipe damage seen and detectable by the MSE analysis are where the damage is uncovered and hence is likely to be due to the lack of a clear pipe-air-pipe interface caused by sand in-fill compared to other locations along the pipe.

4.6 Test 5

The purpose of Test 5 was similar to Test 4. However, in this test, a hole in the pipe with a diameter of 5 cm was covered by a fabric. The reason why this fabric is used is to understand and reconfirm that the GPR are not capable of identifying the damage without

any associated materials passing through the gap. The hole covered with fabric is shown in Figure 4.56. The grid lines used for this experiment were same as in the previous Test 4.

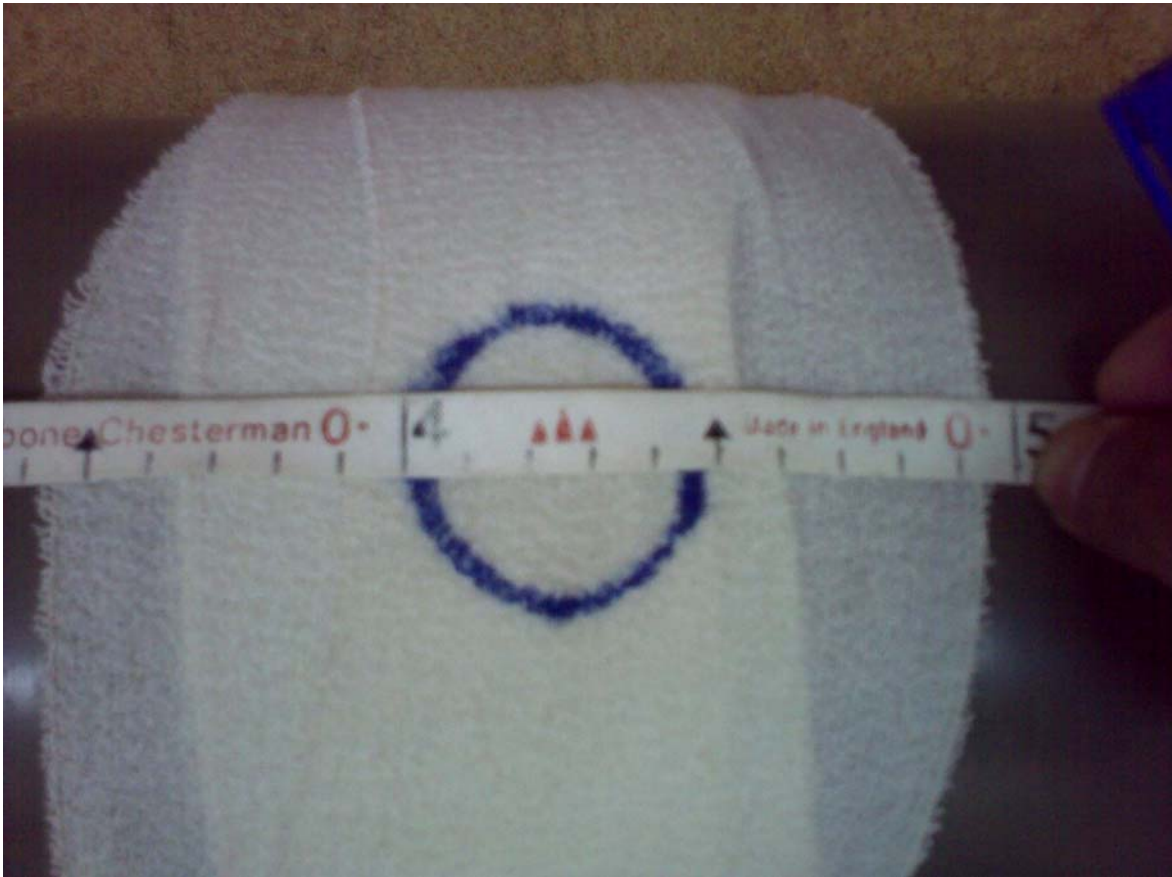


Figure 4.56: Test 5 – 5cm diameter hole in the pipe covered by fabric prior to being covered by sand.

4.6.1 Identifying the signal signature of the damaged and undamaged pipe

Radar scans perpendicular to the pipe and axially along the pipe were conducted in order to identify the signal signature of the damaged and undamaged pipe. As with the previous tests, two types of antenna were tested (i.e. 250MHz and 700MHz). The radar scan results of these experiments perpendicular to the pipes are shown in Figures 4.57 and 4.58. Meanwhile the radar scans along the pipe are shown in Figures 4.59 and 4.60.

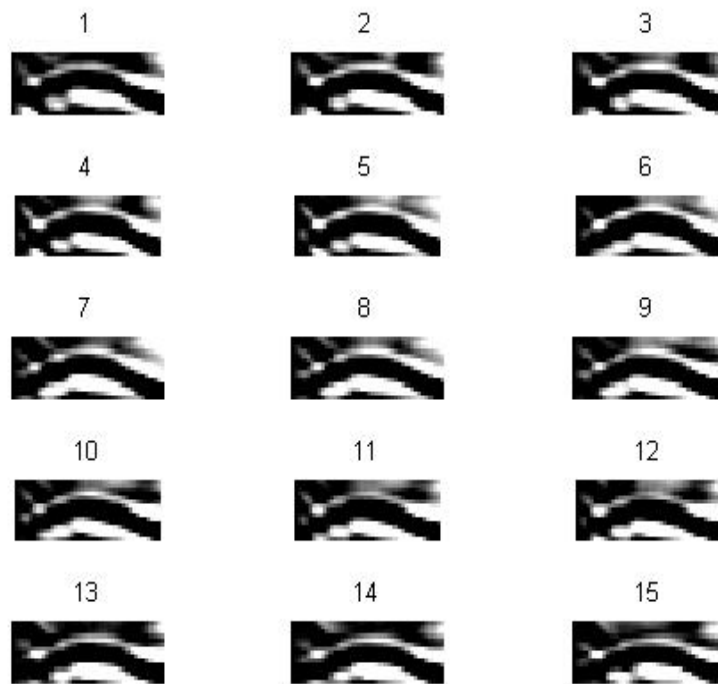


Figure 4.57: 15 radar images perpendicular to the pipes using the 250MHz antenna with 10 integrations (Test 5).

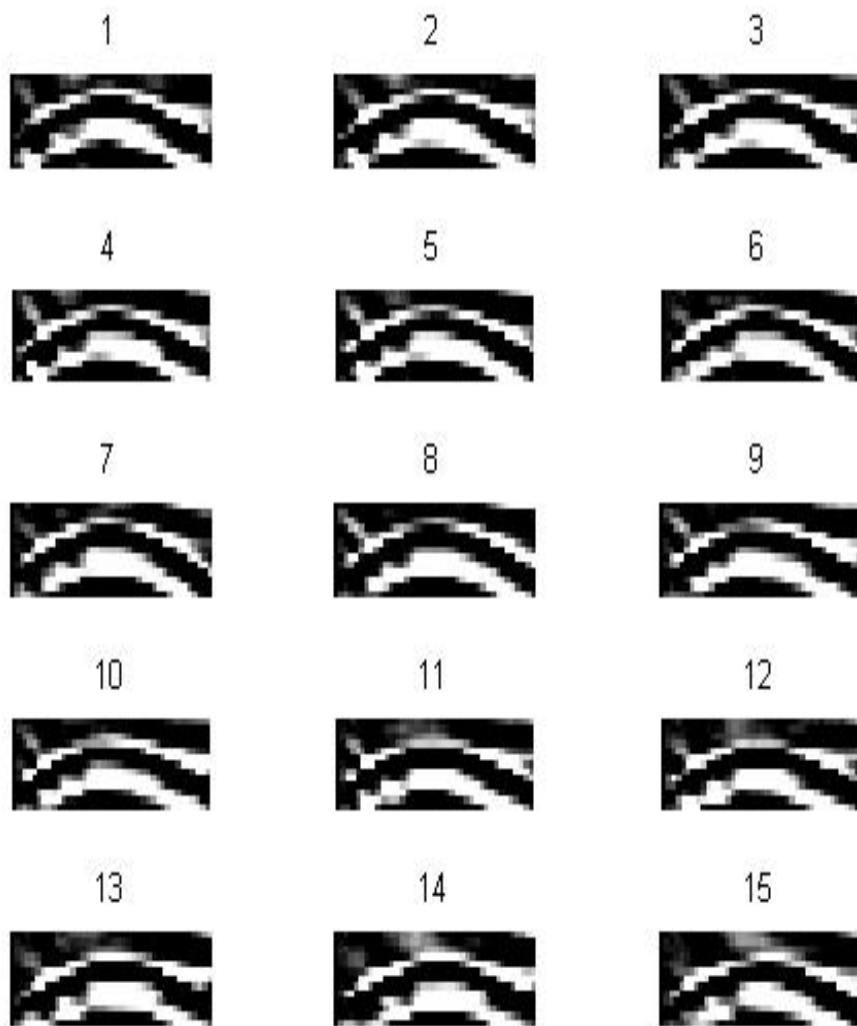


Figure 4.58: 15 radar images perpendicular to the pipes using the 700MHz antenna with 10 integrations (Test 5).

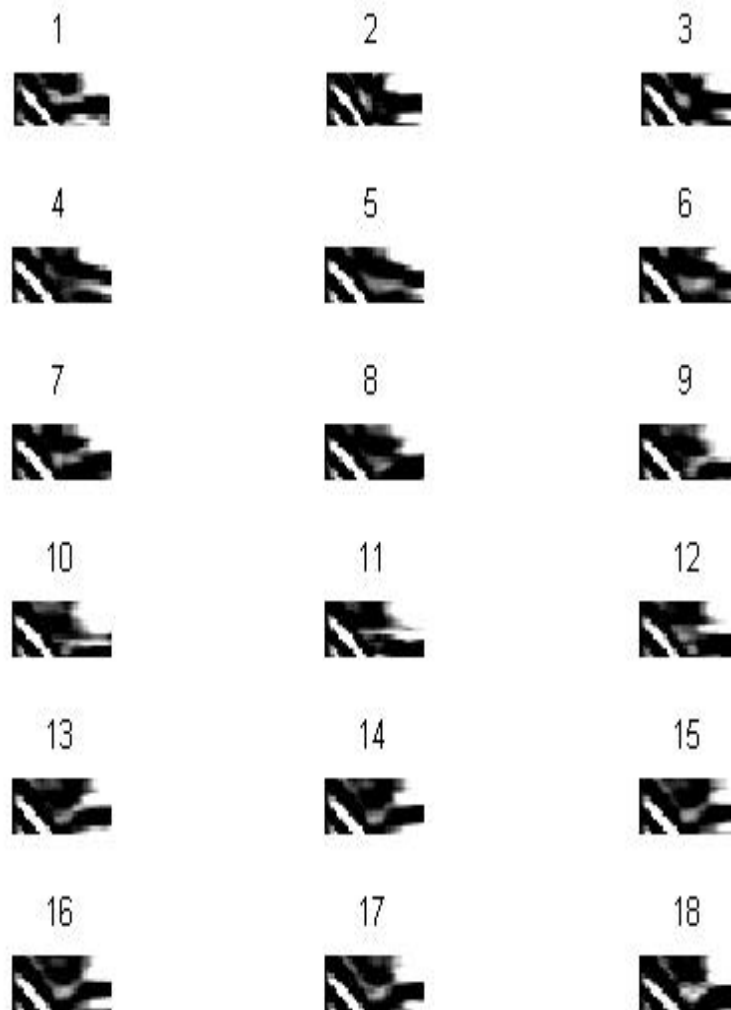


Figure 4.59: 18 radar images axially along the pipes using the 250MHz antenna with 10 integrations (Test 5).

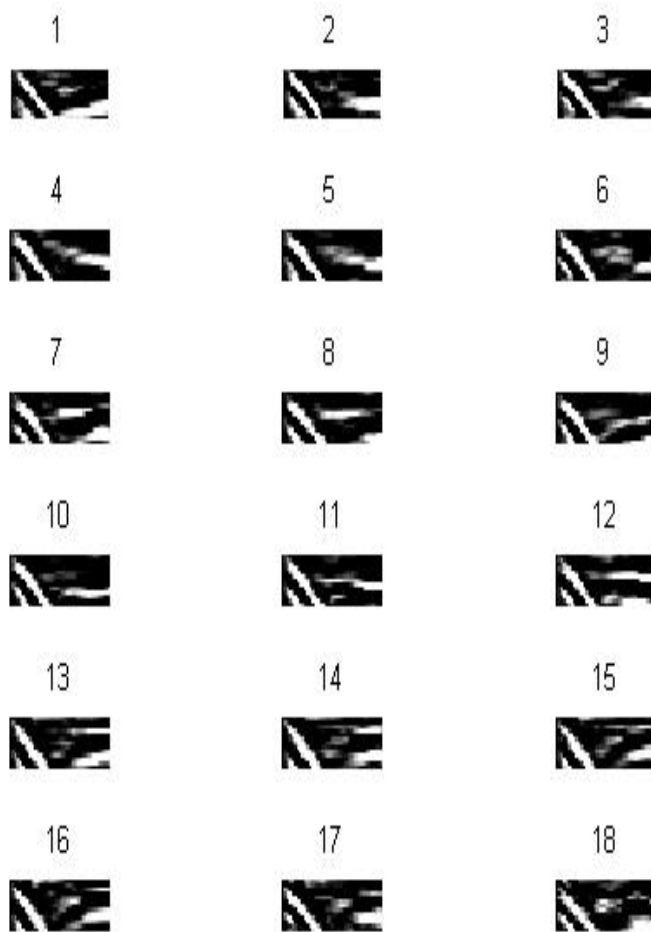


Figure 4.60: 18 radar images axially along the pipes using the 700MHz antenna with 10 integrations (Test 5).

All the radar images for both frequencies in this test could not be used to detect the damaged pipe region by visual inspection. However, MSE analyses were conducted on the radar scans to quantify any differences as shown in the next section.

4.6.2 Identifying the effects of the GPR signal related to the damaged regions relative to the undamaged regions under ‘ideal’ ground conditions

As mentioned in previous experiments, in order to identify and quantify the damaged regions, the MSE was calculated for the various radar scans. The results for the MSE perpendicular to the pipes at 250MHz and 700MHz are shown in Figures 4.61 and 4.62, meanwhile the results for MSE axially along the pipe are shown in Figures 4.63 and 4.64.

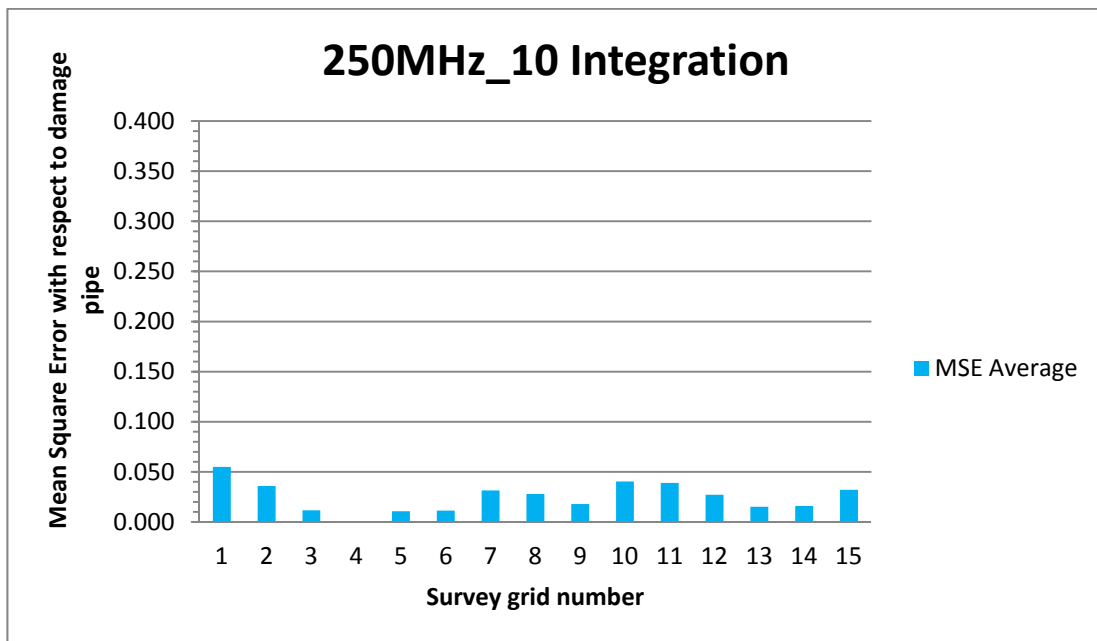


Figure 4.61: MSE for the 250MHz radar at 10 integrations perpendicular to the pipes (Test 5).

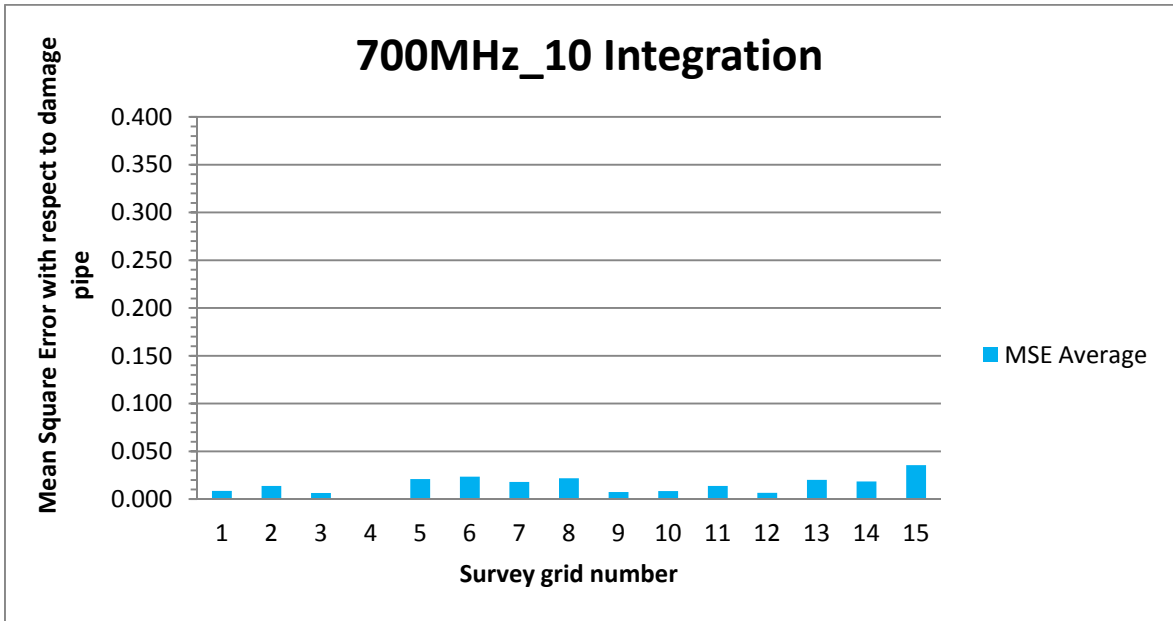


Figure 4.62: MSE for the 700MHz radar at 10 integrations perpendicular to the pipes (Test 5).

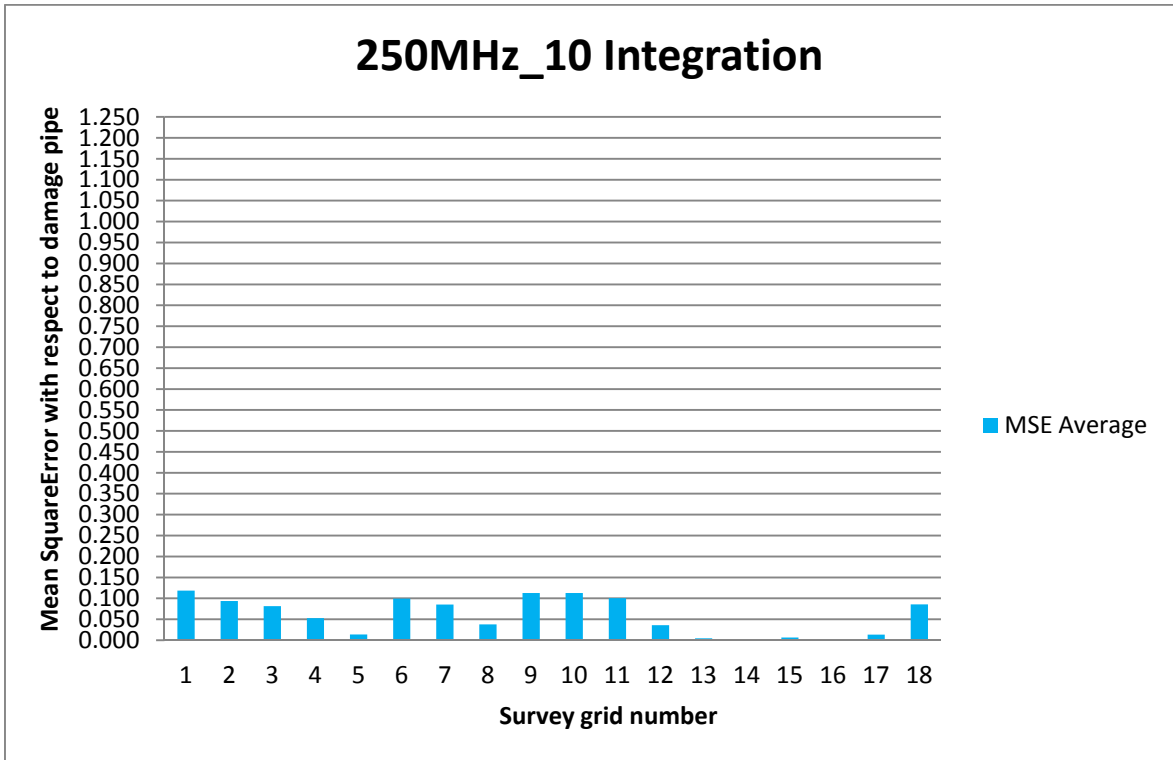


Figure 4.63: MSE for the 250MHz radar at 10 integrations axially along the pipes (Test 5).

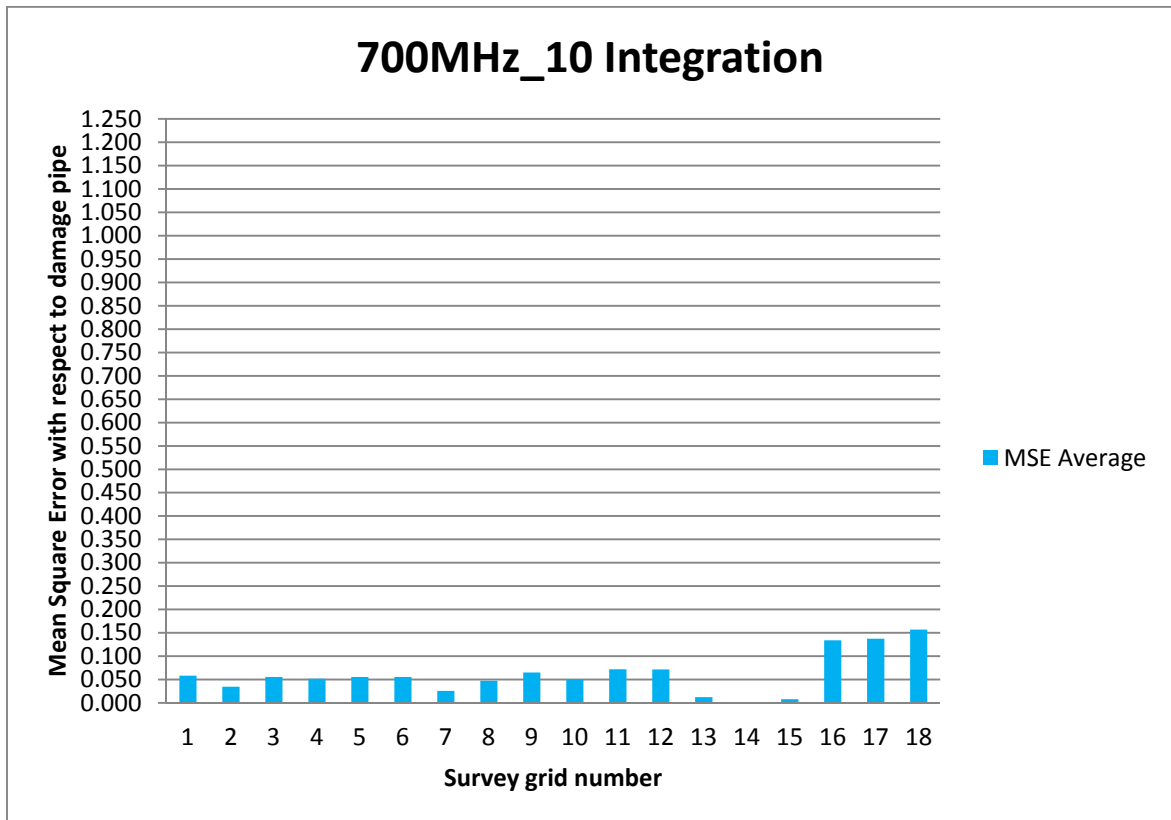


Figure 4.64: MSE for the 700MHz radar at 10 integrations axially along the pipes (Test 5).

In this test, the MSE analyses of the radar images were unsuccessful in identifying the damaged pipe region. Preventing sand entry into the pipe by using the fabric results in no differences in the radar images between the damaged and undamaged pipe sections. This further implies that the damaged pipe section can only be detected if some materials enter the pipe.

The key finding that can be drawn from these results is:

- i. As in previous tests in which the pipe damage was covered by a plastic cover and expanded polystyrene, this test with the fabric cover also indicated that it was not possible to identify a strong anomaly by visual inspection or MSE analysis. This suggests that the sand entering the pipe where the damage in uncovered was crucial in introducing anomalies in the radar scans that led to accurate detection.

4.7 Test 6

The purpose of Test 6 was similar to Test 1. However, in this test, a broken pipe with a 5cm gap under a fabric cover was tested. As in the previous tests, the reason why this fabric is used was to understand and reconfirm that the GPR is not capable of identifying the damage without any associated materials passing through the gap and to see if the material covering the damaged pipe had any influence. The broken pipe covered with fabric is shown in Figure 4.65.



Figure 4.65: Test 6 - Broken pipe with a 5cm gap (sand prevented from passing through the gap by a fabric cover)

4.7.1 Identifying the signal signature of the damaged and undamaged pipe

Radar scans perpendicular to the pipe and along the pipe were conducted in order to identify the signal signatures of the damaged and undamaged pipe. As previously, two types of antenna were tested (i.e. 250MHz and 700MHz). The radar scan results of these experiments perpendicular to the pipes are shown in Figures 4.66 and 4.67. Meanwhile the radar scans axially along the pipe are shown in Figures 4.68 and 4.69.

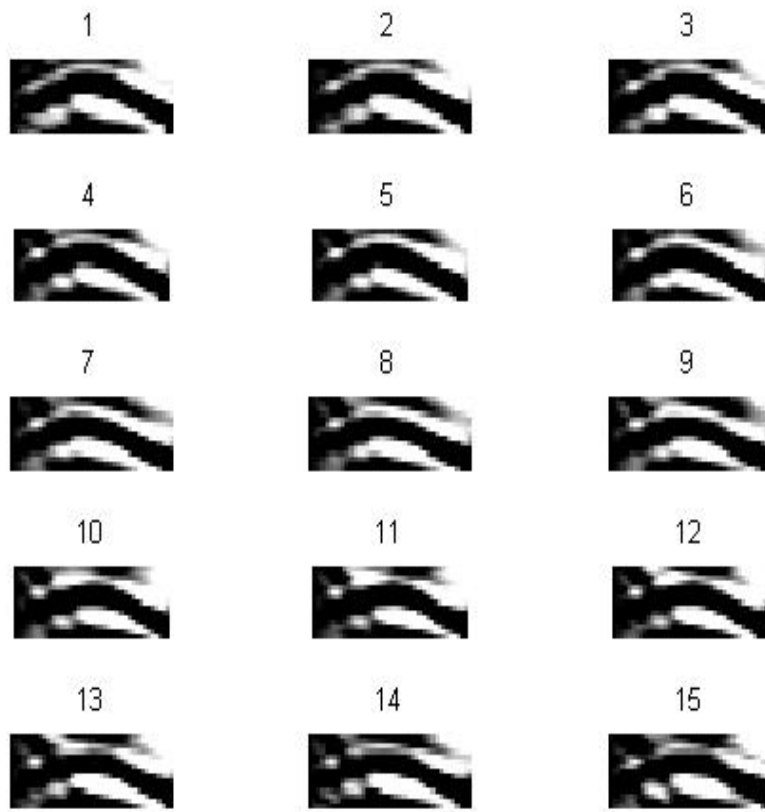


Figure 4.66: 15 radar images perpendicular to the pipes using the 250MHz antenna with 10 integrations (Test 6)

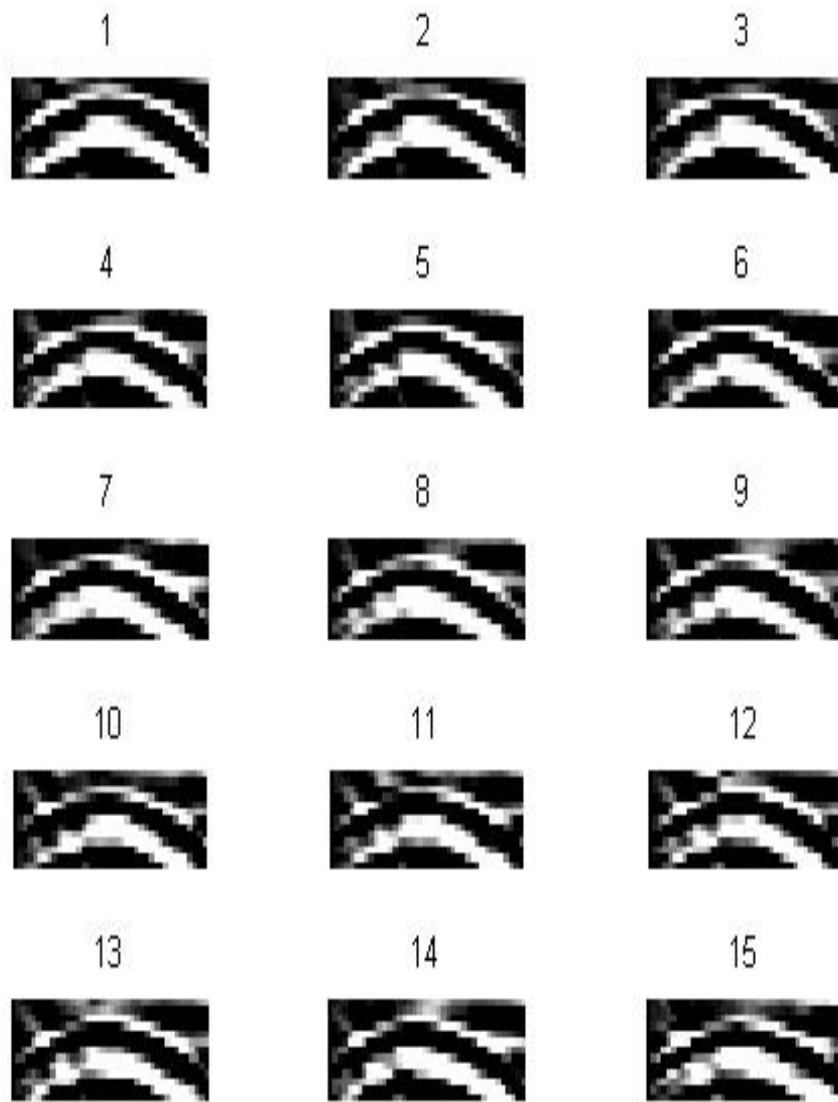


Figure 4.67: 15 radar images perpendicular to the pipes using the 700MHz antenna with 10 integrations (Test 6)

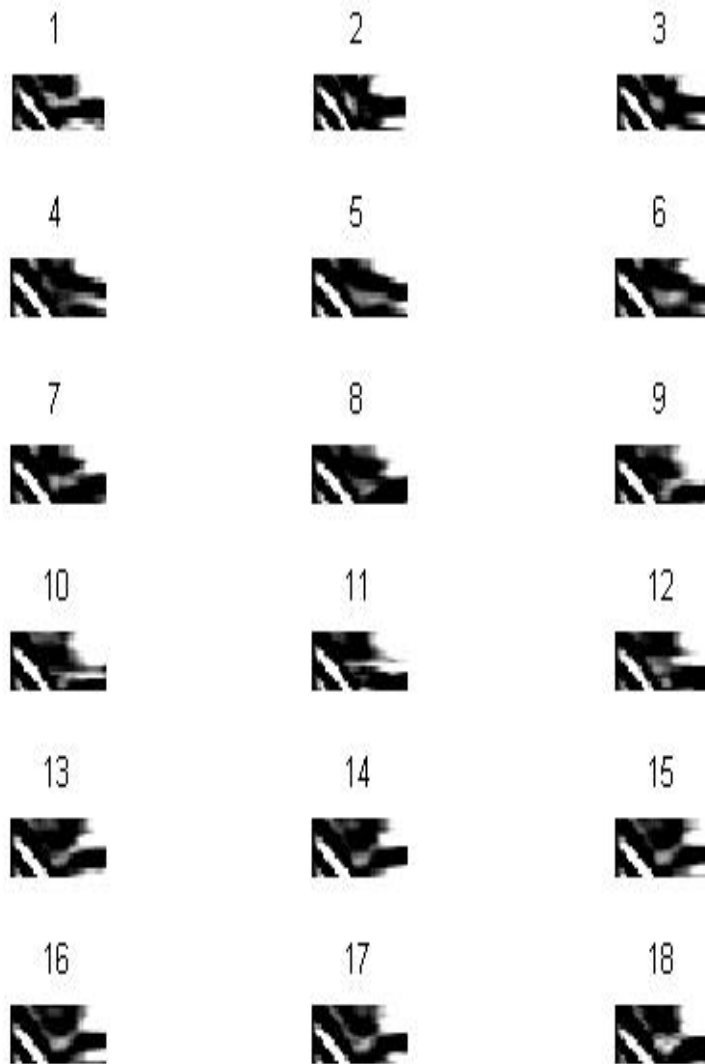


Figure 4.68: 18 radar images axially along the pipes using the 250MHz antenna with 10 integrations (Test 6)

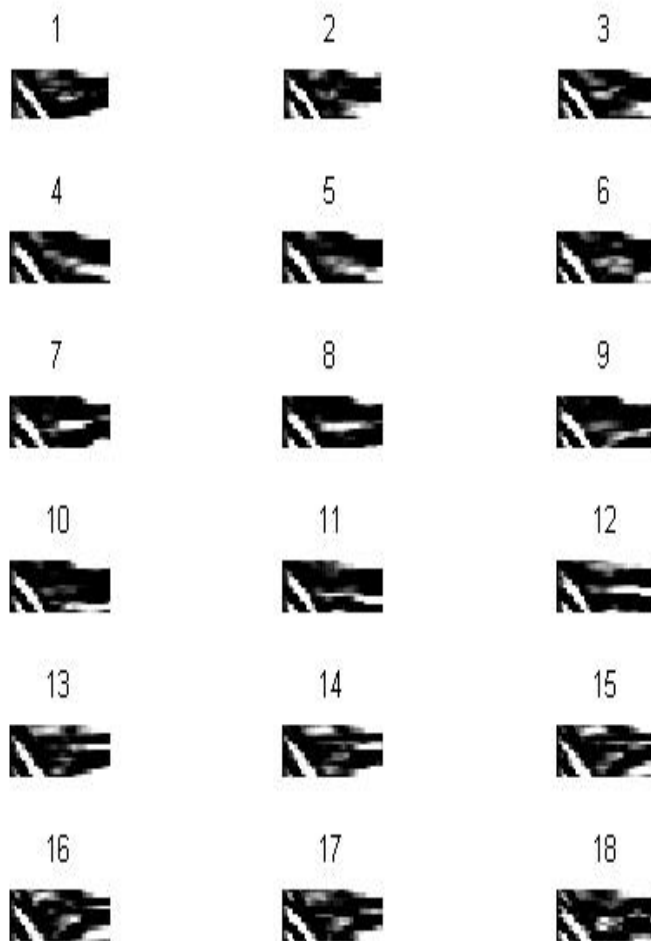


Figure 4.69: 18 radar images axially along the pipes using the 700MHz antenna with 10 integrations (Test 6)

Visual inspection of all the radar images for both frequencies was unable to identify the damaged region in the pipe. However, MSE analyses were conducted on the radar scans to quantify any differences as shown in the next section.

4.7.2 Identifying the effects of the GPR signal related to the damaged regions relative to the undamaged regions under ‘ideal’ ground conditions

As mentioned in previous experiments, in order to identify the damaged regions, the MSE was calculated for the radar scans. The results for the MSE perpendicular to the pipes at 250MHz and 700MHz are shown in Figures 4.70 and 4.71, meanwhile the results for the MSE along the pipe are shown in Figures 4.72 and 4.73.

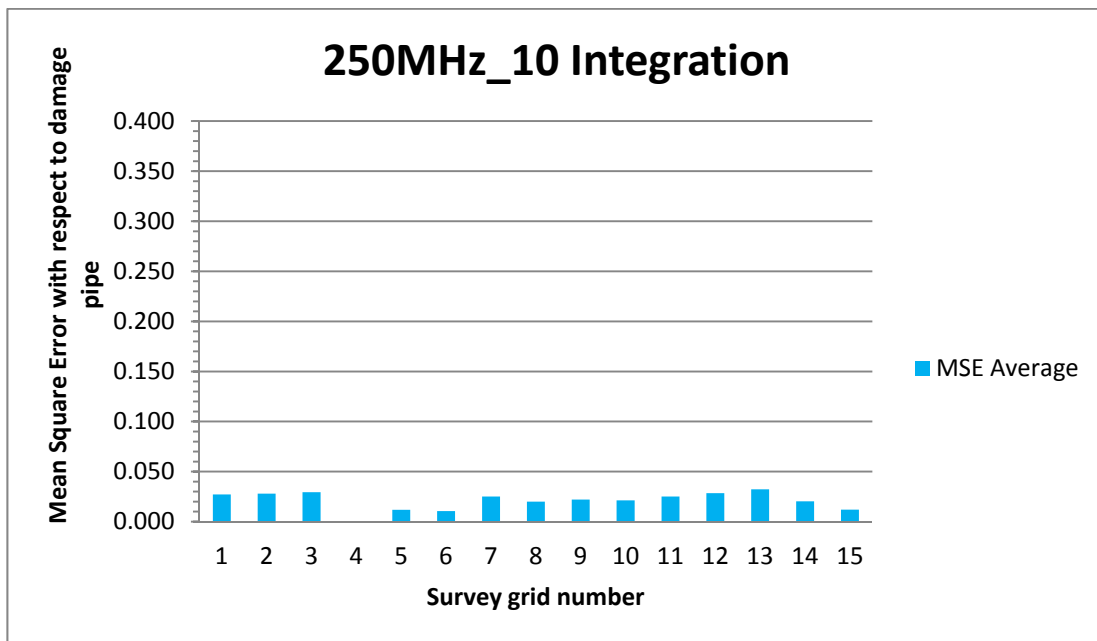


Figure 4.70: MSE for the 250MHz radar at 10 integrations perpendicular to the pipes (Test 6).

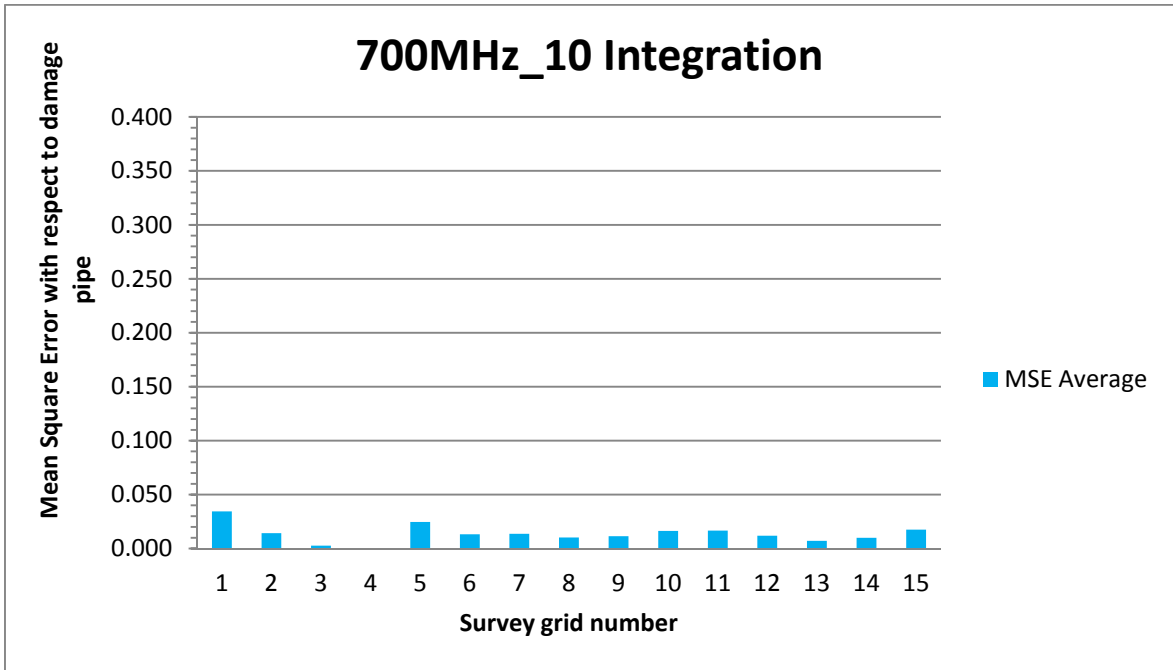


Figure 4.71: MSE for the 700MHz radar at 10 integrations perpendicular to the pipes (Test 6).

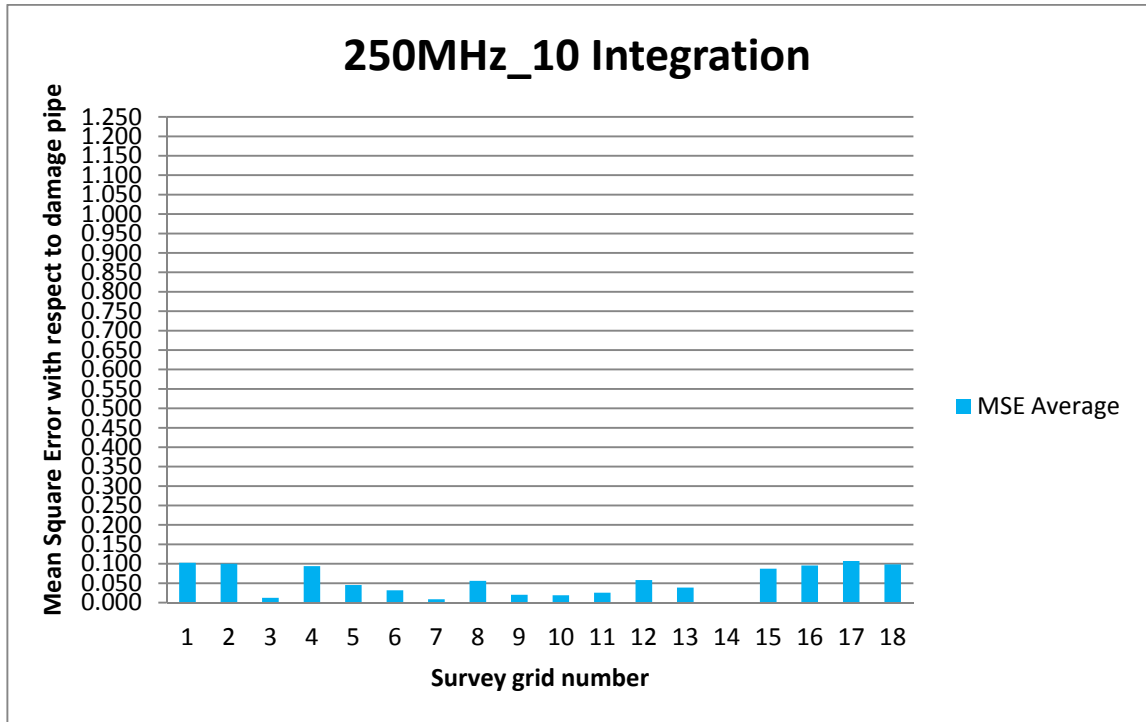


Figure 4.72: MSE for the 250MHz radar at 10 integrations axially along the pipes (Test 6).

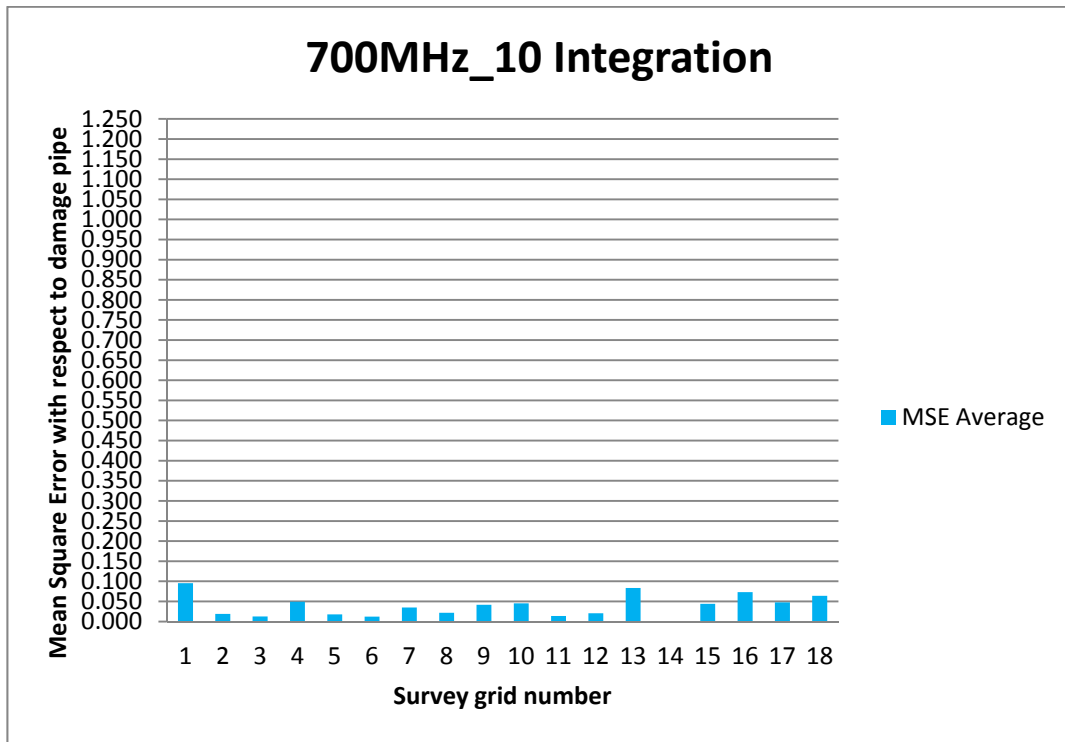


Figure 4.73: MSE for the 700MHz radar at 10 integrations axially along the pipes (Test 6).

A summary of the key findings that can be drawn from these results are:

- i. As with the previous tests where the damaged section was covered and there was no sand allowed to enter the pipe, it was not possible to accurately locate the damage using either visual inspection of the radar traces or the MSE analysis.
- ii. The test further confirms that the anomaly in the radar scans associated with the damaged section of the pipe observed in other tests was caused by the infill of

sand, which resulted in a discontinuity of the pipe-air-pipe interface compared to other regions along the pipe. The test also confirms that the type of damage, such as a small hole or a 5 cm breakage, did not contribute any observable effect to the anomaly.

4.8 Test 7

In this experiment, a hole in the pipe with a diameter of 5cm was created (Figure 4.74). The sand was prevented from passing through the gap by a sponge blocking the hole, but in this test the sponge was removed by drawing it into the pipe as part of the test (Figure 4.75). The GPR data was taken before and after the sponge was pulled out.



Figure 4.74: Test 7 - A 5cm diameter hole in the pipe



Figure 4.75. Test 7 - A sponge was used to block the hole in the pipe that could be subsequently removed

4.8.1 Identifying the signal signature of the damaged and undamaged pipe

Radar scans perpendicular to the pipe and along the pipe were conducted in order to identify the signal signatures of the damaged and undamaged pipe. Two types of antenna were tested (i.e. 250MHz and 700MHz). The radar scan results of these experiments perpendicular to the pipe before the sponge was removed are shown in Figures 4.76 and 4.77. The radar scans after the sponge was removed are shown in Figures 4.78 and 4.79

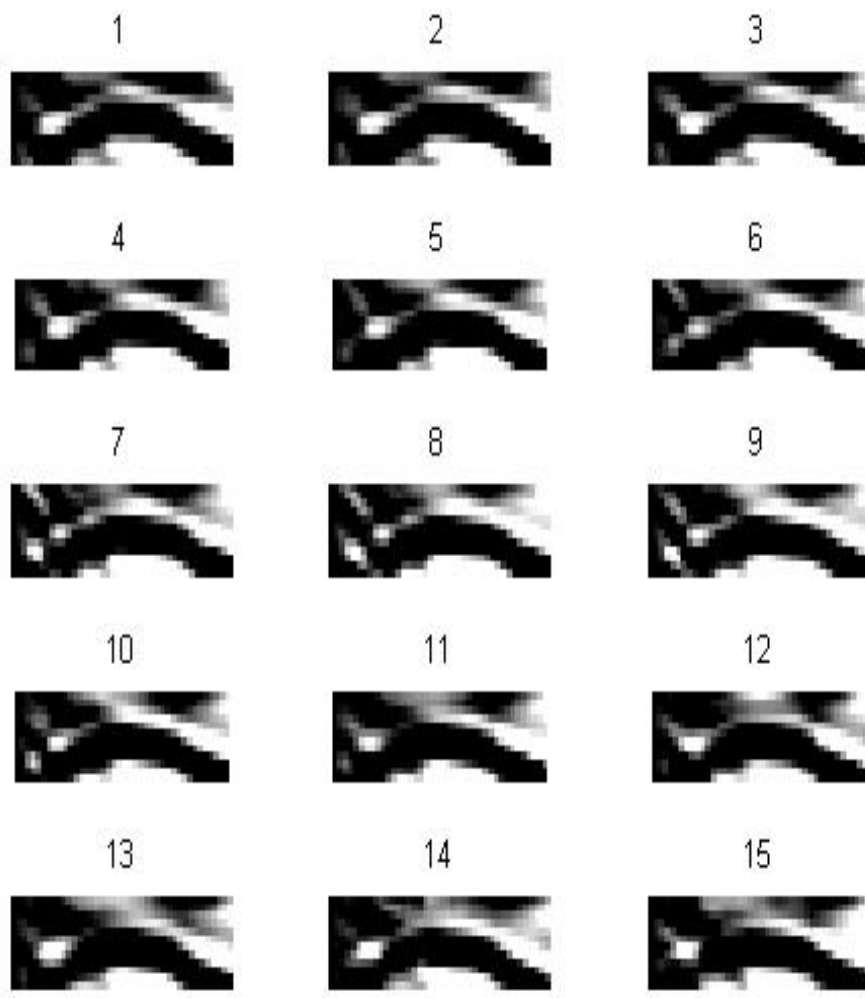


Figure 4.76: Test 7 - 15 radar images perpendicular to the pipes using the 250MHz antenna (before the sponge was removed).

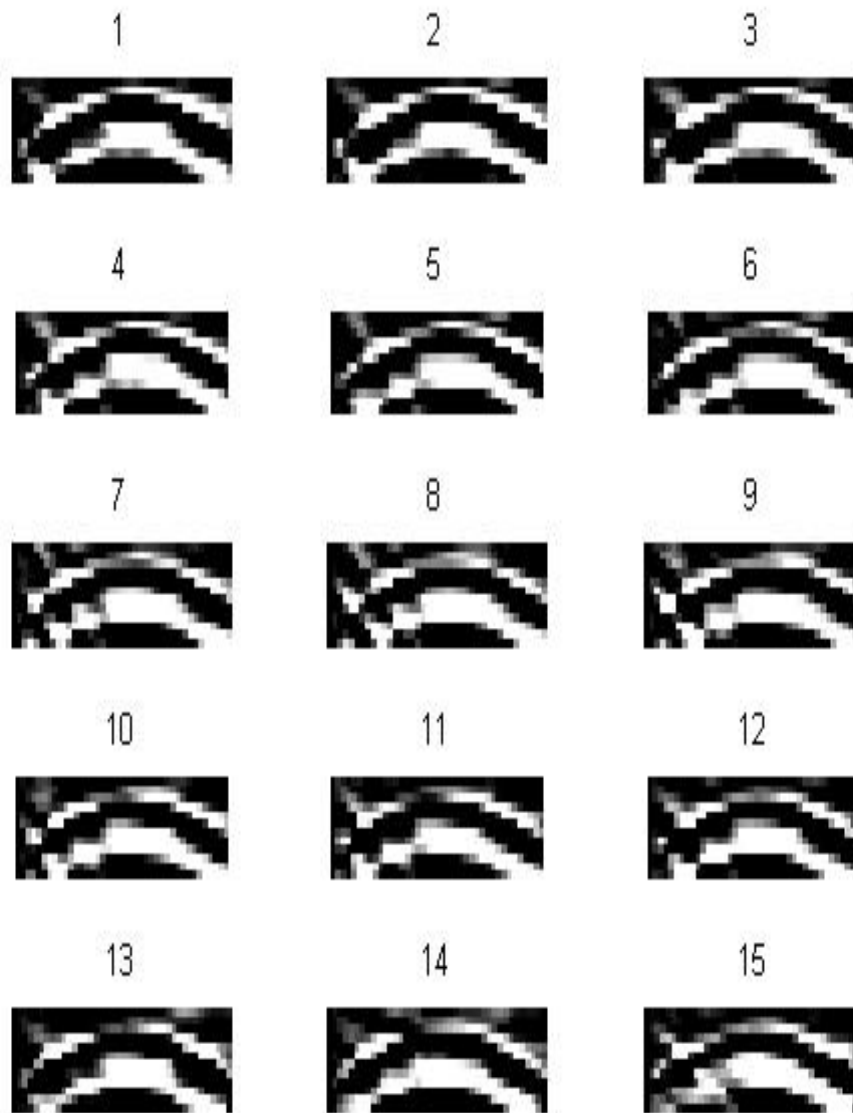


Figure 4.77: Test 7 - 15 radar images perpendicular to the pipes using the 700MHz antenna (before the sponge was removed).

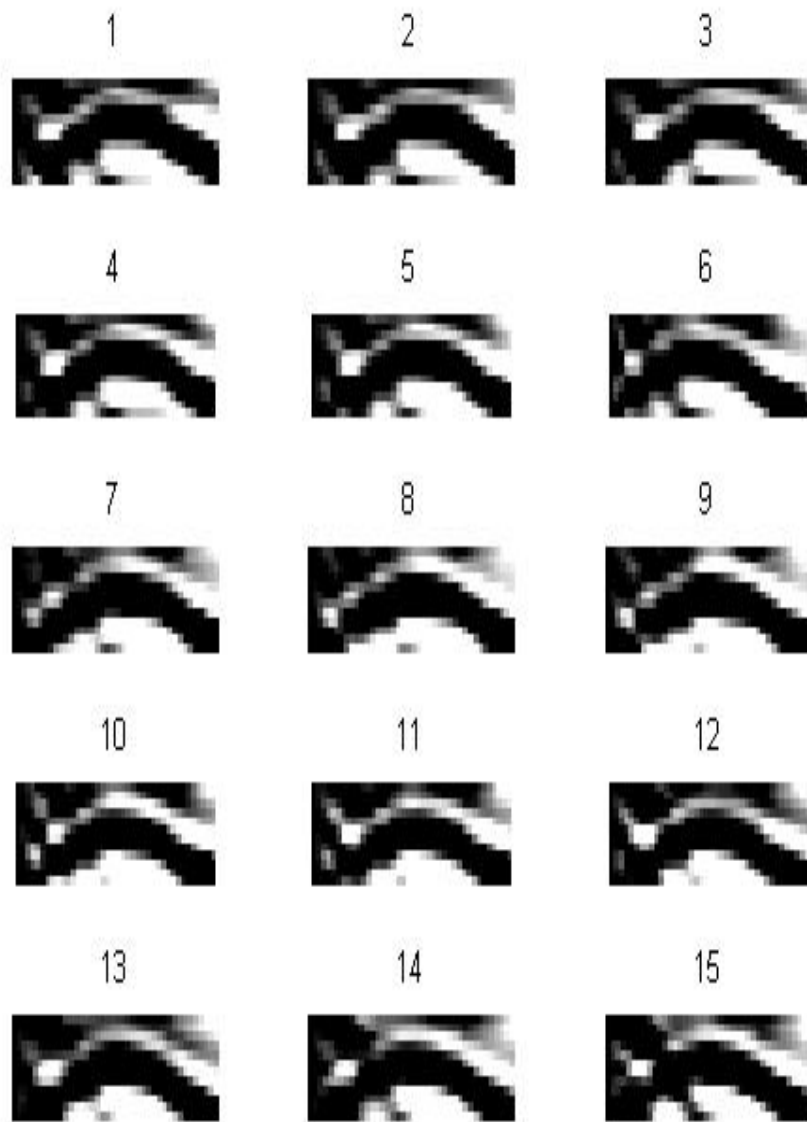


Figure 4.78: Test 7 - 15 radar images perpendicular to the pipes using the 250MHz antenna (after the sponge was removed).

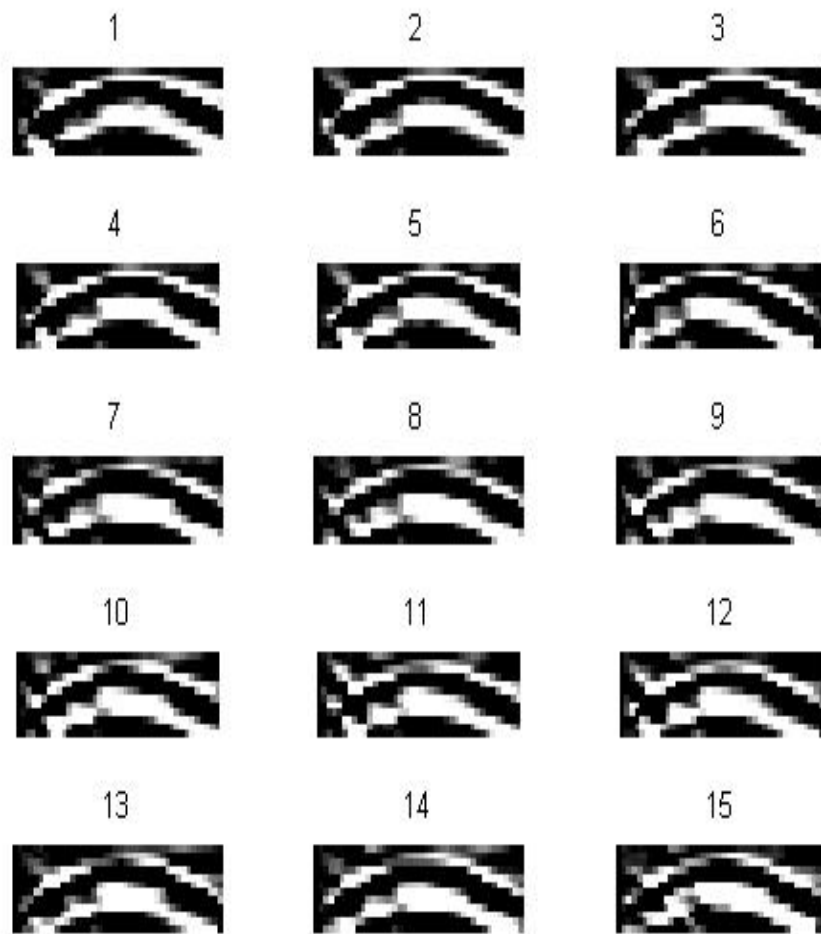


Figure 4.79: Test 7 - 15 radar images perpendicular to the pipes using the 700MHz antenna (after the sponge was removed)

The radar scans along the pipe before the sponge was removed are shown in Figures 4.80 and 4.81. The radar scans after the sponge was removed are shown in Figures 4.82 and 4.83

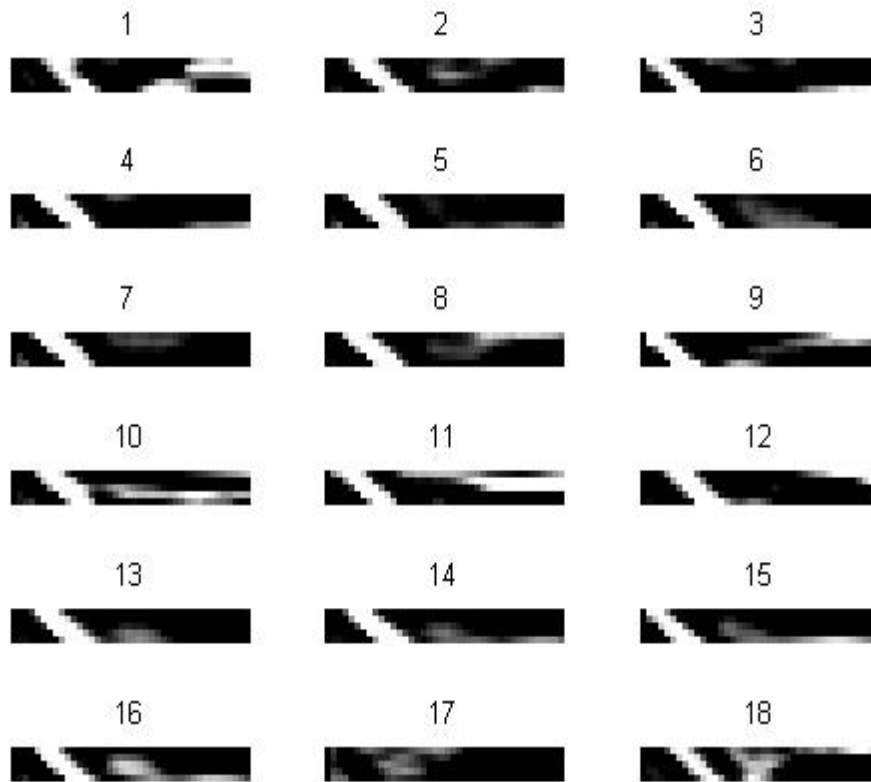


Figure 4.80. Test 7 - 18 radar images axially along the pipes using the 250MHz antenna (before the sponge was removed).

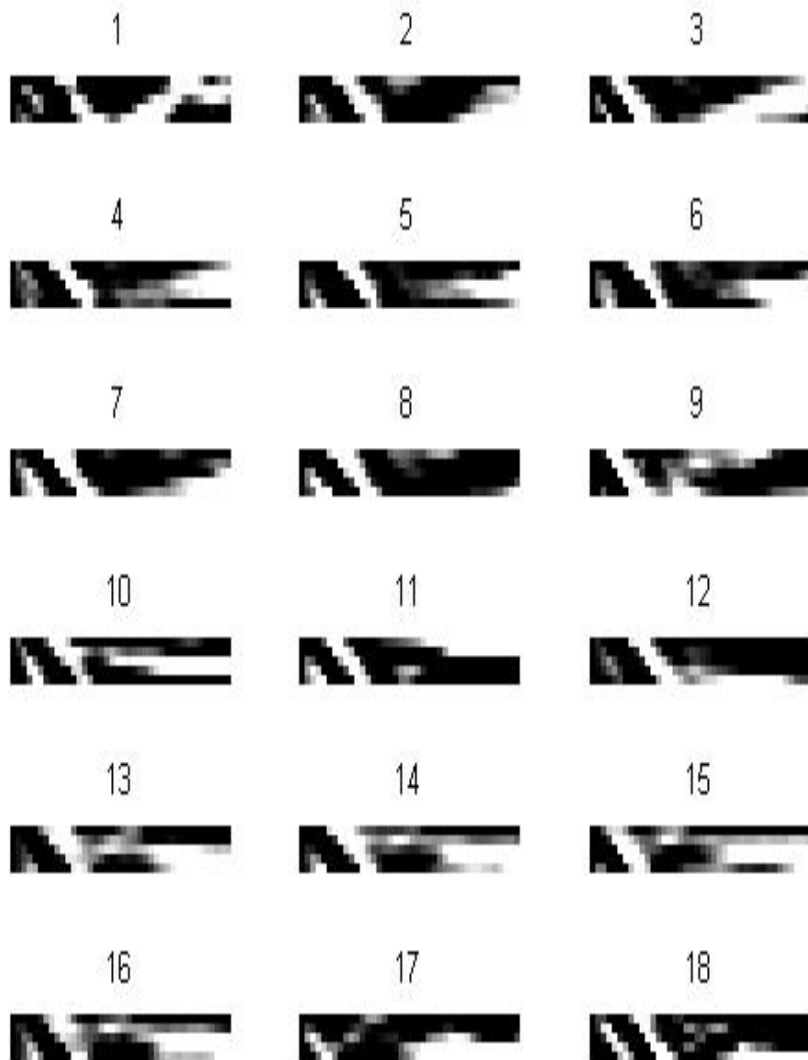


Figure 4.81: Test 7 - 18 radar images axially along the pipes using the 700MHz antenna (before the sponge was removed).

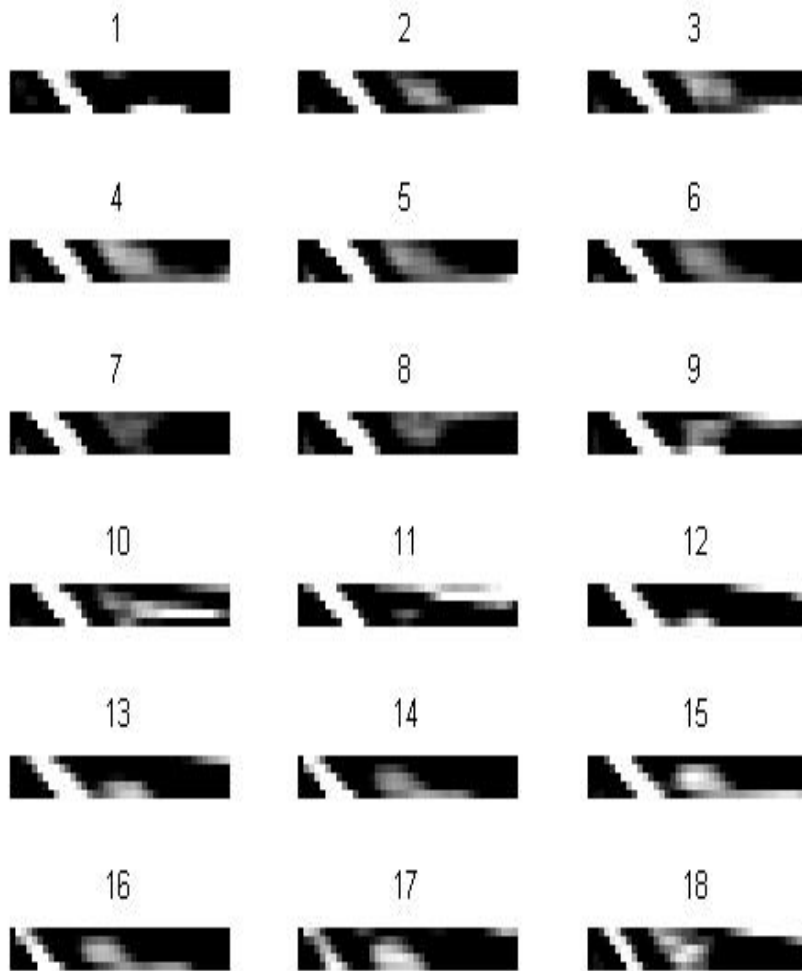


Figure 4.82: Test 7 - 18 radar images axially along the pipes using the 250MHz antenna (after the sponge was removed).

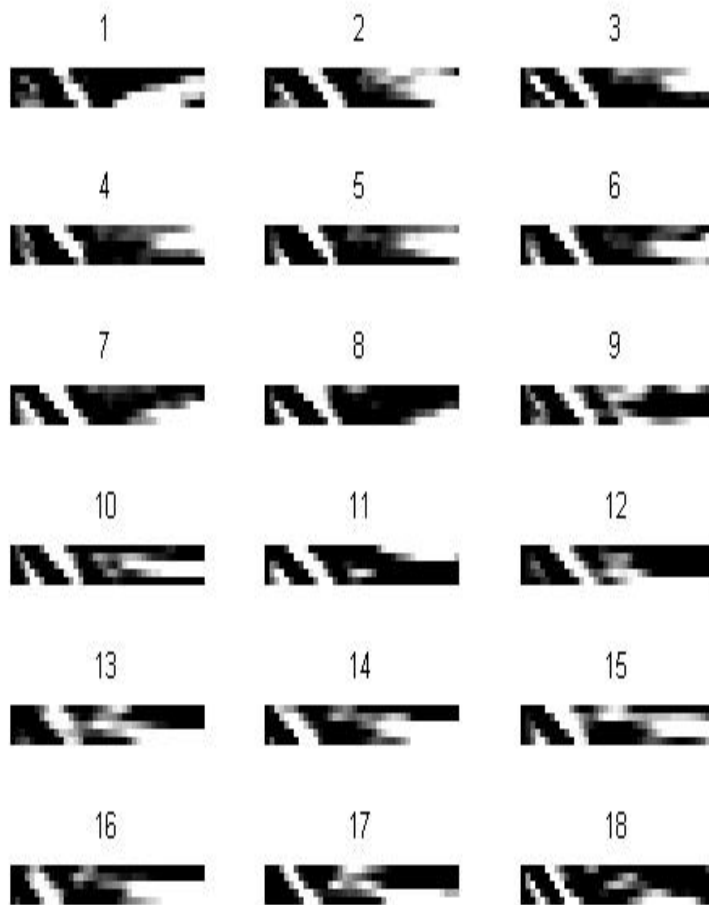


Figure 4.83: Test 7 - 18 radar images axially along the pipes using the 700MHz antenna (after the sponge was removed).

It was not possible to identify using visual inspection the damage in any of the radar images for either frequency. However, MSE analyses were conducted on the radar scans to quantify any differences as shown in the next section.

4.8.2 Identifying the effects of the GPR signal related to the damaged regions relative to the undamaged regions under ‘ideal’ ground conditions

The MSE values were calculated in order to identify the damaged regions. The results from the MSE analysis perpendicular to the pipes at 250MHz and 700MHz before the sponge was removed are shown in Figures 4.84 and 4.85, meanwhile the results for the MSE analysis after the sponge was removed are shown in Figures 4.86 and 4.87. The red dotted circles in these Figures indicate the highest MSE values and hence the likely location of the pipe damage.

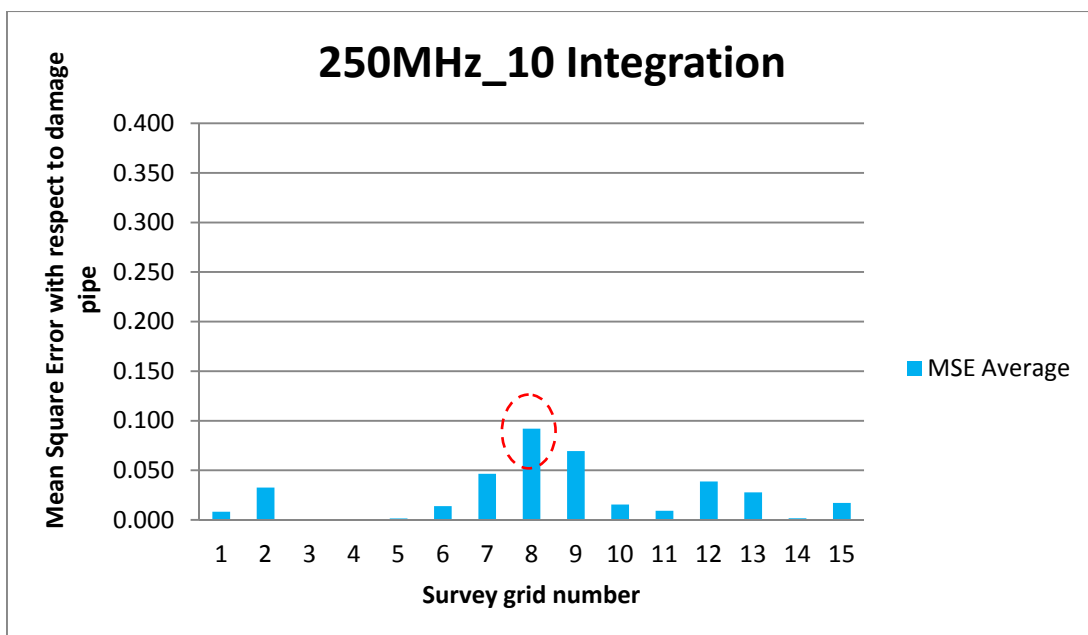


Figure 4.84: Test 7 - MSE for the 250MHz radar at 10 integrations perpendicular to the pipe (before the sponge was removed).

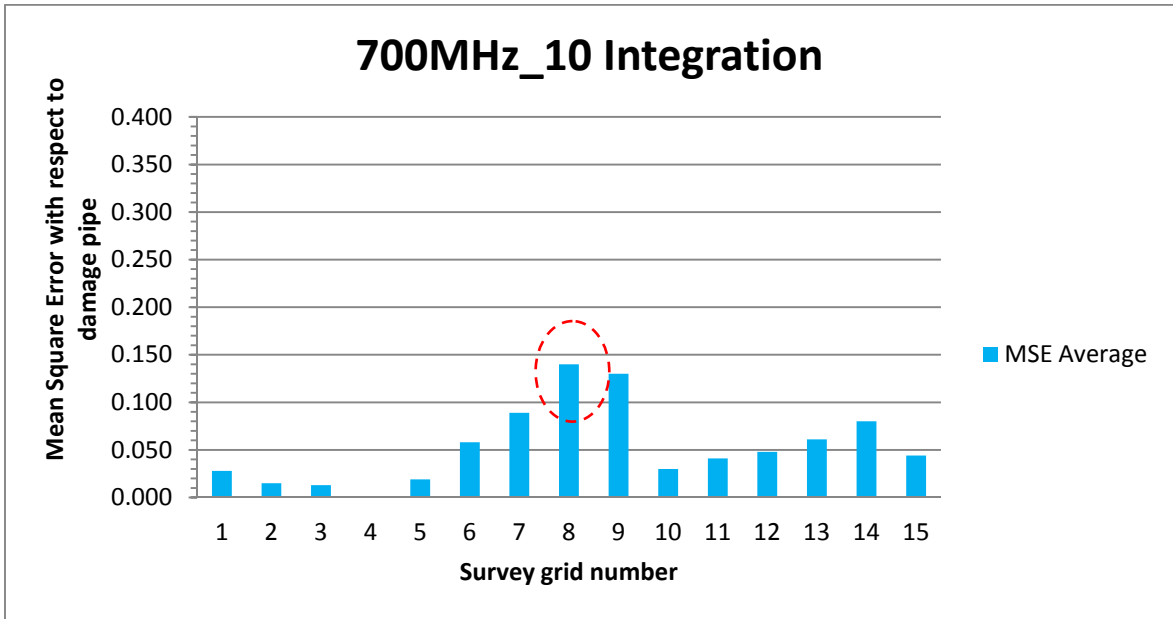


Figure 4.85: Test 7 - MSE for the 700MHz radar at 10 integrations perpendicular to the pipes (before the sponge was removed).

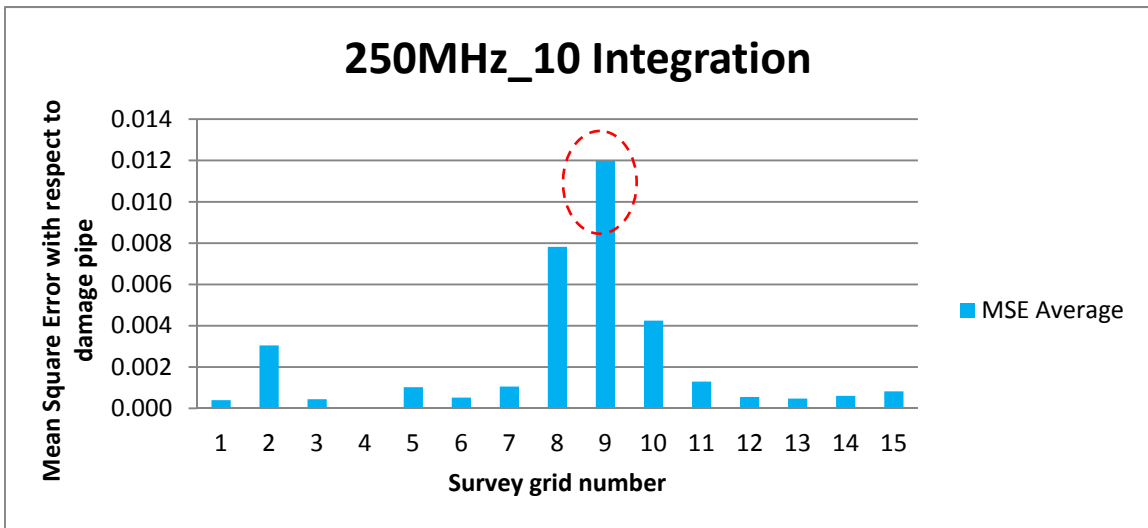


Figure 4.86: Test 7 - MSE for the 250MHz radar at 10 integrations perpendicular to the pipes (after the sponge was removed).

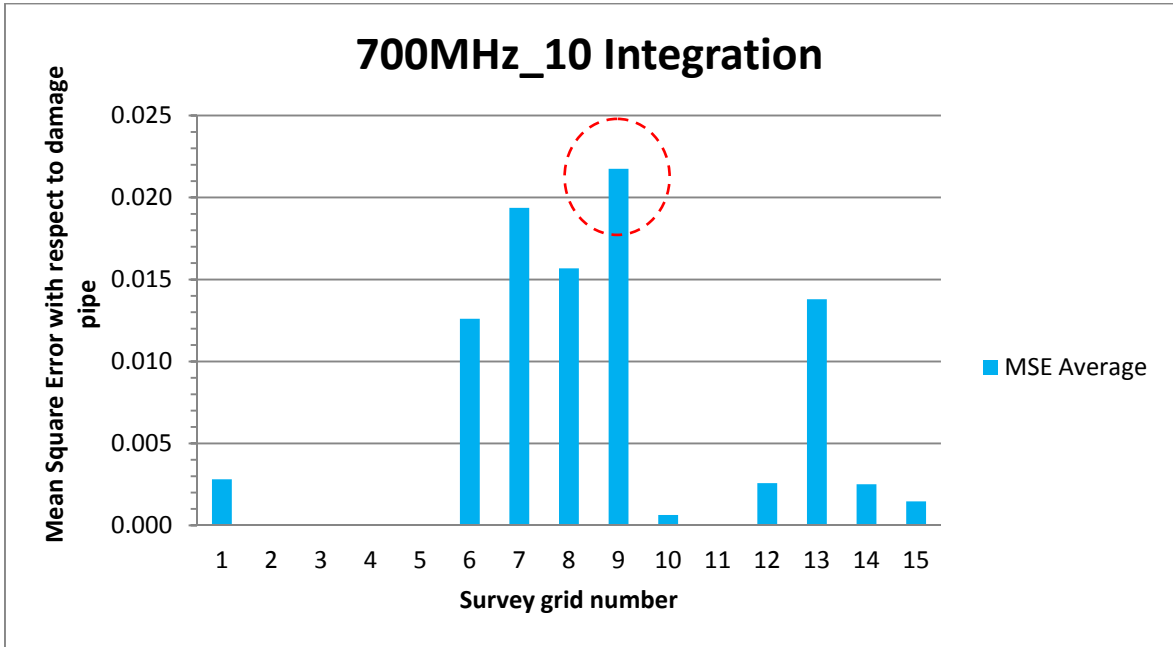


Figure 4.87: Test 7 - MSE for the 700MHz radar at 10 integrations perpendicular to the pipes (after the sponge was removed).

The results for the MSE analysis axially along the pipes at 250MHz and 700MHz before the sponge was removed are shown in Figures 4.88 and 4.89, meanwhile the results for the MSE analysis after the sponge was removed are shown in Figures 4.90 and 4.91.

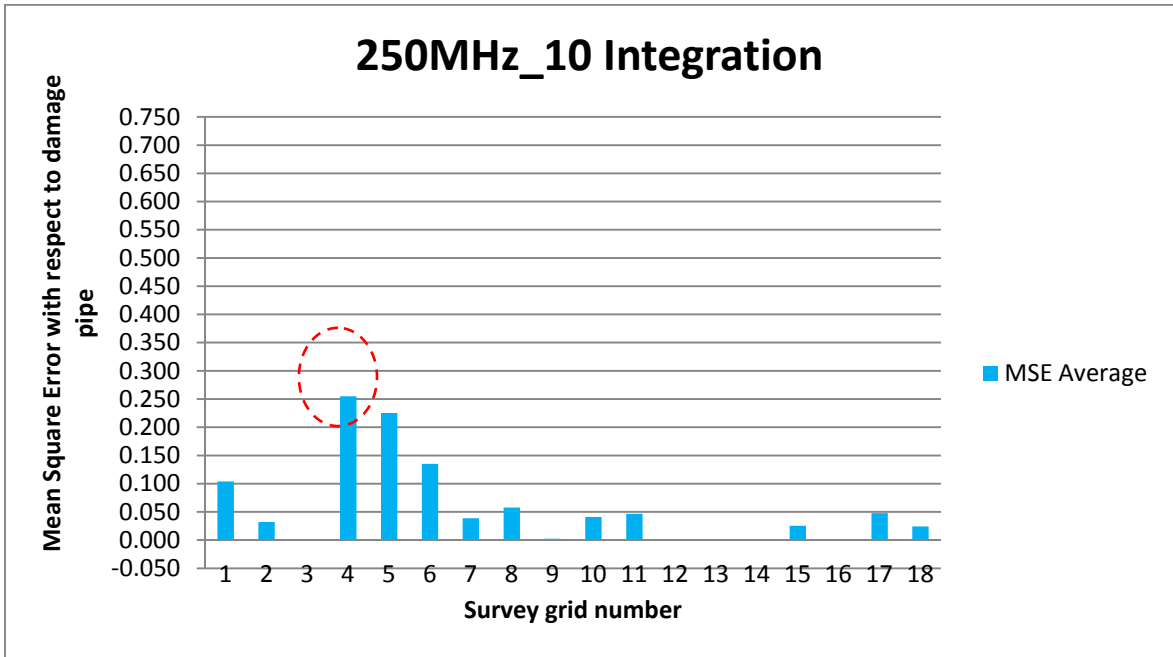


Figure 4.88: Test 7 - MSE for the 250MHz radar at 10 integrations axially along the pipes (before the sponge removed).

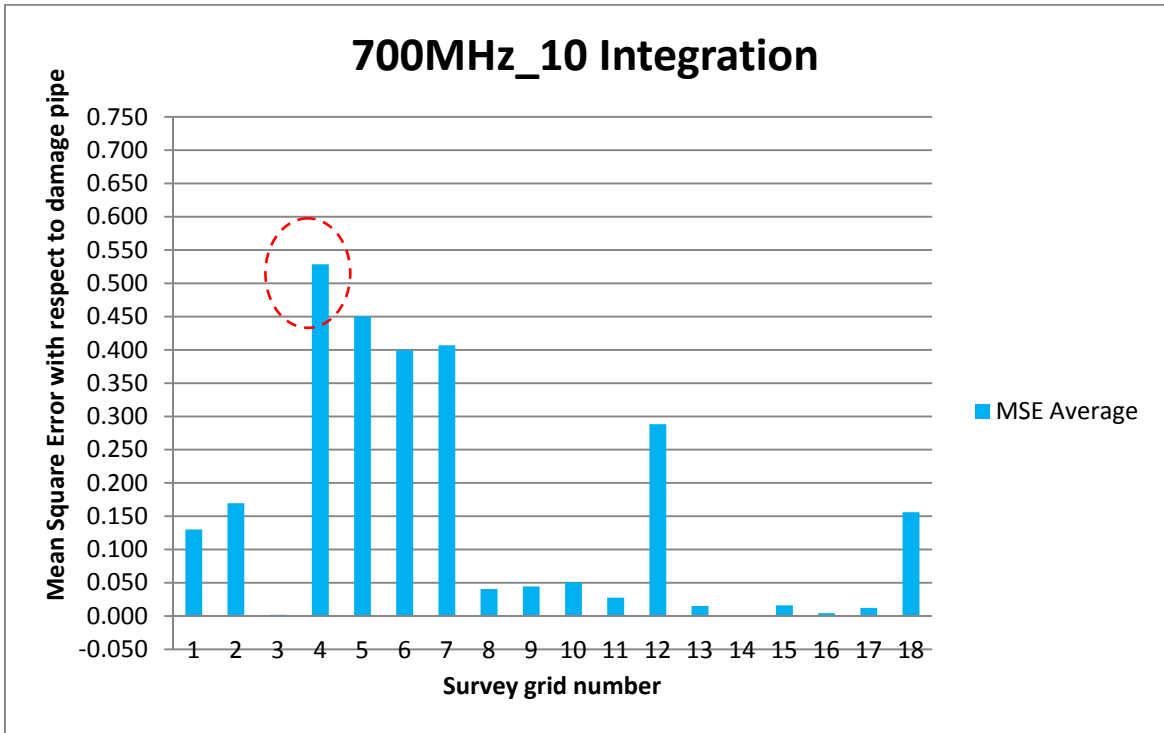


Figure 4.89: Test 7 - MSE for the 700MHz radar at 10 integrations axially along the pipes (before the sponge was removed).

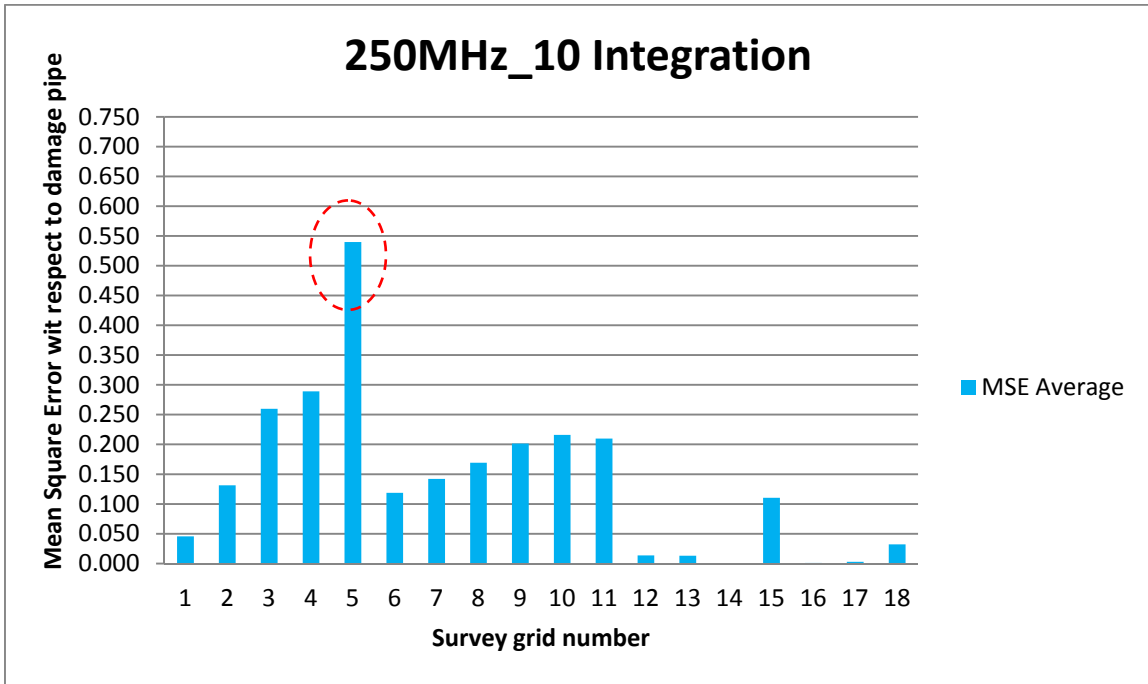


Figure 4.90: Test 7 - MSE for the 250MHz radar at 10 integrations axially along the pipes (after the sponge was removed).

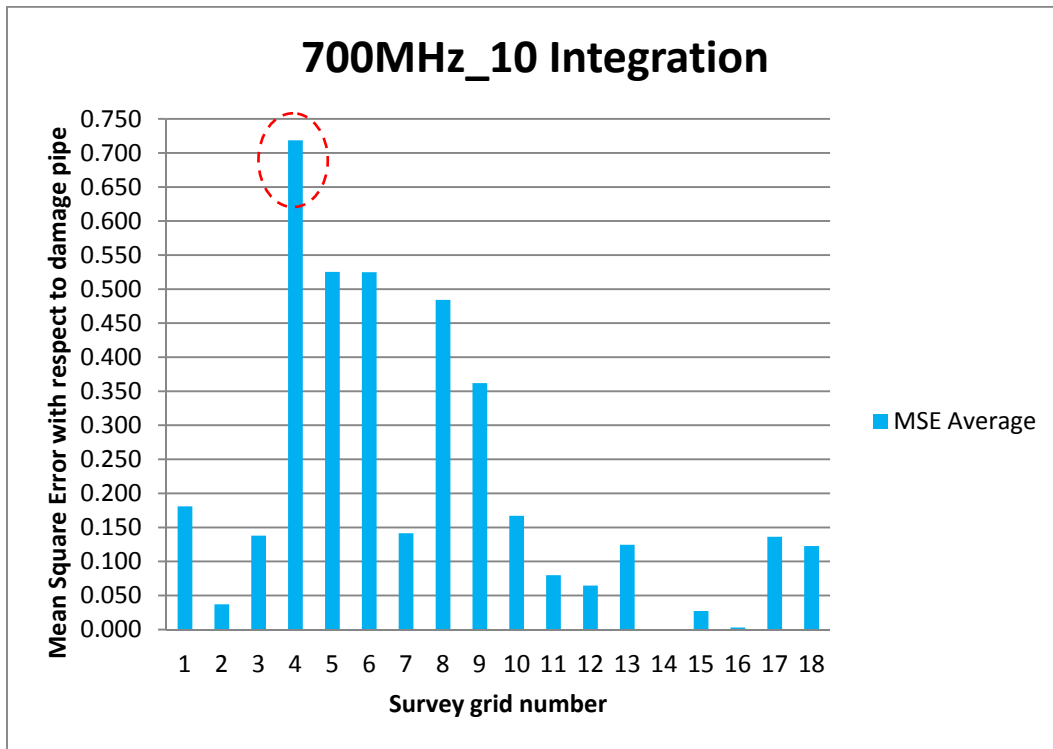


Figure 4.91: Test 7 - MSE for the 700MHz radar at 10 integrations axially along the pipes (after the sponge was removed)

In these tests, it has been shown that the GPR scans could be used to identify the damaged region in the pipe when the scans were conducted both along the pipe and perpendicular to the pipe.

A summary of the key findings that can be drawn from these results are:

- i. The GPR scans could be used to identify the damaged region of the pipe before and after the sponge was removed both perpendicular and axially along the pipe. This would indicate that it is the material in the pipe that is creating the identifiable difference in the GPR signals.

- ii. It is worth noting that with the MSE analysis, the position of the peak value pointed to the location of pipe damage before the sponge was removed. The only difference between this test and the previous tests using coverings over the damage was that the sponge was inside the pipe, which causes a discontinuity to the pipe-air-pipe interface within the pipe compared to other sections of the pipe.
- iii. It is also worth noting that after the sponge was removed, the sand was allowed to enter the pipe and hence replaced the sponge. This also produced an anomaly that could be identified with the MSE analysis, but the position did not always match the position of the pipe damage. This is likely caused by the fact that the sand may not settle uniformly within the pipe. In all cases, the highest MSE peak is not more than one position away from the position of the actual pipe damage.

4.9 Result Comparison and Discussion

From these experiments and interpretation of the radar image via visual inspection, it is not immediately obvious there was any damage to the pipe (sometimes changes to the radar scans can be observed as indicated in the preceding results, but careful inspection is required). It has been shown, however, from the results presented that this can to some extent be addressed by identifying anomalies using a MSE analysis, and hence improve the

identification of defects and locate the position of damage in pipes. However, it is also found that for a defect to be detectable it is mainly attributed to the discontinuity of the pipe-air-pipe interface within the pipe at the damaged location caused by either sand or the sponge in Test 7 being inside the pipe. The actual defect/damage in the pipe made no observable impact on the presence of the anomaly, as demonstrated by the results from the tests where the damage to the pipe was covered and no sand was allowed inside the pipe.

The MSE plot is a measure of deviation, or dissimilarity from the undamaged pipe as imaged by the GPR under the same geophysical conditions. The MSE values can be seen as proportional to the degree of anomaly from that of a "normal", in this case undamaged pipe. While it is possible that a higher peak value for, say Test 1, as compared to the peak value of Test 2 may indicate that the type of damage in Test 1 is more detectable, this may not be consistently valid. The reason is that within each plot, a peak value is also relative to its second largest value. If the second largest value (at an inaccurate damage position) exceeds the value at the accurate position of the damage, then the actual damage would have been missed. In other words, the ease of damage detection also rely upon the relative difference between the peak and the next largest value within the same plot, where the bigger the difference, the easier the process of picking the peak and the more likely the peak will remain a peak in the presence of slight variation in the environment. As a result, comparison across the type of damages using the peak MSE values may not conclusively correlate to the ease of detection of the type of damage. However, in a sufficiently controlled environment (i.e. negligible variation in soil geophysical properties) the

correlation between the magnitude of the MSE peak and ease of detection may well be observed. The following plots, in Figures 4.92 to 4.95, provide a direct comparison of the MSE values for all 7 tests on the same scale, for all 4 different observations of 250 MHz and 700 MHz perpendicular to pipe, and 250 MHz and 700 MHz along the pipe:

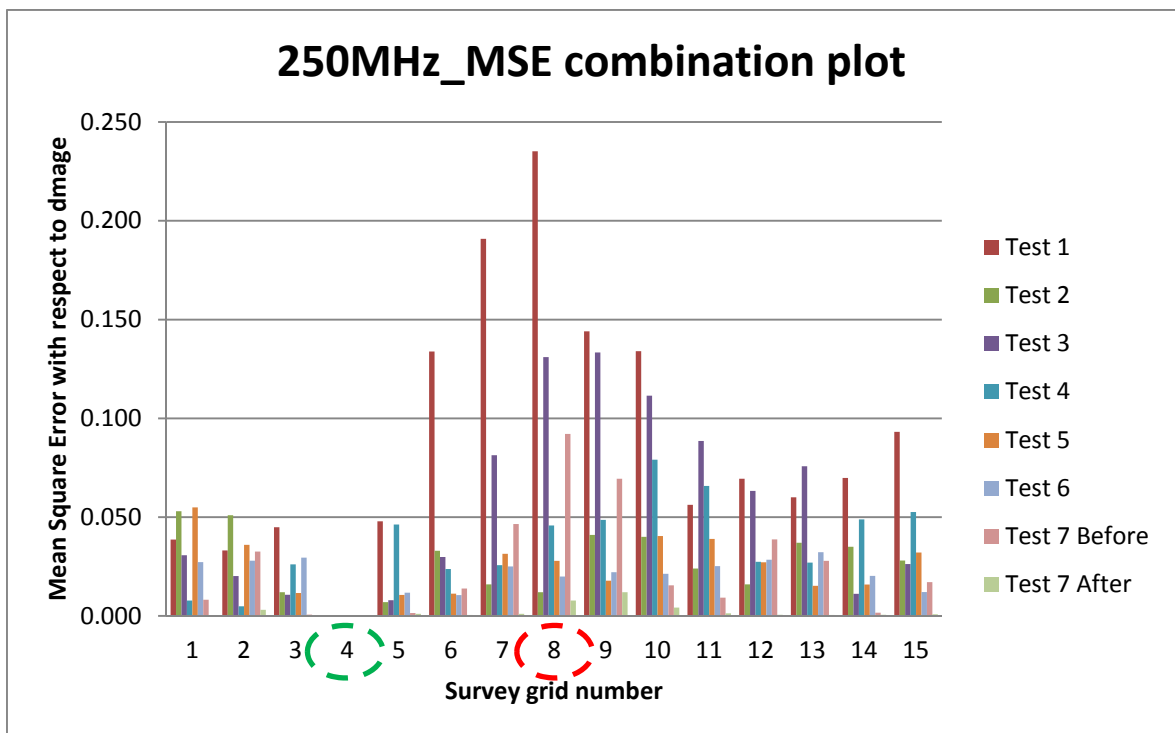


Figure 4.92: All tests of MSE for the 250MHz radar scans perpendicular to the pipes, the green circle highlights position of undamaged pipe, while the red circle highlights position of damaged pipe, both are known *a priori*

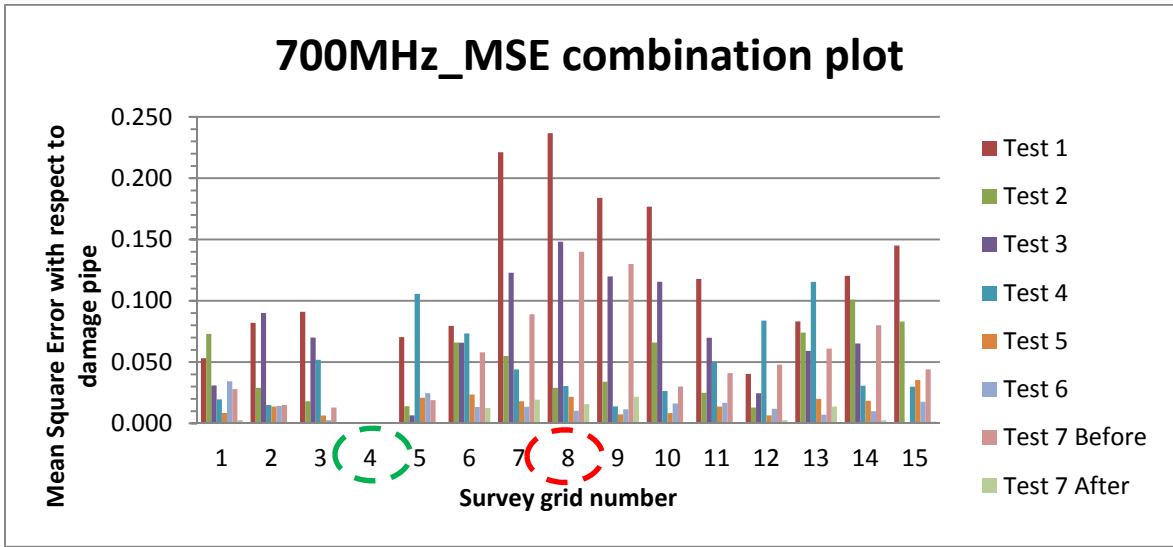


Figure 4.93: All tests of MSE for the 700MHz radar scans perpendicular to the pipes.

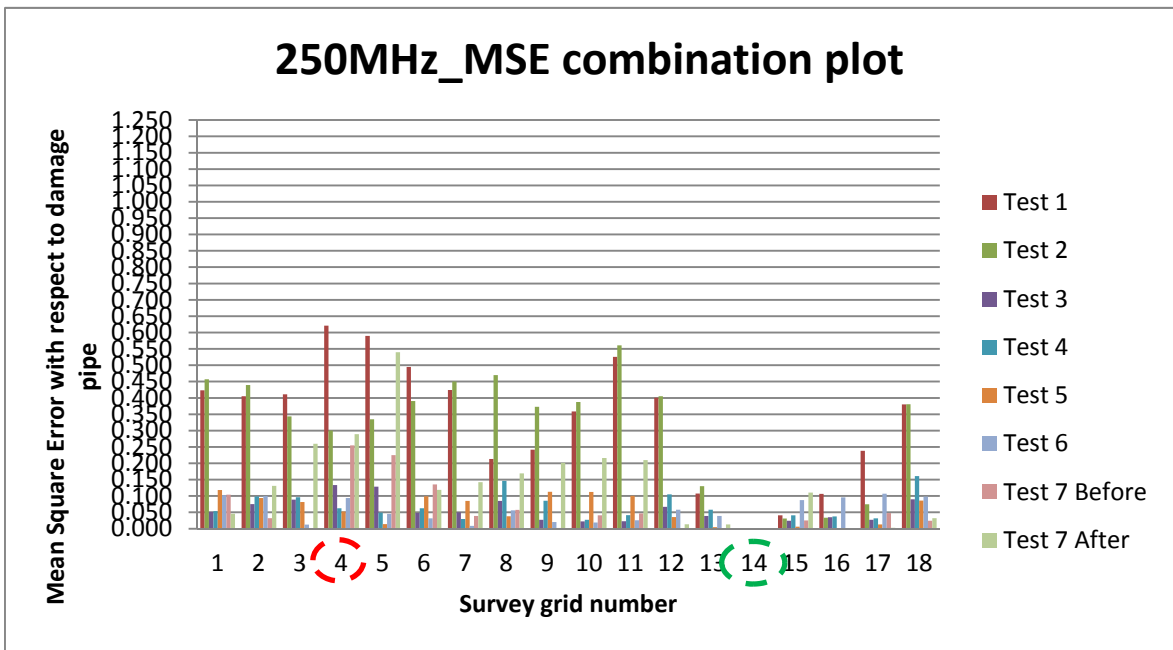


Figure 4.94: All tests of MSE for the 250MHz radar scans axially along the pipes.

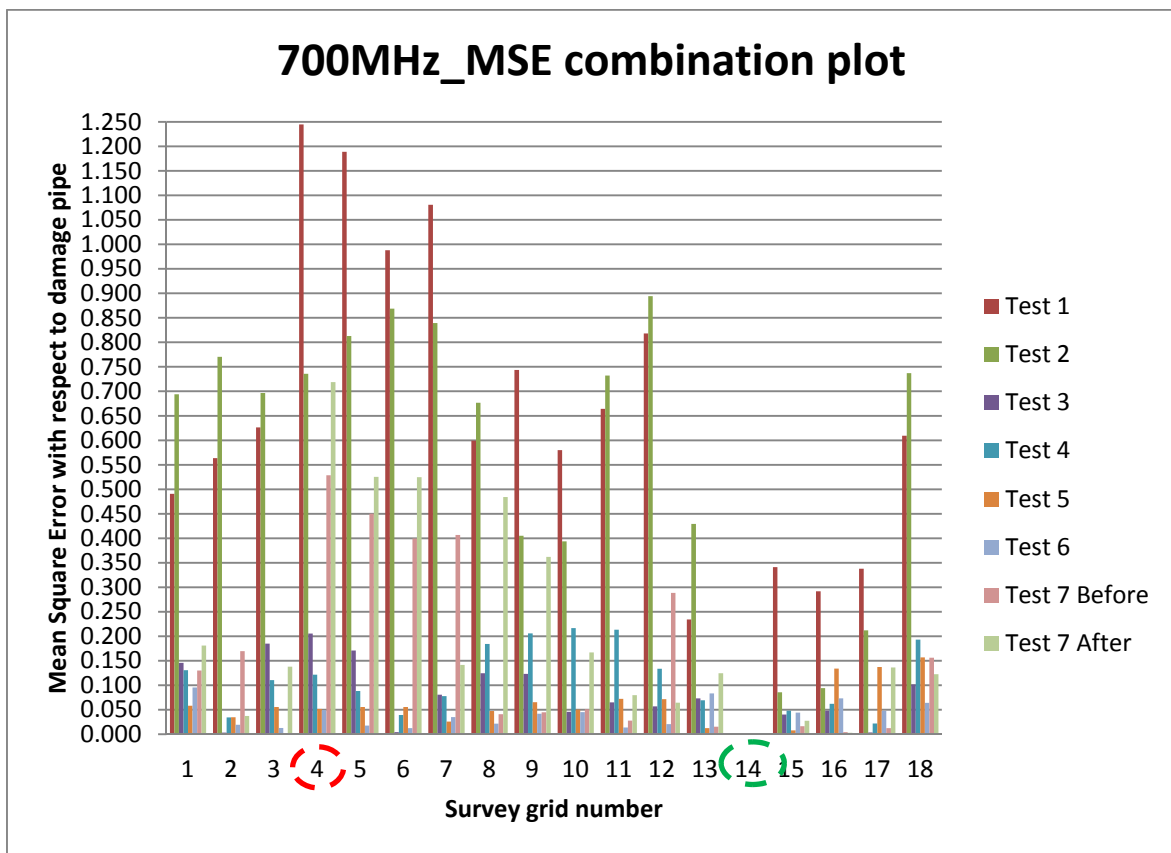


Figure 4.95: All tests of MSE for the 700MHz radar scans axially along the pipes.

By comparing the results on the same graph, it can be observed that in the tests where the damage is not detectable, the overall MSE amplitude is generally lower in relation to the test in which the damage is accurately detectable. This may imply a relationship between the damage and the amplitude of the MSE value, which would potentially be correlated to the condition of the pipe. However, this needs to be further studied by removing the assumption of non-varying geophysical condition so an adaptive reference level can be developed for the MSE analysis.

A further observation from the above results is that the techniques used would be useful in identifying where blockages or deposits of debris exist in a pipe. This would be of use to pipeline operators when devising emergency (i.e. blockages) or routine (i.e. debris deposit) cleaning of pipelines.

Chapter 5

CONCLUSIONS AND RECOMMENDATIONS

5.1 Introduction

This chapter covers the conclusions and recommendations of the study aimed at assessing the condition of existing buried utilities using Ground Penetrating Radar. The conclusions

are made based on the objectives of the project and the results show that the research has achieved the project aim. The results have contributed new knowledge to the field and facilitated further technology development, especially for the Mapping The Underworld project. For the recommendations, these come from the experience and some problems encountered during this study.

5.2 Conclusions

In order to achieve the aim of the research, two key objectives had to be accomplished, taking into account the research available. These were:

1. The design and construction of a suitable test facility that would allow controlled testing to be conducted.
2. The production of a suitable analysis method for the results.

Both of these were successfully achieved during the research with lessons learned for future projects in this field. A Detector Duo GPR unit with shielded dual frequency antennas at 250 MHz and 700 MHz was used in these experiments. The advantage of this dual frequency GPR in a single unit is that it can reduce the time for each test, as it permitted all the targets to be investigated simultaneously with just a single scan. As a result of capturing signal signatures for damaged and undamaged pipes, both frequencies are capable to observe the defective regions, but only in certain conditions and with limitations. Although both frequencies were capable of observing the defective region, the

antenna with 250 MHz frequency has some drawbacks. The radar scan from the 250 MHz antenna was blurred and darker due to reduced signal resolution. In addition, the 250 MHz antenna produced less of a return signal compared to the 700 MHz antenna. This is because the wavelength of the 250 MHz is much longer compared to the 700 MHz. However, the 700 MHz antenna showed more signal attenuation compared to the 250 MHz. Any signal interference from the surroundings such as from radio waves, cellular radio, television, satellite radio and microwaves are factors affecting the radar scan results.

In these experiments, several types of damaged pipe were investigated. The damaged pipe involved broken sections and a hole in the pipe. Both types of damage were tested under different conditions. Firstly, allowing the soil to pass through the damaged region and secondly where the soil was prevented from entering the damaged region. Radar scans were conducted in both directions, i.e. perpendicular to the pipes and axially along the pipes. Two results were identified. Firstly, conducting the radar scan perpendicular to the pipe had a better result compared to scanning axially along the pipes. It was quite hard to interpret the radar scan along the pipe because it just showed one thick straight line and it was very hard to identify any changes in the images and thus hard to quantify and identify the amplitude changes in the damaged region.

Secondly with respect to the damage to the pipe, the vertically broken pipe was easier to identify and to quantify compared to the hole in the pipe. The reason for this involved the amount of soil entering the pipe via the damaged region. More soil in the pipe made for easier interpretation and clarification. However, the vertical break in the pipe and the hole in the pipe could not be identified and detected if the soil was prevented from passing

through the damaged regions. The amount of soil passing through the damaged region is a key factor in identifying the damaged region. The more soil material passing into the pipe, the better the results and the clearer the radar image that is achieved.

All the objectives of the research have been carefully undertaken to achieve the initial aim. By considering the outputs from the analyses and the objectives of this research, it can be concluded that:

- i. Different antenna frequencies will result in different signal signatures between undamaged and damaged pipes in terms of image resolutions and signal attenuation.
- ii. GPR, with careful analysis of the signals, can identify damage in pipes under the controlled conditions in these experiments but with limitations. These limitations depend on the size of the damaged region and the type of damage. However, the damage was easily identified if it was associated with the movement of other materials (soil) into the pipe. Without this material movement, it was hard to identify the damage.
- iii. The GPR signal of the damaged regions relative to the undamaged regions under 'ideal' ground condition depend on the amount of soil (materials) passing through the damaged regions. The more soil passing into the pipe, the better the result in terms of identifying the damaged region.

5.3 Recommendations for Further Work

While the study showed that the location of the damaged section could be detected with anomalies arising from the sand entering the pipe, the current project only used a plastic pipe. Underground assets also consist of pipes of different material such as metal and clay. Damage on metal pipes may exhibit anomalies associated with a different mechanism as the material typically has a strong reflection coefficient compared to the surrounding soil.

Although this project has demonstrated that the MSE approach shows promise when attempting to determine the approximate location of damage in pipes in certain circumstances, there is still further work that can be done into this method, in particular whether the type/extent of the damage can be identified with greater confidence.

A thorough understanding of the pipe damage mechanisms and associated anomalies observable using a GPR would aid in producing a pipe damage matrix based upon pipe material, type of damage, pipe content and surrounding material. As an example, a leaking cast iron water pipe may exhibit anomalies in the form of an enlarged pipe section caused by the surrounding wetted soil near the damage section. These characteristics, if well characterised, could be combined with signal processing techniques to automate and optimise both the detection and identification of pipe damage. This enhances the available toolset for achieving the ultimate goal of long-term monitoring and management of underground assets.

The following recommendations may extend the research in future studies:

- i. To investigate other pipe deterioration mechanisms such as corroded pipes and cracked pipes.
- ii. To investigate other types of pipe such as clay pipes and metal pipes.
- iii. To investigate the effects of burial in other types of soil, such as clay.
- iv. To investigate the effect of different water contents in the soil.
- v. To enhance the analysis and interpretation methods, such as using C-Scan visualisation (tomography) and 3D.
- vi. To include water in the pipe, where a leak is possible into the surrounding ground and to investigate its effect on the GPR, and hence damage identification.
- vii. Signal processing algorithms for the automated detection, identification and potentially prediction of pipe damages.
- viii. To detect blockages or partial blockages (such as debris) deposited in a pipe and alert the operator as to where future blockages might occur and / or where cleaning of the pipe system might be needed.

The outcome of the further research would inform the body of knowledge in applying ground penetrating radar technology as a non-invasive geophysical sensing technique towards the over-arching goal of assessing and monitoring underground assets.

REFERENCES

ASCE. (1994). Manual and reports on engineering practice, Volume 92, Manhole Inspection and Rehabilitation. Reston, VA.

ASCE.(2004). Report card for America's Infrastructure 2003 Progress Report.<http://www.asce.org/reportcard/>, Jan 2010.

Allred, B. J., Fausey, N. R., Peters, L., Chen, C., Daniels, J. J., Youn, H., et al. (2004). Detection of buried agricultural drainage pipe with geophysical methods. *Applied Engineering in Agriculture*, 20(3), 307-318.

Annan, A. P. (2002).GPR—History, Trends, and Future Developments. *Subsurface Sensing Technologies and Applications*, 3, 253-270.

Annan, A. P., Scaife, J. E., & Giamou, P. (1990). Mapping buried barrels with magnetic and ground penetrating radar. *Soc. Expl. Geophys*, 60th Annual. Int. Mtg, 422-423.

Ariaratnam, S. T. & Guercio, N. (2006). *Advances in Engineering Structures, Mechanics & Construction*; In pipe Ground Penetrating Radar for non-destructive evaluation of PVC lined concrete pipe USA. Springer Netherlands,763-772.

Beck, A. R., Fu, G., Cohn, A. G., Bennett, B., & Stell, J. G. (2007).A framework for utility data integration in the UK. In *Urban and Regional Data Management: UDMS 2007*. 26th Urban Data Management Symposium. Stuttgart, Germany. 261-276.

Chen, C.S. & Jeng, Y. (2011). Nonlinear data processing method for the signal enhancement of GPR data. *Applied Geophysics*, 75(1), 113-123.

Costello, S. B., Chapman, D. N. & Metje, N. (2007). Underground asset location and condition assessment technologies. *Tunnelling and Underground Space Technology*, 22, 524-542.

Crocco, L., Prisco, G., Soldovieri, F. & Cassidy, N. J. (2009). Early-stage leaking pipes GPR monitoring via microwave tomographic inversion. *Applied Geophysics*, 67, 270-277.

Daniels, D. J. (1996). *Surface-Penetrating Radar*. London: Institute. Electric. Engineer. 1-18.

Daniels, D. J. (2004). *Ground Penetrating Radar* (2nd edition). London: The Institution of Engineering and Technology. 1-122.

Daniels, D. J., Gunton, D. J., & Scott, H. F. (1988). Introduction to subsurface radar. *Proc. Inst. Elect. Eng. F*, 135, 278-320.

Davenport G, C. (2001). Remote Sensing Applications in Forensic Investigations. *Historical Archeology*, 35(1), 87-100.

Davis, J., & Annan, A. P. (1989). Ground penetrating radar for high resolution mapping of soil and rock stratigraphy. *Geophysics. Prospect*, 3, 531-551.

Doolittle, J., & Collins, M. (1998). A comparison of EM induction and the GPR methods in areas of Karst. *Geoderma*, 85, 83-102.

Dusan, P., & Aleksandar, R. (2007). An underground utility detection technology – our experiences. In PSU-UNS International Conference on Engineering and Environment- ICEE 2007. Songkhla, Thailand.

Eyuboglu, S., Mahdi, H., Al-shukri, H., & Rock, L. (2003). Detection of water leaks using ground penetrating radar. Retrieved from <http://www.dot.state.fl.us>, Nov 2013.

Farley, M., Hamilton, S., Firs, T., Barn, T., Underwood, T., Leakage, K., et al. (2008). Non-intrusive leak detection in large diameter, low-pressure non-metallic pipes: are we close to finding the perfect solution? *World Water*, 1-9.

Fortuny-guasch, J. (2002). A Novel 3-D Subsurface Radar Imaging Technique. *Scenario*, 40, 443-452.

Goodman, D., Novo, A., Astier, G., Morelli, G., Astier, G., Piro, S., et al. (2011). Advances in GPR imaging with multi-channel radar systems from engineering to archaeology. In symposium the application geophysics environmental and engineering problems (Vol. c). South Carolina USA. Retrieved from <http://www.eegs.org>.

Gokhale, S., Abrahams, D. M. & Iseley, T. (1997). Intelligent sewer condition evaluation technologies-an analysis of three promising options. In *Proceedings of the North American No-Dig 97*. Seattle, Washington., 253-265.

Griffin, S., & Piplett, T. (2002). Ground Penetrating Radar. *Geophysical and Remote Sensing Methods for Regolith Exploration*, 144, 80-89.

Grote, K., Hubbard, S., Harvey, J. & Rubin, Y. (2005). Evaluation of infiltration in layered pavements using surface GPR reflection techniques. *Applied Geophysics*, 57, 129 - 153.

Guercio, N. Assessment and modelling of large diameter lined concrete pipe, MS thesis, Del E. Webb School of Construction, Arizona State University (2002).

He, X., Zhu, Z., Liu, Q., & Lu, G. (2009). Review of GPR Rebar Detection. In *PIERS Proceeding*. Beijing, China. 804-813.

Hippel, V. (1954). *Dielectric material and applications*. Wiley, Chichester. Chichester: John Wiley and Sons, Inc.

<http://www.rdg.com.my>, January 2010.

Hulsenbeck.(1926). German Patent. Number 489434.

Inagaki, M., & Okiyasu, Y. (2008). Attenuation coefficients of complex materials. In 12th International Conference on Ground Penetrating Radar. Birmingham.

Jol, H. (2009). *Ground Penetrating Radar: Theory and Applications* (41-54). Oxford: Elsevier Science. 1-143.

Koo, D. H., & Ariaratnam, S. T. (2006). Innovative method for assessment of underground sewer pipe condition. *Automation in Construction*, 15, 479-488.

Kuo, S., Zhao, L., Mahgoub, H., & Suarez, P. (2005). Investigation of ground penetrating radar for detection leaking pipelines under roadway pavements and development of fiber-wrapping repair technique. *Transportation.US*.

Laurens, S., Balayssac, P., Rhazi, J., Klysz, G. & Arliguie, G. (2005). Non-destructive evaluation of concrete moisture by GPR: experimental study and direct modelling. *Materials and structures*, 38, 827-832.

Long, R., Lowe, M., & Cawley, P. (2003). Attenuation characteristics of the fundamental modes that propagate in buried iron water pipes. *Ultrasonics*, 41, 509-519.

Makar, J. (1999). Diagnostic techniques for sewer systems. *Infrastructure Systems*, 5(2), 69-78.

Makar, J. & Rajani, B. B. (2000). Grey cast iron water pipe metallurgy. *Materials in Civil Eng.*, 12(3), 245-253.

Makar, J., Desnoyers, R. & McDonald, S. E. (2001). Failure modes and mechanisms in gray cast iron pipe. In *Underground Infrastructure Research: Municipal, Industrial and Environmental Applications Proceedings*, Ontario. 1-10.

Neal, A. (2004). Ground-penetrating radar and its use in sedimentology: principles, problems and progress. *Earth-Science Reviews*, 66, 261-330.

Neto, P. X., & Medeiros, W. E. d. (2006). A practical approach to correct attenuation effects in GPR data. *Applied Geophysics*, 59, 140-151.

Olheoft, G. R. (1981). Electrical properties of rocks. In: Touloukian. New York: McGraw-Hill, 257-330.

Olheoft, G. R. (1998). Electric, magnetic, and geometric properties that determine ground penetrating radar performance. In *Proceeding of GPR 98, 7th International Conference on Ground Penetrating Radar* Lawrence, KS: University of Kansas, 177-182.

Paniagua, J., Rio, M. D., & Rufo, M. (2004). Test site for the analysis of subsoil. In *10th International Conference on Ground Penetrating Radar*, 21-24 June. Delft, The Netherlands.

Peters, L., Daniels, J. J., & Young, J. D. (1994). Ground Penetrating Radar as a Subsurface Environmental Sensing Tool. *The IEEE* Vol 82, 82(12), 1802-1822.

Pettinelli, E., Soldovieri, F., Redman, D. J. & Annan, A. P. (2008). GPR response from a buried plastic pipes filled with different fluids: An experimental study. In *12th International Conference on Ground Penetrating Radar*. Birmingham: University of Birmingham, 6.

Pickering, D., Park, J. M., & Bannister, D. H. (1993). *Utility Mapping and Record Keeping for Infrastructure*. Washington: The World Bank, 1-69.

Power, M. H. (1997).Modelling frequency-dependent GPR. *The Leading Edge*, (16), 1657-1662.

Power, M. H., &Olheoft, G. R. (1994).Modelling dispersive ground penetrating radar data. In 5th International Conference Ground Penetrating Radar.173-184.

Rana, S. (2011).Subsurface Utility Engineering - A cost effective method to investigate underground without excavation. In *Geospatial World Forum*. Hyderabad, India.

Reppert, P. M, Morgan, F. D., Toksoz, M. N. (2000). Dielectric constant determination using ground-penetrating radar reflection coefficients. *Applied Geophysics*, 43, 189-197.

Reynolds, J. (1997). *An Introduction to Applied and Environmental Geophysics*.Wiley,Chichester. Chichester: John Wiley & Sons Inc.

Rogers, C., Zembillas, N., Metje, N., Chapman, D. N., & Thomas, A. M. (2008). Extending GPR Utility Location Performance - The Mapping The Underworld Project. In 12th International Conference on Ground Penetrating Radar. Birmingham.

Romanoff, M. (1964).Exterior corrosion of cast iron pipe. *The AWWA*, 56(9), 1129-1135.

Silva, D. D., Davis, P., Burn, L. S., Ferguson, P., Massie, D. & Cull, J., (2002). Condition Assessment of Cast Iron and Asbestos Cement Pipes by In-Pipe Probes and Selective Sampling for Estimation of Remaining Life. No Dig. Australia.

Sinha, S. K., & Fieguth, P. W. (2006). Automated detection of cracks in buried concrete pipe images. *Automation in Construction*, 15, 58 - 72.

Sinha, S. K. & Karray, F. (2002). Classification of Underground Pipe Scanned Images Using Feature Extraction and Neuro-Fuzzy Algorithm. *Most*, 13(2), 393-401.

Sinha, S. K. & Knight, M. A. (2004). Intelligent System for Condition Monitoring of Underground Pipelines. *Computer-Aided Civil and Infrastructure Engineering*, 19, 42-53.

Sternberg, B. K., & Levitskaya, T. M. (2001). Electrical parameters of soils in the frequency range from 1kHz to 1GHz, using lumped-circuit methods. *Radio Science*, 36(4), 709-719.

Thomas, A. M., Lim, H. M., Metje, N., Rogers, C., Chapman, D. N., Atkins, P. R., et al. (2006). The complexity of GPR data interpretation in railway foundation surveys. In *Proceeding of RailFound 06, 1st International Conference on Railway Foundations*. Birmingham.

Tong, L. T. (1993). Application of Ground Penetrating Radar to locate underground pipes. *Terr. Atmos. Ocean Sci*, 4, 171-178.

Topp, G., Davis, J., & Annan, A. P. (1980). Electromagnetic determination of soil water content: measurements in coaxial transmission lines. *Water Resources*, 16, 574-582.

Tran, H. U., Investigation of deterioration models for storm water pipe systems, PhD thesis, School of Architectural, Civil and Mechanical Engineering, Victoria University (2007).

USEPA. (2002). The Clean Water and Drinking Water Infrastructure Gap Analysis. Forecast. <http://www.epa.gov/safewater/gapreport.pdf>. Jan 2010.

van Dam, R., & Schlager, W. (2000). Identifying causes of ground penetrating radar reflection using time-domain reflectometry and sedimentological analyses. *Sedimentology*, 47, 435-449.

Walden, J., Oldfield, F., & Smith, J. (1999). Environmental magnetism: a practical guide. (Vol. 6). London: QRA Technical Guide.

Wang, Z. W., Slabaugh, G. & Fang, T. (2008). Partial Differential Equation-based GPR Signature Discrimination for Automatic Detection of Bridge Deck Delamination. In 4th IEEE Conference on Automation Science and Engineering. Washington DC, USA.

Yelf, R. (1990). Appraisal of ground penetrating radar in underground coal mines. Department of Primary Industries and Energy, Canberra, Australia.

Yin, J., & Pineda, J. (1996). Real-Time Full Signature Corrosion Detection of Underground Casing Pipes. In IEEE Instrumentation and Measurement Technology Conference, Brussels, Belgium.138-143.

Zeng, X., & McMechan, G. A. (1997).GPR characterization of buried tanks and pipes.Geophysics, 62, 797-806.

APPENDICES

Appendix 1 – Matlab Script for identifying the related matrices

```
%% Identifying the related matrices
% Creating empty matrix
mse = zeros(1,15);
% for i = 1:number_of_files
fori = 1:15
% Reading the input files in the for loop
if (i< 10)
strn = num2str(i);
str = strcat('LID2000',strn, '.D00');
else
strn = num2str(i);
str = strcat('LID200',strn, '.D00');
end
    data2=idsris_readv4(str);
    map2=data2.MAPPA;
    map2 = map2(50:64,1:42);
%     map2 = corr(map2,0.8);
%     map2 = im2bw(map2);
subplot (5,3,i);imshow(map2);title(num2str(i));
end
```

Appendix 2 – Calculating Mean Square Error (MSE)

```
function dati = idsris_readv4(varargin)

% DATA = IDSRIS_READ('FILENAME')
% La funzione legge il file FILENAME con estensione .dt, .dtp
% o D##
% e carica i dati nella struttura DATA composta dai seguenti campi:
%
% V: len_rec
%     versione_file
% FI: sweep_marker_1
% I: survey_info
% C: comment
% AH: height
% FZ: zone
% FX: x_offset
% FQ: marker_quantum
% FM: sweep_marker
%     position
% AC: n_tx
%     tx_sequence
%     n_rx
%     rx_sequence
%     nacq
% AM: direct
%     l_coord
%     t_coord
% ATR: tx_x0
%     tx_y0
%     tx_alpha
%     tx_freq
```



```
% rx_x0
% rx_y0
% rx_alpha
% rx_freq
% AA: info
% S: S
% canale
% FW: n_canali
% stacking
% interleaving
% id_canale
% SOS_high
% max_sampling_AD
% SW_version
% build_version
% FW_version
% GPS_offset_x
% GPS_offset_y
% H: n_acq_sweep
% n_acq_sample
% n_sampler_x
% n_sampler_y
% enable_x_compress
% n_x_compress
% n_y_compress
% enable_wheel
% wheel_compress
% ad_offset
% radar_freq
% prop_vel
% sweep_time
% sweep_time_tot
```

```

%      scan_freq
%      scan_time_acq
%      sweep_dx
%      wheel_dx
%      x_cell
%      y_cell
%
% CAMPI INSERITI NEI FILE ELABORATI
%
% FS: simboli
% FC: conv_int_volts
% FT: t_soil_sample
% FO: info_operazione
% FN: id_sample_noise
%
% %%%%%%%%%%%%% MAPPA RADAR %%%%%%%%%%%%%
% MAPPA
% mark2
% mark1
% GPSmark
% sweep_non_validi
%
% "Extra"
% X
% Y
% filename
% file_ext
% path
%
%
% Versione:      1.9.0
% Autore:       G. Alli 4/1/2001

```

```

% Rev 1.1: G. Alli 30/10/01 Rendepersistenteil pathname in
modoche'aperturainterattiva di più
%
%                               file in
sequenzavengapositionatanellamedesima directory
% Rev 1.2: G. Alli 05/04/02 'info_operazione' è
inizializzato a '' inveceche []
% Rev 1.3: G. Alli 13/05/02 'S' è inizializzato a ''
inveceche []; modifica
%
%                               nell'estrazione del campo
'canale'
% Rev 1.4: G. Alli 14/05/02
Correzionedell'errorenellaletturacampi ATX e AMX
% Rev 1.5: G. Alli 09/09/02 Modificaestrazione campo
"canale" nelcaso "S" siaassente
% Rev 1.6: G. Alli 18/05/04 Modifica del display deimessaggi
di warning suicampi non letti
% Rev 1.7: G. Alli 18/11/04 Modificasintassiuigetfile per
Matlab 7.1
% Rev 1.8: G. Alli 21/03/05 Modificacontrolloapertura file
interattiva
% Rev 1.9: G. Alli 10/7/05 Allineamento di n_sampler_x al
numero di sweep effettivamente disponibili sul file
%
%                               Modifica del calcolo di Y
poichèoray_cellsiriferisce al tempo di campionamento
%
%                               Estrazione deinuovicampi FI, AH e
FZ
%
%
% Versione: 2.1
% Autore: A. Simi 10/02/09 Leggeilnuovoformatodati
V4.
%
%                               Aggiunticampi "ATR" e
"FW"
% Rev 2.1 G. Alli 10/06/09 Aggiungelettura marker GPS
(GPSmark)

```

```

persistent pathname; %rev 1.1

```

```

%apertura file
if ~isempty(varargin)      %apertura da input
fid = fopen(varargin{1},'r');
if fid ==-1
disp('Impossibile aprire il file');
dati=[];
return
end
[pathname,filename,ext,vers] = fileparts (varargin{1});
pathname=[pathname, '\'];
else%apertura interattiva
[file,
pathname,FILTERINDEX]=uigetfile([pathname, '*.D*'],'Georadar
File Loader');          %rev 1.8
if FILTERINDEX==0
disp('File not selected');
dati=[];
return
end
[scratch,filename,ext,vers]=fileparts(file);
if isempty(file) && isempty(pathname)
fid=-1;
else
% Apertura del file, 'r' sta per accesso in sola lettura
% fid=identificativo di output pari a -1 se l'operazione non
ha avuto successo
fid=fopen(strcat(pathname,file),'r');
end
if fid==-1
disp('File not found');
dati=[];
return

```

```

end
end

%letturacodicelunghezza record
code = fread(fid,4,'integer*1');
if code(1) == double('V');
len_rec=fread(fid,1,'integer*2');
else
disp('File format not recognised');
return
end

%%%%%%%%%%%%%%%%%%%%%%%%%%%%%%%%%%%%%%%%%%%%%%%%%%%%%%%%%%%%%%%%%%%%%%%%
%%%%%%%%%%%%%%%%%%%%%%%%%%%%%%%%%%%%%%%%%%%%%%%%%%%%%%%%%%%%%%%%%%%%%%%%
%%% Inizializzazione e default variabile di output
%%%%%%%%%%%%%%%%%%%%%%%%%%%%%%%%%%%%%%%%%%%%%%%%%%%%%%%%%%%%%%%%%%%%%%%%
%%%%%%%%%%%%%%%%%%%%%%%%%%%%%%%%%%%%%%%%%%%%%%%%%%%%%%%%%%%%%%%%%%%%%%%%

%V
dati.len_rec=len_rec;
dati.versione_file=code(2);           % Versione del file

%FI
dati.sweep_marker_1=[];

%I
dati.survey_info=[];

%C (non implementato)
dati.comment=[];

```

```
%AH
```

```
dati.height=[];
```

```
%FZ
```

```
dati.zone=' ';
```

```
%FX
```

```
dati.x_offset=[];
```

```
%FQ
```

```
dati.marker_quantum=[];
```

```
%FM
```

```
dati.sweep_marker=[];
```

```
dati.position=[];
```

```
%AC
```

```
dati.n_tx=[];
```

```
dati.tx_sequence=[];
```

```
dati.n_rx=[];
```

```
dati.rx_sequence=[];
```

```
dati.nacq=[];
```

```
%AM
```

```
dati.direct=[];
```

```
dati.l_coord=[];
```

```
dati.t_coord=[];
```

```
%ATR
```

```
dati.tx_x0=[];
```

```

dati.tx_y0=[];
dati.tx_alpha=[];
dati.tx_freq=[];
dati.rx_x0=[];
dati.rx_y0=[];
dati.rx_alpha=[];
dati.rx_freq=[];

%AA
dati.info=[];

%S
dati.S='';      %rev. 1.3
% dati.canale=[];

%FW
dati.n_canali = [];
dati.stacking = [];
dati.interleaving = [];
dati.id_canale = [];
dati.SOS_high = [];
dati.max_sampling_AD = [];
dati.SW_version = [];
dati.build_version = [];
dati.FW_version = [];
dati.GPS_offset_x = [];
dati.GPS_offset_y = [];

%H
dati.n_acq_sweep=[];
dati.n_acq_sample=[];
dati.n_sampler_x=[];

```

```

dati.n_sampler_y=[];
dati.enable_x_compress=[];
dati.n_x_compress=[];
dati.n_y_compress=[];
dati.enable_wheel=[];
dati.wheel_compress=[];
dati.ad_offset=[];
dati.radar_freq=[];
dati.prop_vel=[];
dati.sweep_time=[];
dati.sweep_time_tot=[];
dati.scan_freq=[];
dati.scan_time_acq=[];
dati.sweep_dx=[];
dati.wheel_dx=[];
dati.x_cell=[];
dati.y_cell=[];

%%%% Campi inseriti nei file elaborati

%FS
dati.simboli=[];

%FC
dati.conv_int_volts=[];

%FT
dati.t_soil_sample=[];

%FO
dati.info_operazione='';

```



```

%FN
dati.id_sample_noise=[];

%%%%%%%%%%%% MAPPA RADAR %%%%%%%%%%
dati.MAPPA=[];
dati.mark2=[];
dati.mark1=[];
dati.GPSmark=[]; %rev 2.1
dati.sweep_non_validi=[];

%extra (calcolati)
dati.X=[];
dati.Y=[];
dati.filename=filename;
dati.file_ext=ext;
dati.path=pathname;

ifdati.path == '\\'
dati.path=[];
end;

%%%%%%%%%%%% CAMPI OBSOLETI %%%%%%%%%%

%ATX
dati.tx_x0=[];
dati.tx_y0=[];
dati.tx_alpha=[];
dati.tx_freq=[];

```

```

%ARX
dati.rx_x0=[];
dati.rx_y0=[];
dati.rx_alpha=[];
dati.rx_freq=[];

%%%%%%%%%%%%%%%%%%%%%%%%%%%%%%%%%%%%%%%%%%%%%%%%%%%%%%%%%%%%%%%%%%%%%%%%
%%%%%%%%%%%%%%%%%%%%%%%%%%%%%%%%%%%%%%%%%%%%%%%%%%%%%%%%%%%%%%%%%%%%%%%%

pos = len_rec;
fseek(fid,pos,'bof');
code = (fread(fid,4,'integer*1'))';

%%%%%%%%%%%%%%%%%%%%%%%%%%%%%%%%%%%%%%%%%%%%%%%%%%%%%%%%%%%%%%%%%%%%%%%%          LETTURA          HEADER
%%%%%%%%%%%%%%%%%%%%%%%%%%%%%%%%%%%%%%%%%%%%%%%%%%%%%%%%%%%%%%%%%%%%%%%%

while code(1)~= double('R')

%FI
if code(1:2)==double('FI')
    dati.sweep_marker_1=ascii2num(fid,6);

%I
elseif code(1)==double('I')
    temp=fread(fid,len_rec-4,'integer*1');
    dati.survey_info=deblank(char(temp));

%C (non implementato)
elseif code(1)==double('C')

```

```

temp=fread(fid,len_rec-4,'integer*1');
dati.comment=deblank(char(temp));

%AH
elseif code(1:2)==double('AH')
dati.height=ascii2num(fid,16);

%FZ
elseif code(1:2)==double('FZ')
temp=fread(fid,len_rec-4,'integer*1');
dati.zone=deblank(char(temp));

%FX
elseif code(1:2)==double('FX')
dati.x_offset=ascii2num(fid,16);

%FQ
elseif code(1:2)==double('FQ')
dati.marker_quantum=ascii2num(fid,16);

%FM
elseif code(1:2)==double('FM')
dati.sweep_marker=[dati.sweep_marker,ascii2num(fid,6)];
dati.position=[dati.position,ascii2num(fid,16)];

%AC
elseif code(1:2)==double('AC')
dati.n_tx=fread(fid,1,'integer*4');
dati.tx_sequence=fread(fid,1,'integer*4');
dati.n_rx=fread(fid,1,'integer*4');
dati.rx_sequence=fread(fid,1,'integer*4');
dati.nacq=fread(fid,1,'integer*4');

```

```
%AM
```

```
elseif code(1:2)==double('AM')  
dati.direct=char(fread(fid,1,'integer*1'));  
dati.l_coord=ascii2num(fid,16);  
dati.t_coord=ascii2num(fid,16);
```

```
%ATR
```

```
elseif code(1:3)==double('ATR')  
    dati.tx_x0=ascii2num(fid,16);  
    dati.tx_y0=ascii2num(fid,16);  
dati.tx_alpha=ascii2num(fid,16);  
dati.tx_freq=ascii2num(fid,5);  
    dati.rx_x0=ascii2num(fid,16);  
    dati.rx_y0=ascii2num(fid,16);  
dati.rx_alpha=ascii2num(fid,16);  
dati.rx_freq=ascii2num(fid,5);
```

```
%AA
```

```
elseif code(1:2)==double('AA')  
temp=fread(fid,len_rec-4,'integer*1');  
    dati.info=deblank(char(temp));
```

```
%S
```

```
elseif code(1)==double('S')  
temp=fread(fid,len_rec-4,'integer*1');  
temp=char(temp);  
dati.S=[dati.S,temp];
```

```
%Rev. 1.3
```

```
%FW
```

```
elseif code(1:2)==double('FW')
```

```

da_buttare = fread(fid,1,'integer*4');
dati.n_canali = fread(fid,1,'integer*4');
dati.stacking = fread(fid,1,'integer*4');
dati.interleaving = fread(fid,1,'integer*4');
dati.id_canale = fread(fid,1,'integer*4');
dati.SOS_high = fread(fid,1,'integer*4');
dati.max_sampling_AD =ascii2num(fid,16);
temp = fread(fid,10,'char*1');
dati.SW_version = char(temp');
temp = fread(fid,10,'char*1');
dati.build_version = char(temp');
temp = fread(fid,7,'char*1');
dati.FW_version = char(temp');
dati.GPS_offset_x = ascii2num(fid,16);
dati.GPS_offset_y = ascii2num(fid,16);

%H
elseif code(1)==double('H')
scratch=fread(fid,1,'integer*4'); %contiene la lunghezza del
record
%
vienecestinata                                giàestratta e
dati.n_acq_sweep=fread(fid,1,'integer*4');
dati.n_acq_sample=fread(fid,1,'integer*4');
dati.n_sampler_x=fread(fid,1,'integer*4');
dati.n_sampler_y=fread(fid,1,'integer*4');
dati.enable_x_compress=fread(fid,1,'integer*4');
dati.n_x_compress=fread(fid,1,'integer*4');
dati.n_y_compress=fread(fid,1,'integer*4');
dati.enable_wheel=fread(fid,1,'integer*4');
dati.wheel_compress=fread(fid,1,'integer*4');
dati.ad_offset=fread(fid,1,'integer*4');

```

```
%datiscritti in ASCII
```

```
dati.radar_freq=ascii2num(fid,16);  
dati.prop_vel=ascii2num(fid,16);  
dati.sweep_time=ascii2num(fid,16);  
dati.sweep_time_tot=ascii2num(fid,16);  
dati.scan_freq=ascii2num(fid,16);  
dati.scan_time_acq=ascii2num(fid,16);  
dati.sweep_dx=ascii2num(fid,16);  
dati.wheel_dx=ascii2num(fid,16);  
dati.x_cell=ascii2num(fid,16);  
dati.y_cell=ascii2num(fid,16);
```

```
%%%%%%%%%%          LETTURA          HEADER          DATI          ELABORATI  
%%%%%%%%%%
```

```
%FC
```

```
elseif code(1:2)==double('FC')  
dati.conv_int_volts=ascii2num(fid,16);
```

```
%FS
```

```
elseif code(1:2)==double('FS')  
temp=fread(fid,len_rec-4,'integer*1');  
dati.simboli=strvcat(dati.simboli,deblank(char(temp)));
```

```
%FT
```

```
elseif code(1:2)==double('FT')  
dati.t_soil_sample=ascii2num(fid,16);
```

```

%FO
elseif code(1:2)==double('FO')
temp=fread(fid,len_rec-4,'integer*1');

dati.info_operazione=strvcat(dati.info_operazione,deblank(char(temp')));

%FN
elseif code(1:2)==double('FN')
dati.id_sample_noise=fread(fid,1,'integer*4');;

%%%%%%%%%%%%%%%%%%%%%%%%%%%%%%%%%%%%%%%%%%%%%%%%%%%%%%%%%%%%%%%%%%%%%%%% LETTURA          CAMPI          OBSOLETI
%%%%%%%%%%%%%%%%%%%%%%%%%%%%%%%%%%%%%%%%%%%%%%%%%%%%%%%%%%%%%%%%%%%%%%%%

%ATX
elseif code(1:3)==double('ATX')
fseek(fid,53*(dati.tx_sequence-1),0); %rev 1.4:
simuovesullapositionedelleinformazioni del Txcorretto
    dati.tx_x0=ascii2num(fid,16);
    dati.tx_y0=ascii2num(fid,16);
dati.tx_alpha=ascii2num(fid,16);
dati.tx_freq=ascii2num(fid,5);

%ARX
elseif code(1:3)==double('ARX')
fseek(fid,53*(dati.rx_sequence-1),0); %rev 1.4:
simuovesullapositionedelleinformazioni del Rx corretto
    dati.rx_x0=ascii2num(fid,16);
    dati.rx_y0=ascii2num(fid,16);
dati.rx_alpha=ascii2num(fid,16);
dati.rx_freq=ascii2num(fid,5);

```

```
%%%%%%%%%% FINE LETTURA HEADER
%%%%%%%%%%
```

```
else
```

```
    WMSG=['The RIS data field code ',char(code),' = ',int2str(code),' is unknown'];
```

```
    WMSG(find(double(WMSG)==0))=char(32);
```

```
    warning('IDS:UnknownRIScode',WMSG);
```

```
    warningoff
```

```
    disp(['Attenzioneilcodice ',char(code),' = ',int2str(code),' è sconosciuto']);
```

```
    warningon
```

```
%
```

```
end
```

```
pos = pos+len_rec;
```

```
fseek(fid,pos,'bof');
```

```
code = (fread(fid,4,'integer*1'))';
```

```
end
```

```
%ri-posizionamentoall'iniziodeidati
```

```
fseek(fid,pos,'bof');
```

```
%%%%%%%%%% LETTURA DATI RADAR
%%%%%%%%%%
```

```
ifdati.n_sampler_y>0 &&dati.n_sampler_x>0
```

```
dati.MAPPA=fread(fid,[dati.n_sampler_y+2,dati.n_sampler_x],'int16');
```



```

else
disp('Errore: file non caricato');
return
end

%%%%%%%%%%%%%%%%%%%%%%%%%%%%%%%%%%%%%%%%%%%%%%%%%%%%%%%%%%%%%%%%%%%%%%%%%%%%%%
%

%chiusura file
fclose(fid);

%aggiustan_sampler_x se c'è discrepanza col numero di sweep
effettivamente letti
%dati.n_sampler_x=size(dati.MAPPA,2);          %Rev
1.9

%Manipolazione dei dati grezzi
codice_dati=dati.MAPPA([1,2],:);                %codice sweep
dati.MAPPA=dati.MAPPA(3:dati.n_sampler_y+2,:); %elimino le
righe relative al codice sweep

%se il dato di conversione in volts non è stato letto o è = 0
%viene utilizzata la conversione a 16 bit su 10 Volts per i
file .dt
if isempty(dati.conv_int_volts) || dati.conv_int_volts==0
dati.conv_int_volts=10/32768;
end
dati.MAPPA=(dati.MAPPA-dati.ad_offset)*dati.conv_int_volts;
%convertito il dato DT in volt

%se il dato di offset del convertitore AD non è
stato letto viene impostato a 0
if isempty(dati.ad_offset)

```

```
dati.ad_offset=0;
```

```
end
```

```
%calcolo di X e Y in metri
```

```
dati.X=(0:dati.n_sampler_x-1)*dati.x_cell+dati.x_offset;
```

```
dati.Y=(0:dati.n_sampler_y-1)*dati.y_cell;
```

```
%rev 1.9
```

```
%estraegliindici del marker 2 (2386 corrisponde a 'R8' in  
int16)
```

```
dati.mark2=find(codice_dati(1,')==2386);
```

```
%estraegliindici del marker 1 (2130 corrisponde a 'R9' in  
int16)
```

```
dati.mark1=find(codice_dati(1,')==2130);
```

```
%estraegliindici dello "sweep non valido" (338 e 6  
corrispondono a 'R1' '6' in int16)
```

```
dati.sweep_non_validi=find(codice_dati(1,')==338  
&codice_dati(2,')==6);
```

```
%estraegliindici del marker GPS (1874) %line added in  
rev 2.1
```

```
dati.GPSmark=find(codice_dati(1,')==1874); %line added  
in rev 2.1
```

```
%%%%%%%%%%%%%%%%%%%%%%%%%%%%%%%%%%%%%%%%%%%%%%%%%%%%%%%%%%%%%%%%%%%%%%%%  
%%%%%%%%%%%%%%%%%%%%%%%%%%%%%%%%%%%%%%%%%%%%%%%%%%%%%%%%%%%%%%%%%%%%%%%%
```

```
% funzioneausiliaria di lettura di n caratteri e
conversionenumerica
```

```
%%%%%%%%%%%%%%%%%%%%%%%%%%%%%%%%%%%%%%%%%%%%%%%%%%%%%%%%%%
%%%%%%%%%%%%%%%%%%%%%%%%%%%%%%%%%%%%%%%%%%%%%%%%%%%%%%%%%%
```

```
functionnum=ascii2num(fid,n)
```

```
%legge n caratteri dal file (fid) e converte in numero
```

```
temp=fread(fid,n,'char*1');
```

```
num=str2num(char(temp));
```

```
clc;
```

```
clearall;
```

```
closeall;
```

```
% Change the following inputs according to your data
```

```
% Here write the name of the file to compare all others with
it e.g. LID10001.D00
```

```
data=idsris_readv4('LID10004.D00');
```

```
map=data.MAPPA;
```

```
map = map(50:64,1:42);
```

```
tmp = map(:);
```

```
tmp = sort(tmp,'descend');
```

```
tmp = tmp(1:200);
```

```
av1 = mean(tmp);
```

```
% Enter the total number of files here
```

```
number_of_files = 15;
```

```
% Calculating Mean Squared Error
```

```
fori = 1:number_of_files
```

```

% Reading the input files in the for loop
if (i < 10)
strn = num2str(i);
str = strcat('LID1000',strn, '.D00');
else
strn = num2str(i);
str = strcat('LID100',strn, '.D00');
end
data=idsris_readv4(str);
map=data.MAPPA;
map = map(50:64,1:42);
tmp = map(:);
tmp = sort(tmp, 'descend');
tmp = tmp(1:200);
    av2 = mean(tmp);
% Calculating Difference
mse(i) = (av1-av2).^2;
end
%% Displaying the results
%Pipe sorted from good to bad
[MSE,good_to_bad]=sort(mse);
% Here you can change the display name e.g. X-Direction
Pipes or whatever
figure ('Name','X-Direction Pipes');
% Bar Plot
bar (MSE);
% Setting x-axis marks resolution
set(gca, 'XTick', 1:number_of_files);
% Setting x-axis marks labels
set(gca, 'XTickLabel', {good_to_bad(1:end)});
% Label for X-Axis

```

```
xlabel ('Pipe Number =>(Good Pipe on left    Bad Pipe on  
right)');  
% Label for Y-Axis  
ylabel ('Mean Square Error with respect to best Pipe: Pipe  
Number 4')
```